UNIVERSITAT POLITÈCNICA DE VALÈNCIA

DEPARTMENT OF CONSTRUCTION ENGINEERING AND
CIVIL ENGINEERING PROJECTS

Numerical and experimental research on the fire resistance of composite columns with steel sections embedded in concrete and high strength materials

Thesis submitted in partial fulfillment of the requirements
for the degree of Doctor of Philosophy

by

David Medall Martos

Advisors:
Dr. Ana Espinós Capilla
Dr. Manuel L. Romero García

Valencia (Spain), June 2024

Acknowledgements

First, I would like to express my deepest gratitude to my supervisors, Dr Ana Espinós Capilla and Dr Manuel L. Romero, for supporting me through my predoctoral period and for their knowledgeable advice, making this thesis possible.

I also would like to thank my colleagues from Universitat Politècnica de València for being by my side at every step of this path: Roberto, Jorge, Álvaro, Fernando, Dani, and Enrique. A special thanks to Vicente and Carmen, who thought I was suitable for this job and gave me this opportunity. Thanks should also go to all the people from ICITECH and the Department of Construction Engineering and Civil Engineering Projects.

I would also like to sincerely thank Dr Tai Thai for inviting me to the renowned University of Melbourne during my doctoral period and offering his help along the process. I would like to acknowledge the colleagues I made at the Faculty of Engineering and Information Technology during my stay.

I could not have undertaken this journey without my family and friends' constant support and appreciation, so I would like to extend my gratitude to them. Another big thanks to C&SM, for all the adventures. Lastly, I would like to thank Lydia for supporting me, believing in me and always being by my side; this thesis is a bit yours, too.

David Medall Martos

Castelló de la Plana, May 2024

Abstract

Concrete-filled steel tubular (CFST) columns are a type of composite structural members that have gained popularity in recent years owing to their excellent structural performance and rational use of the materials. By embedding a steel profile inside a CFST section, a new and innovative type of composite section is generated: the so-called steel-reinforced concrete-filled steel tubular (SR-CFST) column, which is the focus of this thesis. This typology improves the room temperature capacity of CFST columns, while enhancing their fire performance, as the inner steel profile is thermally protected by the surrounding concrete.

Despite their remarkable load-bearing capacity at both room and elevated temperature, investigations on SR-CFST columns under fire are still scarce. The state of the art on the fire behaviour of SR-CFST columns is reviewed in this thesis, proving that further research is needed to completely understand the performance of this type of columns under elevated temperature.

The fire performance of SR-CFST columns is analysed in this thesis by means of experimental tests and numerical simulations. First, an experimental investigation is conducted to study the behaviour of these composite columns under two scenarios: the first phase of the experimental campaign is focused on the post-fire performance, while the second phase is conducted to determine the thermo-mechanical performance of SR-CFST stub columns under constant load and increasing temperature.

Subsequently, a realistic finite element model is developed to extend the experimental results and analyse in depth the behaviour of SR-CFST columns in fire. The numerical model is validated against the previously performed thermo-mechanical tests, as well as by comparing its predictions with the available experimental results from the literature. A series of parametric studies are conducted to analyse the influence of the relevant geometrical parameters and to study the effect of the use of high-strength materials on the fire performance of the columns. Based on the results of the parametric studies, a simplified proposal is developed to easily determine the cross-sectional temperature distribution at a given fire exposure time. Using the obtained equivalent temperatures and in line with the current provisions in Eurocode 4 Part 1.2, a new design equation is proposed to evaluate the cross-sectional plastic resistance of SR-CFST columns under fire conditions, filling an existing gap in the European design code.

Resumen

Los pilares tubulares de acero rellenos de hormigón (CFST) son un tipo de elementos estructurales mixtos que han ganado popularidad recientemente debido a su excelente comportamiento estructural y al uso racional de los materiales en su fabricación. Con la introducción de un perfil de acero dentro de una sección CFST, surge un nuevo tipo de sección mixta: los pilares tubulares de acero rellenos de hormigón con perfil de acero interior (SR-CFST), en los cuáles se centra esta tesis. Esta tipología incrementa la capacidad portante a temperatura ambiente de los pilares CFST y mejora su comportamiento a fuego, ya que el perfil interior está protegido térmicamente por el hormigón que lo rodea.

Las investigaciones disponibles en la bibliografía sobre pilares SR-CFST aún son escasas, pese a sus significativas capacidades mecánicas tanto a temperatura ambiente como a elevada. En esta tesis se revisa el estado del arte sobre pilares SR-CFST, llegando a la conclusión de que son necesarias más investigaciones para comprender el comportamiento de estas secciones a temperatura elevada.

La presente tesis analizará el comportamiento frente al fuego de pilares SR-CFST mediante ensayos experimentales y simulaciones numéricas. Inicialmente, se lleva a cabo una campaña experimental para analizar el comportamiento de los pilares bajo dos escenarios: una primera fase que estudia el comportamiento de los pilares tras su exposición al fuego, y una segunda en la que se analizará el comportamiento termo-mecánico de pilares cortos SR-CFST bajo carga constante e incremento progresivo de la temperatura.

Tras ello, se desarrolla un modelo de elementos finitos para extender los resultados obtenidos experimentalmente y estudiar en profundidad el comportamiento de los pilares SR-CFST en fuego. El modelo numérico se valida con los ensayos termo-mecánicos realizados anteriormente, así como comparando sus predicciones con los resultados experimentales extraídos de la bibliografía. Con el modelo desarrollado se realizan una serie de estudios paramétricos para examinar la influencia de los parámetros geométricos más relevantes, así como para analizar el efecto del uso de materiales de alta resistencia en el comportamiento a fuego de los pilares. En base a los resultados obtenidos de los estudios paramétricos, se lleva a cabo una propuesta para determinar de forma sencilla la distribución de temperaturas seccional en un tiempo de exposición al fuego dado. Empleando las temperaturas equivalentes obtenidas y en línea con las directrices del Eurocódigo 4 Parte 1.2, se propone una nueva expresión para evaluar la resistencia plástica seccional de los pilares SR-CFST bajo la acción del fuego. Esta propuesta cubre un campo de aplicación que actualmente no está contemplado en la normativa europea.

Resum

Els pilars tubulars d'acer plens de formigó (CFST) són un tipus de membres estructurals mixtes que han guanyat popularitat recentment degut al seu excel·lent comportament estructural y a l'ús moderat de materials en la seua construcció. Amb la introducció d'un perfil d'acer dins d'una secció CFST, s'obté un nou tipus de secció mixta: els pilars tubulars d'acer plens de formigó amb perfil d'acer interior (SR-CFST), al voltant dels quals se centra esta tesi. Esta tipologia incrementa la capacitat a temperatura ambient dels pilars CFST i millora el seu comportament a foc, ja que el perfil interior està protegit tèrmicament pel formigó que l'envolta.

Les investigacions disponibles a la bibliografia sobre pilars SR-CFST encara són escasses, malgrat les seues significatives capacitats mecàniques tant a temperatura ambient com a elevada. En esta tesi es revisa l'estat de l'art sobre pilars SR-CFST, concloent que són necessàries més investigacions per tal de comprendre el comportament d'estes seccions a alta temperatura.

En la present tesi s'analitzarà el comportament a foc dels pilars SR-CFST per mitjà d'assajos experimentals i simulacions numèriques. Inicialment es desenvolupa una campanya experimental per tal d'analitzar el comportament dels pilars en dos situacions: una primesa fase estudia el comportament dels pilars després de la seua exposició al foc i una segona en què s'analitza el comportament termo-mecànic de pilars curts SR-CFST subjectes a una càrrega constant i a un increment progressiu de la temperatura.

Seguidament es desenvolupa un model d'elements finits realista per tal d'estendre els resultats obtinguts experimentalment i estudiar en profunditat el comportament dels pilars SR-CFST en foc. El model numèric es valida amb els assajos termo-mecànics realitzats anteriorment, així com comparant les seues prediccions amb els resultats disponibles a la bibliografia. Amb ajuda del model desenvolupat es realitzen una sèrie d'estudis paramètrics per tal d'examinar la influència dels paràmetres geomètrics més rellevants així com l'efecte de l'ús de materials d'alta resistència en el comportament a foc dels pilars. Basat en els resultats obtinguts dels estudis paramètrics, es desenvolupa una proposta per determinar, de forma senzilla, la distribució de temperatures seccional en un temps d'exposició al foc concret. Amb les temperatures equivalents obtingudes i en línia en les indicacions de l'Eurocódi 4 Part 1.2, es proposa un nou mètode per avaluar la resistència plàstica seccional de pilars SR-CFST baix l'acció del foc. Esta proposta cobreix un camp d'aplicació que actualment no està contemplat en la normativa europea.

MOTIVATION AND OUTLINE OF THIS THESIS

The present thesis is developed in the scope of the National Project HIFICOMP (Grant PID2019-105908RB-I00) and with the help of the author's pre-doctoral contract (Grant PRE2020-093106) funded by MCIN/AEI/10.13039/501100011033 and by "ESF Investing in your future". The main objective of this project, led by Dr Romero and Dr Espinós, was to study the performance of innovative steel-concrete composite columns in fire and analyze the benefits of the inclusion of high-strength materials in these sections. The work presented in this thesis follows the research line on the fire behaviour of innovative composite structures in the framework of the aforementioned project.

This work is motivated by previous research conducted by the research group of the thesis supervisors at Universitat Politècnica de València (Spain), where the fire behaviour of innovative steel-concrete composite sections and their benefits as compared to traditional concrete-filled steel tubular (CFST) columns was studied. One of the most promising typologies investigated was the steel-reinforced CFST (SR-CFST) columns, which gave rise to the need of studying these sections specifically under fire conditions.

Given the reduced number of both experimental investigations and numerical studies on SR-CFST columns, this thesis aims to both extend the available experimental data in the literature and to analyze the response of these columns by numerical means. That is why, a comprehensive experimental campaign was conducted in this thesis – as part of the experimental program planned in the project HIFICOMP –, along with the development of a realistic numerical model, which was subsequently used to conduct extensive parametric studies to investigate the influence of the relevant geometrical and physical parameters of the SR-CFST columns under fire.

To acquire a deeper knowledge on the finite element modelling of steel-concrete composite columns in fire, the author of this thesis performed a research stay at the University of Melbourne (Australia) during the last stage of the doctoral period to collaborate with Dr Tai Thai, who had a broad experience in this field.

As an outcome of the numerical and experimental work developed within this thesis, a simplified calculation method was developed. This method allows to evaluate the temperature field of an SR-CFST section at a given fire exposure times through a set of equivalent temperatures representing the different parts of the section. With those temperatures, the cross-sectional plastic resistance of an SR-CFST column in fire can be easily obtained with a design formula based on the provisions of Eurocode 4 Part 1-2.

The document starts with an introductory part consisting of Chapters 1, 2 and 3. Chapter 1 presents a revision of the theoretical background of the fire behaviour of CFST and SR-CFST columns. Next, Chapter 2 presents a review of the state of the art on this field, covering the available numerical models and experimental investigations in SR-CFST sections exposed to fire. The aim and scope of this thesis is subsequently exposed in Chapter 3, after generating the need for this research.

Chapter 4 includes the experimental investigations conducted in the scope of this thesis. The first phase of the experimental program (phase A) was designed to study the thermal behaviour of the column and its post-fire resistance to axial compression and to calibrate the experimental set-up. With the findings extracted from this campaign, phase B was designed to study the thermo-mechanical behaviour of SR-CFST stub columns in a fire scenario. Important conclusions were drawn from this study and the experimental data extracted was subsequently used as a reference for validation of the numerical model.

In Chapter 5 the development of the numerical model is presented, together with the validation process and a series of sensitivity analyses conducted to adequately calibrate the model.

The results of a series of parametric studies conducted with the numerical models are included in Chapter 6. The effect of the geometrical parameters of SR-CFST sections and the use of high-strength materials on the fire performance of these columns is discussed in this chapter.

Chapter 7 presents a new method for evaluating the sectional capacity of SR-CFST columns in fire. A simplified proposal is firstly introduced to predict the temperature evolution of the section by means of a single representative equivalent temperature for each part. Then, a simplified design equation is proposed based on the formulation in EN 1994-1-2 to predict the cross-sectional plastic resistance of SR-CFST columns in fire.

Finally, Chapter 8 includes the major conclusions drawn from the work presented in this thesis and presents suggestions for future work.

Four articles were published in peer-reviewed international journals containing part of the work presented in this thesis, which are included in open access version in Annex I of this document. Additionally, a series of conference papers were presented based on the findings of this work. The details of these publications are included hereafter:

ARTICLES PUBLISHED IN SCIENTIFIC JOURNALS

Article 1

"Simplified proposal for the temperature field of steel-reinforced CFST columns exposed to fire"
David Medall, Ana Espinós, Vicente Albero, Manuel L. Romero
Engineering Structures 273 (2022) 115083
https://doi.org/10.1016/j.engstruct.2022.115083

Article 2

"Experimental residual capacity of steel-reinforced concrete-filled steel tubular stub columns after fire exposure"
David Medall, Carmen Ibáñez, Vicente Albero, Ana Espinós, Manuel L. Romero
Thin-Walled Structures 189 (2023) 110900
https://doi.org/10.1016/j.tws.2023.110900

Article 3

"Thermo-mechanical compression tests on steel-reinforced concrete-filled steel tubular stub columns with high performance materials"
David Medall, Carmen Ibáñez, Ana Espinós, Manuel L. Romero
Steel and Composite Structures 49 (2023) 533-546
https://doi.org/10.12989/scs.2023.49.5.533

Article 4

"Fire design of steel-reinforced CFST stub columns with high-strength materials"
David Medall, Manuel L. Romero, Huu-Tai Thai, Ana Espinós
Journal of Constructional Steel Research 218 (2024) 108692
https://doi.org/10.1016/j.jcsr.2024.108692

CONFERENCE PAPERS

Congress on Numerical Methods in Engineering – CMN 2022 (Las Palmas de Gran Canaria, Spain)

"Modelo numérico bidimensional para la evaluación del comportamiento térmico de columnas tubulares de acero rellenas de hormigón con perfiles embebidos en situación de incendio"
David Medall, Ana Espinós, Vicente Albero, Carmen Ibáñez, Manuel L. Romero
CMN 2022, Congress on Numerical Methods in Engineering, (2022) 219-236
ISBN: 978-84-123222-9-3

The International Colloquium on Stability and Ductility of Steel Structures - SDSS 2022 (Aveiro, Portugal)

"Numerical Investigation on the Thermal Behaviour of Steel-reinforced CFST Columns in Fire"
David Medall, Ana Espinós, Vicente Albero, Carmen Ibáñez, Manuel L. Romero
ce/ papers, 5(4), (2022) 429-438
http://dx.doi.org/10.1002/cepa.1774

12th International Conference on Structures in Fire - SIF22 (Hong Kong)

"Experimental investigation on steel-reinforced CFST columns after fire exposure"
David Medall, Carmen Ibáñez, Vicente Albero, Andrés Lapuebla, Ana Espinós, Manuel L. Romero
Proceedings of the 12th International Conference on Structures in Fire, (2022) 157-167
ISBN: 978-962-367-869-8

The 10th Eurosteel Conference - Eurosteel 2023 (Amsterdam, Netherlands)

"Experimental evaluation of the load-bearing capacity of steel-reinforced CFST stub columns under a fire scenario"
David Medall, Carmen Ibáñez, Ana Espinós, Manuel L. Romero
ce/papers 6(3-4), (2023) 2127-2132
http://dx.doi.org/10.1002/cepa.2525

7th International Conference on Mechanical Models in Structural Engineering - CMMoST 2023 (Málaga, Spain)

"Finite element model for the proposal of a simplified temperature field in SR-CFST columns subjected to fire"
David Medall, Carmen Ibáñez, Vicente Albero, Andrés Lapuebla, Ana Espinós, Manuel L. Romero
7th International Conference on Mechanical Models in Structural Engineering, (2023) 103-106
ISBN: 978-84-19214-79-9

9th International Conference on Thin-Walled Structures - ICTWS 2023 (Sydney, Australia)

"Experimental fire performance of slender steel-reinforced concrete-filled steel tubular columns"
David Medall, Carmen Ibáñez, Ana Espinós, Manuel L. Romero
Proceedings of the Ninth International Conference on Thin-Walled Structures - ICTWS2023, (2023) 898-908

TABLE OF CONTENTS

LIST OF FIGURES

LIST OF TABLES

NOTATION

Latin upper case letters

A_a	Cross-sectional area of the steel tube
A_c	Cross-sectional area of the concrete
A_f	Cross-sectional area of the inner steel profile flanges
A_{sp}	Cross-sectional area of the inner steel profile
A_w	Cross-sectional area of the inner steel profile web
A_m/V	Section factor
B	Outer dimension of a square section
D	Outer diameter of a circular section
$E_{s,\theta}$	Modulus of elasticity of steel at the temperature θ
$E_{c,\theta}$	Tangent modulus of concrete at the temperature θ
$E_{c,sec,\theta}$	Secant modulus of concrete at the temperature θ
E_s^t	Tangent modulus of steel
$(EI)_{fi,eff}$	Effective flexural stiffness in the fire situation
$I_{a,\theta}$	Second moment of area of the steel profile at the temperature θ
$I_{c,\theta}$	Second moment of area of the concrete at the temperature θ
$I_{f,\theta}$	Second moment of area of the inner steel profile flanges at the temperature θ
$I_{w,\theta}$	Second moment of area of the inner steel profile web at the temperature θ
L	Length of the column
N	Applied axial load
N_{exp}	Experimentally applied axial load
N_{calc}	Numerically obtained axial load
$N_{fi,cr}$	Elastic critical load in the fire situation
$N_{fi,pl,Rd}$	Design cross-sectional plastic resistance to axial compression in fire
$N_{fi,Rd}$	Design axial buckling load of the column in the fire situation
$N_{post,exp}$	Experimentally applied axial load in the post-fire scenario
N_u	Ultimate resistance of the column at room temperature
P_m	Perimeter of the section
R	Standard fire resistance

Latin lower case letters

b	Width of the inner steel profile
c_p	Specific heat
f_c	Compressive cylinder strength of concrete at room temperature
$f_{c,post}$	Compressive cylinder strength of concrete in the post-fire scenario
$f_{c,u}$	Ultimate compressive cylinder strength of concrete at room temperature
f_y	Yield strength of structural steel at room temperature
$f_{y,,post}$	Yield strength of structural steel in the post-fire scenario
$f_{y,u}$	Ultimate yield strength of structural steel at room temperature
$f_{ui,post}$	Yield strength of reinforcing steel at room temperature

h_j	Thermal gap conductance
h	Height of the inner steel profile
$\dot{h}_{net}$	Net heat flux
$k_{i,\theta}$	Reduction factor for a material property at elevated temperature
q	Heat flux vector per unit surface
t	Thickness of the steel tube
t_f	Thickness of the flanges of the steel profile
t_w	Thickness of the web of the steel profile
u_s	Concrete cover

Greek lower case letters

α_c	Coefficient of heat transfer by convection
ε	Strain
ε_f	Emissivity of the fire
ε_m	Emissivity of the exposed surface
Φ	Configuration factor
$\gamma_{M,fi}$	Partial factor for a material property in the fire situation
μ	Axial load level ($\mu = N/N_{Rd}$)
λ_i	Thermal conductivity
θ	Temperature
ρ_i	Density
σ	Normal stress
υ	Poisson coefficient

Abbreviations

CES	Concrete encased section
CFDST	Concrete Fillet double steel tube
CFST	Concrete filled steel tube
CFSST	Concrete filled stainless steel tube
CFT	Concrete filled tube
CHS	Circular hollow section
EN 1991-1-2	Eurocode 1 Part 1-2
EN 1992-1-2	Eurocode 2 Part 1-2
EN 1993-1-2	Eurocode 3 Part 1-2
EN 1993-1-12	Eurocode 3 Part 1-12
EN 1994-1-1	Eurocode 4 Part 1-1
EN 1994-1-2	Eurocode 4 Part 1-2
FE	Finite element
FEA	Finite element analysis
F-F	Fixed-fixed supporting conditions
FT	Failure time
HSC	High strength concrete

HSS	High strength steel
LVDT	Linear Variable Differential Transformer
NSC	Normal strength concrete
NSS	Normal strength steel
P-F	Pinned-fixed supporting conditions
P-P	Pinned-pinned supporting conditions
pr EN1992-1-2	New draft version of Eurocode 2 Part 1-2
pr EN1994-1-2	New draft version of Eurocode 4 Part 1-2
RC	Reinforced concrete
RCFST	Reinforced concrete
RHS	Rectangular hollow tube
RSI	Residual strength index
SHS	Square hollow section / Steel hollow section
SI	Strength index
SRC	Steel reinforced concrete
SFRC	Steel fibre reinforced concrete
SR-CFST	Steel reinforced concrete filled steel tube
TC	Thermocouple

1.

INTRODUCTION

This first chapter presents a summary of the innovative steel-reinforced concrete-filled steel tubular (SR-CFST) columns and their behaviour under fire conditions. The emerge of these new sections, the advantages they provide and several examples of their use in construction are included in this chapter. Next, the fire behaviour of these types of composite sections is analysed.

1.1. BACKGROUND

Concrete-filled steel tubular columns (CFST) have been broadly used in recent years due to their significative structural performance, ductility, and energy absorption capabilities, combining the effect of the steel and the concrete (Han et al., 2014). As the inner concrete is confined by the outer steel tube, the compressive strength of the column is increased, therefore boosting the resistance to local buckling (Johansson, 2002). Additionally, it also eliminates the need for formwork as the outer steel provides the shape to the section and confines the inner concrete, reducing the cost and time in construction.

A large list of examples of high-rise buildings that use composite sections for the main load-bearing elements are available all around the world. While this trend in civil construction began in the United States in the 70's, nowadays, most examples of composite construction are found in Asia, more precisely in China (Liew et al., 2021). Some examples of the use of composite sections could be the Otemachi Tower in Tokyo, Japan (Matsumoto et al., 2014) or the Guangzhou West Tower in Guangzhou, China (Fang et al., 2010). These types of composite sections have also been introduced in Europe, as in the Millennium Tower in Wien, Austria (Romero et al., 2016) or the VDEh Steel Institute in Dusseldorf, Germany (Hassanein et al., 2017).

Despite their extended use and advantages, slender CFST columns have shown to prematurely fail when exposed to fire conditions (Espinos et al., 2015). That is why, in recent years a wide variety of innovative alternatives (see Figure 1.1) has appeared to improve both the load-bearing capacity and the fire behaviour of steel-concrete composite sections (Han et al., 2014; Liew et al., 2021).
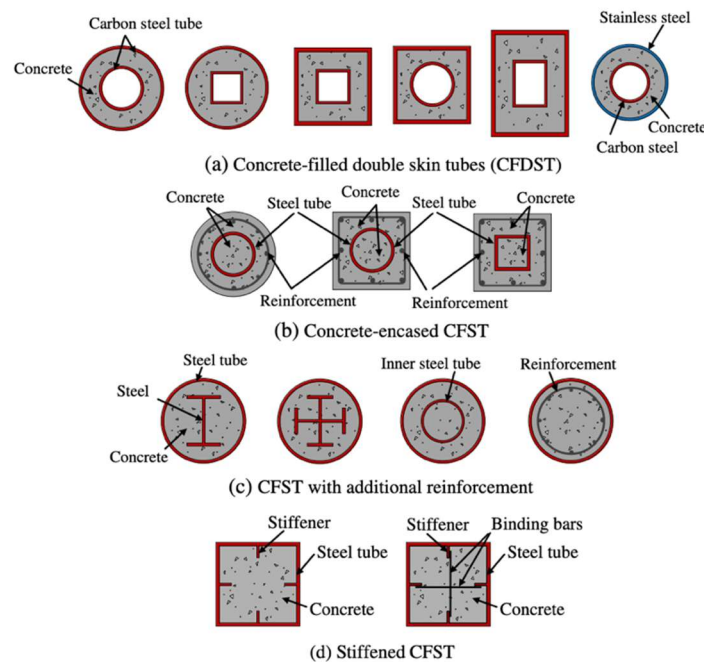
Figure 1.1   Different types of CFST cross-section variations (Han et al., 2014).

The mechanical performance of regular square and rectangular CFST columns is inferior when compared to their circular counterparts, and the local buckling of the outer tube tends to occur more often in these geometries (Tao et al., 2008). That is why, some authors proposed the inclusion of longitudinal or traverse stiffeners to increase the ductility of the square CFST columns (see Figure 1.1d). Many different configurations have been tested to find the best stiffening scheme in terms of the strength and ductility of the columns (Huang et al., 2002; Tao et al., 2005) while the addition of binding bars has also been examined for similar purposes (Tao et al., 2007; Zheng et al., 2013).

Numerous authors have proposed the addition of an inner steel tube as a solution to this issue, which have been studied with two different approaches. One of them is the so-called "double skin", which consists of two concentric steel tubes that confine a concrete area (see Figure 1.1a). This proposal has been studied with numerous combinations for the tubes: double circular (Essopjee & Dundu, 2015; Tao et al., 2004; Uenaka et al., 2010), double square (Tao & Han, 2006; Zhao & Grzebieta, 2002), and other configurations (Elchalakani et al., 2002; Han et al., 2004). The other typology is known as "double tube", in which the concrete ring between the tubes and the inner part of the section (inside the second tube) are filled with concrete. Most of the work on these columns has been performed in double circular configurations, and some authors have studied the introduction of ultra-high strength to enhance the mechanical properties of the sections (Ibañez et al., 2017; Liew & Xiong, 2010; Romero et al., 2017).

Another category of composite section is constructed around an inner CFST section surrounded by reinforced concrete (see Figure 1.1b), similar to the well-known steel-reinforced concrete (SRC) member. The inner tube provides confinement to the embedded concrete, enhancing its load-bearing capacity, while the steel tube is thermally protected by the outer concrete zone (Han et al., 2009; Han & An, 2014).

While less common, another proposal is the concrete-filled steel tubular columns with a solid steel core. The section consists of a regular CFST section with a massive section of steel embedded in the centre of the column, which significantly enhances the load-bearing capacity of the column (Hanswille & Lippes, 2008). The mechanical behaviour of this typology has been tested under fire conditions proving that, as the inner steel is protected by the other elements of the section, the fire resistance enhancement when compared to CFST sections is considerable (Espinos et al., 2016; Neuenschwander et al., 2010, 2013; Schaumann & Kleibömer, 2015).

In line with these last proposals, an alternative consisting of embedding a different steel profile emerged from the literature (see Figure 1.1c). The solution consists of embedding an open steel profile within the concrete infill of the CFST section (Wang et al., 2003), generating the so-called steel-reinforced concrete-filled steel tubular (SR-CFST) section (see Figure 1.2). The contribution to the column resistance is the combined strengths of the embedded steel profile, the surrounding concrete, and the steel outer tube, providing a significant improvement to the load-bearing capacity and ductility of the column (Cai et al., 2015; Ding et al., 2017; He et al., 2010; Wang et al., 2004). Furthermore, the inner steel profile becomes thermally protected by the surrounding concrete and therefore, its degradation at high temperatures is delayed, resisting the applied load during a longer period, thus enhancing the fire resistance of the column (Dotreppe et al., 2010; Chu et al., 2016; Espinos et al., 2016).

a)   b)
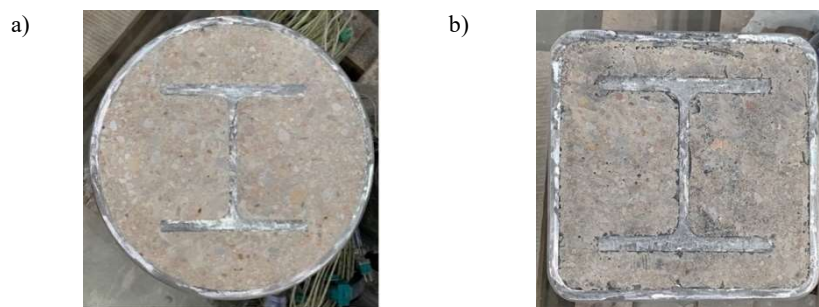
Figure 1.2   SR-CFST sections: a) circular; b) square.

Even though the available studies point out that the advantages of SR-CFST columns are notable in both standard and high-temperature conditions, at present, there are no specific design guidelines and calculation methods applicable to these sections. Therefore, the present thesis focuses on SR-CFST sections and their behaviour under fire conditions with the aim of expanding the study of these innovative composite sections and providing insightful knowledge about their thermal and mechanical performance.

1.1.1. Practical applications

Since the 70s, composite sections, such as CFST, have been increasingly used in modern construction for high-rise and super high-rise buildings, bridges, electricity poles, industrial structures, or subway infrastructure (Zhao et al., 2010) due to their constructive advantages and good performance under different actions.

A vast majority of buildings with composite columns can be found in China where this typology has been used widely in the last three decades. A great number of high-rise buildings and skyscrapers have been built using CFST sections such as the SEG Plaza in Shenzhen, the tallest building in China erected with these sections. The building is 76 floors tall with four basements and a total height of 361 meters. Huge columns with diameters between 900 mm and 1600 mm were used and its steel tube was shipped mounted in lengths corresponding to three stories. This procedure allowed to simultaneously build the deck floors while filling the columns with concrete, which accelerated the construction proving to be a significantly efficient method. (Han et al., 2014; Zhong & Zhang, 1999). The trend continued during the 2000's, with buildings like the Wuhan International Securities Building in Wuhan being constructed in 2008 (Han & Yang, 2007) or the Canton Tower in Guangzhou finished the next year (Han et al., 2014) using CFST sections as a primary load-bearing element.

The CFST also have been vastly used in the construction of arch bridges in China offering significant benefits in the building process because the outer tubes can serve as stiffened skeletons to sustain their own weight in the construction process and do not need additional formwork, which makes it a versatile and adaptable construction method. Up to the present time, more than 400 CFST arch bridges have been built in China and they hold several records with the Zangmu Yarlung Tsangpo River Bridge (Lhasa–Nyingchi Railway) and the Hejiang Yangtze River Bridge being the highest and longest CFST arch bridges in the world, respectively (Zheng & Wang, 2018; Zhou & Zhu, 1997). According to Chen and Wang (2009), there are five main types of CFST bridges, depending on their erection method and geometric parameters: the deck true arch, half-though true arch, through deck-stiffened arch, through rigid-frame tied arch and fly bird type arch. The first CFST bridge constructed in the country, a through deck-stiffened arch type, was the Wangchang Bridge, finished in 1990. Among the vast number of CFST bridges found in China, it is worth mentioning the Wushan Yangtze River Bridge, the longest CFST arch bridge in the world and an example of the half-though true arch typology.

The use of these composite sections in the Asian country has not only been reserved for large buildings and bridges but also has been introduced in the construction of subway infrastructure like the Jiangmen subway station and the transportation centre in Tianjin, or in long-span transmission towers (Han et al., 2014).

As CFST columns have proven their efficacy under earthquake conditions, these sections have been broadly used in Japan. One of the first documented examples of CFST columns used in this country is the Mitsui Soko Hakozaki Building, finished in 1989 in Tokyo, a 19-story building in whose structural frame was supported by prefabricated CFST columns (Twilt et al., 1996). The Nakanoshima Festival tower in Osaka (Okada et al., 2014) and the Toranimon Hills in Tokyo (Karasaki et al., 2015) are more modern examples in which square and circular CFST sections were used for the core of the building with significantly large dimensions. The mentioned composite sections were also used in civil infrastructure, as in the case of the Techno Station in Tokyo, whose main columns were designed as circular CFST sections with high-strength steel tubes (780 MPa) filled with ultra-high-strength concrete (160 MPa). This approach permitted a significant reduction in the diameters of the columns allowing for more usable space in the building (Endo et al., 2011).

Other countries in Asia and Oceania, have also observed the advantages of composite structures and adopted them in their projects. Some examples would be the Riverside Office Building in Australia, with huge concrete-filled reinforced CHS sections of diameters up to 600 mm (Twilt et al., 1996), the Lotter World Tower in Korea or the Taipei 101 in Taiwan (Liew et al., 2021).

Canada and the United States also led the construction of buildings with concrete-filled steel tubular columns. In Seattle, the Two Union Square (Samarakkody et al., 2017) and the Museum of Flight at Kink County Airport are good examples of the use of CFST members to archive the required fire protection and reduce the space occupied by the columns. The St. Thomas Elementary School in Hamilton, Ontario, is another instance of civil infrastructure in the EEUU fabricated with composite sections, specifically circular hollow sections (CHS) filled with concrete mixtures of different strengths (Kodur & Mackinnon, 2000).

Europe has not been left behind in this matter, as recently numerous buildings have been erected using this typology (Twilt et al., 1996). In the UK, the Rockdale Bus Station was built using SHS columns 150 mm wide and 3.3 m tall, filled with steel fibre reinforced concrete (SFRC). The Darlington Memorial Hospital is also an example on the island as rectangular hollow sections (RHS) filled with concrete were used in the internal columns of the 8 and 9-story developments of the building. In France, a wide range of concrete-filled square hollow sections (SHS) columns of 250 mm in width were used to construct the Microsoft Head Office in Villebon-sur-Yvette. In the construction of the Technocent Building in Oulu, Finland, both circular (CHS) and square (SHS) steel sections were used as load-bearing members, which were filled with concrete and reinforced with steel bars.

More recently, Liew and Xiong (2021) pointed towards a new trend in composite construction: the use of high-strength materials for the steel and concrete used in these sections. In their work, they presented several examples from around the globe where these materials are being used in composite sections. In China, buildings like the Guangzhou West Tower (2010) or the Goldin 117 Tower (2022) of 432 m and 597 m in height, respectively, are cases that prove the use of high-strength steel and concrete CFST columns in high-rise skyscrapers. Similar examples of the use of CFST sections with high-performance materials can be found in Japan with the W-Comfort Towers and the Obatashi Tech Research Institute in Tokyo or the highest skyscraper in the country, the Abeno Harukas erected in Osaka.

It is worth mentioning the abundance of buildings constructed with composite sections and high-strength materials in Singapore, lately. A vast number of buildings have been constructed using CFST sections, i.e., the Robinson Tower (2019), the New Afro-Asia i-Mark building (2020) or the integrated development project at 88 Market Street (2021); and with concrete encased sections (CES), i.e., the Outram Community Hospitals (2019) or the National Cancer Center (2020).

Even though SR-CFST sections are relatively new and still have not been included in the design codes, several constructions have already implemented them in constructive projects. The Haiyi Hotel in Jiangmen is a great example, among some other public buildings in China that have adopted SR-CFST columns as the main load-bearing structural members (Zhou et al., 2014).

This typology has also been introduced in Europe, i.e., in the Millennium Tower in Wien, a fifty-storey building, 202 m high with CFST columns built with CHS tubes with an outer steel of grade S355 and concrete C40 and C60 as infill. The internal columns were embedded with H profiles to increase their load-bearing capacity. The Amsterdam Mees Lease Building is also an example of an SR-CFST application in which HEA profiles were embedded in CHS columns of 323 mm in diameter (Twilt et al., 1996).

1.1.2. Advantages of SR-CFST columns

SR-CFST columns emerge from a modification of conventional CFST columns to improve their mechanical performance, and their use is expanding as these characteristics are acknowledged by designers and engineers. The interaction between the different components of SR-CFST columns provide many advantages to these sections, several of them included hereafter:

- The combined effect of the steel tube, inner concrete, and steel embedded profile provide the columns with a high load-bearing capacity, stiffness, and ductility even with smaller sections as compared to CFST. The inner profile greatly contributes to enhancing the mechanical capacities of the column without increasing the total cross-sectional area.

- As in CFST sections, the external tube confines the inner concrete, boosting its load-bearing capacity (in circular sections). Additionally, the tube physically protects the concrete from disaggregating when it reaches its maximum load while the inner concrete protects the outer tube from inward local buckling. Consequently, both elements take advantage of this configuration to increase their mechanical performance.

- Even though CFST sections have a good energy absorption property, SR-CFST further improve this property in impact tests or earthquake situations.

- SR-CFST columns require no formwork as the outer tube serves both as a mechanical element of the column and an "in situ" formwork. Therefore, the concrete casting times are reduced an so the construction costs.

- By embedding the steel profile, it is possible to obtain smaller sections that resist the same design load, therefore reducing the overall carbon footprint in the construction process. Moreover, the reduced section allows a higher net usable floor area in construction leading to more open and pleasant spaces. The reduction in the section also leads to a reduction in the painting and corrosion protection of the elements, further reducing the material consumption.

- Finally, one of the main improvements of SR-CFST columns is the fire performance. As the inner embedded profile is thermally protected by the outer tube and the surrounding concrete, the section maintains its load-bearing capacity for longer periods while exposed to fir without any additional protection. Furthermore, as the outer tube expands (due to the high temperatures) an air gap is formed between this element and the concrete core, which delays even more the heating of the section.

1.2. FIRE BEHAVIOUR OF SR-CFST COLUMNS

Depending on the length-outer dimension ratio (*L/D* or *L/B*), columns loaded in compression behave differently. Shorter columns (lower *L/D* ratios) performance is mainly due to the strength of the cross-section while longer columns (higher *L/D* ratios) are governed by stability. The failure of shorter or stub sections is due to the reach of the ultimate capacities of the materials that are part of it, i.e., the yield of steel or crushing of concrete. In contrast, longer or slender columns usually fail to elastic or inelastic column buckling (Chu, 2009).

While the room temperature properties of SR-CFST columns have been studied by several authors in recent years (Cai et al., 2015; Ding et al., 2017; Zhao, 2020; Zheng et al., 2013), the fire performance of these sections is still under investigation. Therefore, the following section aims to expose the mechanisms that influence the behaviour of SR-CFST when exposed to high-temperature conditions and the physical principles that are at play.

In CFST sections, the inner concrete filling enhances the fire performance of the column with a double effect: on one hand, the concrete slows the heating of the section, due to its lower thermal conductivity, and on the other, its mechanical contribution helps sustain the load and avoids the inward local buckling of the steel tube (Espinós, 2012). By adding an open steel profile section in the concrete core, the load-bearing capacities of the column and fire resistance are significantly boosted as the inner profile is thermally protected by the other elements of the cross-section (Espinos et al., 2016).

Recent investigations have reached similar conclusions: the fire resistance of SR-CFST columns has been proven to be significantly better than regular CFST columns under the same conditions (Meng et al., 2021). The inner profile plays a significant role in this enhancement and affects the failure mode and behaviour of the rest of the components. While in conventional CFST sections, in the final stages of the fire exposure, the inner concrete crashes and fails, the inner profile embedded inside provides an additional confinement to the inner concrete and prevents the apparition of cracks (Mao et al., 2021).

Regarding the thermal behaviour of SR-CFST columns, another important consideration is the concrete moisture content. As in CFST sections, the moisture content of the concrete infill in SR-CFST sections directly impacts their fire performance: higher moisture content implies slower heat transferring along the cross-section of the column. When heated, the water content within these sections evaporates, absorbing a great amount of heat energy in the process, and thus delaying the heating of the section. From the construction point of view, a series of ventilation holes must be made in the ends of the columns (at least 20 mm in diameter) to allow the release of this vapor and avoid a rise in the internal pressure of the column (Kodur & Mackinnon, 2000; Twilt et al., 1996).

Figure 1.3 shows the load distribution percentage for each element of an SR-CFST stub column under axial compression in fire. In the first steps of a fire scenario, an SR-CFST section behaves similarly to a CFST section: the steel tube expands faster than the other two elements, bearing most of the applied load in this period. The concrete has a lower expansion coefficient, and the steel profile, as it is embedded within, is prevented from expanding as the outer tube. As the expansion happens also transversally, an air gap is formed in the interface between the concrete outer wall and the inner part of the steel tube. This phenomenon, together with the more favourable thermal properties of concrete, reduce the heat diffusion into the section. Once a certain fire exposure time has been reached, the steel tube starts to lose its mechanical properties due to the higher temperatures therefore receding its elongation and transferring part of the load to the concrete core and inner steel profile. The inner parts of the column bear the applied load as they expand, due the heat diffusion to the inner parts of the column, generating a "second expansion" phase.

As temperature increases, the mechanical capacities of the elements are slowly degraded. While in CFST the loss of mechanical properties of the concrete core led to the failure of the column, SR-CFST columns have a considerably longer failure time, as the inner profile is thermally protected by the concrete and remains unaffected by the thermal degradation for longer. Finally, once the inner profile loses part of its strength, the column cannot hold the load and fails due to global buckling (slender columns) or sectional failure (stub columns).
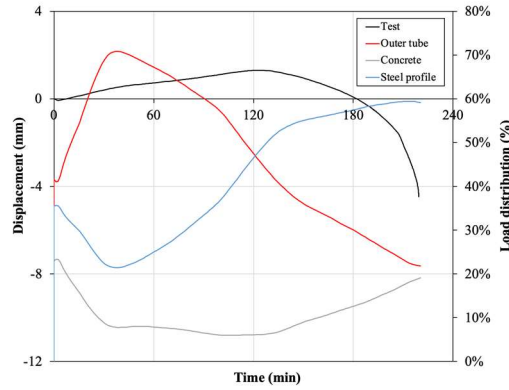
Figure 1.3   Load distribution in the different elements of an SR-CFST section.

The general evolution of an SR-CFST stub column and slender column is included in Figure 1.4, represented in terms of axial displacement of the top of the column versus the fire exposure time. As can be seen, a more abrupt failure occurs in slender columns (see Figure 1.4b) in contrast to the slower descent of stub columns (see Figure 1.4a). This is due to the different failure modes: stub columns have a sectional failure in which the column slowly loses capacity over time and eventually fails upon steel yielding and/or concrete crushing, in contrast to slender SR-CFST columns, which fail by global buckling (i.e. instability).
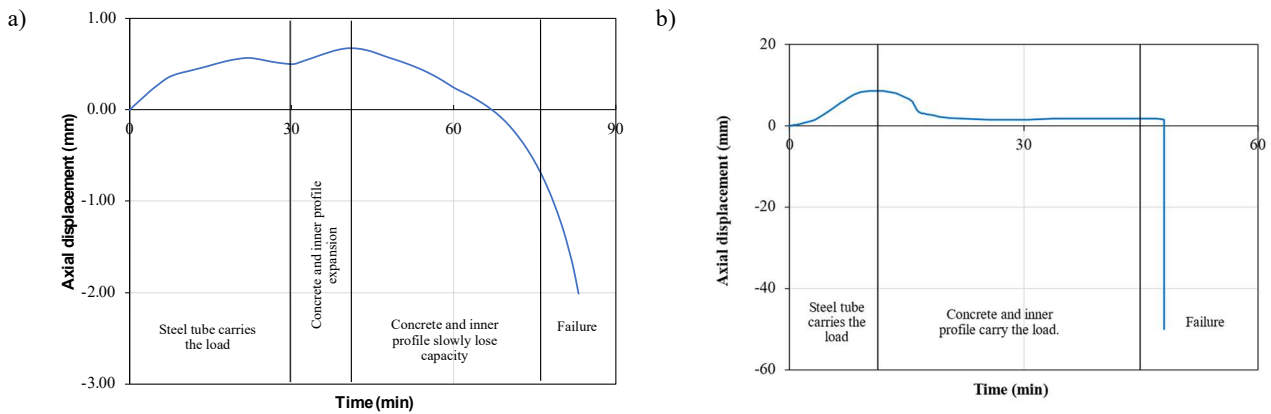
Figure 1.4   Evolution of a) stub and b) slender SR-CFST columns under fire exposure.

2.

STATE OF THE ART

This chapter presents the available literature regarding the fire behaviour of SR-CFST columns. A general overview is first given, and the main numerical and experimental investigations are thoroughly revised and described, to understand the present state of the research on this topic. Lastly, the available calculation methods for predicting the fire resistance of these composite columns and similar typologies are reviewed.

2.1. GENERAL

While a vast extent of investigations in concrete-filled steel tubular sections with several geometries (circular, square, rectangular, elliptical…) can be found in the literature, the novel SR-CFST sections still lack sufficient research to predict their thermal and mechanical behaviour adequately. Research studies become even more scarce when considering their behaviour at high temperatures.

Although numerous authors have provided the analytical resolution of transient heat conduction in composite columns, most research is focused on CFST sections. One of the first works that tackled this matter is the one by Lie (1984), who provided a method to calculate the temperature field in the inner concrete core and steel tube by dividing the area of the section into multiple layers in circular CFST columns (Lie, 1994; Lie & Chabot, 1990) or elements, in rectangular CFST columns (Lie & Irwin, 1995). Several investigations applied and extended their previously proposed Rankine resolution method for steel frames (Tang & Tan, 2001) to CFST columns, both unreinforced (Tan & Tang, 2004b) and reinforced (Tan & Tang, 2004a) in fire scenarios. Wang and Tan (2006), on the other hand, analysed the behaviour of concrete-filled CHS columns based on Green's function solution. With this approach they were able to calculate the temperature distribution and heat flux inside of the column and at the steel-concrete interface.

Even though several researchers have developed equations and methods to predict the behaviour of SR-CFST columns at room temperature (Wang et al., 2006; Zhu et al., 2010) and some formulations have tentatively been developed to predict the post-fire behaviour of this typology (Meng et al., 2019; Yang et al., 2020), the available models are still limited. The multiple steel-concrete interfaces and the complex thermal gradient caused by the inner embedded profile have made it difficult to develop analytical solutions and led authors to develop numerical methods to address this difficulty.

The work of Espinós et al. (2016) is one of the first numerical studies to introduce and study the behaviour of SR-CFST columns under fire conditions, among several types of pioneering composite sections proposed to improve the thermo-mechanical response of CFST columns. Since then, several studies on the fire response of SR-CFST sections can be found in the literature for square (Mao et al., 2020; Meng et al., 2020) and circular (Meng et al., 2021) geometries and for the use of different materials in the constituting elements of the section, such as the inclusion of stainless steel in the outer tube (Tan et al., 2019a, 2019b).

The fire behaviour of SR-CFST columns has limited experimental investigations due to the novelty of these sections and the elevated associated costs of these tests. One of the first thermo-mechanical experimental tests in this field was conducted by Dotreppe et al. (2010) at the University of Liege. Since then, a great number of tests have been conducted at different universities in China, both at the Shanghai University for Science and Technology (Meng et al., 2020, 2022; Zhu et al., 2016) and at the Southeast University (Mao et al., 2021, 2022, 2023). In the field of fire investigations, studies on the post-fire behaviour of SR-CFST stub columns have become available in recent years. While a few square stub specimens were tested by Meng (2019) in different heating conditions, Yang et al. (2020) performed an extensive experimental campaign on similar specimens that studied the influence of several geometrical and mechanical parameters. A short experimental campaign of longer specimens was carried out at the Shanghai University for Science and Technology (Sun, 2023). The most recent work on this topic comes from the investigation of Wang et al. (2024) at the Huaqiao University.

This chapter provides an extensive revision of the state of the art on SR-CFST columns subjected to fire conditions. The main numerical and experimental investigations of this topic are included as well as the available calculation models. As this column typology is relatively novel and most of the design

guidance and available literature do not include a specific methodology for their evaluation, a review of potentially applicable methods used for other steel-concrete composite sections is included.

2.2. NUMERICAL MODELS

One of the first appearances of SR-CFST sections in numerical investigations can be found in the work of Espinós et al. (2016), where the fire response of different types of innovative steel-concrete composite columns was analysed, and strategies for enhancing the fire resistance of traditional CFST columns by using inner steel profiles were proposed. The authors found that dividing the outer steel tube area of a CFST section and including the most amount of steel in the inner part of the section significantly augmented the fire resistance by thermally protecting the steel and slowing its degradation. Additionally, it was discovered that the performance of the SR-CFST section could be further improved by using high-strength steel at the embedded inner profile.

Tan et al. (2019a, 2019b) developed a numerical model for composite SR-CFST circular and square cross-sections using stainless steel in the outer tube (also called SR-CFSST). The model was validated with experimental data from CFST experiments with stainless steel in the outer tube (CFSST) and SR-CFST experiments from Dotreppe et al. (2010) and Zhu (2016). Afterwards, parametric studies were performed to analyze and improve the fire performance of the SR-CFST studied sections and quantify the increase in fire performance between sections with and embedded inner steel profile compared to the reference CFST section. Two series were proposed: Series 1, in which the same area of steel was divided between the outer steel tube and the inner profile, and Series 2, in which all the columns had the same axial load-bearing capacity at room temperature. The simulated SR-CFSST columns demonstrated an improved fire resistance compared to their CFST and CFSST counterparts with the same cross-sectional area (Series 1) or load-bearing capacity (Series 2).

More recently, square SR-CFST under fire conditions were studied numerically by Mao et al. (2020) to assess the influence of several column parameters such as the slenderness, the steel ratio between the outer tube and inner profile or the concrete and steel strength. The numerical model was then validated with an experimental campaign performed at the Shanghai University for Science and Technology (Zhu et al., 2016). Parametric studies were conducted to study the influence of the slender ratio, concrete and steel strength, and the total steel area distribution on fire performance. It was found that the proportions of steel used at the outer steel and inner profile significantly impacts the fire resistance of SR-CFST columns. The potential of using high-strength steel at the inner embedded profile for enhancing fire resistance was suggested by the authors, which was aligned with the conclusions obtained by Espinós et al. (2016).

One of the most recent numerical evaluations on SR-CFST sections can be found in the works of Meng et al. for both square (2020) and circular geometries (2021). A finite element model was developed to simulate the behaviour of SR-CFST columns subjected to non-uniform fire conditions and was validated against the experiments of Zhu et al. (2016). The finite element mesh and initial geometric imperfection were modelled based on the suggestions of Espinós et al. (2010) for CFST columns, while the outer tube was modelled using S4R shell elements. The outer steel tube and inner concrete interface were modelled via a constant value of 200 W/m^{2}K for the gap conductance. Good agreement was found between the developed model and the experiments. Within these studies, a series of parametric studies were conducted to evaluate the applicability and accuracy of the existing fire design method of CFST columns to SR-CFST columns, as at that moment, there was no specific method in the literature or normative that covered these sections. The fire design approach proposed by Albero et al. (2016) – currently used in Europe in the new version of EN1994-1-2: prEN1994-1-2 (CEN, 2021) – was applied to SR-CFST columns exposed to 4-sides while the reduction method proposed by Yang et al. (2013) was applied to 3-sided exposed specimens.

It is worth noting that the tested specimens were beyond the application scope of the method from Annex H (i.e., reinforcement ratio and slenderness), and the inner steel section was assumed to be a reinforcement in a CFST section. The research concluded that further research is needed to provide accurate predictions for different load eccentricities and fire exposure conditions (i.e., non-uniform fire). While the steel tube was found to have some contribution to the performance of the column, the steel section was the critical factor regarding the load-bearing capacity of the column under fire conditions.

2.3. EXPERIMENTAL INVESTIGATIONS

Regarding the existing experimental investigations on SR-CFST composite columns, various tests have been conducted on the mechanical performance of these sections in the last two decades. The first experimental campaign regarding axially loaded SR-CFST columns is the work performed by Wang et al. (2004) where after a review of several innovative ways to enhance the fire resistance of CFST columns, the SR-CFST typology was proposed to unify the advancement of concrete-encased and CFST columns.

The axial compression bearing capacity of SR-CFST sections at room temperature has been deeply studied by several authors under concentric (Chen et al., 2022; Ding et al., 2017; Ma et al., 2019; Zhu et al., 2010) and eccentric loads (Zhao, 2020), finding several advantages in this innovative section arrangement. The performance of square-shaped SR-CFST sections under biaxially eccentric compression was tested by Li et al. (2020), showing a significant improvement compared to regular CFST sections. Some experiments on the behaviour of circular SR-CFST sections under lateral shear load were conducted by Shi et al. (2019), and later, the dynamic response to lateral impact load was studied by the same research group (Xian et al., 2020). Lately, other authors analysed the performance of SR-CFST sections under long-term loading and preload on the steel tube (Wang et al., 2023).

As has been exposed, the mechanical behaviour of SR-CFST sections has been thoughtfully analysed. Even though extensive work has been conducted on the fire behaviour of composite columns, such as CFST columns (Espinos et al., 2015), few of these investigations have considered the SR-CFST columns due to their novelty. Consequently, a compilation of the different available fire tests performed on SR-CFST columns is included hereafter, regarding both post-fire mechanical tests and coupled thermo-mechanical experiments.

2.3.1. Post-fire experimental investigations

While the advantages of SR-CFST sections may result appealing to the research community, the investigations on their fire and post-fire structural response are rather limited, particularly those that examine the post-heating behaviour. More evidence is needed in the performance of SR-CFST sections after a fire scenario to accurately predict the residual capacity of this typology and to determine the main parameters that influence its post-fire behaviour.

The research conducted by Meng et al. (2019) is one of the first experimental studies that appear on the post-fire behaviour of SR-CFST columns. Three square SR-CFST stub columns of 600 mm in length were tested in uniform and non-uniform heating conditions (4-sided, 3-sided, and 2-sided). The square section had an outer dimension of 300 × 300 × 6 mm, and the embedded section was a HW 150 × 150 × 7 × 10 mm in all the specimens. The concrete infill had a compressive strength of 47.2 MPa after 28 days and both the outer steel tube and the inner profile had a nominal yield strength of 368 MPa. The sections were heated inside a small mobile electric furnace for 300 minutes, the estimated temperature by the authors for the inner steel to reach 400 ºC. Afterwards, the columns were let to cool off until ambient temperature was reached and then were loaded incrementally until failure. As expected, a significant reduction of the mechanical capacity of SR-CFST in the post-fire situation was found with the protected columns

performing better than the unprotected. The high ductility of the columns was addressed in the study, and equations to predict the residual capacity of these columns in post-fire situations were proposed based on parametric studies.

Yang et al.(2020) conducted an extensive experimental campaign on 135 SR-CFST stub columns of 600 mm in length. The columns were designed to have the same outer steel SHS section of 200 × 200 mm with thicknesses between 2.94 mm and 4.78 mm. Three different sizes of open-section steel profiles were embedded inside the columns: 100 × 68 × 4.5 × 7.6 mm, 100 × 100 × 6 × 8 mm and 125 × 125 × 6.5 × 9 mm. Both the steel tube and the embedded profile were made of Q235A steel, while for the concrete core different mixtures with nominal strengths of C20, C30 and C40 were used. In this research, 108 specimens were heated to certain heating times (between 30 min up to 130 min) while the rest served as a control group and reference. The tests were heated up to the specified time, and then cooled until ambient temperature. Next, axial compression tests were performed until the columns reached failure. The authors found that the inner steel section ratio was the most influential parameter in the post-peak behaviour of the columns while the maximum temperature had the greatest effect on the residual bearing capacity. It must be noted that, despite the high number of tests, the variation was narrow, as all the tests had the same external dimensions and similar outer tube thickness, and only three types of embedded sections were tested.

More recently, a short experimental campaign was conducted at the Fengxian Campus of Shanghai Normal University consisting of two SR-CFST square columns of 1800 mm in length (Sun, 2023). The specimens had an outer SHS section of 300 × 300 × 6 mm and an HW 150 × 150 × 7 × 10 mm embedded steel section. The inner concrete infill had an estimated compressive strength of 55 MPa and the outer tube and inner steel yield strength were obtained by the characteristic coupon tests and were approximately 360 MPa and 345 MPa, respectively. This investigation is one of the few amongst the available literature in which the columns were heated with an applied load (40% of the room temperature capacity). The columns were heated in an electric furnace with non-uniform conditions (2-sided and 1-sided heating) for 240 min. Then, the initial load was released, and the specimens were left to cool off for two days. The columns were then axially loaded until failure. Amongst the conclusions, the author find that the non-uniformity of the heating had a great impact on the temperature distribution and the residual capacity of the column. Additionally, the design method proposed by Meng et al. (2019) was tested and provided a reasonable agreement with the tests.

One of the most contemporary experimental studies on SR-CFST columns in a post-fire scenario is the one performed at Huaqiao University (Wang et al., 2023). A total of 18 thin-walled SR-CFST stub circular columns of 630 mm in length were tested. The columns had an outer steel section of 210 × 1.5 mm and an embedded H-shaped steel section of 125 × 125 × 6.5 × 9 mm. The columns had two different mixtures of concrete (C30 and C60), and the steel yield strength for the outer tube and inner steel profile were approximately 320 MPa and 260 MPa, respectively. 12 of the columns were heated in a large gas furnace for up to 45 or 90 min, and the rest of the columns were tested unheated to serve as a reference. Once the columns were at room temperature after the thermal test, increasing axial load was applied until failure. This research evidenced the high ductility of SR-CFST columns in the post-fire scenario and found that the ratio of inner steel had a positive effect on the residual strength and stiffness of the columns.

The most recent experimental available campaign by the previously commented research group (Wang et al., 2024) consisted of six SR-CFST columns, three circular and three-square sections, with embedded cruciform steel profiles, were tested under axial loading and temperature. The embedded steel sections had dimensions of 160 × 90 × 5 × 8 mm and 140 × 70 × 5 × 8 mm for the square and circular sections, respectively. The concrete used as an infill was C50 and C70, depending on the specimen, while the steel for the outer tube was of grade S355 and the one used for the inner steel profile was of grade S275.

The heating times ranged between 25 to 40 minutes, and the columns were loaded during the high-temperature tests at load levels between 0.4 and 0.5. After the fire tests, the columns were loaded increasingly until failure. The study highlighted the important effect of the initial loading on the post-fire performance of the columns.

This literature analysis confirms the fact that the number of available post-fire test results on SR-CFST columns is still scarce and needs to be expanded and thoughtfully analysed before any conclusions are drawn about the behaviour of these composite sections after being exposed to fire conditions.

2.3.2. Thermo-mechanical experimental investigations

Considering the novelty of SR-CFST sections it is comprehensible that the number of available experimental investigations is still scarce. Regardless, the increased popularity of composite construction is leading to constant technological and scientific advancements in this field of research.

One of the first works to be published on the thermal behaviour of SR-CFST columns was experimental investigation of the tests conducted at the Fire Engineering Laboratory University of Liege (Dotreppe et al., 2010). The experimental program consisted of ten columns with circular and square shapes and five different configurations were used for the cross-sections, in which two were SR-CFST sections with an embedded HEB120 profile. The sectional dimensions of the tested SR-CFST columns were $\varnothing$219.1 mm for the circular specimens and #200 mm for the square ones, and the columns had a total length of 3310 mm. They were tested at a load level of 0.4 and the fire resistance times ranged from 39 up to 79 minutes, thanks to the application of intumescent painting to some of the tested specimens.

Another set of ten columns were tested under axial compression and ISO-834 standard fire conditions at the Shanghai University for Science and Technology, eight of which were SR-CFST specimens (Meng et al., 2021; Meng et al., 2020; Zhu et al., 2016). The investigation proved that the inclusion of an inner steel profile significantly boosted the fire performance of the columns, exceeding 240 minutes in some tests. The outer dimensions of the columns were $\varnothing$300 mm and #300 mm for circular and square specimens, respectively and had a total length of 1800 mm although only 1200 mm were heated. The embedded steel profile was an open steel HW150 section with dimensions $150 \times 150 \times 7 \times 10$ mm. The columns were tested under load levels of 0.3 and 0.4 and subjected to uniform and non-uniform heating. The research proved that the SR-CFST sections significantly improve the fire resistance of the column as compared to CFST sections.

An extensive experimental campaign was conducted at the facilities of Southeast University, China (Mao et al., 2021, 2022, 2023). A total of twenty SR-CFST columns were tested at elevated temperatures with circular and square outer shapes with cruciform embedded sections with a total length of 3810 mm. The outer dimension of the circular outer tubes was $\varnothing$325 mm while for the square tubes it was #300 mm. The embedded steel sections had dimensions of $140 \times 70 \times 5 \times 8$ mm and $160 \times 90 \times 5 \times 8$ mm for the circular and square sections, respectively, and the concrete used as infill was C50 and C70, depending on the specimen. The columns were tested at a wide range of load levels (from 0.39 up to 0.8) and with two different eccentricity values (0,50 mm and 80 mm). Four of them were protected with a thick fire-resistive coating (with thicknesses between 12 mm and 17 mm) whereas four were tested with non-uniform heating (3-sided, 2 sided-adjacent, 2-sided-opposite, and 1-sided). The fire resistance times of the specimens varied between 14 min up to 103 min for the protected specimens. The authors found out that the eccentricity, the load ratio, and the fire exposure conditions significantly affected the fire performance of SR-CFST sections. The inclusion of the embedded profile improved the fire behaviour of the columns in all scenarios as compared to regular CFST columns.

2.4. AVAILABLE CALCULATION METHODS

The increase in the use of steel-concrete composite structures and the numerous experimental and numerical investigations on the topic have pushed the inclusion of design guidelines in international codes regarding this typology of sections. Even though some typologies like the CFST sections or the concrete encased sections (CES) have been included in these codes, the SR-CFST has yet to be incorporated, possibly due to its novelty and lack of sufficient experimental evidence. Therefore, in this section a review of the existing design guidance for composite CFST columns is provided, given their similarities to the SR-CFST sections studied in this thesis.

In the European steel-concrete composite structures normative (CEN, 2005c), there are several design procedures included for composite columns design: tabulated data and simple and advanced calculation models. The first approach is rather simple and provides design tables for composite columns made of partially or totally encased steel sections and concrete-filled hollow sections with reinforcing bars. The second option, simple calculation methods, are the most broadly utilized among the fire design of structures and can be used in the same typologies as the previous one. A specific method is provided in Annex H of the same code for composite unprotected concrete filled hollow sections. Advanced calculation procedures can be applied in the design of composite columns and can be applied to any type of cross-section as per Clause 4.4 of EN1994-1-2 (CEN, 2005c) with the specific thermal and mechanical particularities of the calculated column. This approach can provide a more precise estimation of the behaviour of the system, considering a wide range of variables, as compared to the other two more conservative design methodologies. It is worth mentioning at this point that the research group at the Polytechnic University of Valencia (Albero et al., 2016) proposed an innovative design procedure for the fire behaviour of CFST columns that has been approved by the Technical Committee CEN/TC250/SC4 (CEN, 2017) to be included in the new version of EN1994-1-2: prEN1994-1-2 (CEN, 2021) as a replacement of the current Annex H. The temperature distribution for the composite section is obtained in this method by three equivalent temperatures for each part of the column: steel tube, concrete core, and reinforcement bars.

In Australia and New Zealand, the AS/NZS 2327 (Standards Australia & Standards New Zealand, 2014) adopted the proposal by the research group at the Polytechnic University of Valencia (Albero et al., 2016) with a similar approach, based on the three equivalent temperatures. Tabulated data for the design of fully encased steel sections and CFST sections is provided. The simplified method includes equations for the temperature calculation of the steel tube, concrete core, and reinforcement of CFST sections. Finally, a series of requirements are provided if advanced calculation models are used.

The British standard BS5950 Part 8 (BSI, 2003) gives indications for fire resistant design of steel-concrete composite structures. The code provides two approaches to fire resistance: through standard fire tests for all types of members and through calculation using provided design methods. A method for CFST sections is provided to derive the necessary thickness of fire protection material depending on the section factor (A_m/V). For additional information on the design of these sections, the code refers to the Corus Tubes guide (Hicks et al., 2002) and the CIDECT guide (Twilt et al., 1996).

A different approach is taken by Chinese code GB-50936 (Chinese Standards, 2014) for CFST columns exposed to fire. Two calculation methods are provided: one to obtain the load-bearing capacity of the column using an average temperature for the concrete and steel tube, and another to obtain the critical temperature of the cross-section depending on the thickness of the outer steel tube. These methods only consider columns subjected to axial compression.

Similar to the Chinese proposal, the Japanese code (AIJ, 2008) provides a simplified equation that calculates the critical temperature of the outer steel tube, only depending on the heating time of the specimen.

A design equation was proposed by Kodur and co-workers (Kodur, 1999, 2007; Kodur & Mackinnon, 2000) that incorporated the parameters affecting the high-temperature behaviour of CFT columns. Their work has been incorporated into the American Society of Civil Engineers (ASCE, 2003), the Steel Design Guide 19 of the American Institute of Steel Construction, the National Building Code of Canada (CCBFC, 2005) and the American Concrete Institute (ACI, 1989).

Apart from the design codes, several works can be found in the literature to facilitate the calculation of the load-bearing capacity of composite columns in case of fire. Some of the most relevant works are mentioned hereafter in chronological order.

One of the first works focused on predicting the behaviour of CFST columns in fire conditions is the formulation proposed by Kodur (1999) that was derived from parametric studies. This equation calculated the fire resistance time depending on geometrical and mechanical parameters such as the outer dimension of the column, the concrete strength, and the applied load. The formula was then tested against available experimental tests from the literature. Later, Wang and Kodur (1999) developed an approach for evaluating the squash load and rigidity of CFST sections in the fire scenario, inspired by the EN1994-1-2 (CEN, 2005c) normative, through the analysis of the results of a broad parametric study where numerical modelling techniques were used. This proposal was later extended by Wang (2000) to circular fire-protected and unprotected CFST columns.

In the following years, a formulation to determine the fire resistance of circular and square CFST sections was presented by the research group at Fuzhou University (Han et al., 2003a, 2003b; Han & Huo, 2003). Based on the results of experimental tests complemented with parametric studies, they suggested a formula to obtain the fire resistance time and a formula to obtain the thickness of necessary protection to obtain the desired fire resistance.

Tan and Tang from the Nanyang Technological University, Singapore, proposed an extension of their Rankine method for reinforced concrete (RC) columns in fire conditions (2004a) to concrete-filled steel tubular columns (CFST) applicable to both reinforced and not reinforced composite sections (2004b). They provided general recommendations on the fire performance of the studied columns and assessed the accuracy of their method with experimental data from the literature.

At Seoul University, Park et al. (2007, 2008) presented an empirical formula for square CFT columns subjected to axial load. The equation depended on the width of the column, the mechanical properties of the concrete infill and the axial load applied.

Given the inaccuracy found in the method of Annex H in EN1994-1-2 (CEN, 2005c), Espinós (2012) provided a simple method for calculating the fire resistance of unreinforced CFST columns under axial load. Equivalent temperature equations were proposed for the outer steel tube and concrete core of the section to evaluate the plastic resistance and flexural stiffness of the column at elevated temperatures, with which the design value of the fire buckling load of the column can be calculated. The method was later extended to bar-reinforced circular and elliptical CFST sections (Espinos et al., 2013) and its final version (Albero et al., 2016) is now being included in the new version of the Eurocode 4, prEN1994-1-2 (CEN, 2021) as previously commented.

A research group from Wuhan University in China suggested a solution procedure for CFST columns based on Eurocode 4 provisions and a previous formula proposed by the same authors (Yu et al., 2013). The calculation method used an average temperature approach for the outer steel tube and inner concrete and proposed a unified calculation procedure with Eurocode 4, which was validated with numerous experimental data. After several studies and proposals (Yu et al., 2014, 2018a, 2018b) the authors came up with a unified method to obtain the fire resistance of CFST columns under different conditions (protected and unprotected), geometries (circular and polygonal), and mechanical properties (normal strength and high strength) of the steel and concrete (Yu et al., 2022).

A modified Rankine approach based on the one previously proposed for steel columns and frames by Tang and Tan (2001) is proposed in the work of Hu et al. (2015). This approach considers non-uniform distribution in the concrete and includes the effect of the shear bond into Rankine´s formula. Several parametric studies were conducted, and the FE results were compared with the predicted results with the equation obtaining a good agreement between both.

Han (2024) proposed an equation based on a regression analysis of the obtained results from an extensive FEA. The formula is suitable for different eccentricity ratios, normal and high-strength concrete (from 30 MPa up to 90 MPa), and steel grades up to 500 MPa.

Liew and Xiong (2021) proposed a series of recommendations on the fire design of composite sections (CFST and CES) for both normal-strength and high-strength materials. The fire design methods of the European normative, are revised and recommendations are provided, focusing on the use of HSS and HSC in these sections.

Lately, a design equation was proposed to calculate the axial load-bearing capacity under fire conditions of reinforced CFST (RCFST) columns by a research group of the Harbin Institute of Technology, Shenzhen (Shao et al., 2022). The formula considered the difference between strength steel grades and concrete strength of the section (only normal strength materials), proposing a series of material partial factors to calculate the axial compressive strength at high temperatures.

Some authors have proposed formulations that predict the axial load capacity of SR-CFST columns at room temperature. The work performed by Wang (2006) provided a series of equations to predict the mechanical behaviour of circular SR-CFST columns under axial loads for different values of relative slenderness based on previous design methods for CFST sections. This formulation was later extended to square-shaped SR-CFST columns by the same research group (Zhu et al., 2010).

One of the few works available in the prediction of the performance of SR-CFST columns related to fire in the post-fire scenario is a set of formulas proposed by Meng and co-workers (2019) that predicted the residual strength of SR-CFST columns in a post-fire situation with different fire exposures: four-sided, three-sided, and two-sided. The formulation was dependent of the fire duration time, the sectional dimensions, the section steel index, and the confinement index. Instead, the work of Yang et al. (2020) proposed a model that considered a "highly confined" concrete area between the flanges of the embedded steel profile of an SR-CFST section. After proposing a formula for the room temperature ultimate strength of square SR-CFST stub columns, the authors proposed a series of parameters to account for the temperature degradation of the materials after being exposed to fire and cooled off. The parameters included the heating time, the section steel ratio and a confinement coefficient.

By reviewing the existing design guidance for steel-concrete composite columns, it becomes clear that no specific formulation is available for the calculation of the fire performance of SR-CFST sections. Although some authors have tentatively applied the CFST calculation models to SR-CFST sections (Meng et al., 2020b, 2021; Mao et al., 2021, 2022), there is an urge to develop a specific and accurate method for predicting the thermal and mechanical behaviour of these innovative sections in the fire situation. Thus, the present thesis aims to expand the available knowledge in this area and shed light on this topic.

3.

AIM AND SCOPE OF THIS THESIS

In this chapter, the general aim of this investigation is presented, together with the specific objectives. Additionally, the scope and limitations of this thesis are established.

3.1. AIM OF THIS THESIS

This thesis aims to investigate the fire behaviour of axially loaded SR-CFST stub columns. With this aim, numerical and experimental investigations will be carried out to fully understand the behaviour of these types of columns subjected to elevated temperatures.

A numerical finite element model will be developed and validated against the available literature. The influence of relevant geometric parameters and the effect of high-strength materials on the thermal behaviour of the SR-CFST cross-sections will be analysed by means of parametric studies. Regarding the experimental campaign, two phases will be conducted: a first phase that will study the post-fire performance of the columns and a second phase that will evaluate their thermo-mechanical performance.

As shown in the state-of-the-art review, these sections represent an innovation in composite columns, and, therefore, the number of studies concerning their fire behaviour is limited. The main aim of this thesis is therefore to shed light on the thermo-mechanical behaviour of this composite column typology and provide calculation methods and design recommendations for evaluating their load-bearing capacity under fire conditions, which could serve as guidance for future designers and researchers.

3.1.1. Specific objectives

The specific objectives that will be addressed in the present thesis are:

- Review of the available guidance in the literature and design codes to characterise the behaviour of composite cross-sections under the fire action.
- Review of the current experimental and numerical investigations on SR-CFST sections and their behaviour in fire conditions.
- Design and plan an extensive experimental campaign that modifies several parameters of the SR-CFST columns, such as the shape, embedded steel profile and the material properties of the specimens.
- Analysis of the experimentally obtained results.
- Development of a two-dimensional thermal nonlinear finite element model for SR-CFST sections under fire scenarios
- Analysis of the influence of the main geometric characteristics of SR-CFST columns on their behaviour under fire conditions.
- Validation of the numerical two-dimensional model with experimental campaigns of composite cross-sections available in the literature.
- Performance of parametric studies with the two-dimensional model that cover different geometric parameters from commercially available sections to analyse their influence.
- Development of a three-dimensional nonlinear finite element model for SR-CFST columns under fire conditions that adequately represents the performance of these composite cross-sections.
- Validation of the numerical three-dimensional model with experimental results obtained from experimental tests.
- Performance of parametric studies with the three-dimensional model covering different geometric parameters and material properties to study their effect on the column fire performance.
- Development of a simple calculation method for the temperature distribution and plastic resistance of SR-CFST sections in fire that extends the present scope of Eurocode 4 Part 1.2 (CEN, 2005c).

3.2. SCOPE AND LIMITATIONS OF THIS THESIS

The scope of the present thesis is restricted to unprotected SR-CFST columns of square and circular shape subjected to concentric loads. The eccentrically loaded columns will be left out for future investigations. The materials studied in this research will range from normal strength to high strength for both the embedded steel profile and the concrete core of the cross-section.

This thesis will focus on the analysis of short (stub) columns and, therefore, will analyse the cross-sectional plastic resistance of these types of specimens. Slender columns are out of the scope of this thesis.

4.

EXPERIMENTAL PROGRAM

The present section aims to expose the organization and phases of the conducted experimental campaign. The main goals of this campaign are to expand the number of available fire tests in the literature regarding SR-CFST columns and to use them as a validation framework to develop an advanced numerical model to extract relevant conclusions about the behaviour of these composite columns under the fire action.

The experimental campaign is divided into two main phases:

- Phase A: Post-fire stub column tests.
- Phase B: Thermo-mechanical stub column tests.

Even though initially it was not the objective of the research to investigate the post-fire properties of the SR-CFST sections, this phase was considered of interest to be included, due to two reasons: First, it allowed for the testing and calibration of all the equipment and facilities that were going to be used in the subsequent phase (electrical furnace, hydraulic jack, thermocouple data acquisition hardware and software…) individually. These helped to detect anomalies in the furnace performance that were subsequently investigated and solved thanks to this initial phase. Secondly, the extracted thermal results are useful for a better understanding of the temperature fields and distribution of an SR-CFST section, while the mechanical results provide valuable information for future developments in the post-fire design of these sections.

4.1. SPECIMEN PREPARATION

All the column specimens were manufactured at the facilities of ICITECH, Universitat Politècnica de València (Spain). Initially, the inner steel profiles were set in an upright position. Then, a steel plate of $300 \times 300 \times 10$ mm was welded to the bottom end of the steel profiles (Figure 4.1a). The thermocouples were then installed in the middle section of the column as established in the indications provided in ISO 834-11:2014 (ISO, 2014). To both adequately extract the thermocouples and ventilate the water vapour during the heating of the specimens, a hole was drilled at the top end of the steel outer tube (Figure 4.1b and Figure 4.1c). The bottom of the tube was then welded to the plate and the concrete was poured into the column and vibrated with a needle vibrator (Figure 4.1d). To avoid an excessive drying velocity in the process of the concrete curing, a plastic cover was placed on the top of the specimen.

When the concrete was dry, the upper part of the specimen was smoothed to ensure planarity and make sure that all the parts of the composite column contacted the top plate of the column. Then, another plate of the same dimensions as the bottom one was welded to the top end of the column to seal the column and provide good support for the load application (Figure 4.1e).
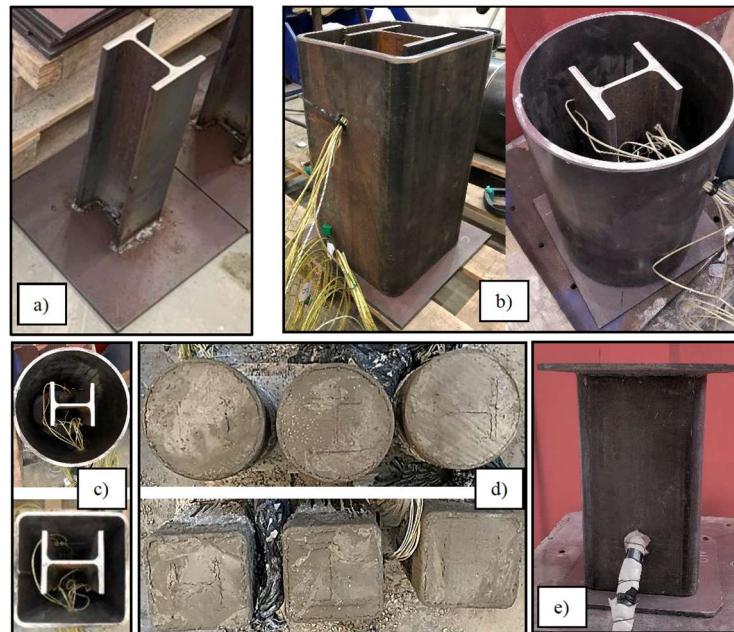
Figure 4.1   Columns preparation: a) Steel plate welded at bottom end of the embedded profile; b) Positioning of hollow steel tube; c) Positioning of thermocouples; d) Columns after casting; e) Column finished

4.2. POST-FIRE STUB COLUMNS TESTS

4.2.1. Test specimens

In this phase, a total of six SR-CFST stub columns were tested in a post-fire scenario: three square-shaped and three circulars (see Figure 4.2). The columns were initially heated until a certain reference temperature and then let them cool off. After the columns had dissipated all the heat, mechanical compression tests were conducted with increasing load until the failure of the columns was achieved.
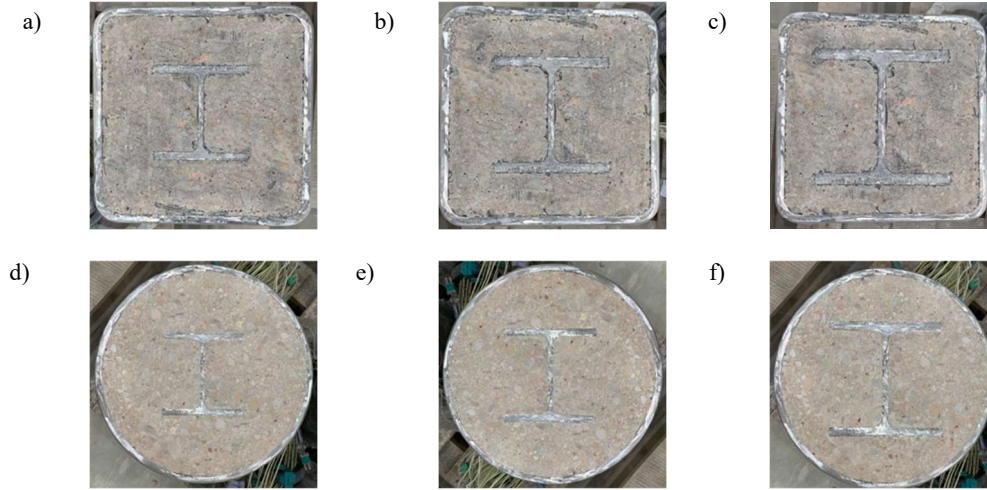
Figure 4.2   Sectional view of the specimens of the post-fire tests: a) SR-CFST-S-T1; b) SR-CFST-C-T1; c) SR-CFST-S-T2; d) SR-CFST-C-T2; a) SR-CFST-S-T3; b) SR-CFST-C-T3.

The selected square and circular tubes had roughly the same cross-sectional area with a maximum difference of 2.51%, for comparison purposes. All three specimens of each series had a different embedded inner steel section ranging from an HEB100 to an HEB140. Table 4.1 summarizes the cross-sectional geometry and mechanical characteristics of all the columns tested in this experimental program, Additionally, it also includes the experimental residual loads tested after being exposed to fire that will be discussed further in chapter 4.2.5.5. The test specimens are named as follows: SR-CFST-X-Ti, where X stands for the outer tube cross-sectional shape (C for circular sections and S for square sections) and i represents the test number, each related to the dimensions of the inner steel profile, where T1 stands for HEB100, T2 for HEB120 and T3 form HEB140. Note that the open steel HEB100 section has the following dimensions: $h = b = 100$ mm ($t_f = 10$ mm, $t_w = 6$ mm); the HEB120: $h = b = 120$ mm ($t_f = 11$ mm, $t_w = 6.5$ mm); and the HEB140: $h = b = 140$ mm ($t_f = 12$ mm, $t_w = 7$ mm). The total length of the specimens was 400 mm.

Table 4.1   List of specimens of the post-fire tests.

Specimen	D/B (mm)	t (mm)	f_{yo} (N/mm²)	f_{uo} (N/mm²)	Inner section	f_{yi} (N/mm²)	f_{ui} (N/mm²)	f_c (N/mm²)	Moist. (%)	$N_{post, exp}$ (kN)
SR-CFST-C-T1	273	10	451	504	HEB100	315	445	24.3	7.952	4799
SR-CFST-C-T2	273	10	451	504	HEB120	308	437	24.3	7.952	>5000
SR-CFST-C-T3	273	10	451	504	HEB140	315	441	24.3	7.952	>5000
SR-CFST-S-T1	220	10	560	680	HEB100	315	445	24.3	7.952	4153
SR-CFST-S-T2	220	10	560	680	HEB120	308	437	24.3	7.952	4615
SR-CFST-S-T3	220	10	560	680	HEB140	315	441	24.3	7.952	4896

Note: D and B are the outer diameter or dimension for circular and square sections respectively; t is the outer steel tube thickness; f_{yo} and f_{yi} are the yield strength of steel for the outer steel tube and inner embedded section respectively; f_{uo} and f_{ui} are the ultimate strength of steel for the outer steel tube and inner embedded section respectively; f_c is the concrete cylinder compressive strength and $N_{post,exp}$ is the experimental residual load after fire.

Steel

The steel tubes used in this experimental campaign were cold-formed welded structural hollow sections as per EN10219 (CEN, 2007) and had a nominal yield strength of S355. The open HEB steel profiles were hot rolled in accordance with EN10025-1 (CEN, 2006) with a nominal yield strength of S275. For both elements, the corresponding coupon tests were performed to obtain the real values of the yield strength (f_{yo} for the outer tube and f_{yi} for the embedded steel profile) and the ultimate strength (f_{uo} for the outer tube and f_{ui} for the embedded steel profile). The obtained values are included in Table 4.1. The modulus of elasticity was taken as 210 GPa as recommended in the European standards.

Concrete

All the specimens of this phase were filled with normal-strength concrete. The mixture was prepared in a planetary mixer and cured in standard conditions for 28 days at the laboratories of the Concrete Science and Technology Institute (ICITECH), Universitat Politècnica de València. Two sets of three samples (cylindrical and cubic shaped) were prepared to obtain the real compressive strength (f_c) and the moisture content of the concrete. The compressive uniaxial strength tests were performed on the cylindrical samples in accordance with EN1992-1-1 (CEN, 2004a), while the moisture content was measured with the cubic ones as stated in ISO 12570:2000 (ISO, 2000) at the beginning of the experimental program. The results of both tests can be found in Table 4.1.

4.2.2. Thermal test set-up

The specimens were heated using a small vertical electric furnace with a power of 10 kW. The furnace consisted of two semicylinders joined by a hinge and had an inner diameter of 400 mm. The electric resistance elements were evenly distributed in parallel layers on the inner refractory wall of the semicylinders throughout their whole length as shown in Figure 4.3.

The furnace temperature was controlled by five thermocouples placed at different levels and positions within the furnace. One thermocouple was placed at the upper part of the furnace, three at the mid-length level, and one at the lower level (refer to detail in Figure 4.3).
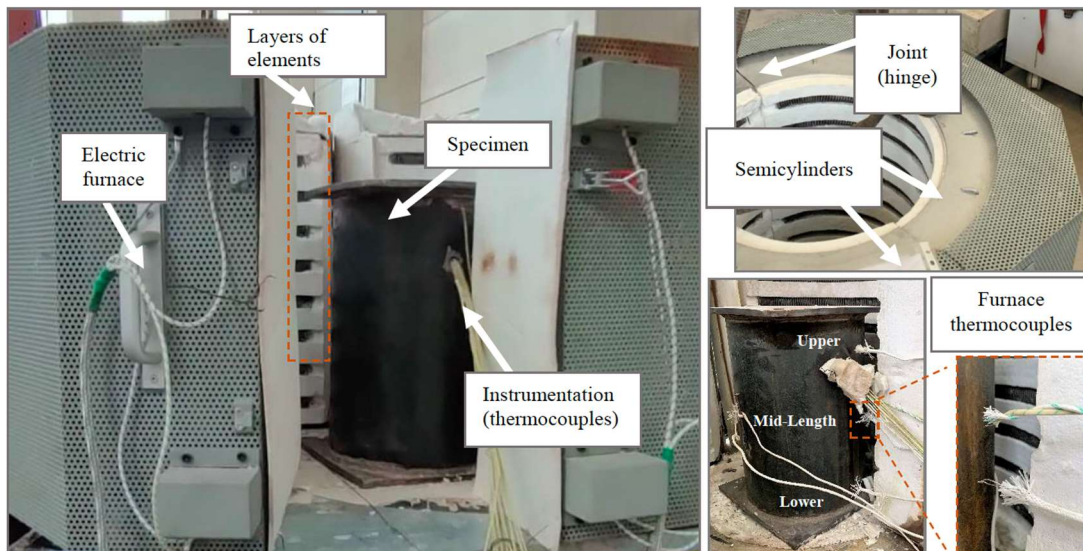
Figure 4.3   Thermal test-set up of the post-fire tests.

For each specimen, their thermal response was recorded using 12 thermocouples placed at specific points of interest at the mid-length cross-section of the column, according to the outline displayed in Figure 4.4. Thermocouples 1 and 6 were welded to the outer surface of the steel tube, while thermocouples 11 and 12 were attached to the inner surface of the tube. Thermocouples 7 to 10 were installed at different points of flanges and web of the embedded HEB, thus documenting the thermal evolution of the inner steel profile. Finally, thermocouples 2 to 5 were embedded in the concrete core, with numbers 2 to 4 placed equidistantly with a separation of 1/6 of the section width, and number 5 placed at 1/4 of the width.
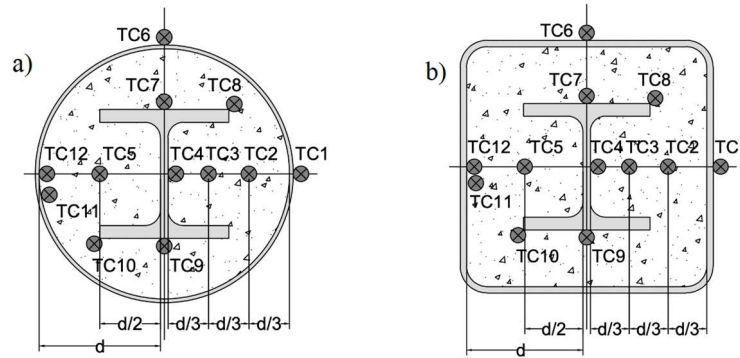
Figure 4.4   Thermocouple layout of the post-fire tests: a) circular sections; b) square sections.

4.2.3. Mechanical test set-up

The set-up for the mechanical tests consisted of a hydraulic jack of 5000 kN of capacity attached to a vertical frame. The boundary conditions of the stub columns in all tests were pinned-fixed (P-F) as they were placed in the testing platform and their bottom end was welded.

The mechanical behaviour of the column was monitored by means of four LVDTs attached to the four sides of the column to record the axial displacement of the top end. Additionally, sets of two strain gauges were installed at the four sides of the column (a total of 8 gauges) in the longitudinal and transversal directions as depicted in Figure 4.5.
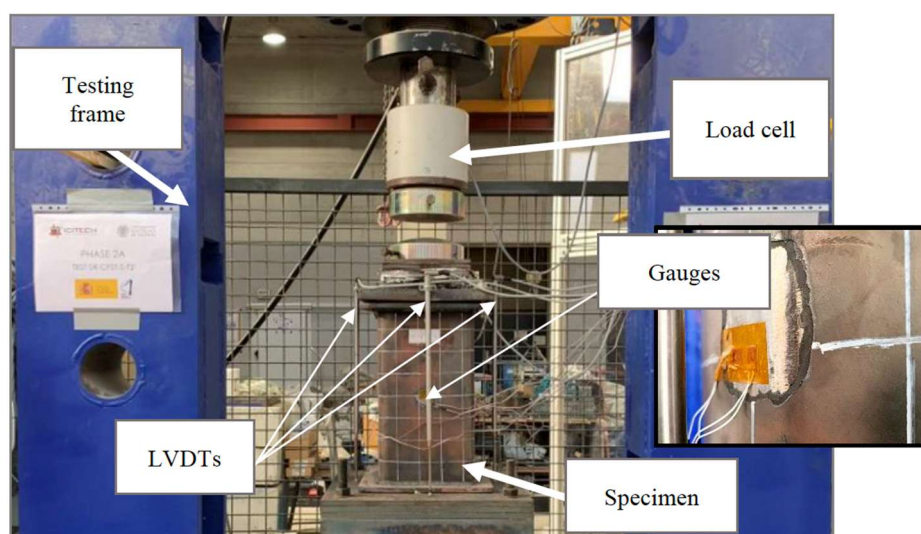
Figure 4.5   Mechanical test-set up of the post-fire tests.

4.2.4. Test procedure

Initially, the columns were heated unloaded in the previously described electric furnace, as this state is considered more conservative when evaluating the residual strength of concrete after heating. The column was placed inside the furnace, and the top and bottom ends were covered with blank fibre to avoid a significant heat loss. The test was conducted to ensure that the inner steel profile was affected by the temperature field and decreased its properties until the outer steel tube reached a maximum temperature of 1000 ºC. Due to the limitation in the electric power of the furnace and the initial heat inertia, the heating times for all specimens in the series exceeded 240 minutes. Once the target temperature was achieved, the furnace was turned off and opened, letting the columns cool off until they regained room temperature. The temperatures in the locations where the thermocouples were installed were monitored during the heating process and part of the cooling.

Once the columns had cooled off, mechanical compression tests were performed to obtain the residual strength of the thermally affected SR-CFST section. The specimens were mounted in the testing platform, aligned with the hydraulic jack, and welded. Then, a pre-loading phase started, during which, using the data from the LVDTs, the uniformity and verticality of the specimen were ensured. The displacement-controlled test was then conducted at a loading rate of 0.1mm/min, which was measured by the loading cell internal displacement sensor, which allowed to record and extract the data from each test, showing the shortening of the columns as the load increased. The LVDTs and strain gauge data were also recorded during the mechanical test.

4.2.5. Results

4.2.5.1. Cross-sectional temperatures

Figure 4.6 displays the temperature changes across the cross-section recorded during the heating and initial cooling stages. While 12 thermocouples were monitored, only four are presented in the figure, along with the furnace temperature evolution for clarity purposes. Unfortunately, during the testing of specimen SR-CFST-C-T1, a connection issue was experienced in some of the thermocouples, resulting in missing temperature data from TC1 starting at 130 min, TC3 and TC9 from 150 min, and TC8 from approximately 180 min onwards.

As observed in Figure 4.6, the impact of the thermal protection of the outer steel tube and the low thermal diffusivity of concrete is evident in the delay of temperature increase in the concrete core for both series. Generally, temperatures are higher in the square SR-CFST columns than their circular counterparts, possibly due to the section factor, which means a higher exposed perimeter for the same cross-sectional area. In specimens SR-CFST-C-T3 and SR-CFST-S-T3, the steel profile embedded in HEB140 experiences higher temperatures than in the other section types probably due to the higher dimensions of the embedded steel profile, which translates into a lesser concrete cover protection.
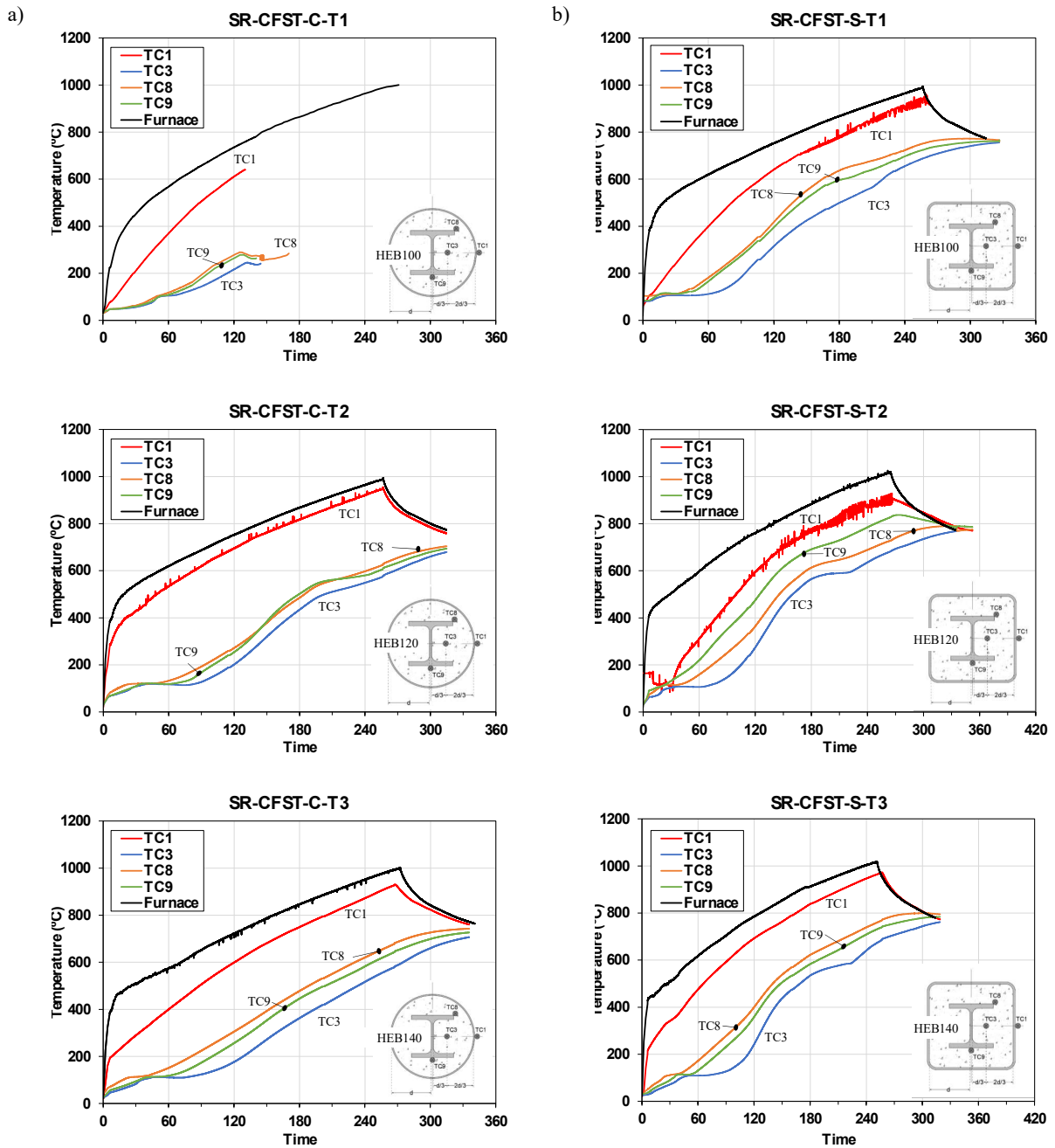
Figure 4.6   Cross-sectional temperatures of a) circular and b) square specimens T1 to T3.

Regarding the visual modification of the columns after the thermal tests, the change in colour of the external surface of the steel tubes was noticeable. The surface became dark burgundy, substituting the normal orange colouration of the columns in their initial state. Figure 4.7 shows a close-up of specimens SR-CFST-C-T2 and SR-CFST-S-T2 where it can be observed that a thin layer of the outer tube shed off the tube wall during the heating process. Figure 4.9a shows the final state of all the columns after the heating process.

Figure 4.7   External surface of the columns after the heating tests: a) SR-CFST-C-T2; b) SR-CFST-S-T2.

After specimens SR-CFST-C-T1 and SR-CFST-S-T1 were tested they were cut longitudinally to examine the inner state of the column internal elements: the inner steel profile and the concrete core (refer to Figure 4.8). The concrete degraded and changed its pigmentation to a yellow colour in the areas more affected by the heat, maintaining its original colour in the more internal and protected areas. This area is outlined in Figure 4.8 with a red dotted line for clarity. This area comprises the outer part of the core and the upper part of the column, as the heat travels to the upper part of the furnace, heating it further. As previously shown in Figure 4.6b, the temperatures at the end of the heating test for the SR-CFST-S-T1 specimen reached between 600 and 800ºC. This may explain the colouring change of the concrete, as its microstructure changes above temperatures of 600 ºC.
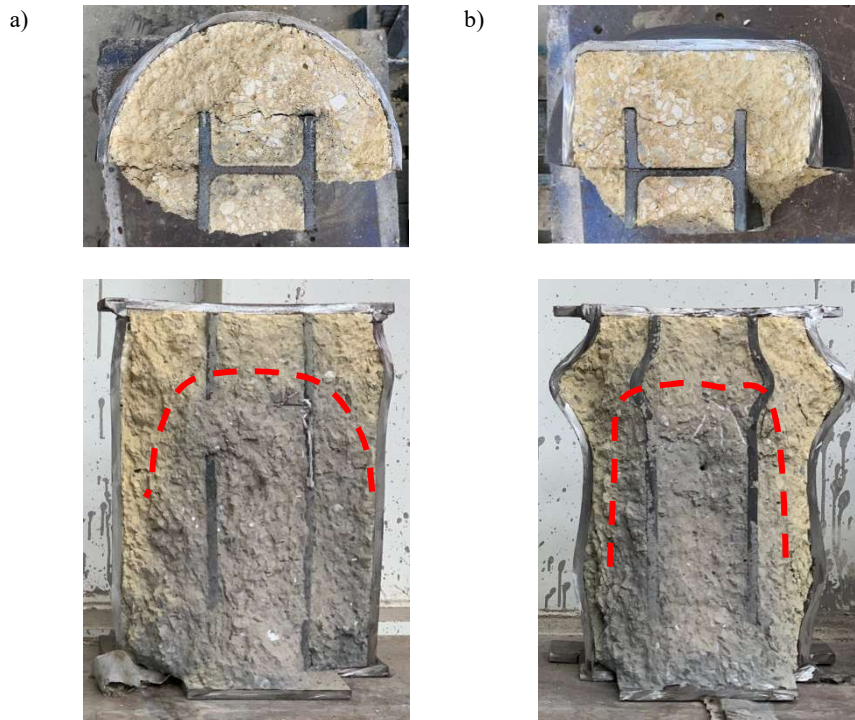
Figure 4.8   Internal state of the post-fire specimens after test: a) SR-CFST-C-T1; b) SR-CFST-S-T1.

4.2.5.2. Failure modes

Figure 4.9 shows the six tested specimens of this phase after the thermal tests (Figure 4.9a) and after the completion of the post-fire compression tests (Figure 4.9b). After the completion of the mechanical phase, the columns were severely damaged and showed a local buckling of the outer steel tube, most outstandingly in the square specimens of the series. This characteristic elephant foot shape appears due to the different thermal expansion of the materials of the column and the uneven temperature field causing the steel outer tube to support the axial load and bend.
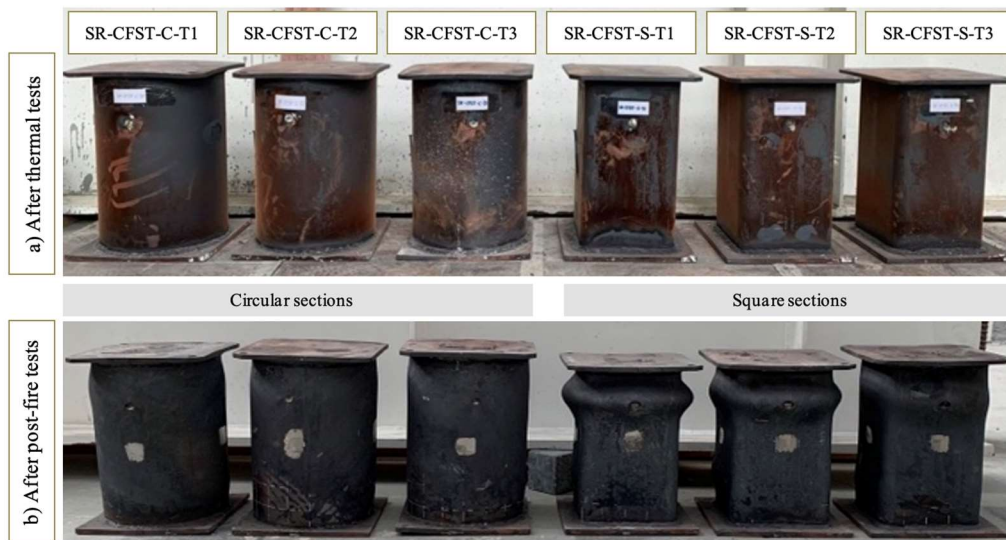
Figure 4.9   Post-fire test specimens after the thermal tests and post-fire mechanical tests.

As can be observed in both Figure 4.8 and Figure 4.9b, the bulges appeared near the top end of the column instead of the middle section. This displacement may be due to the position of the evaporation hole, drilled in the upper part of the section. Additionally, the upper part of the mechanical set-up (as stated in 4.2.3) had a pinned boundary condition, caused by the ball joint of the load cell, which contributed further to the local buckling in this upper section.

Precisely on the bulge area, a gap appeared between the steel tube and the inner damaged concrete (see Figure 4.8). The bonding capacity of concrete was reduced considerably due to the high-temperature exposition during the test. This concrete crumbled when touched as it lost part of its integrity. Yang et al. (2020) experienced the same behaviour on the top end of their specimens, as no plates were welded to them. In the surface smoothing stage, after the thermal tests and before the mechanical post-fire ones, small parts of the concrete's aggregates scattered from the surface. In this research, however, this issue was not experienced as the welded plates assured the planarity of the end of the column.

It is worth noting that, while conducting the mechanical post-fire tests, a series of shear slippage lines (see Figure 4.10a) appeared in the outer tube wall. These lines described an angle of 45º with respect to the main compression stress direction (longitudinal axis) and portrayed the plane of maximum tangential stress. These lines started to appear when the applied load reached about 3000 kN (approximately 60-75% of the maximum load) when the outer tube entered a plastic stage, as will be later discussed in 4.2.5.3. This phenomenon continued to develop in the final stages of all the conducted tests and became more prominent until the ultimate capacity of the tested specimens was reached.
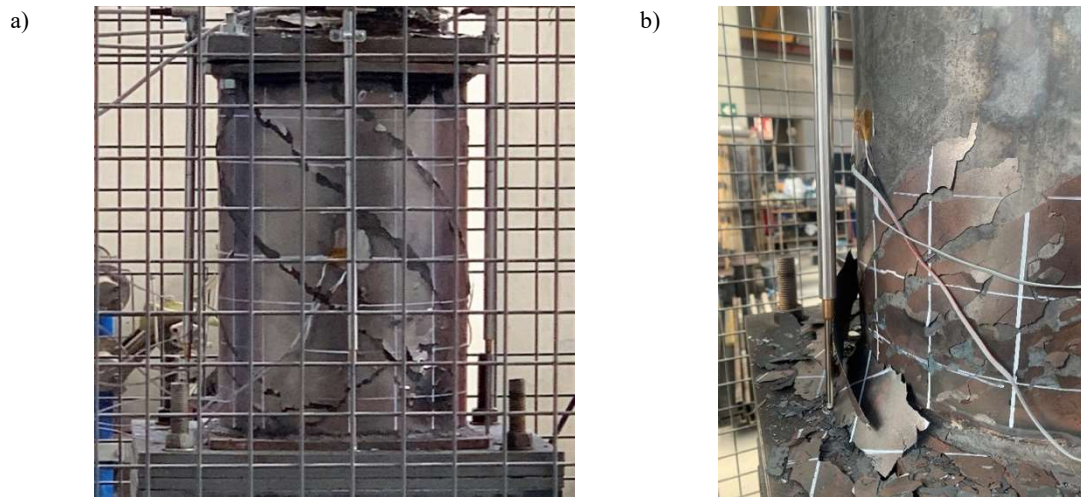
Figure 4.10   Shear slippage lines in the mechanical tests: a) SR-CFST-C-T1 during the test; b) SR-CFST-C-T2 bottom end detail after the test.

Figure 4.10b also shows how a very thin layer of the outer tube steel peeled off and separated from the rest of the tube while conducting the test. This is the so-called mill scale (also known as "calamine"), a surface oxidation layer generated during the hot rolling process of the piece. The main purpose of this layer is to protect the tube while in storage, to avoid further oxidation and degradation. The calamine has a smaller thermal expansion coefficient than the rest of the steel from the tube, which makes it very fragile and vulnerable to temperature gradients. After the heating process it is more fragile, which causes it to separate and fall from the rest of the tube.

4.2.5.3. Stress analysis of the outer steel tube

The outer tube stress levels were registered during the mechanical post-fire tests by using sets of vertical and horizontal strain gauges located at the four sides of the column (0º, 90º, 180º and 270º) as described in section 4.2.3 (see Figure 4.11).
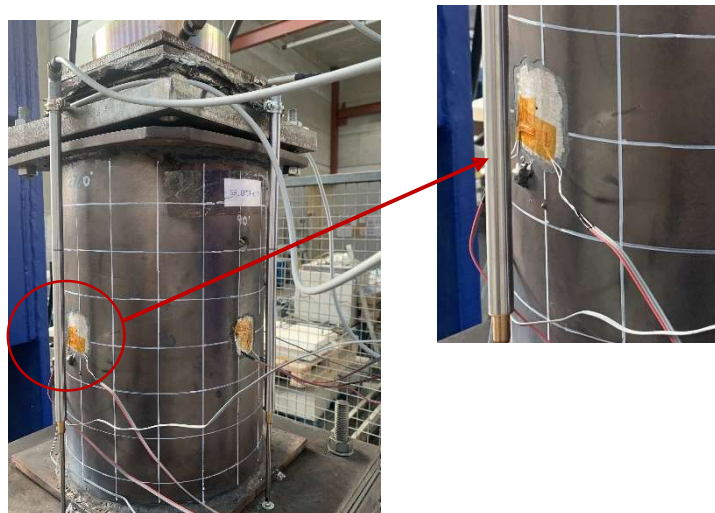
Figure 4.11   Detail of the strain gauges attached to the outer steel tube walls.

The obtained measurements from these gauges are provided in Figure 4.12. In these sets of graphs, the positive strain indicates contraction while the negative strain implies elongation.
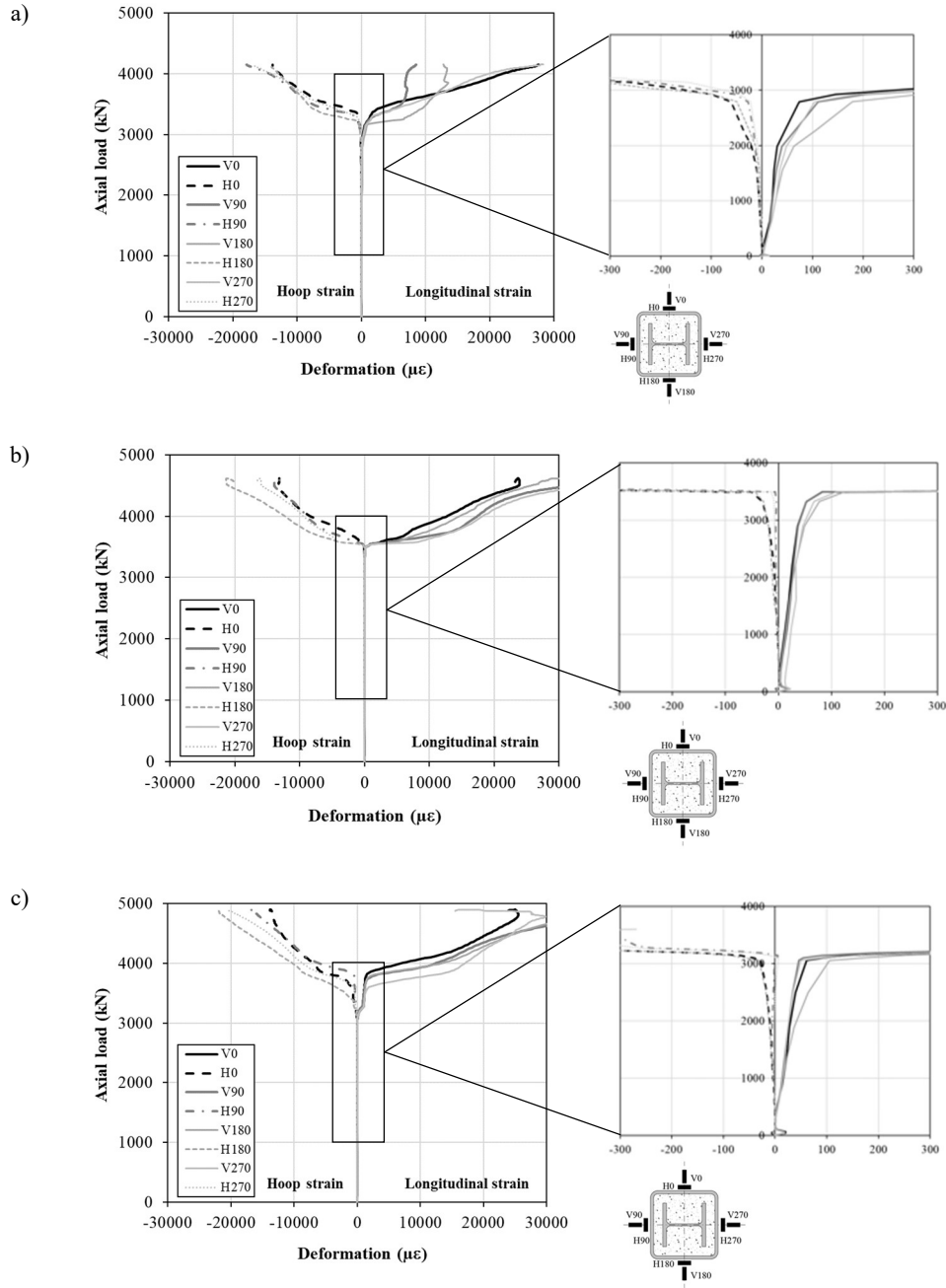
Figure 4.12   Post-fire test specimens after the thermal tests and post-fire mechanical tests: a) SR-CFST-S-T1; B) SR-CFST-S-T2; C) SR-CFST-S-T3.

From the presented strain readings, the hoop (σ_h) and vertical (σ_v) stress at the linear elastic range can be directly obtained by assuming a state of plane stress at the outer surface of the steel tube, according to Hooke's law:

$$\sigma_h = \frac{E_s}{1 - v_s^2}(\varepsilon_h + v_s \varepsilon_v) \tag{4.1}$$

$$\sigma_v = \frac{E_s}{1 - v_s^2}(\varepsilon_v + v_s \varepsilon_h) \tag{4.2}$$

where ε_h and ε_v are the transverse and longitudinal strain, respectively, v_s is the Poisson's ratio of steel at the elastic range and E_s is the elastic modulus of steel.

Then, according to the elastic-plastic theory, the Von Misses equivalent stress can be calculated as:

$$\sigma_{eq,VM} = \frac{\sqrt{2}}{2}\sqrt{(\sigma_h - \sigma_v)^2 + \sigma_v^2 + \sigma_h^2} \qquad (4.3)$$

where σ_h and σ_v are the transverse and longitudinal stress at the outer tube wall's surface, respectively.

Nonetheless, in the elastic-plastic range, the expressions given in equations (4.1) and (4.2) are not applicable; consequently, the real stress-strain relations can be obtained based on an incremental procedure, as proposed by Zhang et al. (2005), in which the tangent modulus of steel (E_s^t) is re-calculated at each strain increment:

$$E_s^t = \frac{(f_y - \sigma_{eq,VM})\sigma_{eq,VM}}{(f_y - f_p)f_p} E_s \qquad (4.4)$$

and the same applies to the Poisson's ratio:

$$\nu_{sp} = \frac{\sigma_{eq,VM} - f_p}{f_y - f_p} + \nu_s \qquad (4.5)$$

The stress state of the outer steel tube surface during the loading process of the mechanical tests was obtained by the described procedure. It is worth noting that, the mechanical properties of steel were assumed to have been affected by the greatest temperature in the heating part of the test. Thus, the corresponding post-fire residual factors were applied to f_y, f_p and E_s according to the highest temperature recorded at the outer steel tube for each column.

In Figure 4.13 it can be observed the evolution of the hoop (H) and vertical (V) stresses at each location studied (0º, 90º, 180º and 270º) for column SR-CFST-S-T3. In this graph, the positive stresses correspond to compression stresses while the negative denote tensile stresses.
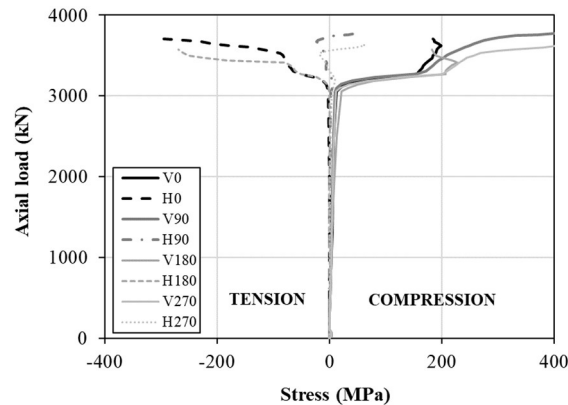
Figure 4.13   Stress evolution at the outer tube Surface for specimen SR-CFST-S-T3 for each orientation studied.

In the initial loading phase, the outer steel is in the elastic range; thus, the vertical stresses increase linearly while the transverse (hoop) stresses increase slightly and at a slower pace. While the axial compression load increases, the steel enters the elastic-plastic regime, where the slope of the curves reduces progressively leading to the plastic range. In this state, both types of stresses show a rapid progression, indicating a possible effect of the lateral confinement stresses between the inner concrete core and the steel tube. This event occurs at a load of 3000 kN (60-75% of the ultimate load) which matches the apparition of the shear slippage 45º lines exposed previously in this chapter, indicating a plastic failure of the tube.

In this stage, the stresses continue increasing even though the load level rise is not significant developing a plateau, as seen in Figure 4.14. Between 200 and 400 MPa, a strain hardening phase appears, at the end of which, the stresses stabilize again and ultimately the steel tube fails. By computing the equivalent Von Misses stress at this endpoint, the obtained values were close to the post-fire ultimate strength of steel corresponding to the maximum temperature reached by the outer tube. As an example, in column SR-CFST-S-T3 the higher temperature reached in the thermal test at the outer tube was 989 ºC which, according to Pons et al. (2022) corresponds to a post-fire reduction coefficient of the ultimate strength of steel of 0.577. Therefore: $f_{uo, post} = 0.577 \cdot f_{uo, 20} = 0.577 \cdot 688$ MPa = 392 MPa. From this point, the tube loses its load-bearing capacity and transmits it to the concrete core and inner steel profile until, eventually, the column fails.
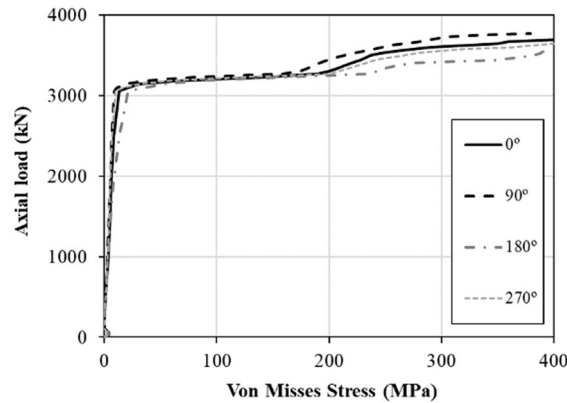
Figure 4.14   Axial load vs. Von Misses equivalent stress for specimen SR-CFST-S-T3.

4.2.5.4. Force-displacement response.

Figure 4.15 displays the load versus displacement curves for all the studied specimens in this experimental campaign. The response was initially linear elastic until 60-75% of the peak load ($N_{post,exp}$) was reached which is analogous to the obtained response of the experimental studies of Meng et al. (2019). After this stage, the columns entered the plastic range and the stiffness of the columns reduced progressively. The peak load value, once reached it remained constant for a substantial period instead of presenting a sudden descent, exhibiting the high ductility of the SR-CFST columns. Refer to Table 4.1 to consult the peak load values of all experiments.
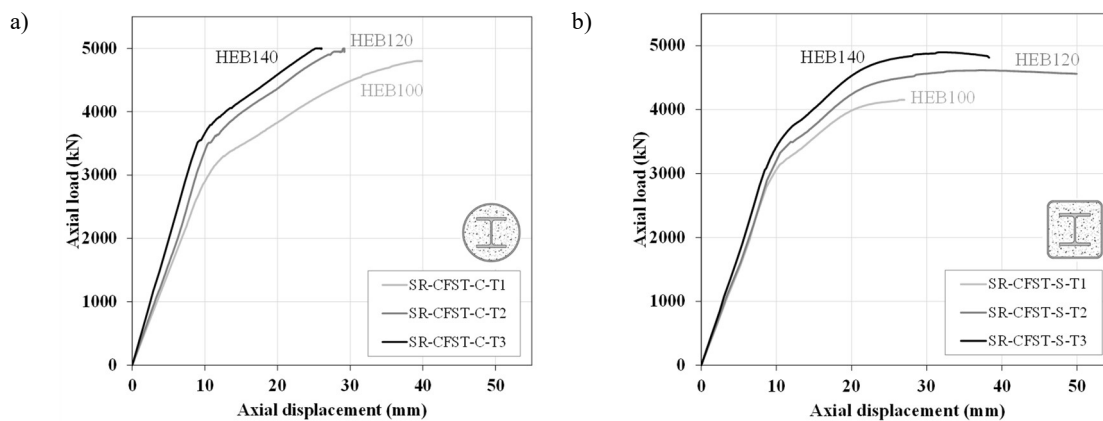
Figure 4.15   Axial load vs. displacement curves for: a) circular specimens; b) square specimens.

It is worth mentioning that, as can be observed in Figure 4.15a, the mechanical tests for columns SR-CFST-C-T2 and SR-CFST-C-T3 were manually stopped due to the limitations of the vertical testing frame and the hydraulic jack capacity (5000 kN) which prevented the obtainment of the maximum load experimentally (included as ">5000" in column $N_{post,exp}$ of Table 4.1).

Figure 4.16 shows a comparison between each pair of test specimens with similar steel cross-sectional areas. The circular specimens had higher peak loads than their square counterparts and the peak load value increased as the size of the inner steel profile did. The maximum values of axial load for each series were obtained for the sections with an embedded HEB140 (specimens SR-CFST-S-T3 and SR-CFST-C-T3).

a)

b)

c)
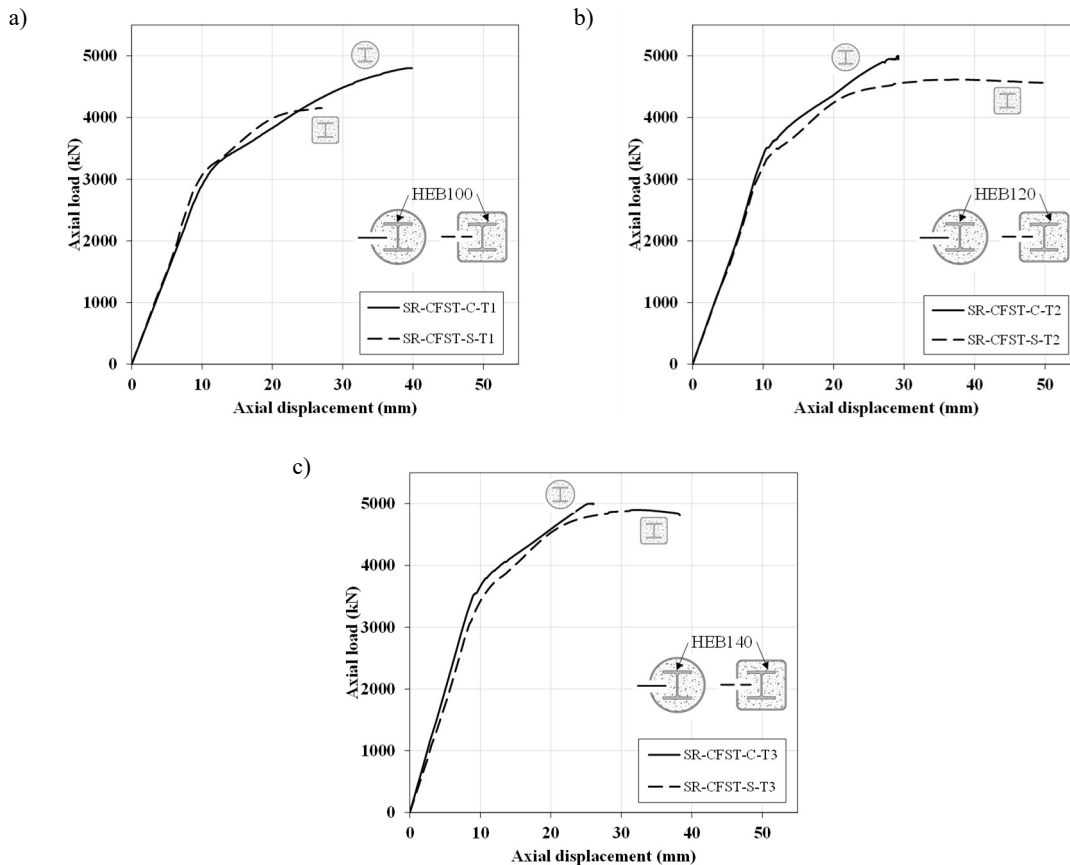
Figure 4.16   Axial load vs. displacement curves for each pair of specimens with different embedded profiles: a) HEB100; b) HEB120; c) HEB140.

4.2.5.5. Residual Strength Index

To measure the load-bearing capacity decrease of the thermally affected columns, an indicative is defined: the Residual Strength Index (RSI). The proposed approach by Han et al. (2005) is adopted where the RSI is defined as:

$$\text{RSI} = \frac{N_{post,exp}}{N_{u,0}} \tag{4.6}$$

where $N_{u,0}$ and $N_{post,exp}$ are the room temperature ultimate load and the experimentally obtained ultimate load of the columns, respectively.

To obtain the room temperature ultimate load ($N_{u,0}$) of the columns, the equations in Clause 6.7.3.2 of Eurocode 4 Part 1-1 (CEN, 2004c) are used and adapted from CFST sections to the tested SR-CFST sections in this study. To consider the effect of the inner steel profile, its contribution to the plastic resistance of the cross-section ins added in the summation of components.

For the square SR-CFST sections, the confinement effect at room temperature is neglected, thus the $N_{u,0}$ is obtained by adding the plastic resistances of each component of the cross-section as per Clause 6.7.3.2(1) of EN1994-1-1 (CEN, 2004c):

$$\mathrm{N}_{u,0} = A_a f_{uo} + A_c f_c + A_{sp} f_{ui} \tag{4.7}$$

where A_a and f_{uo} are the cross-sectional area and ultimate strength of the steel outer tube; A_c and f_c are the cross-sectional area and compressive cylinder strength of the concrete infill; and A_{sp} and f_{ui} are the cross-sectional area and ultimate strength of the embedded steel profile.

For circular SR-CFST columns, the confinement of the cross-section at room temperature is considered as specified in Clause 6.7.3.2(6) of EN1994-1-1 (CEN, 2004c), given that the relative slenderness does not exceed 0.5 ($\bar{\lambda} < 0.5$) and a load eccentricity to diameter ratio less than 0.1, which is the case for the tested columns. The ultimate resistance is therefore obtained by the following equation:

$$\mathrm{N}_{u,0} = \eta_a A_a f_{uo} + A_c f_c \left(1 + \eta_c \frac{t}{D} \frac{f_{uo}}{f_c}\right) + A_{sp} f_{ui} \tag{4.8}$$

where t is the wall thickness of the steel tube; D is the external diameter of the column; and η_a and η_c are the factors associated with the confinement of concrete. For axially loaded members, these factors are calculated as:

$$\eta_a = 0.25(3 + 2\bar{\lambda}) \tag{4.9}$$

$$\eta_c = 4.9 - 18.5\bar{\lambda} + 17\bar{\lambda}^2 \tag{4.10}$$

In EN1994-1-1 (CEN, 2004c) these equations are used with the design value for the yield strength of steel and compressive strength of concrete, which have been replaced in this calculations by the ultimate strength of steel and the concrete strength obtained with the cylinder material tests as stated in 4.2.1. This modification is done to calculate the ultimate sectional capacity of the specimens. Table 4.2 presents the $N_{u,0}$ calculated values along with the experimentally tested $N_{post,exp}$:

Table 4.2   Calculated ultimate load ($N_{u,0}$), post-fire test results ($N_{post,exp}$) and RSI.

	Specimen	$N_{u,0}$ (kN)	$N_{post,\,exp}$ (kN)	RSI
	SR-CFST-C-T1	8774	4799	0.547
	SR-CFST-C-T2	9016	>5000	0.554*
	SR-CFST-C-T3	9331	>5000	0.536*
	SR-CFST-S-T1	7547	4153	0.550
	SR-CFST-S-T2	7856	4615	0.587
	SR-CFST-S-T3	8245	4896	0.594

*Note: For columns SR-CFST-C-TM2 and SR-CFST-C-TM3 the RSI values are calculated assuming a $N_{post,exp}$ of 5000 kN even though the values would be slightly higher as the columns retained a higher load-bearing capacity.

Additionally, the RSI values have been plotted in Figure 4.17 for clarity. The RSI values for both series of specimens are around the same values, retaining between 55 and 60% of their initial load capacity. The fact that the circular columns lose the same amount of capacity as the square ones denotes that the confinement effect, initially considered in the $N_{u,0}$ calculation for circular specimens, is still active in the post-fire columns. Regarding the effect of the embedded HEB profiles in the square sections, the difference in RSI values is minor (an additional 7.4% for the HEB120 and 1.2% for the HEB140 as compared to the SR-CFST-S-T1 which has an embedded HEB100). This fact denotes that the higher cross-sectional area of the bigger profiles gets compensated by a greater degradation of the steel, as it becomes less protected by the concrete, due to its dimensions. As previously stated, the SR-CFST-C-T2 and SR-CFST-C-T3 cases were manually stopped due to the load limitations of the hydraulic jack. Therefore, the obtained RSI values should be greater than the ones exposed in Figure 4.17, following a similar increasing trend as the square ones.

It is worth mentioning that the conclusions drawn from this experimental research and the exposed calculations are valid for heating times of 240 minutes at the t-T curve applied in these tests. Further research is essential to properly evaluate the behaviour of SR-CFST columns in post-fire conditions.
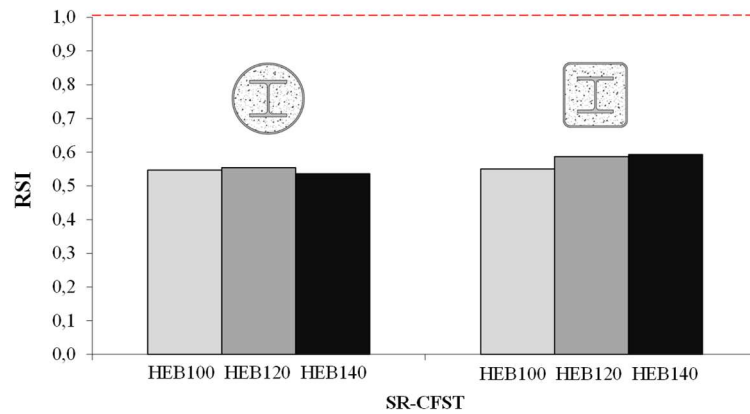
Figure 4.17   Residual Strength Index (RSI) for all specimens in the post-fire tests.

4.2.6. Proposed design procedures

This final section aims to evaluate the residual post-fire capacity of SR-CFST columns by using the available design guidelines and considering the residual strength of the concrete and steel materials after being exposed to fire conditions.

Since the European normative, in EN1994-1-2 (CEN, 2005c), does not provide any specific guidelines to calculate the residual post-fire plastic strength of SR-CFST columns, the expressions provided in EN1994-1-1 (CEN, 2004c) for room temperature design will be adapted by using the residual material properties after fire exposure. As indicated in the previous chapter, accounting for the inner embedded profile will be done by including an additional term in the equation, as in equations (4.7) and (4.8), but considering the post-fire effect in the material properties.

Despite Annex C of Eurocode 4 Part 1-2 (CEN, 2005c) provides a formula to obtain the residual strength of concrete after being exposed to fire – also included in the last draft version of Eurocode 2 Part 1-2 (prEN1992-1-2:2021-09) (CEN, 2021), the steel post-fire properties still lack regulation in the available normative. That is why several researchers have conducted investigations to shed light on this matter and characterize the material properties of steel after fire. These proposals will be assessed in predicting the residual load-bearing capacity of SR-CFST columns against the experimental results obtained in this campaign.

The British normative, specifically Annex B of BS5950-8:2003 (BSI, 2003), states in Clause B.2.1 that the mechanical properties of structural steels are not significantly affected until the material reaches temperatures of 600 ºC or higher. The normative stipulates that, for micro-alloyed steels of grade S355, 75% of their strength can be assumed to be regained after cooling.

Some authors, such as Tao et al. (2013), proposed several equations to obtain the residual strength of structural and reinforcing steel obtained from a statistical analysis of available data from the literature experiments. Likewise, Molkens et al. (2021) revised the available post-fire campaigns of structural steel in the literature (a total of 718 tests) and conducted a statistical analysis. A series of residual factors were recommended for normal, high-strength and very high strength steel after being exposed to fire conditions, which were designed with a severe drop in the mechanical properties of any of the steels at around 500-600 ºC.

Finally, the post-fire residual properties of steel were also investigated by co-workers Pons et al. (2022), as part of the project in which this investigation is comprised. Different samples obtained from various steel hollow steel were tested and a series of post-fire residual factors were proposed for temperatures ranging from 20 up to 1000 ºC.

The residual plastic resistance of SR-CFST sections will be calculated by dividing the cross-section with the presented scheme in Figure 4.18. The three elements of the section are clearly differentiated, and the central parameter of this proposal is the maximum temperature achieved in each sub-division. As can be observed, while the outer steel tube is considered as a whole, the embedded profile is divided into two parts: the web (more protected by the surrounding concrete) and the flanges (more exposed to the fire). Since the concrete core has a non-uniform field along its depth, a subdivision in four concentric rings (circular) or layers (square) is proposed, similar to the analytical approach taken by Lie and co-workers (1994, 1995) in CFST columns in fire. A representative maximum temperature is assigned to each division of the concrete infill.

The representative maximum temperatures assigned to each section are the maximum recorded temperatures in the experimental investigation (see Section 4.2.5.1). The steel tube temperature ($\theta_{a,max}$) ranges between 920 ºC and 970 ºC. The temperatures for the flanges ($\theta_{f,max}$) and web ($\theta_{w,max}$) of the inner steel profile range between 700 ºC and 800 ºC. Each subdivision of the concrete is assigned a design temperature ($\theta_{c,i,max}$) according to the maximum temperature of the corresponding thermocouple (refer to Figure 4.18).
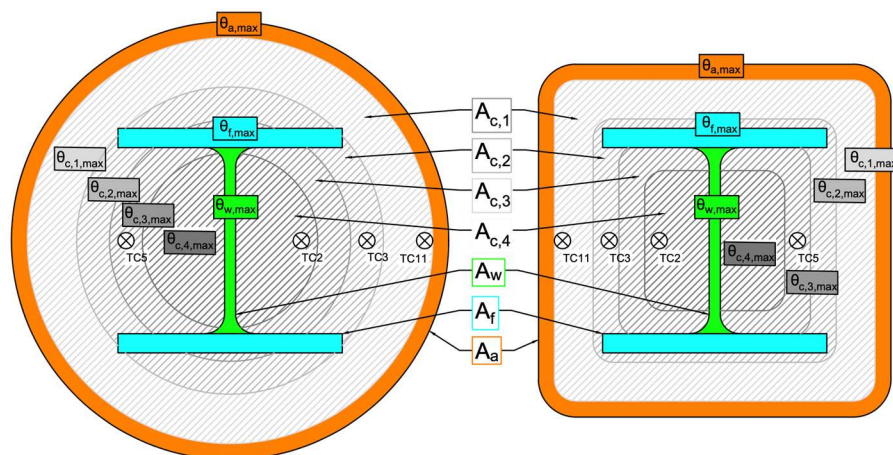
Figure 4.18   Zone sub-division of the SR-CFST cross-sections.

Hence, the plastic resistance to compression of SR-CFST sections in post-fire scenario will be obtained by means of the following equations:

For square SR-CFST sections (no confinement):

$$N_{u,0} = A_a f_{uo,post}(\theta_{a,max}) + \sum_{i=1}^{4} A_{c,i} f_{c,post}(\theta_{c,i,max}) + A_f f_{ui,post}(\theta_{f,max}) + A_w f_{ui,post}(\theta_{w,max}) \tag{4.11}$$

where $A_{c,i}$ is the cross-sectional area of the i concrete ring or layer; $f_{c,post}$ is the ultimate concrete compressive strength affected by the matching residual factor for the assigned temperature $\theta_{c,i,max}$; A_f and A_w are the cross-sectional areas of the flanges and the web of the embedded steel profile, respectively; and $f_{uo,post}$ and $f_{ui,post}$ are the ultimate strength of the outer steel tube and the embedded steel profile affected by the corresponding residual factors for the peak temperatures $\theta_{a,max}$, $\theta_{f,max}$ and $\theta_{w,max}$, respectively.

For circular SR-CFST sections (confinement effect considered)

$$N_{u,0} = \eta_a A_a f_{uo,post}(\theta_{a,max}) + \sum_{i=1}^{4} A_{c,i} f_{c,post}(\theta_{c,i,max})\left(1 + \eta_c \frac{t}{D}\frac{f_{uo}(\theta_{a,max})}{\overline{f_{c,post}}}\right) \tag{4.12}$$
$$+ A_f f_{ui,post}(\theta_{f,max}) + A_w f_{ui,post}(\theta_{w,max})$$

where the average compressive strength of the concrete core, after being exposed to high temperatures which accounts for the confinement effect in the post-fire situation is calculated as:

$$\overline{f_{c,post}} = \frac{\sum_{i=1}^{4} A_{c,i} f_{c,post}(\theta_{c,i,max})}{A_c} \tag{4.13}$$

Therefore, the residual axial capacity for the six tested stub SR-CFST columns is obtained and compared to the experimentally obtained results. For the concrete core, the formula from Annex C of EN1994-1-2 (CEN, 2005c) will be used to obtain its residual mechanical properties while for the steel in the outer tube and inner profile, the four previously exposed models and formulation will be tested and compared. Table 4.3 presents a summary of the obtained values following this procedure in which the post-fire plastic resistance of the columns ($N_{calc,j}$) with each approach is presented, where the numbers at the subscripts j correspond to 1, British Standard (BSI, 2003); 2, Tao et al. (2013); 3, Molkens et al. (2021); and 4, Pons et al. (2022). The experimentally obtained load-bearing capacity of the columns (see Table 4.3) is included in the table for reference.

Table 4.3   Post-fire plastic resistance for the SR-CFST columns calculated under different approaches ($N_{calc,j}$).

	Specimen	$N_{post,exp}$ (kN)	$N_{calc,1}$ (kN)	$N_{calc,2}$ (kN)	$N_{calc,3}$ (kN)	$N_{calc,4}$ (kN)
	SR-CFST-C-T1	4799	5785,9	6724,9	5118,1	4821,3
	SR-CFST-C-T2	>5000*	6077,3	7054,5	5446,3	5163,4
	SR-CFST-C-T3	>5000*	6447,0	7422,0	5632,4	5383,1
	SR-CFST-S-T1	4153	5255.6	6202.1	4639.3	4368.2
	SR-CFST-S-T2	4615	5530.0	6483.9	4837.3	4556.4
	SR-CFST-S-T3	4896	5902.8	6831.2	4951.4	4726.9

Note: 1, BS5950-8:2003 (BSI, 2003); 2, Tao et al. (2013); 3, Molkens et al. (2021); and 4, Pons et al. (2022).

Table 4.4 includes a comparison between the calculated values with each approach and the experimental results with the relation $N_{post,exp}/N_{calc,j}$, in which a value higher than one indicates a conservative prediction, while lower indicates a non-conservative evaluation. Additionally, the values for the mean and standard deviation of each approach are included in the table. It is worth mentioning that, as previously stated in Table 4.1, the SR-CFST-C-T2 and SR-CFST-C-T3 columns are marked with * to indicate that they have been calculated assuming a load-bearing capacity of 5000 kN. These values have been neglected in the calculation of the mean and standard deviation of each case.

Table 4.4 $N_{post,exp}/N_{calc,j}$ for the different approaches compared.

	Specimen	$N_{post,exp}/$ $N_{calc,1}$	$N_{post,exp}/$ $N_{calc,2}$	$N_{post,exp}/$ $N_{calc,3}$	$N_{post,exp}/$ $N_{calc,4}$
	SR-CFST-C-T1	0.83	0.71	0.94	1.00
	SR-CFST-C-T2	0.82*	0.71*	0.92*	0.97*
	SR-CFST-C-T3	0.78*	0.67*	0.89*	0.93*
	SR-CFST-S-T1	0.79	0.67	0.90	0.95
	SR-CFST-S-T2	0.83	0.71	0.95	1.01
	SR-CFST-S-T3	0.83	0.72	0.99	1.04
	Mean	**0.82**	**0.70**	**0.94**	**1.00**
	SD	**0.02**	**0.02**	**0.04**	**0.04**

Despite all the proposals significantly reducing the steel properties for temperatures higher than 500-600 ºC, some differences are appreciable between the analysed models. As can be observed in Table 4.4, both the British Standard proposal (BSI, 2003) and the one from Tao et al. (2013) are non-conservative as they significantly overestimate the residual plastic capacity of the steel after fire with this second one the least accurate of the tested models with a mean of the obtained errors equal to 0.7. The reduction factors proposed by Molkens et al. (2021) provide a better agreement with the experimental data with a slightly non-conservative prediction (with a mean of 0.94).

The best residual factors are found to be the ones proposed by co-workers Pons et al. (2022), providing the most accurate predictions with an average error value equal to one and a relatively small standard deviation (4%). In their proposal, Pons et al. (2022) recommend a more progressive loss of capacity for the steel, in contrast with other proposals that only discriminate between temperatures higher or lower than a certain boundary. As can be observed, the use of EN1992-1-2 (CEN, 2005c) coefficients for concrete, together with this proposal, provides an accurate prediction of the post-fire resistance of SR-CFST stub columns.

It is worth noting that the approach exposed in this section is nothing, but a preliminary proposal based on a limited number of experimental tests and should not be considered definitive. Further research, experimental tests and numerical models are needed to adequately validate and develop a valid proposal for the residual strength of SR-CFST columns after exposure to fire conditions. It should also be considered that the circular residual loads were calculated accounting for the confinement of the steel tube as displayed in equation (4.12). Not doing so would have given significantly low predictions (highly conservative) for the ultimate load of the circular specimens. This seems to point out that the confinement effect remains active after the columns have been cooled off and contributes actively to the resistance of the section, which should be further confirmed and verified with additional research.

4.3. THERMO-MECHANICAL STUB COLUMN TESTS

4.3.1. Test specimens

In this phase of the experimental research campaign, a total of twelve stub columns, square and circular-shaped, were tested under axial load at elevated temperatures. Two of the specimens were a circular and a square hollow tube and ten were SR-CFST specimens grouped in two series according to their geometry. Table 4.5 shows the main characteristics of all the specimens included in this experimental campaign.

Table 4.5   List of thermo-mechanically tested columns.

Specimen	D/B (mm)	t (mm)	f_{yo} (N/mm²)	f_{uo} (N/mm²)	f_{yi} (N/mm²)	f_{ui} (N/mm²)	f_c (N/mm²)	Moist. (%)	μ (%)	N_{exp} (%)	FT (min)
CHS-TM0	273	6.3	413.33	483.28	-	-	-	-	40	1020.7	63
SR-CFST-C-TM1	273	6.3	413.33	483.28	315	441	29.73	6.28	40	2812.3	267
SR-CFST-C-TM2	273	6.3	413.33	483.28	777.2	853.68	29.73	6.28	40	3488.9	405
SR-CFST-C-TM3	273	6.3	413.33	483.28	315	441	86.16	2.11	40	3936.8	317
SR-CFST-C-TM4	273	6.3	413.33	483.28	777.2	853.68	86.16	2.11	40	4624.3	383
SHS-TM0	220	6.3	495.84	549.65	-	-	-	-	40	1154.3	43
SR-CFST-S-TM1	220	6.3	495.84	549.65	315	441	29.73	6.28	40	2377.4	239
SR-CFST-S-TM2	220	6.3	495.84	549.65	777.2	853.68	29.73	6.28	40	3097.9	308
SR-CFST-S-TM3	220	6.3	495.84	549.65	315	441	86.16	2.11	40	3306.5	285
SR-CFST-S-TM4	220	6.3	495.84	549.65	777.2	853.68	86.16	2.11	40	4027.0	294
SR-CFST-S-TM5	250	10	824	864	315	441	29.73	6.28	30	3406.5	274
SR-CFST-S-TM6	250	10	824	864	777.2	853.68	86.16	2.11	30	4821.7	395

*Note: *D* and *B* are the outer diameter or dimension for circular and square sections respectively; *t* is the outer steel tube thickness; f_{yo} and f_{yi} are the yield strength of steel for the outer steel tube and inner embedded section respectively; f_{uo} and f_{ui} are the ultimate strength of steel for the outer steel tube and inner embedded section respectively; f_c is the concrete cylinder compressive strength; μ is the load level; N_{exp} is the applied load; and *FT* is the failure time.

To classify them properly, the specimens are named as follows: SR-CFST-X-TMi (i.e. SR-CFST-S-TM1), where X stands for the outer cross-sectional shape of the column (C for circular sections and S for square sections), TM stands for "Thermo-Mechanical" and *i* represents the test number, each corresponding to a different combination of materials for both the inner steel profile and the concrete infill of the section. For the two hollow tube tests a different notation was used, labelling them as CHS and SHS followed by TM0 to indicate that they served as a reference case for the other SR-CFST cases. For the square specimens S-TM1 to S-TM4, a hollow steel SHS section was used of dimensions #220 × 6.3 mm; meanwhile, for the circular ones, a CHS section of dimensions ϕ273 × 6.3 mm was utilized. These two sections had a very similar steel area, with a difference lower than 0.57%, to assure the equivalence in steel usage between the two series of stub columns. The two distinctive square sections, S-TM5 and S-TM6, had a bigger outer hollow steel SHS section with dimensions #250 × 10 mm. It is worth noting that this steel tube was made of high-strength steel as it will be further discussed in this section. The embedded profile of all sections across the two groups consisted of an HEB140 steel section with dimensions *h = b = 140 mm* (*t_f* = 12 mm, *t_w* = 7 mm). The length of all specimens was 600 mm.

<u>Steel</u>

The specimens TM0 to TM4 of this experimental program utilized cold-formed hollow steel tubes with grade S355. Meanwhile, for square specimens TM5 and TM6, hot-rolled quenched and tempered hollow steel tubes with steel grade S770 were used. As for the embedded steel profiles, five of the SR-CFST columns utilized hot-rolled sections with steel grade S275, while the other five utilized welded high-strength steel plates of grade S700MC. All the hollow steel tubes and embedded steel profiles underwent

three coupon tests (per sample) to determine their yield strength (f_{yo} and f_{yi}) and ultimate strength (f_{uo} and f_{ui}). The averages of the measured values are listed in Table 4.5.

Concrete

Concrete mixes of both normal (30 MPa) and high strength (90 MPa) were prepared in a planetary mixer and cured in standard conditions for 28 days at the laboratories of the Concrete Science and Technology Institute (ICITECH), Universitat Politècnica de València. To obtain the compressive strength and the moisture content of each concrete mix, two sets of three samples were prepared: three cylindrical and three cubical. These samples were used to perform the corresponding uniaxial compression tests according to EN1992-1-1 (CEN, 2004a) to obtain the real mechanical characteristics of the mixture. The moisture content values of each mix were obtained following the standard procedure indicated in ISO 12570:2000 (ISO, 2000).
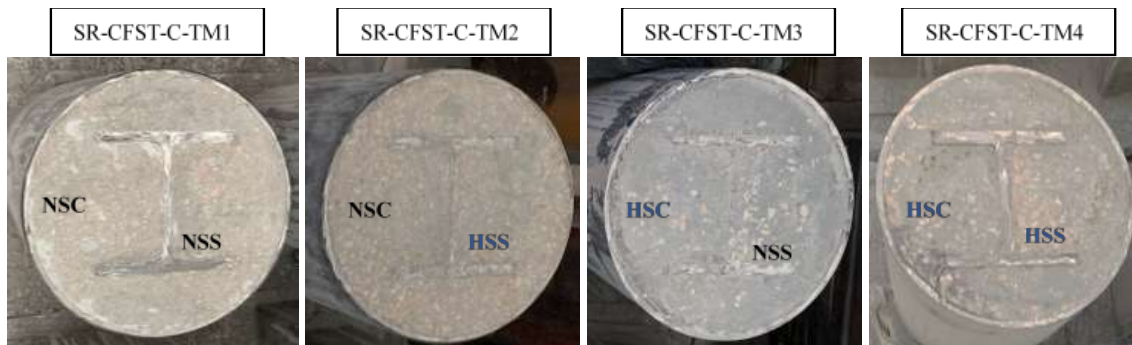
Figure 4.19   Circular specimens φ273×6.3 mm

Figure 4.20   Square specimens #220×6.3 mm

Figure 4.21   Square specimens #250×10 mm

Note: NSC and HSC stand for Normal and High Strength Concrete respectively; NSS and HSS stand for Normal and High Strength Steel respectively.

The layout of the thermocouples positioned in the mid-section of the column can be seen in Figure 4.22. The thermocouples were distributed along all elements, conforming to the composite sections to ensure that the thermal behaviour of each of them could be properly characterized. At the inner steel profile, five thermocouples were installed: thermocouple 4 was installed at the web, and thermocouples 7 to 10 were installed at the flanges of the profile. Thermocouples 2, 3 and 5 were located at the inner concrete core: the first two were positioned equidistantly, ensuring that they had a separation of 1/6 of the section width; meanwhile, thermocouple 5 was positioned at ¼ of the section width. Finally, thermocouples 1 and 6 were welded to two faces of the outer steel tube (90º between them) at the same height.
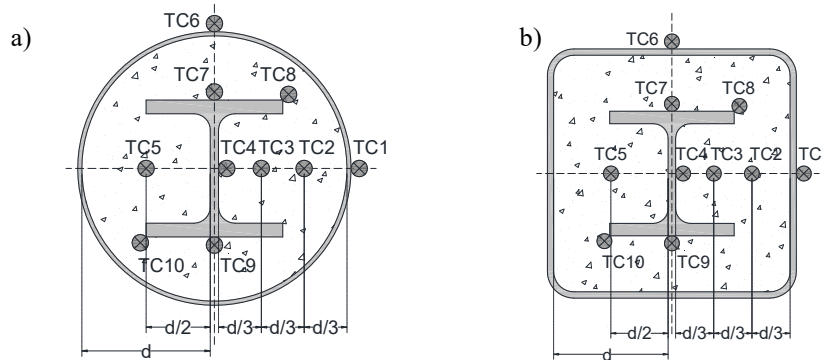
Figure 4.22   Layout of the thermocouples for: a) circular sections; b) square sections.

4.3.2. Test set-up.

A thermo-mechanical testing method was designed to conduct the experiments of Phase B. The procedure consisted of applying a fixed load to the stub SR-CFST columns while concurrently being heated by an electric furnace. A general view of the test set-up of the experiments can be observed in Figure 4.23. A vertical testing frame with an attached hydraulic jack of 5000 kN was used to apply the load as portrayed. The heating was provided by an electric furnace of 10000 W of power, attached to the testing platform. The inner diameter of the furnace was 400 mm and consisted of two semicylinders united at one end by a hinge. The electric resistances of the furnace were distributed along the semi-cylindrical walls in parallel layers to ensure uniform heating of the column as can be observed in Figure 4.24.
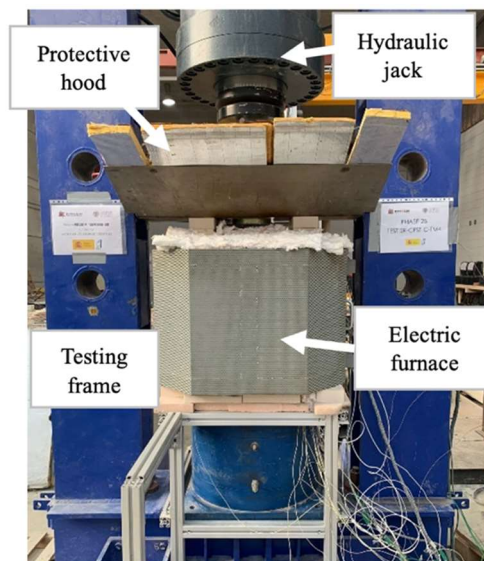
Figure 4.23   General view of the test set-up
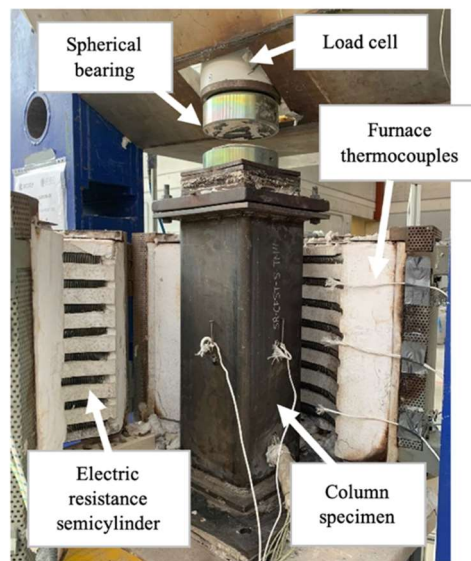
Figure 4.24   Specimen inside of the electric furnace prepared for testing.

The loading system was controlled by a loading cell attached to the hydraulic jack that permitted the application of the desired load. The furnace temperature was monitored and controlled by three thermocouples positioned at the top of the furnace chamber, middle and bottom. Additional thermocouples were placed at the bottom of the testing frame and near the loading cell to ensure these areas were not heating excessively. A steel protective hood with a fibre blanket was placed at the top of the furnace to ensure that the released heat did not affect the hydraulic jack. The furnace top and bottom cavities were insulated using a fibre blanket to minimize heat loss. Additionally, the contact plates of the top and bottom of the column were isolated with several layers of a thinner fibre blanket to avoid the conduction of heat towards the loading cell.

Following a non-constant heating rate, a transient heating regime was applied during the tests. Due to the limitation of the furnace power and the high inertia of the first stages of the heating process, the standard ISO-834 curve (ISO, 2014) was not followed by the furnace temperature. The size of the specimen is comparable to the size of the furnace, which creates a considerable delay in the heating process. That is why in the comparison and result discussion of this phase, the final time the columns failed is referred to as "failure times" instead of "standard fire resistance times".

The applied load of specimens TM1 to TM4 for both series was computed as 40% of the ultimate capacity of the columns at room temperature with the measured material properties. For specimens S-TM5 and S-TM6, with a considerably higher ultimate load, this percentage was set to 30% of the ultimate column load due to a limitation in the capacity of the hydraulic jack. The values for the load level (μ) and applied load (N_{exp}) are in Table 4.5. Initially, the load was applied concentrically to the top end of the columns through a spherical bearing connected to the top of the specimen with several bolts. Once the specified load level was reached, it was maintained during the test, and the specimen was heated, not restricting the elongation of the column.

4.3.3. Results

4.3.3.1. Cross-sectional temperatures

Figure 4.25 to Figure 4.27 show the cross-sectional temperature evolution for the tested columns. Additionally, the furnace temperature is plotted alongside to provide a reference of the chamber heat evolution. Only five representative thermocouples are included in the graphs of specimens TM1 to TM6 for the sake of clarity.

a)

b)
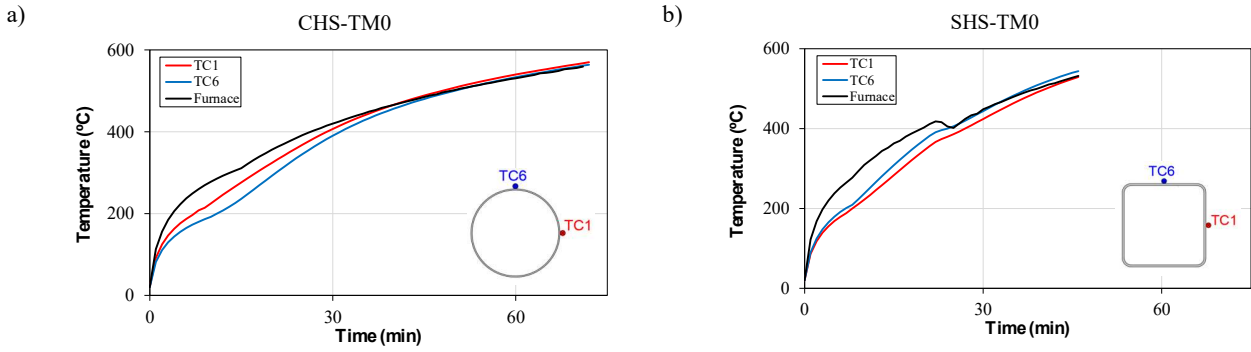
Figure 4.25   Cross-sectional temperatures of the hollow specimens a) CHS-TM0 and b) SHS-TM0.

a)

b)
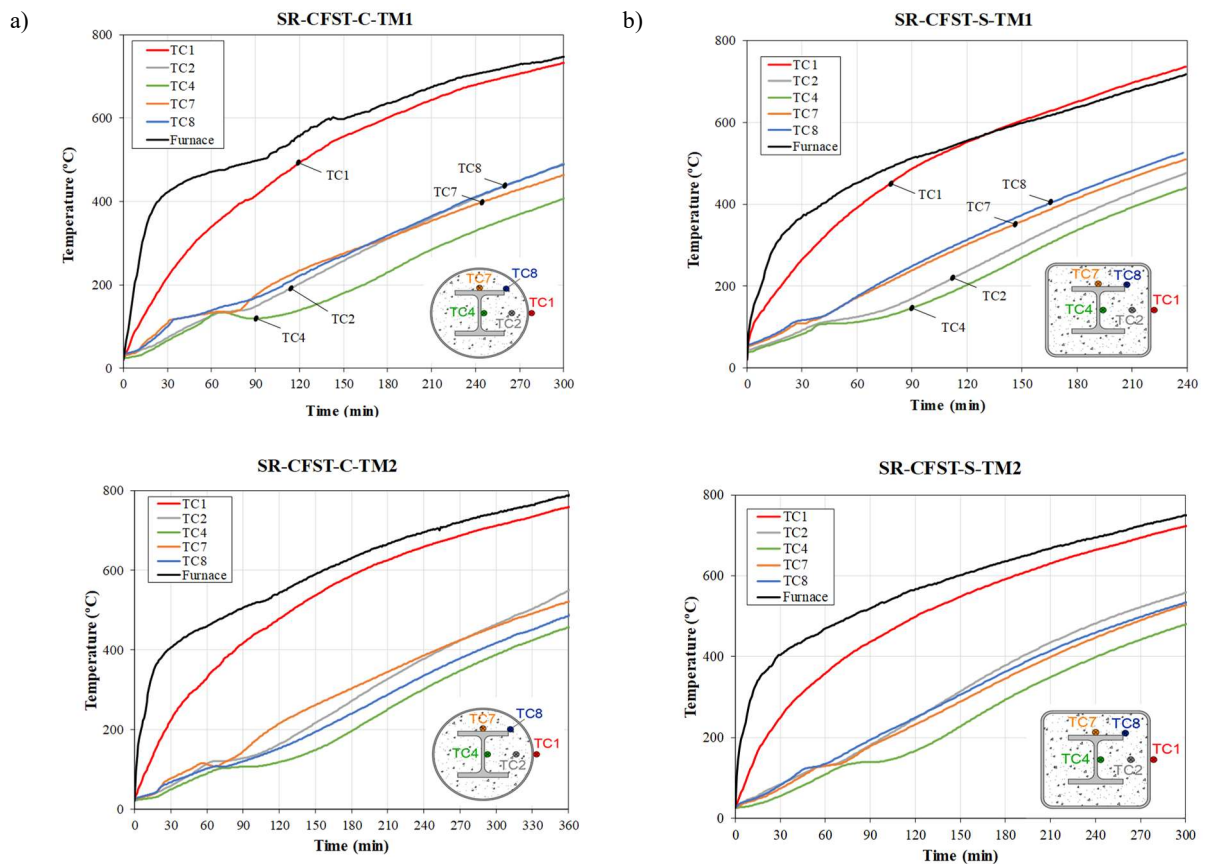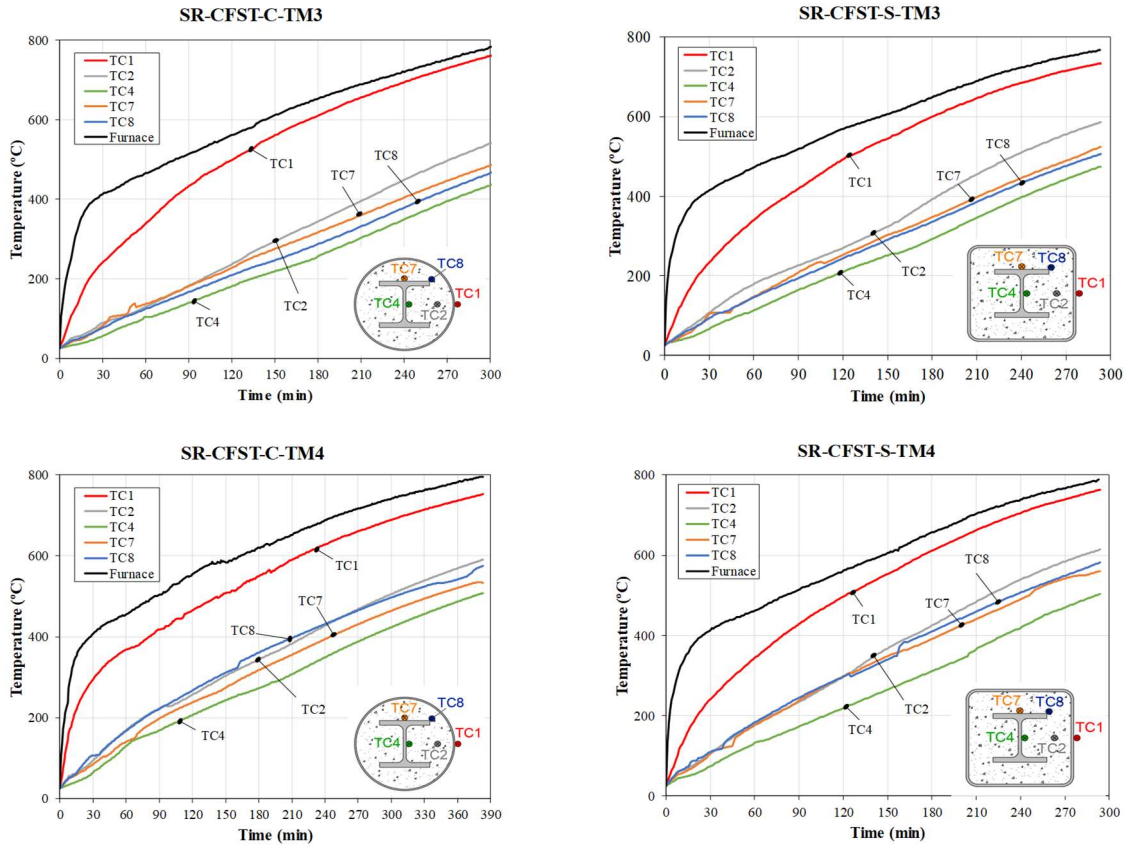
Figure 4.26   Cross-sectional temperatures of a) circular and b) square specimens TM1-TM4.
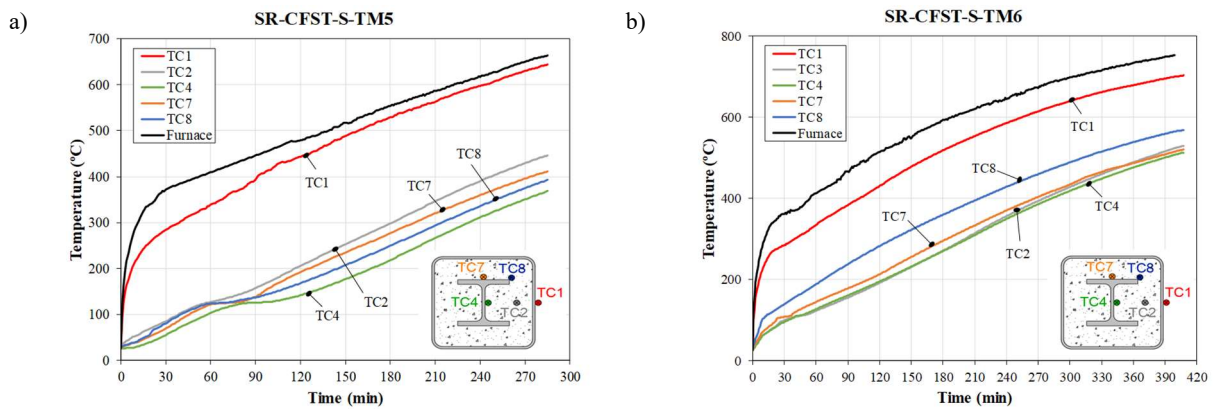
Figure 4.27   Cross-sectional temperatures of square specimens a) S-TM5 and b) S-TM6.

The square SR-CFST specimens registered a high-temperature field compared to their circular counterparts in every case, even in cases CHS-TM0 and SHS-TM0, e.g., by comparing the temperature of the steel tube at 30 minutes. The effect of the section factor may be what causes this increased heating in the square columns. For the same cross-sectional area, this geometry possesses a higher fire-exposed perimeter. Both types of specimens of series TM1-TM4 show a delay in the inner steel profile heating. As a result of the outer steel tube protection and the surrounding concrete, the section heats considerably slower, which retardates its degradation due to fire. By comparing cases CHS-TM0 and SHS-TM0 with any case in the other series, it becomes clear that the heating process is slowed, i.e., at 30 minutes, case CHS-TM0 reaches 400 ºC while in the SR-CFST-C series, this does not occur until 90 minutes of heating.

A similar thing happens when comparing case SHS-TM0 and the SR-CFST-S series. It is worth mentioning that, due to the difference in moisture content of the concrete mixtures, the cases with a higher percentage of water show a higher delay in heating the inner elements of the column. Cases TM1 and TM2 of both geometries show a "valley" at the inner section and concrete temperatures around 100 ºC when the water vaporisation occurs. This occurrence is much less noticeable in cases TM3 and TM4, where there is almost no delay in the temperature rise. The effect of this difference on the mechanical behaviour of the columns will be discussed in chapter 4.3.3.3.

Figure 4.27 shows the temperature evolution of square cases S-TM5 and S-TM6. These cases have a larger section, with a #250x10 mm high-strength steel tube. The increase of the overall column section and the thickness of the outer tube produces a significantly lower heating rate than the other square sections. As discussed, the outer tube provides inbuilt fire protection to the column, delaying its degradation by slowing the thermal conduction along the other internal elements.

4.3.3.2. Failure modes

Figure 4.28 to Figure 4.30 show the final state of the specimens after the performances of the thermo-mechanical tests. As can be observed, the outer tube of the specimens experienced a local buckling in the middle of the section, which was more evident for the hollow tubes CHS-TM0 and SHS-TM0. The square specimens experienced a more noticeable bulge as compared to the circular specimen. In columns TM0-TM4, a change of colour from the characteristic orangey rust to darker red can be observed, due to the changes in the microstructure of the steel when exposed to high temperatures. This is less appreciable in columns TM5 and TM6 probably due to both a difference in the outer steel composition and the lower temperatures reached by the tube in the tests (see Figure 4.30).

Figure 4.28   Hollow columns after the thermo-mechanical tests.

a) Circular SR-CFST sections
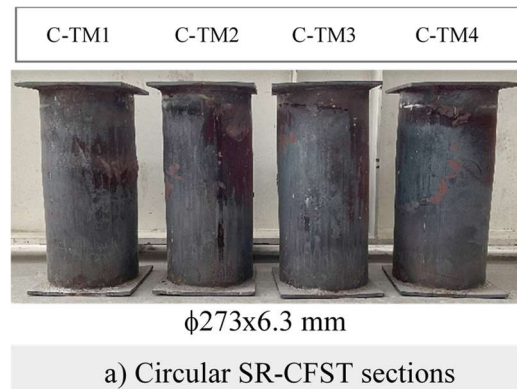
Figure 4.29   Circular SR-CFST columns after the thermo-mechanical tests.
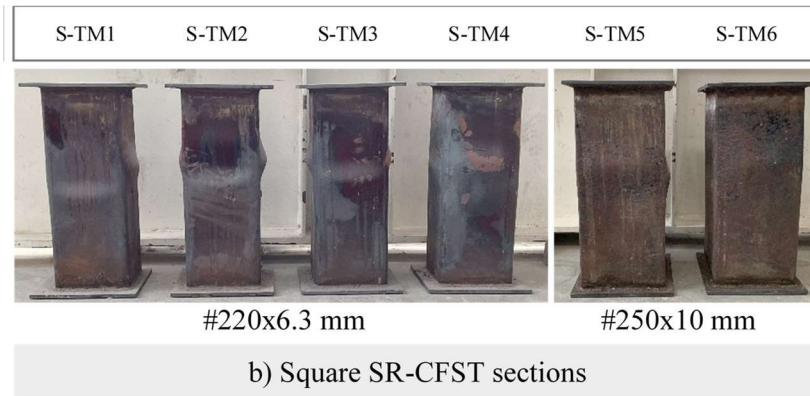
Figure 4.30   Square SR-CFST columns after the thermo-mechanical tests.

The evolution of the axial displacement of the top end of the columns along the duration of the thermo-mechanical tests is displayed in Figure 4.31 to Figure 4.33. As established in EN1363 Section 11.1 (CEN, 2020), a homogenous criterion was defined for determining the failure time of the columns where, for vertical members in compression, failure is established when one of the following two criteria is met:

- Vertical contraction limit: L /100 mm
- Contraction velocity limit: 3 L /1000 mm/min

where h is the initial length of the column. As the test specimens had a length (L) of 600 mm, the vertical contraction limit for the tests was set to 600/100 = 6 mm and the contraction velocity limit to 3·600/1000 = 1.8 mm/min. The hollow tubes test met the velocity criterion first, while all the others reached the vertical contraction limit earlier.

For all specimens, the displacement evolution followed three main phases: initially the expansion of the outer steel tube produced a positive displacement; subsequently, a gradual shortening of the column occurred after the outer tube lost gradually its mechanical properties due to the thermal exposure; and a final stage when eventually the failure criteria established at the beginning of the test is reached.
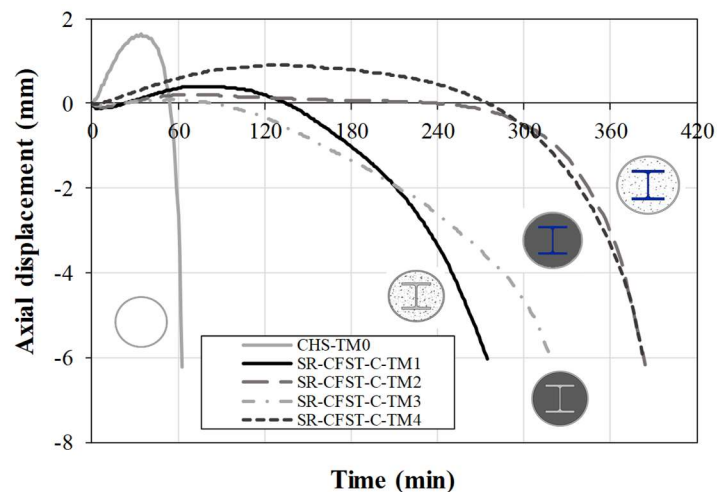
Figure 4.31   Axial displacement versus time curves for specimens C-TM0 to C-TM4.
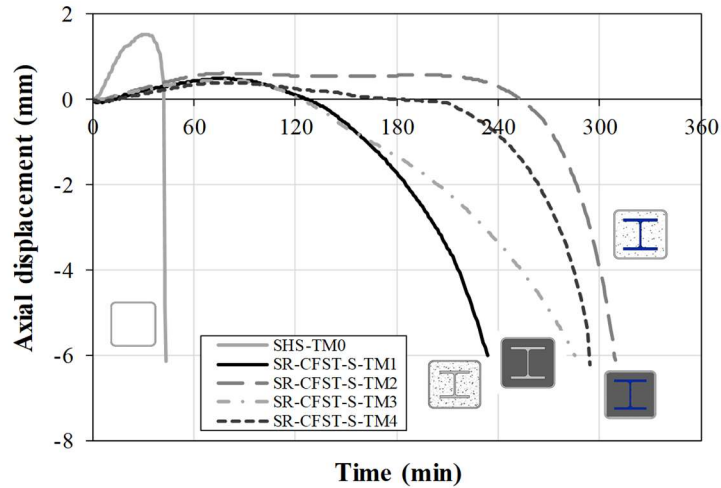
Figure 4.32   Axial displacement versus time curves for specimens S-TM0 to S-TM4.
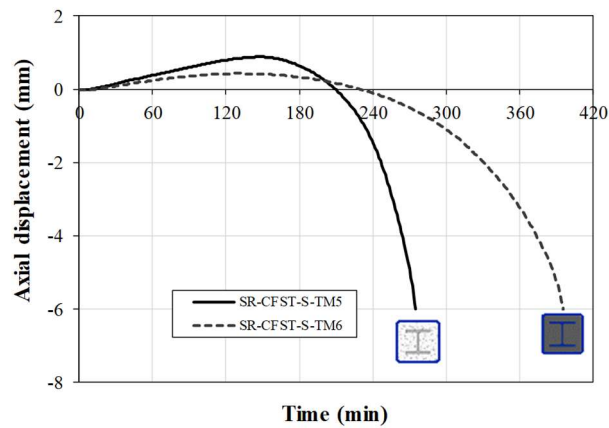
Figure 4.33   Axial displacement versus time curves for specimens S-TM5 and S-TM6.

By observing these time-displacement curves a few conclusions can be extracted. In the first phase, the direct exposition of the outer tube to the heat causes it to expand, and its higher thermal expansion than concrete causes it to support the whole applied load. After the tube has lost some of its mechanical properties due to a higher temperature, the tube descends and passes part of the load to the concrete core and the inner steel profile. The lower thermal degradation of the inner elements due to the higher thermal capacity of the concrete core slows the heating process, enabling the column to sustain the transferred load for a substantial time. After some time, when the degradation of the inner concrete and steel profile occurs, the column loses its capacity to sustain the load and progressively decreases until one of the failure criteria is met.

4.3.3.3. Thermo-mechanical performance

By observing Figure 4.34 it becomes clear that circular specimens performed better than square specimens, enduring the applied load during a longer heating time. The hollow tubes failed earlier and expanded more than the SR-CFST specimens, as expected, not only due to a lower mechanical capacity but because the heating of this specimens was extremely fast as compared to the other sections (refer to Figure 4.25).

In series TM1-TM4 it is possible to observe that the inclusion of high-strength materials extends the failure time of the column as compared to TM1. Moreover, the use of a high-strength embedded steel profile combined with normal-strength concrete (TM2) provides the longest failure time, even higher than its combination with high-strength concrete (TM4). The phenomena can be explained by the moisture content

of the normal-strength concrete as compared to the high-strength concrete (6.28% vs. 2.11%). The higher water content extends the water evaporation plateau in the temperatures field, slowing the degradation of the inner elements of the section and enhancing the thermo-mechanical behaviour of the column. Additionally, this effect may also explain the lower improvement in the failure time when using high-strength concrete (TM3) as its advantage; the high-strength concrete degrades rapidly when the temperature rises.

Regarding specimens TM5 and TM6, although their failure times are higher, considering they possess a bigger and thicker high-strength outer tube, they are lower than estimated. For comparison purposes, they will be associated to specimens SR-CFST-S-TM1 and SR-CFST-S-TM4. FT for specimens S-TM1 and S-TM4 was 239 min and 294 min, respectively; meanwhile, for S-TM5 and S-TM6, they were 275 min and 396 min, respectively. Considering the delayed heating of columns TM5 and TM6 and their wider sections, this limited improvement leads to believe that the outer tube losses its properties rapidly, acting merely as a thermal barrier for the inner components. As it rapidly degrades due to its exposure to high temperatures, the use of high-strength materials in this area is not advisable, as its high-performance material properties will not be taken advantage of. This phenomenon was already observed for double-tube concrete-filled steel tubular composite columns (DT-CFST) by Romero et al. (2017) after a series of fire tests. One of the main conclusions drawn from that study was that, in a fire scenario, a good design strategy consists of designing the column to have the maximum area of steel in the inner part of the section, thermally protected by the surrounding concrete. For this type of section (SR-CFST), this same phenomenon has been observed in the numerical two-dimensional model (refer to section 0).

To analyse the mechanical contribution of the different configurations of materials in the experimental research, a new mechanical ratio is defined: the high-performance ratio (HPR). This ratio will serve to evaluate the advantages of a certain combination of materials as compared to the column with normal-strength materials. This way, the influence of the high-performance materials on the failure time of SR-CFST columns will be assessed. The HPR is calculated as the ratio between the failure time achieved by a column of each series (FT C-TMi or FT S-TMi) with respect to the failure time (FT) obtained for the TM1 column of the corresponding series, as reference (FT C-TM1 or FT S-TM1). Consequently, a value higher than one in the HPR ratio will mean that the contribution is positive, providing a higher FT to the specimen. HPR will only be computed for specimens TM2 to TM4, circular and square, as they share the same cross-sectional dimensions and steel usage area as the reference case TM1.

For circular SR-CFST columns, Eq. 4.14 will be used:

$$\text{HPR}_{\text{Ci}} = \frac{FT_{C-TMi}}{FT_{C-TM1}} \tag{4.14}$$

And for square SR-CFST columns, Eq. 4.15:

$$\text{HPR}_{\text{Si}} = \frac{FT_{S-TMi}}{FT_{S-TM1}} \tag{4.15}$$

The HPR calculate values are included in Table 4.6 and represented graphically in Figure 4.34.

Table 4.6   HPR values for the tested specimens.

Specimen	*FT* (min)	HPR (-)
SR-CFST-C-TM1	267	-
SR-CFST-C-TM2	405	1.52
SR-CFST-C-TM3	317	1.19
SR-CFST-C-TM4	383	1.43
SR-CFST-S-TM1	239	-
SR-CFST-S-TM2	308	1.29
SR-CFST-S-TM3	285	1.19
SR-CFST-S-TM4	294	1.23
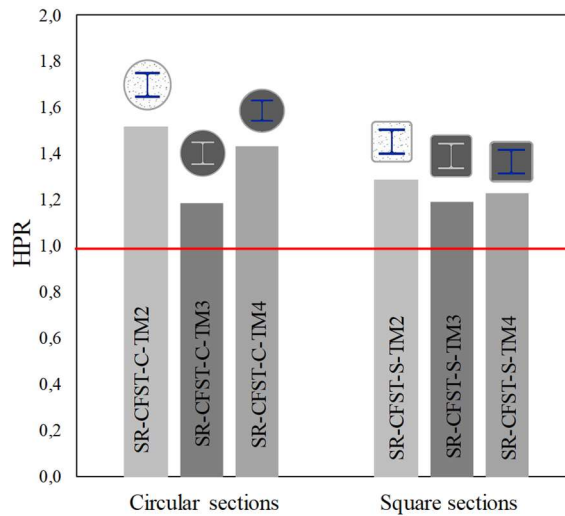
Figure 4.34   HPR for circular and square tested specimens.

The values obtained for the HPR of both series make it clear that designing the section to have the high-strength steel located in the inner steel profile is the most effective way to improve the behaviour of SR-CFST stub columns exposed to fire. This effect is more prominent in the circular sections probably due to their lower section factor, decelerating their heating further.

As previously exposed, in both TM3 cases, the improvement of the column failure time is limited, as the lower moisture content accelerates the heating of the column thus lowering its performance under a fire scenario. This singularity also explains the better behaviour of columns TM2 as compared to TM4, even though the second had been filled with high-strength concrete. It is worth noting that, with the same moisture content for both mixtures, the effect of the high-strength concrete would have been more notable.

An additional calculation is made, regarding the specimens S-TM5 and S-TM6, where the first will be compared to specimen S-TM1 and the latest to specimen S-TM4 as they share the same usage of materials at the inner steel profile and concrete core, even though not at the outer steel profile. Note that specimens S-TM5 and S-TM6 have a 76.38% increase in the sectional steel area and a 25.53% in the sectional concrete area. The HPR obtained for these two combinations is included in Table 4.7.

Table 4.7   HPR values for the square specimens TM5 and TM6.

Specimen	FT (min)	HPR (-)
SR-CFST-S-TM1	239	-
SR-CFST-S-TM5	275	1.15
SR-CFST-S-TM4	285	-
SR-CFST-S-TM6	385	1.35

Considering the greater section, high-strength outer tube and lower load applied in cases S-TM5 and S-TM6 (30% vs. 40% in TM0-TM4), the improvement is scarce and lower than expected. This supports the previous conclusion that placing most of the steel in the inner and thermally protected areas leads to a higher gain in the column thermo-mechanical performance and discourages the use of high-strength steels in the exposed areas as they quickly lose their mechanical properties.

Thanks to the experimentally obtained results analysis, a few conclusions can be drawn about using high-strength materials in SR-CFST stub columns. As has been observed, including these materials in the inner parts of the section (concrete and inner steel profile) leads to an improvement in the thermo-mechanical behaviour of the stub columns. The HSS at the steel profile significantly improved the resistance of the columns in terms of FT. The use of HSS and NSC leads to the best combination of materials in terms of fire performance due to the improved thermal properties of NSC. The HSC improved the ductility of the section, but due to the higher applied load and its reduced water content, the improvement is nuanced. Finally, using HSS at the outer steel tube is not recommended as it rapidly loses its enhanced properties due to being directly exposed to the fire source.

5.

DEVELOPMENT OF THE NUMERICAL MODEL

This section describes the numerical finite element model developed in this thesis. An initial two-dimensional (sectional) thermal model was developed and extended to a thermo-mechanical three-dimensional model. The selection of the relevant properties and parameters of the model are justified through previous research studies and sensitivity analyses. Finally, the thermal and mechanical performance of the model are validated against experimental investigations performed in the framework of this thesis, as well as with available literature data.

5.1. CHARACTERISTICS OF THE NUMERICAL MODEL

5.1.1. Geometry and finite element mesh

Initially, a two-dimensional (2D) finite element model for simulating the thermal behaviour of SR-CFST sections was developed utilizing the general-purpose nonlinear finite element analysis package ABAQUS (Dassault Systèmes, 2021). The use of a 2D model is suitable in this scenario since the primary goal of the numerical model is to evaluate the cross-sectional plastic resistance and flexural stiffness values at the critical section of the columns. In cases of non-uniform fire exposure, this decision may yield conservative results. Additionally, the thermal model used in this case assumes a generalized fire at the compartment (post-flashover) and does not account for localized fires; therefore, the column is assumed to be uniformly exposed along its entire length.

The parameters of the developed 2D numerical model were:

- the column shape (circular or square),
- the outer tube dimensions (D for circular and B for square cross-sections),
- the thickness of the outer steel tube (t)
- the dimensions of the embedded inner profile.

The geometry of the model is comprised of three distinct components - an outer steel tube, concrete encasement, and inner steel profile. Each of these components has been assigned specific thermal properties and interactions between them.

In this analysis, three-node linear heat transfer triangles (DC2D3) with nodal temperature degree of freedom were used for meshing the parts. After conducting a mesh sensitivity study (refer to section 5.2.2.1), it was determined that a maximum finite element (FE) size of 10 mm is appropriate for accurately predicting the cross-section fire behaviour. The assembled and meshed models are included in Figure 5.1.
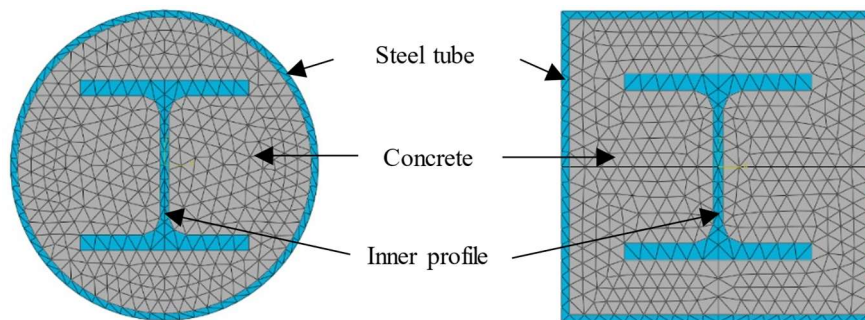
Figure 5.1   Finite element mesh of the two-dimensional model.

After validating and performing a series of parametric studies, the exposed sectional model was extended to a three-dimensional numerical model to simulate the thermo-mechanical behaviour of SR-CFST stub columns under fire conditions. The main properties of this 3D model were:

- the column shape (circular or square),
- the outer dimension (D or B for circular and square columns, respectively),
- the outer tube thickness (t),
- the dimensions of the embedded inner profile,
- the applied axial load level (μ),
- the material properties of both the concrete infill and the inner steel profile.

As the boundary conditions of the columns were not symmetrical, the column was modelled in complete length for the validation process. Two additional parts were added to the model: the upper and lower loading plates (see Figure 5.2). The concrete core and steel profile were modelled as solid objects, while the outer steel tube and the loading plates were defined as shell elements. The shell elements are more accurate in reproducing the local buckling in the outer tube.
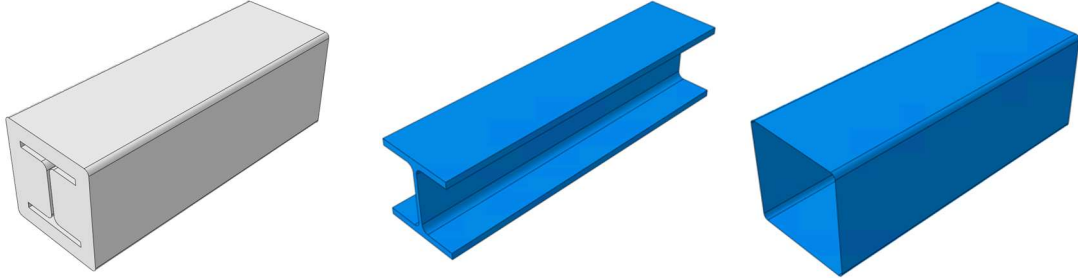
Figure 5.2   Parts of the three dimensional finite element model.

Both loading plates were modelled as perfectly elastic parts and used to transmit the axial load to the rest of the elements of the column. All parts were assembled and assigned their respective material properties, and their thermal and mechanical interactions were defined. Figure 5.3 shows a detailed view of the assembled model.
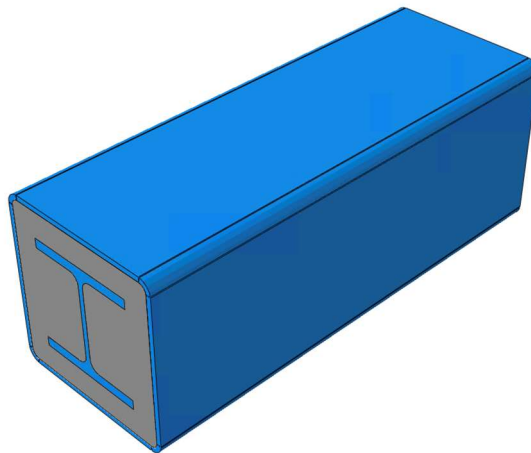
Figure 5.3   Assembly of the three-dimensional finite element model (shell thickness rendered).

For the thermal analysis, the inner steel profile and concrete core were meshed with 4-node linear heat transfer tetrahedrons (DC3D4) with nodal temperature degree of freedom. The outer tube was meshed using 4-node heat transfer quadrilateral shell elements (DS4) with nodal temperature degree of freedom.

In the mechanical analysis, the concrete infill and embedded steel profile were designed with 4-noded linear tetrahedron elements (C3D4), while the outer tube was meshed with 4-noded doubly curved thin shell elements (S4R) with reduced integration. The auxiliary plates were designed as discrete rigid elements with 4-noded 3-D bilinear rigid quadrilateral elements (R3D4).

In the three-dimensional version, the mesh density of the solid elements was set to a maximum element size of 20 mm, while the maximum element size of the shell elements was set to 15 mm. While providing reasonable computing times, these values proved to be accurate enough to predict the behaviour of SR-CFST stub columns adequately. The finite element mesh for an SR-CFST specimen is included in Figure 5.4.
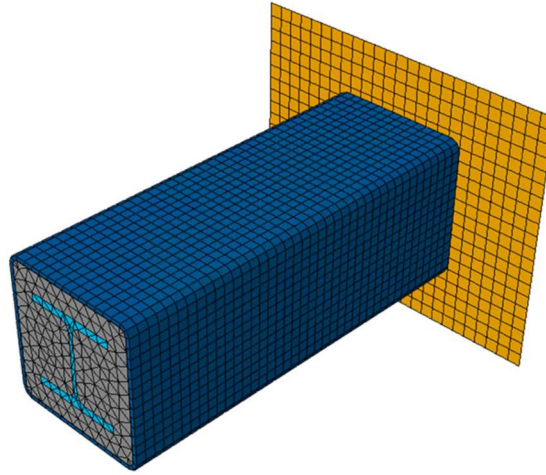
Figure 5.4   Assembly and finite element mesh of the three dimensional model.

5.1.2. Material properties at elevated temperatures

<u>Thermal properties</u>

In the numerical model, the materials were designed with thermal properties that depend on temperature. For steel, the thermal properties, specific heat (c_p), and thermal conductivity (k) specified in EN 1993-1-2 (CEN, 2005b) were used. The thermal properties of concrete at elevated temperatures were taken from EN 1992-1-2 (CEN, 2004b). However, the new method proposed in the draft version of prEN 1992-1-2:2021 (CEN, 2021) was used to model the thermal conductivity. This method recommends transitioning between the upper and lower conductivity limits in temperatures between 140 and 160 ºC. The equations used for this new formulation are included hereafter:

$$\lambda_c = 2 - 0{,}2451(\theta_c/100) + 0{,}0107(\theta_c/100)^2 \qquad \text{for } \theta_c \leq 140ºC \qquad (5.1)$$

$$\lambda_c = -0{,}02604\,\theta_c + 5{,}324 \qquad \text{for } 140 < \theta_c < 160ºC \qquad (5.2)$$

$$\lambda_c = 1{,}36 - 0{,}136(\theta_c/100) + 0{,}0057(\theta_c/100)^2 \qquad \text{for } \theta_c \geq 160ºC \qquad (5.3)$$

To include the latent heat of water vaporization, a peak value was added to the specific heat (cp) calculation of concrete between 100 and 200 ºC, as specified in Clause 3.3.2(8) of EN 1994-1-2 (CEN, 2005c). The concrete was assumed to have a moisture content equal to 4% of its weight, which is the recommended value in Clause 3.3.2(7) of EN 1994-1-2 (CEN, 2005c). This was considered in the specific heat calculation through a peak value of 5577.9 J/kg·K.

<u>Mechanical properties</u>

The mechanical properties of the materials were introduced in ABAQUS (Dassault Systèmes, 2021) with several plasticity models. An isotropic elastic-plastic model with the von Mises yield criterion was used for steel, while the Drucker Prager model was used for concrete. The input parameters for the Drucker Prager model were the friction angle, which was set to 25º, a flow-stress ratio of 0.8 and a dilation angle of 5º.

The constitutive models included in EN1994-1-2 (CEN, 2005c) for the uniaxial behaviour at elevated temperatures were used for the steel and concrete. Thermal elongation was also included in the material definition in the mechanical model as defined in Clauses 3.3.1(1) and 3.3.2(1) of EN1994-1-2 (CEN, 2005c). Regarding the mechanical properties of high-strength steel and high-strength concrete, several sensitivity studies were performed testing the accuracy of available literature models, which will be appropriately discussed in section 5.3.2.

5.1.3. Thermal contacts

To properly simulate the heat flux along the column, a series of thermal contacts should be defined between the different parts of the model. These definitions are presented hereafter.

5.1.3.1. Thermal contacts at the outer steel tube-concrete interface

Under elevated temperatures, the outer steel tube detaches transversely from the inner concrete core, creating a physical space between both materials. This phenomenon appears due to the differences in the thermal expansion coefficients of both materials and is generally addressed as an "air gap". It generates a high thermal resistance between both materials that significantly influences the behaviour of the section, as documented in Espinós (2012).

In ABAQUS (Dassault Systèmes, 2021), the heat flow along a surface interface can be introduced through convection and radiation. The heat transfer is assumed to flow in the normal direction of the surfaces, and the radiation component is not included as, when compared to the conductive component, its effects are negligible (Espinós, 2012). The modelling of the conduction between surfaces in ABAQUS is exposed next.

The conductive heat transfer between the surfaces in contact is given by:

$$q = k(\theta_A - \theta_B) \tag{5.4}$$

where q is the heat flux per unit of area crossing the surface interface from point A (on one surface) to point B (on the other); θ_A and θ_B are the temperatures of points A and B; and k is the gap conductance. This gap conductance can be directly defined in ABAQUS (Dassault Systèmes, 2021) as a function of several variables:

$$k = k(\bar{\theta}, d, p, \overline{f_\gamma}, \overline{|\dot{m}|}) \tag{5.5}$$

where:
- $\bar{\theta} = \frac{1}{2}(\theta_A + \theta_B)$ is the average temperature between temperatures of surfaces A and B,
- d is the distance between surfaces A and B,
- p is the contact pressure transmitted at the A-B interface,
- $\overline{f_\gamma} = \frac{1}{2}(f_\gamma^A + f_\gamma^B)$ is the average of any predefined field variables in A and B, and,
- $\overline{|\dot{m}|} = \frac{1}{2}(|\dot{m}|_A + |\dot{m}|_B)$ is the average of the magnitudes of the mass flow rates per unit area of surfaces A and B.

The gap conductance coefficient k can be modelled in ABAQUS (Dassault Systèmes, 2021) as a function of clearance, contact pressure or both. Several models were studied in the sensitivity analysis which is presented later in section 5.2.2.2. Ultimately, a constant value of 200 W/m²K for the gap conductance between the concrete and the outer tube was fixed, as it was deemed to be the one that provided the most accurate results.

5.1.3.1. Thermal contacts between the inner profile and concrete

As the inner steel profile is embedded in the concrete core at the centre of the section, the heat transmission is assumed to be instantaneous. Therefore, the contact is modelled by assuming a massive gap conductance value (see equation (5.5)) to emulate the direct temperature transmission between the concrete and the inner steel profile surface.

5.1.4. Mechanical contacts

Several contacts were defined between the different parts of the model. A contact interaction property was defined to model the interaction between steel and concrete. The Tangential behaviour of this interaction was defined by a friction coefficient of 0.3, while the Normal behaviour is modelled as a "Hard contact". The interaction between the steel profile and the concrete and the outer steel tube and the concrete is defined with this property. The steel profile and outer steel tube are tied to the lower plate to emulate the welding of the experimental specimens. The same is defined for the outer tube and upper plate. The rest of the contacts between the concrete and steel parts (concrete-lower plate, concrete and steel profile-upper plate) are modelled with the previously defined contact property.

5.1.5. Analysis procedure

Two approaches can be taken when developing a thermo-mechanical model: a sequentially coupled thermal-stress analysis or a fully coupled thermal-stress analysis.

The first type of analysis is used to simultaneously solve the stress/displacement and the temperature fields due to a strong interaction between the mechanical and the thermal solutions of the problem. While this type of analysis gives more realistic results, it is highly non-linear, significantly increasing the computational costs of the simulation. The second type is more simplistic and less time-consuming. It considers that the stress/displacement solution depends on a temperature field, but the dependency is not inverse. Therefore, this type of analysis is conducted in two phases: first, the pure heat transfer problem is solved, and then the temperatures are imported to a stress analysis as a predefined field.

A sequentially coupled analysis is chosen for the model due to the high computational costs of the first approach. Therefore, an initial uncoupled pure thermal analysis of the model is conducted on the model, extracting the temperature field in all the analysed nodes. Then, a stress/deformation analysis is conducted in which the mechanical boundaries are defined, and the obtained temperatures are imported as a temperature field. A schematic representation of the sequentially coupled analysis is presented in Figure 5.5. The suitable results obtained in the validation process further justify the decision to perform a sequentially coupled analysis, therefore reducing the time and computational cost associated with the analysis.
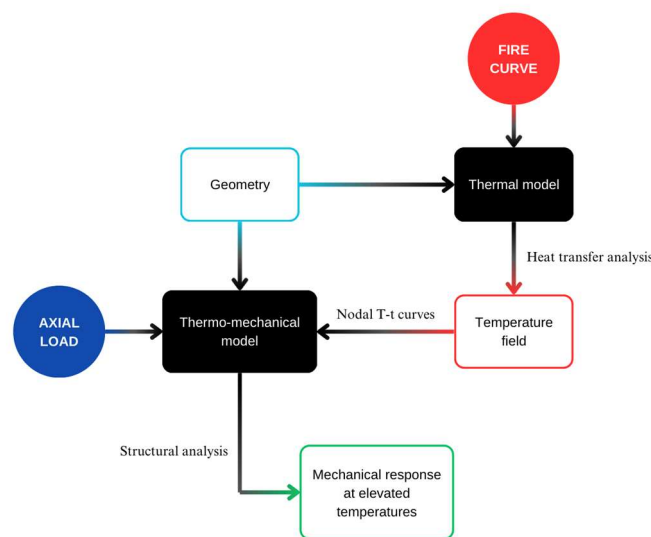
Figure 5.5   Scheme of the sequentially-coupled analysis procedure.

5.1.5.1. Thermal analysis

A non-linear heat transfer analysis was conducted in ABAQUS (Dassault Systèmes, 2021) to compute the temperature field of the modelled SR-CFST stub columns. The thermal actions that must be considered in the heat transfer analysis are stated in Section 3 of EN1991-1-2 (CEN, 2002). These are given by the net heat flux ($\dot{h}_{net}$) to the surface member, the outer wall of the steel tube in SR-CFST sections. On surfaces directly exposed to fire, as the outer tube of an SR-CFST section, the net heat flux ($\dot{h}_{net}$) can be calculated by the addition of the convection component and the radiation component:

$$\dot{h}_{net} = \dot{h}_{net,c} + \dot{h}_{net,r} \ [W/m^2] \tag{5.6}$$

The net heat flux convective component is obtained by computing the difference between the gas temperature and the surface temperature of the member:

$$\dot{h}_{net,c} = \alpha_c (\theta_g - \theta_m) \ [W/m^2] \tag{5.7}$$

where:

- α_c is the coefficient of heat transfer by convection in W/m²K. The coefficient of heat transfer by convection is set to 25 W/m²K when using the standard or external temperature-time curve, to 35 W/m²K when adopting a parametric fire curve and to 50 W/m²K when assuming the hydrocarbon temperature-time curve.
- θ_g is the gas temperature near the exposed member in ºC.
- θ_m is the temperature of the structural member in ºC.

The radiative component of the neat heat flux can be obtained as:

$$\dot{h}_{net,c} = \Phi \cdot \varepsilon_m \cdot \varepsilon_f \cdot \sigma \cdot ((\theta_r + 273)^4 - (\theta_m + 273)^4) \ [W/m^2] \tag{5.8}$$

where:

- Φ is the configurator factor, according to the indications provided in (7) of Section 3.1 of EN1991-1-2 (CEN, 2002).
- ε_m is the surface emissivity of the member.
- ε_f is the emissivity of fire.
- σ is the Stephan Boltzmann constant (=5.67·10⁻⁸ W/m²K⁴).
- θ_r is the effective radiation temperature of the fire environment in ºC. In fully engulfed members, the radiation temperature (θ_r) may be taken as the gas temperature (θ_g) around the member.
- θ_m is the temperature of the structural member in ºC.

For the specific case of SR-CFST composite sections, Section 2.2(2) of EN 1994-1-2 (CEN, 2005c) states that the emissivity coefficient for steel and concrete related to the surface of the member should be taken as $\varepsilon_m = 0.7$. Additionally, the emissivity of the fire is assumed to be $\varepsilon_f = 1.0$.

To conduct the thermal sectional analysis for the validation processes, the characteristic furnace curve was applied to each case at the exterior surface of the outer steel tube of the sections through convection and radiation boundary conditions. The ISO-834 curve (ISO, 2014) was used in the validation cases where no information about the furnace temperature was provided and in all the parametric study cases. It is worth noting that, in the experimental campaign used for the validation of the thermo-mechanical model (see section 4.3), as the temperature distribution along the vertical length of the furnace varied significantly, three exposure areas (lower, mid and upper part of the column) were defined in the validation of the model to adequately simulate the experimental conditions inside of the furnace (see Figure 5.16).

For the parametric studies conducted with this FE model, the exposure was constant along the length of the columns and was set to follow the standard ISO-834 curve (ISO, 2014) as stated in Eurocode 1991 Part 1.2 (CEN, 2002):

$$\theta_g = 20 + 345 \log_{10}(8t + 1) \tag{5.9}$$

where:

- θ_g is the gas temperature in the fire compartment in ºC.
- t is the time in minutes.

The results obtained from the described nonlinear heat transfer analysis are the temperature evolution of all the nodes of the FE model mesh (NT11). These results will then be imported into the thermo-mechanical model to perform the second part of the sequentially coupled analysis.

5.1.5.2. Mechanical analysis

A sequentially coupled thermo-mechanical analysis was conducted; the temperature evolution was retrieved from the previous thermal model, and the results were imported into the mechanical model. This type of analysis requires the thermal field previously calculated and the definition of the temperature-dependent mechanical properties of the materials introduced in the model. This way, each time the temperatures change, the mechanical properties are updated, therefore computing the load-bearing capacity of the column along time until the failure of the column.

The applied load is introduced in the model as a concentrated force applied in the centre of the upper plate. The load is calculated as a percentage of the plastic resistance to compression of the section by adding the plastic resistances of its components as stated in Clause 6.7.3.2 of EN1994-1-1 (CEN, 2004c).

The boundary conditions at each end of the column are modelled as limitations in the displacement and rotation of the model at those points. In the validation (see section 4.3), the columns are modelled as pinned-fixed (P-F) to simulate the experimental conditions at the tests (welded at the bottom, hinge at the top). For the parametric studies, the boundary conditions of the columns are pinned-pinned (P-P).

ABAQUS (Dassault Systèmes, 2021) employs the Newton-Raphson to method solve nonlinear problems. The solution is obtained by gradually applying the specified loads and incrementally working toward the solution. This way, ABAQUS divides the simulation into a series of "load increments" and obtains the equilibrium configuration at the end of each increment. The sum of all the incremental responses is the approximate solution to the nonlinear problem. Further details of the Newton-Raphson formulation can be found in the ABAQUS manual (Dassault Systèmes, 2021).

5.2. SECTIONAL THERMAL MODEL

5.2.1. Validation

5.2.1.1. Validation against available SR-CFST column tests in the literature

The numerical two-dimensional model was validated with experiments available in the literature. The recorded temperature evolution of several experimental fire tests was compared to the thermal distribution obtained by subjecting the model to the same conditions. The specimens used to validate this model were the ones performed by Chu et al. (2016) and Zhu et al. (2016).

The circular and square-shaped specimens 3A and 4A from Chu et al. (2016) investigation were used to validate the temperatures. Section 3A consisted of an outer CHS of 219.1 × 5 mm, while section 4A consisted of a SHS tube of 200 × 5 mm, both with an embedded steel HEB120 section. The concrete infill reported moisture content was 6%. The comparison results between the numerically obtained temperatures and the experimentally recorded ones can be observed in Figure 5.6. Additionally, tests 3B and 4B were included in the validation even though they were thermally protected with intumescent paint.

The experimental program of Zhu et al. (2016) consisted of four square (S1H, S2H, S3H and S4H) and two circular (C2H and C4H) SR-CFST sections. The dimensions of the outer steel tubes were 300 × 300 × 6 mm for the square specimens and 300 × 8 mm for the circular specimens. The inner embedded section was an H-section HW150×150 (150 × 150 × 7 × 9 mm) as established in the Chinese standard GB706-2008 (Chinese Standards, 2016). These columns were subjected to non-uniform fire exposure and consequently, such conditions were replicated in the numerical model. The material used to isolate the specimens in the model was a ceramic fibre blanket with a thermal conductivity of 0.1 - 0.2 W/mºC in the three, two and one-side exposed columns. The reported moisture content was 5%. The results of comparing the calculated and experimentally obtained temperatures at the C4H and S4H specimens is included in Figure 5.7.
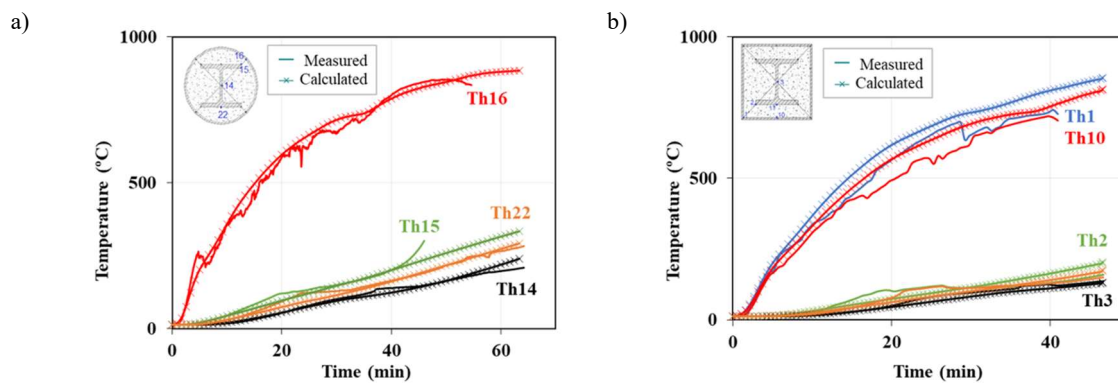
Figure 5.6   Comparison between measured and computed T-t curves for the cases specimens tested by Chu et al. (2016): a) 3A; b) 4A.
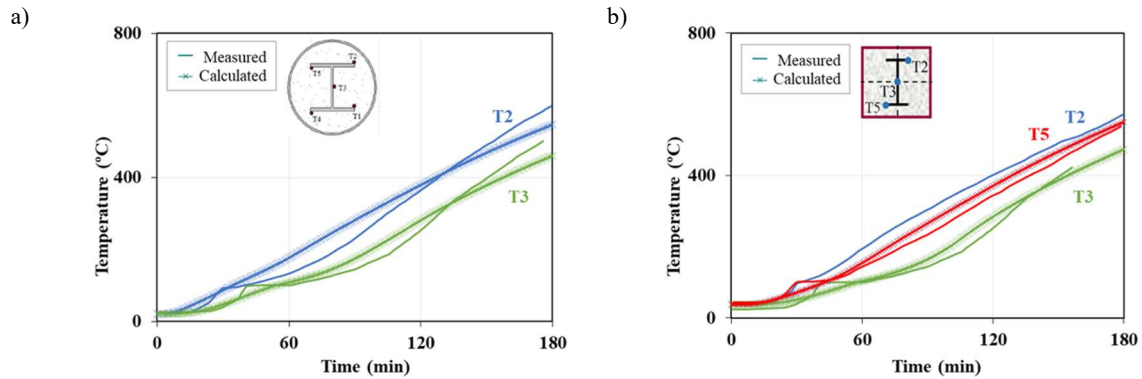
Figure 5.7   Comparison between measured and computed T-t curves for the cases specimens tested by Zhu et al. (2016): a) C4H; b) S4H.

5.2.1.2. Validation against available CES column tests in the literature

As the experimental evidence available in the thermal behaviour of SR-CFST columns is scarce, the validation was extended by experimental campaigns of a different type of composite cross-section: Concrete Encased Sections (CES). These sections consist of reinforced concrete with an embedded steel profile inside and will help to validate and test the thermal response of the model and extend the validation thanks to the similarities between SR-CFST and CES sections. The specimens used in this part of the validation process were extracted from the works of Huang et al. (2008), Mao & Kodur (2011), Han et al. (2015) and Du et al. (2021).

The test specimens RCC03, SZCC03 and SZCC04 from Huang et al. (2008) were tested, which consisted of a square section of dimensions 300×300 mm, 350×350 mm and 400×400 mm respectively. The embedded steel section of the columns was a UC152 $\times$ 152 $\times$ 37 mm, a UC 254 $\times$ 254 $\times$ 73 mm and a UC305 $\times$ 305 $\times$ 97 mm, respectively. The moisture content of the concrete was assumed to be 4%, as no value was provided. The thermal validation for these tests is included in Figure 5.8 and Figure 5.9.

Four sections were considered from the campaign performed by Mao & Kodur (2011): three rectangular sections with outer dimensions of 350×250 mm and a square section with 300×300 mm. The dimensions of the embedded inner profiles were $175 \times 175 \times 7.5 \times 11$ mm for the square section and $200 \times 150 \times 6 \times 9$ mm for the rectangular sections, and the average moisture content obtained at the time of the thermal tests was 5.79%. The numerically predicted temperatures versus the experimentally obtained ones can be observed in Figure 5.10.

A single specimen (SRC1-1) was considered from Han et al. (2015), consisting of a square-shaped section of 300x300 mm and an HW150 $\times$ 150 $\times$ 10 $\times$ 10 mm as the inner profile. Without available test data, the moisture content was assumed to be 4%. The comparison between the temperature evolution of the section and the temperatures obtained from the FE model is included in Figure 5.11.

Finally, a peculiar specimen was validated from the experimental campaign of Du et al. (2021). SRHSC-1 was a square-section column with an embedded inner profile of dimensions $200 \times 200 \times 8 \times 12$ mm filled with ultra-high-strength concrete. Steel fibres with a 0.5% dosage in volume and 0.15% fibres of polypropylene were added to the mixture to improve its ductility and prevent spalling at elevated temperatures. The moisture content stated in the study was lower than 3%. Figure 5.12 shows the temperature field at the thermocouple locations of the section versus the results obtained from the numerical simulation.
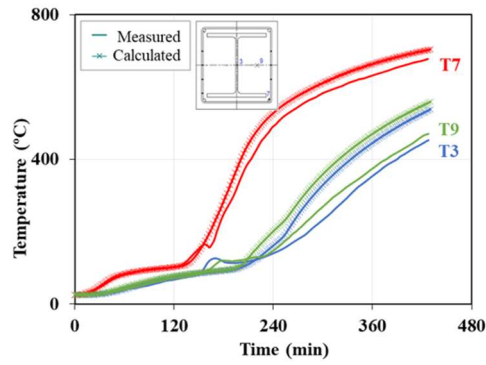
Figure 5.8   Comparison between measured and computed T-t curves at the relevant points of the section for case RCC03 from Huang et al. (2008)

a)

b)
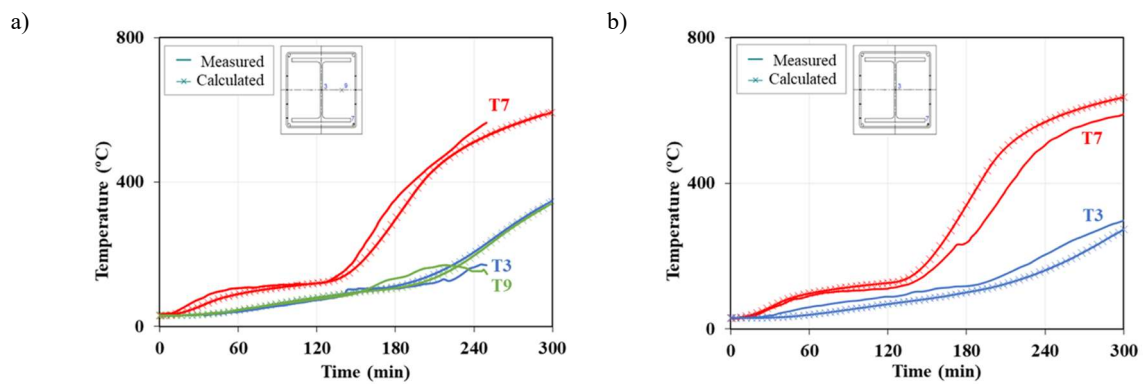
Figure 5.9   Comparison between measured and computed T-t curves for the case specimens from Huang et al. (2008): a) SZCC03, b) SZCC04.

a)

b)
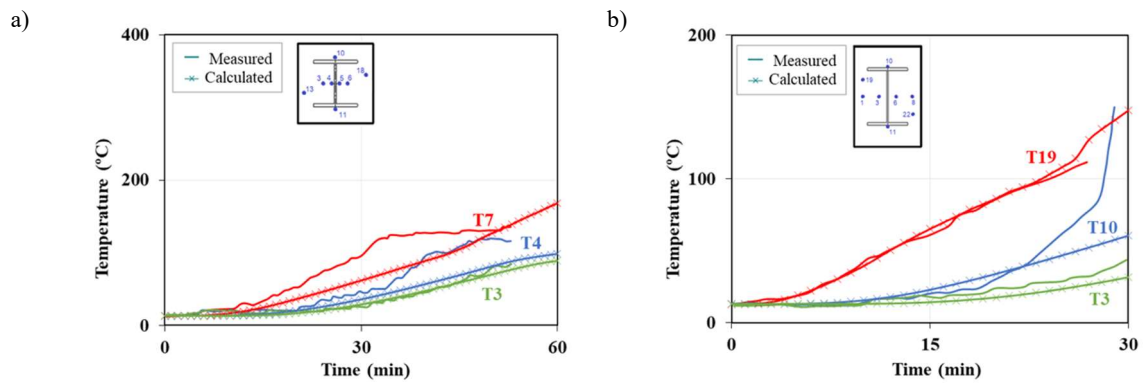
Figure 5.10   Comparison between measured and computed T-t curves for the case specimens from Mao & Kodur (2011): a) FR4S06, b) FR4S38.
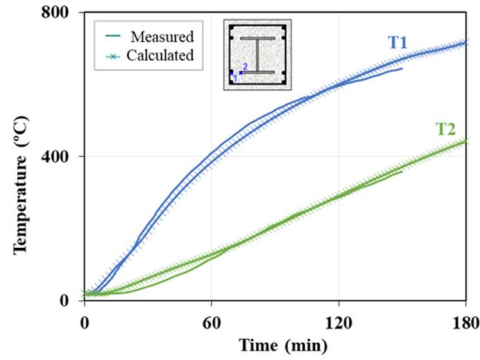
Figure 5.11   Comparison between measured and computed T-t curves at the relevant points of the section for case SRC1-1 from Han et al. (2015).
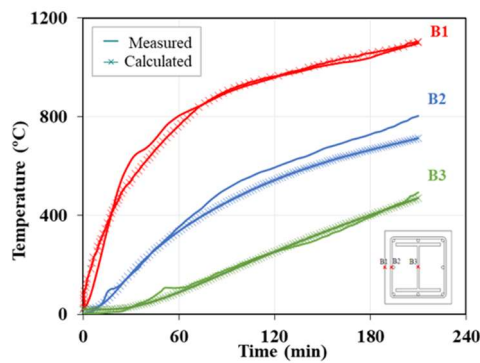
Figure 5.12   Comparison between measured and computed T-t curves at the relevant points of the section for case SRHSC-1 from Du et al. (2021).

5.2.1.3. Summary of the validation

Table 5.1 and Table 5.2 summarize the SR-CFST and CES cases used in the validation of the two-dimensional numerical model, respectively.

Table 5.1   List of SR-CFST columns analysed from the literature.

Specimen	D or B (mm)	t (mm)	f_a (N/mm²)	Inner profile	f_y (N/mm²)	f_c (N/mm²)	Exposure type	Moisture
3A (Chu et al., 2016)	219.1	5	420	HEB120	375	35	4-side	6%
3B (Chu et al., 2016)	219.1	5	420	HEB120	375	35	4-side	6%
4A (Chu et al., 2016)	200	5	510	HEB120	375	35	4-side	6%
4B (Chu et al., 2016)	200	5	510	HEB120	375	35	4-side	6%
C4H (Zhu et al., 2016)	300	8	360	HW 150×150	345	55	4-side	5%
C2H (Zhu et al., 2016)	300	8	360	HW 150×150	345	55	½-section	5%
S4H (Zhu et al., 2016)	300	6	360	HW 150×150	345	55	4-side	5%
S3H (Zhu et al., 2016)	300	6	360	HW 150×150	345	55	3-side	5%
S2H (Zhu et al., 2016)	300	6	360	HW 150×150	345	55	2-side	5%
S1H (Zhu et al., 2016)	300	6	360	HW 150×150	345	55	1-side	5%
C2H (Zhu et al., 2016)	219.1	5	420	HEB120	375	35	4-side	6%

Table 5.2   List of CES columns analysed from the literature.

Specimen	*D or B* (mm)	Inner profile	f_y (N/mm²)	f_c (N/mm²)	Exposure type	Moisture
RCC03 (Huang et al., 2008)	300 ×300	UC152 × 152 × 37	320	43	4-side	4%
SZCC03 (Huang et al., 2008)	350 × 350	UC254 × 254 × 73	320	44	4-side	4%
SZCC04 (Huang et al., 2008)	400 × 400	UC305 × 305 × 97	400	44	4-side	4%
FR4S06 (Mao & Kodur, 2011)	300 × 300	175 × 175 × 7.5 × 11	242.3 - 281.3	40	4-side	5.79%
FR4S38 (Mao & Kodur, 2011)	350 × 250	200 × 150 × 6 × 9	242.3 - 281.3	40	4-side	5.79%
FR3S37 (Mao & Kodur, 2011)	350 × 250	200 × 150 × 6 × 9	242.3 - 281.3	40	3-side	5.79%
FR3S65 (Mao & Kodur, 2011)	350 × 250	200 × 150 × 6 × 9	242.3 - 281.3	40	3-side	5.79%
SRC1-1 (Han et al., 2015)	300 × 300	150×150×10×10	307	38	4-side	4%
SRHSC-1 (Du et al., 2021)	300 × 300	200×200×8×12	380	121.1*	4-side	<3%

* ultra-high-strength concrete with 0.5% steel fibers and 0.15% polypropylene fibers in volume

Furthermore, Figure 5.13 compares the predicted and tested temperatures at the thermocouple locations for all cases, plotted at standard fire exposure times (30, 60, 90, and 120 minutes). Most points of this comparison fall between the ± 15% margins, which signals a good agreement between the model and the real thermal behaviour of the sections.
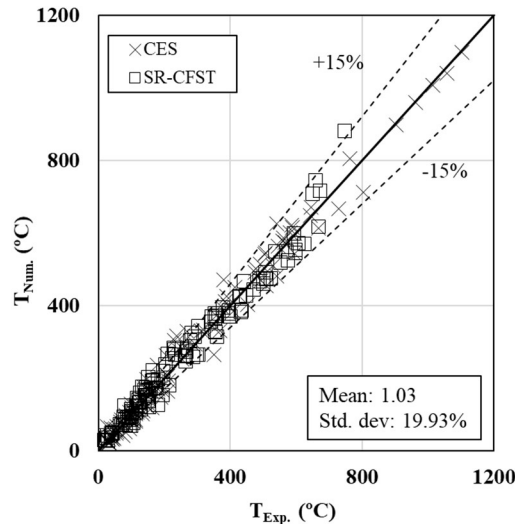
Figure 5.13   Numerically predicted temperatures versus experimental temperatures at the available thermocouple locations for the different cases used for validation

Table 5.3 summarizes the mean and standard deviation values of the temperature comparison between the numerical model and the thermocouple history from the experimental literature. The evaluation of the accuracy has been calculated as $\theta_{num}/\theta_{exp}$, where a mean value greater than 1 implies a conservative approach (the numerical temperature is higher than the experimentally recorded temperature).

Table 5.3   Prediction errors in the validation of the thermal sectional model *($\theta_{num}/\theta_{exp}$)*

Section type	$\theta < 300$ ºC		$\theta > 300$ ºC		All range of θ	
	Mean	Std. dev.	Mean	Std. dev.	Mean	Std. dev.
SR-CFST	1.06	0.30	1.04	0.17	1.06	0.26
CES	1.03	0.26	1.01	0.08	1.02	0.21
All	1.06	0.24	0.99	0.08	1.03	0.20

An average mean value of 1.03 is obtained for all the models with a standard deviation of 20%, confirming the developed model's accuracy and providing a slightly conservative prediction. Additionally, the results have been divided into two groups: temperatures above 300 ºC and below that value to evaluate the concrete evaporation effect on the accuracy of the model. As can be seen, the mean value for the higher than 300 ºC subdivision provides a narrow dispersion (with a standard deviation of 8%) and a mean value of 0.99. In contrast, the evaporation of the water content in the concrete, which takes place between 100 ºC and 200 ºC, affects the precision of the model, as it generates a temperature plateau difficult to replicate. However, the obtained results in this temperature range are primarily conservative, and once the plateau ends, the model is capable of adequately predicting the thermal behaviour of the section.

Considering the wide range of cases and different sections included in the validation of the models and the lack of some critical parameters in some of them, such as the concrete moisture content, the validations are considered sufficient. Therefore, the model is considered reliable for conducting parametric studies on the thermal behaviour of SR-CFST sections, which will be explained and developed in section 6.1.

5.2.2. Sensitivity analysis

5.2.2.1. Finite element mesh size

To select the optimal size of the finite elements in the thermal model and to evaluate the effect of this parameter in the accuracy of the model, a mesh sensitivity study was performed. Three different finite element sizes where compared: 5, 10 and 20 mm.

Specimens 3A and 4A from Chu et al. (2016) experimental campaign were selected to perform this study, to compare the effects on a square and circular section and simulated using each of the mesh densities. The obtained results are included in Figure 5.14.
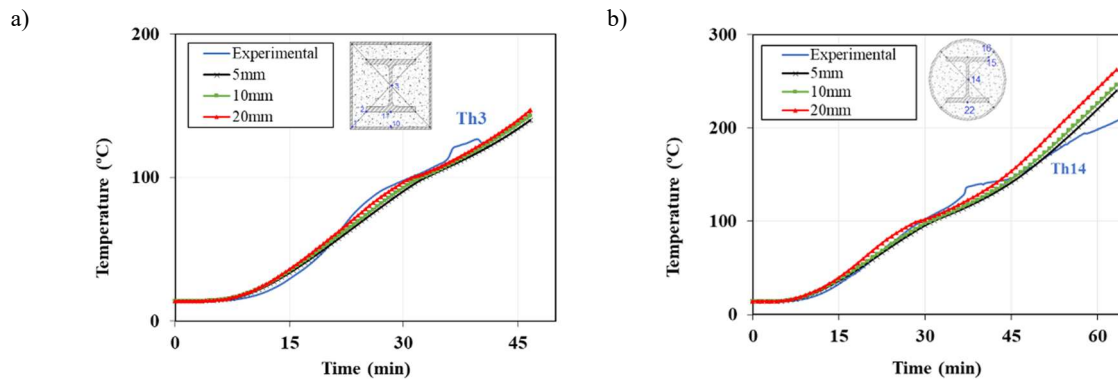
Figure 5.14   Mesh sensitivity analysis. Comparison with Chu et al. (2016) specimens: a) 3A; b) 4A.

As can be observed, a rougher mesh with a greater element size (20 mm) provides significant deviations in the thermally predicted temperatures at the thermocouple locations compared, increasing with the exposure time. The FE sizes of 5 mm and 10 mm provided a better agreement between the numerical and experimental data and were fairly accurate in the temperature prediction. Therefore, a FE size of 10 mm was deemed optimal and selected for the model, as a more refined mesh does not provide increase accuracy and leads to a higher computational cost.

5.2.2.2. Gap conductance

In this section, a sensitivity study regarding the steel-concrete interface between the steel outer tube and the inner concrete will be performed. As exposed in 5.1.3, an "air gap" appears between the two materials when the tube detaches as its temperature increases.

Ghojel (2004) analysed this effect concluding that this phenomenon creates a thermal resistance boundary between the outer tube and the concrete. After conducting a series of experiments, Ghojel proposed an equation to evaluate the thermal conductance at the air gap in both circular and square CFST sections as a function of the temperature:

$$k = 160.5 - 63.8 \cdot \exp(-339.9 \cdot \theta_a^{-1.4}) \ W/m^2K \tag{5.10}$$

where θ_a is the outer steel tube surface temperature in degrees Celsius.

A proposal from other authors was also studied. Tao and Ghannam (2013) suggested a set of expressions to adequately describe the thermal contact conductance, depending on the cross-sectional dimensions of the column.

For circular sections:

$$k = 516 \left(\frac{D}{100}\right)^{-2.373} \ W/m^2K \tag{5.11}$$

and for square or rectangular sections:

$$k = 115 \left(\frac{B}{100}\right)^{-0.85} \ W/m^2K \tag{5.12}$$

where D is the outer diameter of the circular tube and B is the outer side length of a square or rectangular tube in mm.

This model stabilizes at a specific constant value for massive columns (> 300 mm for the outer dimension) equal to 38.1 W/m^{2}K for circular columns and 45.2 W/m^{2}K for square or rectangular columns, indicating that the Tao and Ghannam model considers the air gap effect more prominent in circular sections as compared to square/rectangular ones.

Lastly, a last approach was tested, following the proposal of Espinós et al. (2010), where a constant value of k = 200 W/m^{2}K was taken to simulate the thermal behaviour of the steel-concrete interface in CFST columns.

A summary of the sensitivity analysis results can be observed in Figure 5.15. The numerically obtained temperatures are compared with the experimentally obtained at different thermocouple locations of the section to compare the accuracy of each model.

It can be observed that the temperature predictions of the three models are relatively similar for the three models compared. Nevertheless, in Figure 5.15a, where the temperature of the concrete infill and steel tube interface is recorded, the best prediction is obtained with a constant gap conductance value. The same occurs in the second case (see Figure 5.15b), where the inner steel temperature prediction for the fixed value is the most accurate. Other specimens and thermocouple locations have been studied and concluded the better performance of the fixed conductivity model of Espinós et al. (2010).

a)

b)
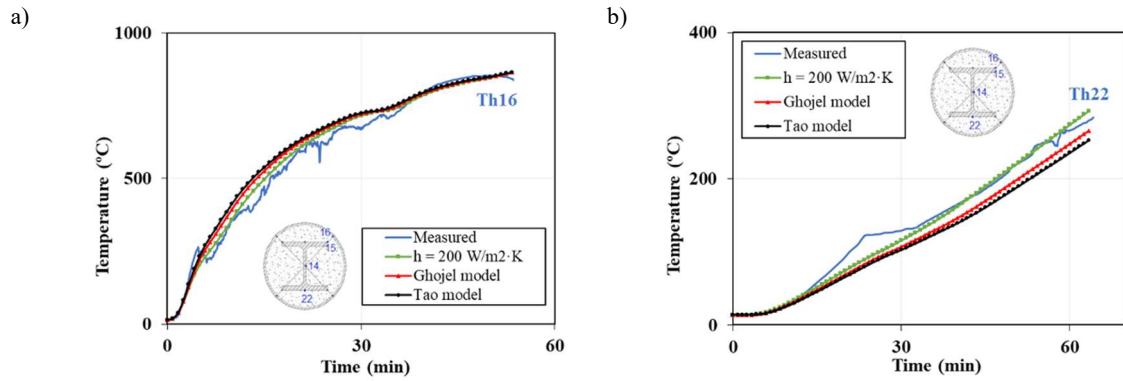
Figure 5.15   Gap conductance sensitivity analysis results. Compared with case 3A by Chu et al. (2016) at thermocouples a) Th16 and b) Th22.

What is more, the Ghojel (2004) model, even though it provides good and similar predictions to the fixed value model, consumes a vast amount of computational time, as the value is recalculated each step as the outer tube temperature rises. Therefore, assuming a fixed $k = 200$ W/m²K, as suggested by Espinós et al. (2010), is deemed to be the optimal case in this study as it provides the most accurate response with a small computational cost associated to it.

5.3. THREE-DIMENSIONAL THERMO-MECHANICAL MODEL

5.3.1. Validation

This section describes the thermal and mechanical validation of the numerical model. The model is validated with available data from the previously described stub SR-CFST thermo-mechanical experimental campaign (see section 4.3).

5.3.1.1. Validation of the thermal response

For the validation procedure, the time-temperature evolution inside the furnace was measured using three thermocouples located at different heights (see section 4.3.2) and modelled accordingly in the numerical model. As the temperature distribution along the vertical dimension of the furnace varied significantly, three temperature exposure zones (upper, middle, and lower part of the column) were modelled in the validation to simulate the experimental conditions properly (see Figure 5.16).
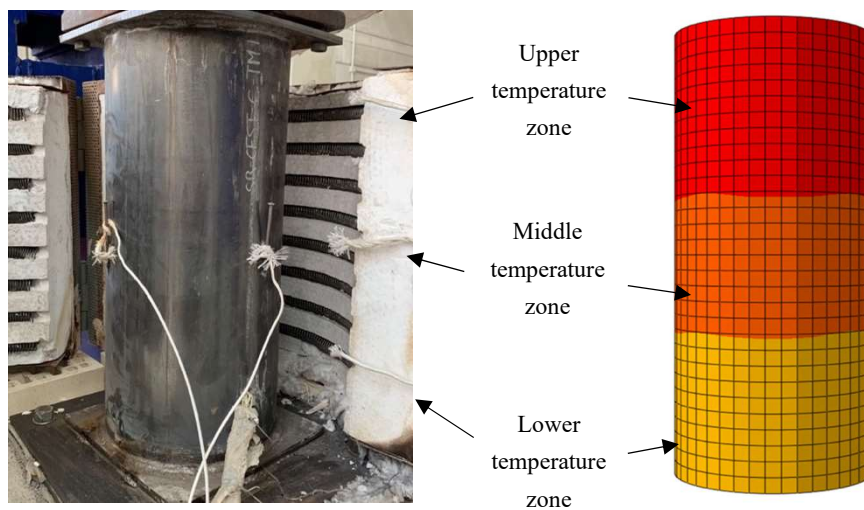
Figure 5.16   Temperature exposure zones included in the FE model as compared to the experimentally measured thermocouples in specimen SR-CFST-C-TM1.

The thermal response of the columns is validated by comparing the temperature evolution obtained with the FE model to the experimental data obtained from the thermocouples. Several thermocouples were placed in the mid-section of the column in different parts: the concrete core, the inner steel profile flanges, and web and the outer tube. The nodal temperature at those positions (NT11) is compared to the recorded temperature evolution of the TCs. The middle cross-section temperature field of the simulated SR-CFST-S-TM1 column can be observed in Figure 5.17 at two standard fire periods (60 and 120 min).
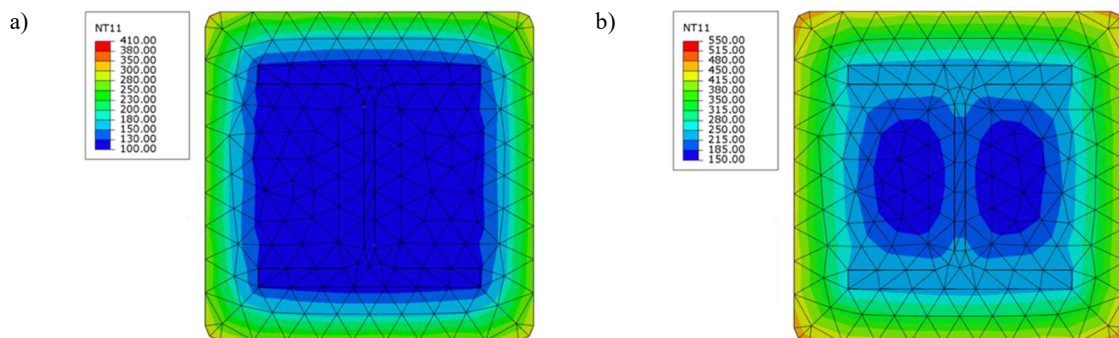
Figure 5.17   Numerically obtained temperature fields of the SR-CFST-S-TM1 (see section 4.3) stub column tested at a) 60 min and b) 120 min.

Figure 5.18 to Figure 5.20 include a comparison between the experimentally obtained temperatures and the numerically obtained ones. Only a few representative thermocouples for each element of the cross-section are included for clarity: TC1 for the steel tube, TC2 for the concrete infill, TC4 for the inner steel profile web and TC7 and TC8 for the steel profile flange.
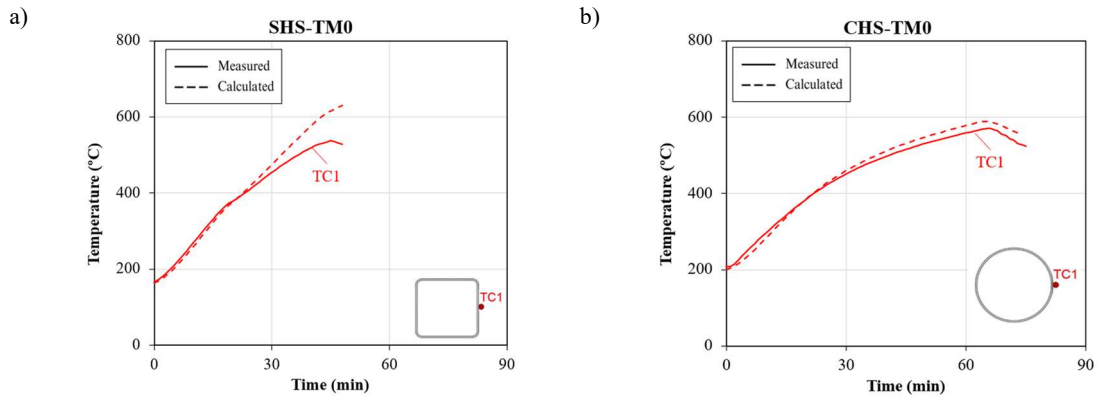
Figure 5.18   Comparison between measured and computed temperature–time curves for the case specimens a) SHS-TM0 and b) CHS-TM0.
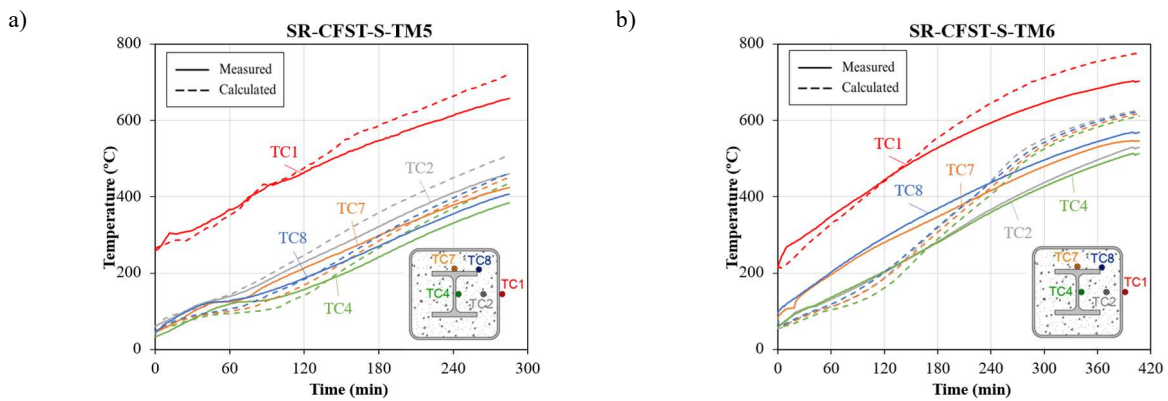
Figure 5.19   Comparison between measured and computed temperature–time curves for the case specimens a) S-TM5 and b) S-TM6.
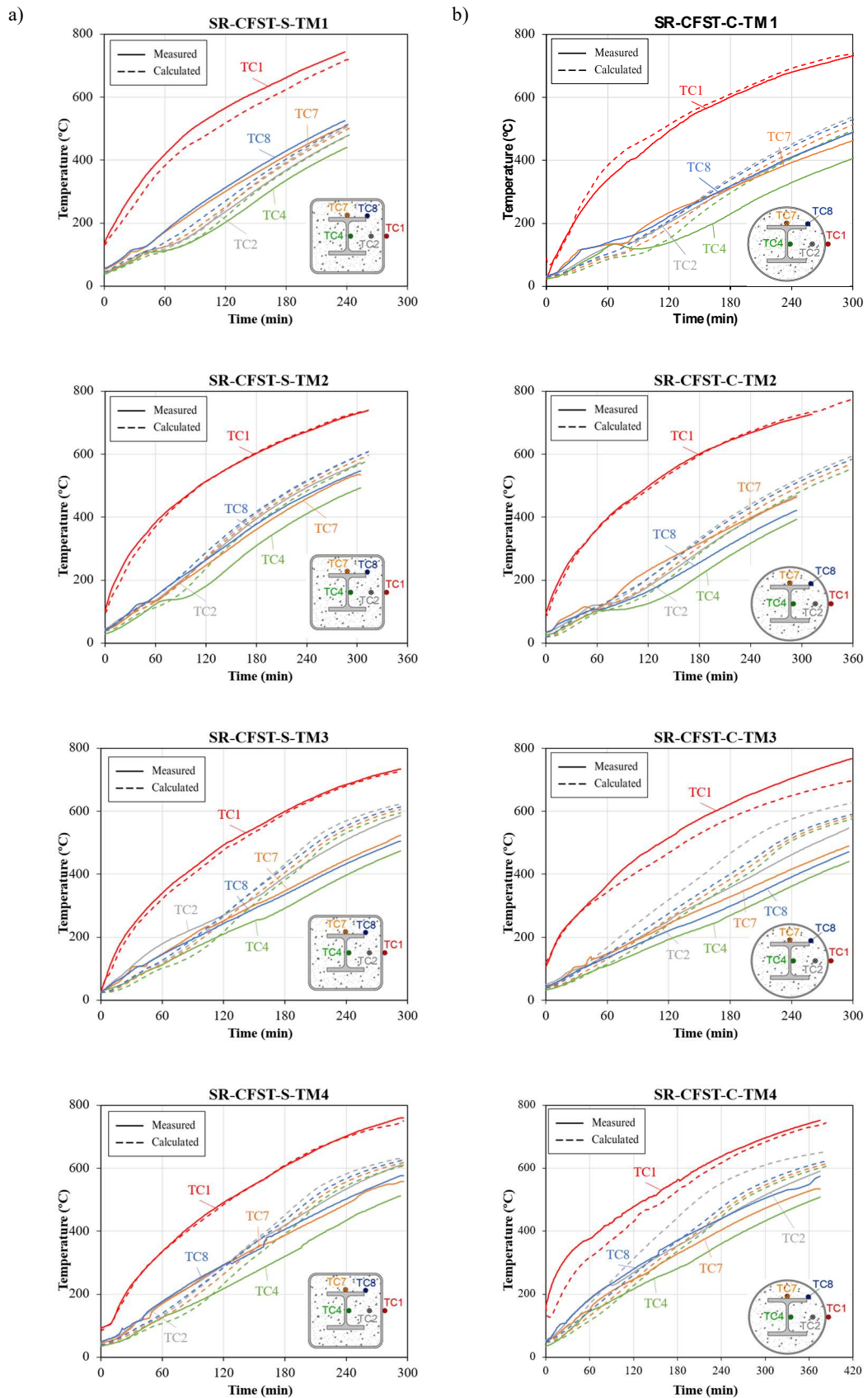
Figure 5.20   Comparison between measured and computed temperature–time curves for a) square and b) circular case specimens TM1 to TM4.

5.3.2. Sensitivity analysis

Before proceeding with the mechanical validation, the following section presents a sensitivity analysis conducted on the use of different formulations to define the mechanical properties at elevated temperatures of high-strength concrete (HSC) and high-strength steel (HSS).

5.3.2.1. High-strength steel mechanical models at elevated temperatures

The investigation of Qiang et al. (2012) presented a series of experimentally obtained coefficients for high-strength S690 steel at temperatures between 20-700 ºC. Li & Young (2017) studied experimentally the material properties of high-strength steel of yield strengths from 690 to 960 MPa exposed to temperatures up to 1000 ºC. The work of Shakil et al. (2020) presented several coefficients for the mechanical properties of S700 MC steel at high temperatures up to 800 ºC. Authors Li & Song (2020) investigated the mechanical properties of TMCP Q690 HSSS at elevated temperatures ranging from 200 to 800 ºC. Finally, as the range of application of EN1993-1-2 (CEN, 2005b) has been extended up to steel grades of S700 with the publication of the EN1993-1-12 (CEN, 2015), it will also be considered in the sensibility study.

The exposed models are tested for specimens SR-CFST-S-TM2 and SR-CFST-C-TM2 in which the inner steel profile was made of high-strength steel while the materials of the concrete infill and steel outer tube remained normal-strength. This way, the influence of the selected steel model can be isolated from the other material variables (see Figure 5.21).

While the coefficients proposed by Qiang et al. (2012) have a good agreement in the S-TM2 case (see Figure 5.21a), they fail to predict the steel behaviour in the circular case effectively (see Figure 5.21b). As can be observed, while all the tested models provide good agreement with the experimental results, the model that gives the most precise simulations is the EN1993-1-2 (CEN, 2005b) formulation. This material model provides the best agreement regarding failure time as in terms of total column expansion and, therefore, will be used in the validation process.
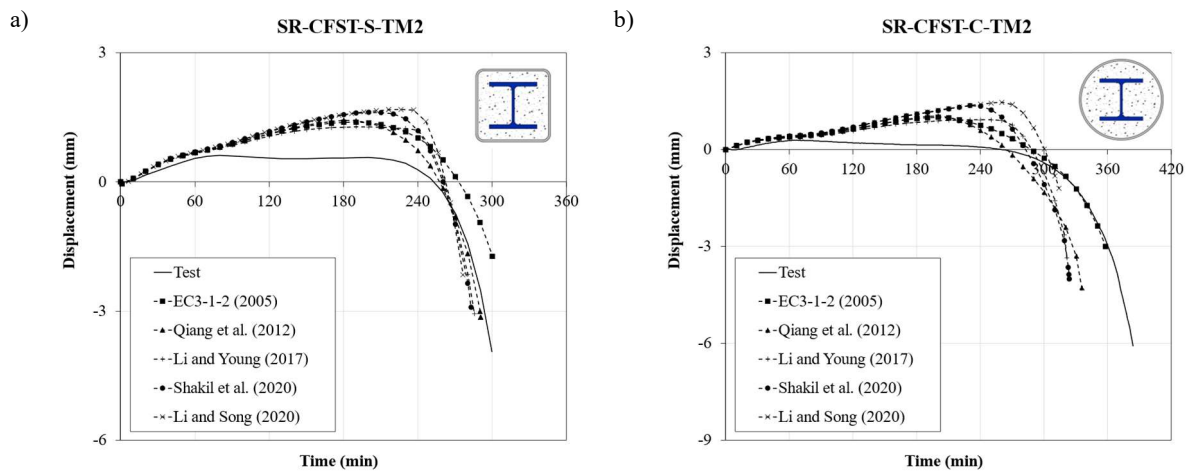
Figure 5.21   Sensitivity analysis on the HSS material models for specimens a) SR-CFST-S-TM2 and b) SR-CFST-C-TM2.

5.3.2.2. High-strength concrete mechanical models at elevated temperatures

Phan and Carino (2003) proposed a series of strength-temperature relationships for high-strength concrete based on the results of several experiments. Other authors, such as Kodur et al. (2004), proposed a numerical model which predicted the behaviour of high-performance concrete (HPC) columns exposed to fire. Several experimental tests were conducted by Matsudo et al. (2008) for HSC specimens at temperatures ranging between 100 and 800 ºC. They proposed a series of mathematical expressions to characterize the mechanical behaviour of HSC. More recently, Aslani and Bastami (2011) developed a constitutive relationship for normal-strength and high-strength concrete exposed to fire conditions, where the compressive and tensile properties of HSC are analysed. Finally, the provisions of EN1992-1-2 (CEN, 2005c) include several coefficients for the mechanical properties of concrete at high temperatures depending on its grade.

A comparison between the previously mentioned high-strength concrete material models is included in Figure 5.22. Experimental columns SR-CFST-S-TM3 and SR-CFST-C-TM3 are tested with the exposed models for comparison purposes, as they are the only specimens with high-strength concrete in the infill with a normal-strength steel inner profile.

The validation of both specimens shows a good agreement of the numerical response when the Aslani and Bastami (2011) material model is used in the HSC. This model does not reduce the mechanical properties of concrete as aggressively as other models, extending its load-bearing capacity further than any of the others. The rest of the models provide a rather conservative response, slightly more precise in the case of the EN1992-1-2 (CEN, 2005c) and Kodur et al. (2004) expressions. Considering the validation of the concrete model, the Aslani and Bastami (2011) proposed coefficients will be used to conduct the validation process. As the EN1992-1-2 (CEN, 2005c) provides conservative and fairly precise results and is the current European normative for HSC, it will be used to perform the parametric studies exposed in section 6.2.
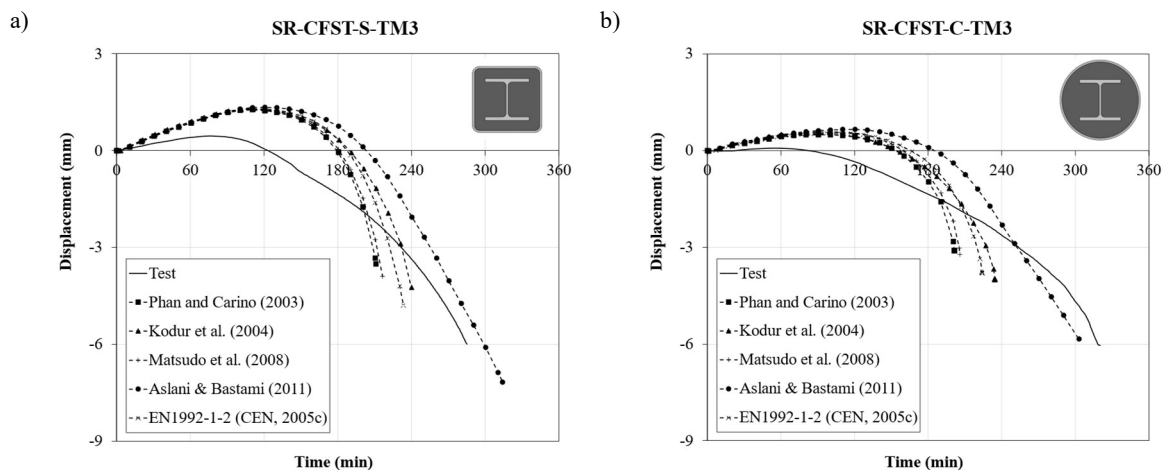
Figure 5.22   Sensitivity analysis on the HSC material models for specimens a) SR-CFST-S-T3 and b) SR-CFST-C-TM3.

5.3.2.3. Validation of the mechanical response

The displacement-time curves obtained from the thermo-mechanical experimental campaign are compared with the ones obtained with the FE numerical model. Figure 5.23 to Figure 5.25 compare the experimental and numerical axial displacement results for the twelve specimens, showing good agreement between the FE simulations and the experiments.

a)

b)
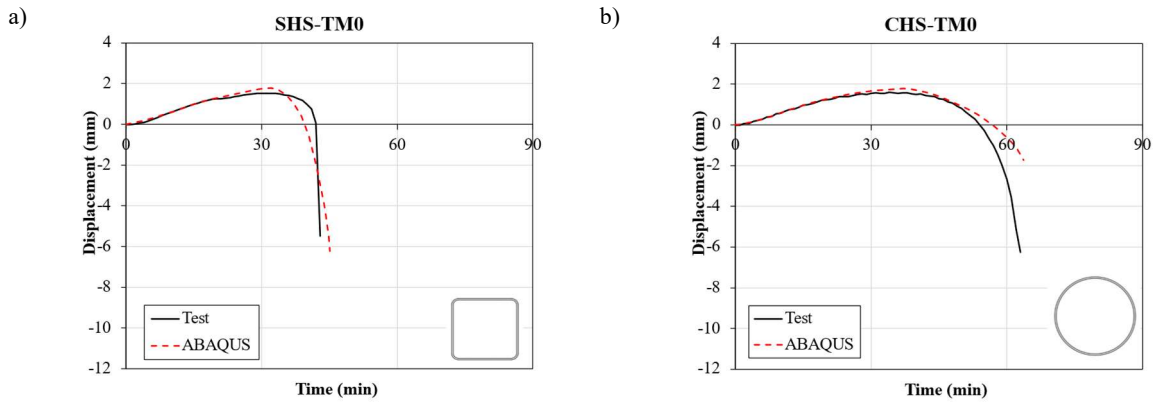
Figure 5.23   Mechanical validation of specimens a) SHS-TM0 and b) CHS-TM0.

a)

b)
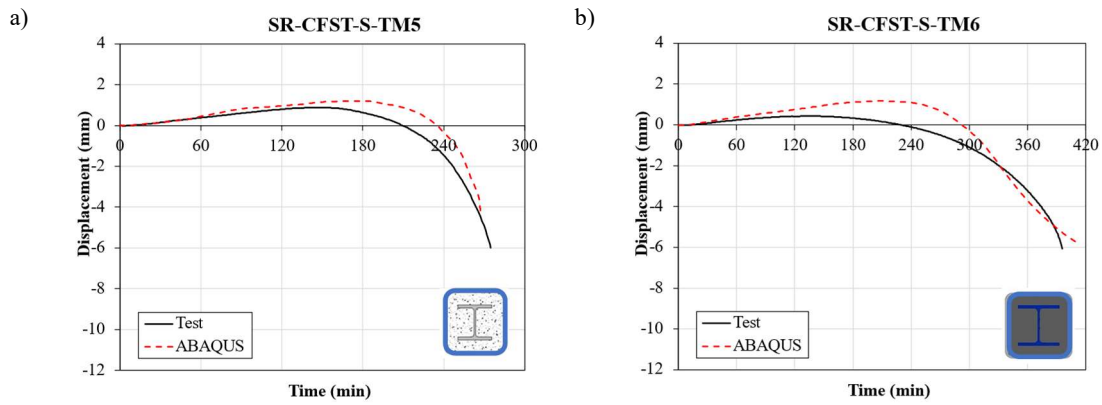
Figure 5.24   Mechanical validation of specimens a) TM5 and b) TM6.

a)

b)
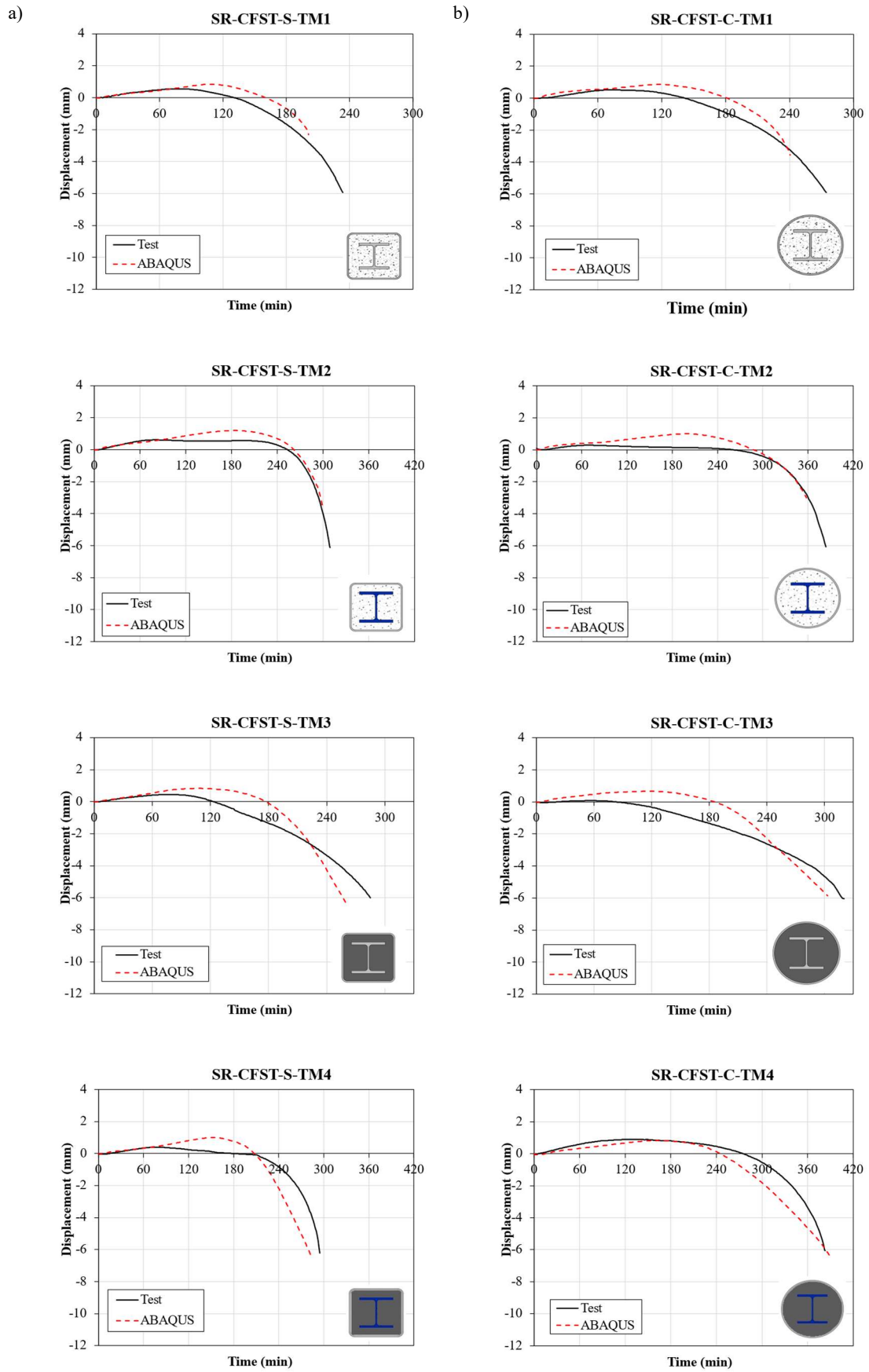
Figure 5.25   Mechanical validation of a) square and b) circular specimens TM1 to TM4.

Additionally, Figure 5.26 compares the experimentally tested tubes and the FE model deformed column shape obtained from the numerical simulation. As can be observed, the model correctly simulates both the failure mode of the column and the bulge location on the outer tube.

a)   b)
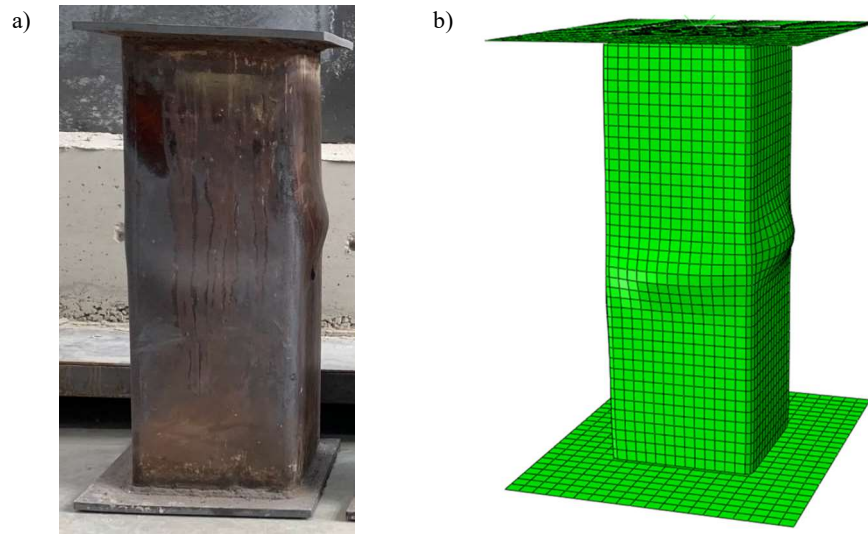
Figure 5.26   Comparison between a) the experimental test results for specimen SR-CFST-S-TM1 and b) the mechanical results obtained with the FE model.

The mechanical response of the columns under fire was validated by comparing the experimentally recorded failure times to the numerically obtained ones. Figure 5.27 plots the numerically predicted FT versus the experimentally obtained ones. Table 5.4 shows the relative error of the numerically simulated cases, FT_{exp}/FT_{num}, in terms of failure time, where values greater than 1 mean a safe prediction and lower than 1 mean an unsafe prediction.

As can be observed in both the figure and the table, an average value of 1.06 and a standard deviation of 6% are obtained, which denotes a good agreement and consistency between the numerically modelled cases and the experimental tests.
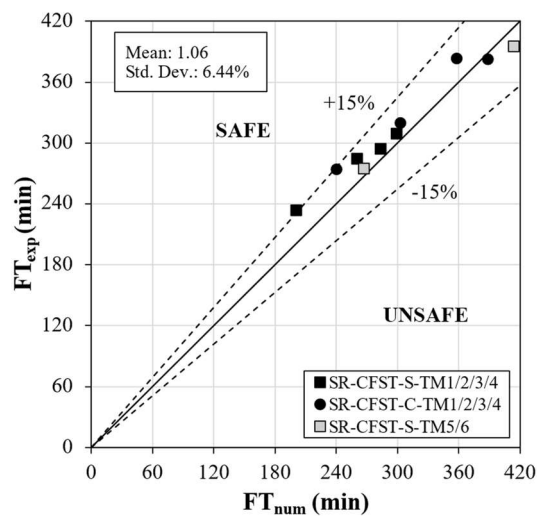
Figure 5.27   Numerically predicted failure times (FT_{num}) versus experimental failure times (FT_{exp}) for the cases used in the validation.

Table 5.4   Comparison between the experimental and the numerically obtained failure times of the validation.

Specimen	FT_{exp}	FT_{num}	FT_{exp}/FT_{num}
CHS-TM0	63.00	63.76	0.99
SR-CFST-C-TM1	274.63	240.53	1.14
SR-CFST-C-TM2	383.80	358.02	1.07
SR-CFST-C-TM3	320.13	303.02	1.06
SR-CFST-C-TM4	382.83	389.02	0.98
SHS-TM0	43.01	45.03	0.95
SR-CFST-S-TM1	233.76	201.01	1.16
SR-CFST-S-TM2	309.27	299.71	1.03
SR-CFST-S-TM3	285.12	260.57	1.09
SR-CFST-S-TM4	294.48	283.81	1.04
SR-CFST-S-TM5	274.89	267.19	1.03
SR-CFST-S-TM6	395.79	414.02	0.96
		Average	1.06
		Std. Dev.	0.06

As has been presented, the developed thermo-mechanical model adequately predicts the fire behaviour of SR-CFST stub columns in terms of temperature evolution and time-displacement response. Therefore, the model is deemed suitable for conducting parametric studies to analyse the effect of several parameters on the fire performance of these composite columns.

6.

PARAMETRIC STUDIES

In this section, a series of parametric studies are conducted, using the previously developed and validated numerical model. Initially, a set of two-dimensional cases will be computed to analyse the thermal behaviour of SR-CFST sections. Afterwards, the thermo-mechanical performance of SR-CFST stub columns will be analysed by modelling a wide range of three-dimensional cases. The effect of different geometrical parameters and the use of high-strength materials over the thermo-mechanical behaviour of these columns in the fire situation will be studied along this section.

6.1. THERMAL PARAMETRIC STUDIES

Based on the previously developed and validated finite element model (Section 5.2), a series of parametric studies are conducted in this section to study the influence of various relevant parameters over the thermal behaviour of the SR-CFST cross-sections under elevated temperatures.

6.1.1. Cases of the parametric studies

A parametric study was conducted using the thermal numerical model described in Section 5. The influence of several parameters affecting the cross-sectional capacity of SR-CFST sections under the fire action was studied. The studied parameters were the external dimension of the outer steel tube (*D* or *B* for circular and square columns, respectively), the outer steel tube wall thickness (*t*), the inner steel profile dimensions and the moisture content of concrete covering a broad range of cases that can be found in practice. Table 6.1 summarizes the cases analysed in this parametric study.

Table 6.1   Summary of the sectional parametric study cases.

a)   **Circular Sections**   b)   **Square Sections**

D (mm)	t (mm)	Inner profile	B (mm)	t (mm)	Inner profile
193.7	4 8	HE100A HE100B	150	4 8	HE100A HE100B
219.1	4 8	HE120A HE120B	175	4 8	HE120A HE120B
273	5 10	HE140A HE140B	220	5 10	HE140A HE140B
323.9	6 10	HE140A – HE180A HE140B – HE180B	260	6 10	HE140A – HE180A HE140B – HE180B
355.6	6 12.5	HE100A – HE200A HE100B – HE200B	300	6 12.5	HE100A – HE200A HE100B – HE200B
406.4	7 14.2	HE120A – HE220A HE120B – HE220B	325	7 14.2	HE120A – HE220A HE120B – HE220B
457	8 10	HE100A – HE180A – HE280A HE100B – HE180B – HE280B	350	8 10	HE100A – HE180A – HE280A HE100B – HE180B – HE280B
508	8 10	HE100A – HE200A – HE300A HE100B – HE200B – HE300B	400	8 10	HE100A – HE200A – HE300A HE100B – HE200B – HE300B

Note: All cases were simulated using a 4, 7 and 10 % of concrete moisture content.

Two sets of cross-section geometries were studied consisting of eight circular geometries in one set and eight square-shaped geometries in the other. To properly compare the circular and square pairs, they were selected from a range of commercially available sections to have a similar cross-sectional area, with a maximum difference of below 2% between each set. Two different outer tube thicknesses were analysed for each geometry: a thinner tube and a thicker one. The outer hollow SHS and CHS sections in this study all met the criteria for non-slender sections stated in EN1993-1-1 (CEN, 2005a), with specimen 508 × 8 as an exception which is classified as Class 4. Different inner steel profiles from the European flange beams catalogue were selected for each geometry for the inner steel profile. Both HEA and HEB sections were embedded in the sections, increasing their dimensions as the tube progressively increased theirs. The wider tubes were tested with two or three profiles in their core as their dimensions allowed them to be embedded inside. In contrast, the narrow tubes were only tested with one profile, given the space limitations within the section. Altogether, 120 cases were generated through the parametric study, 60 cases for each geometry.

Moreover, the moisture content of the concrete infill was modified, testing three different percentages: 4, 7 and 10%, resulting in 360 cases.

The yield strength and compressive strength nominal values were set to 355 MPa and 30 MPa, respectively, even though the mechanical response was not analysed in this numerical investigation. The concrete was considered to have calcareous aggregates regarding its thermal response.

6.1.2. Sectional integration for computing plastic resistance and stiffness

The sections were meshed using triangular elements to conduct the thermal simulation (see section 5.1.1). Thus, the temperature at each node is extracted from the calculated temperature field. Each triangular i-element of the mesh can be characterized by its position (z_i, y_i), area (A_i), temperature (θ_i) - which is obtained by linear interpolation of the temperatures of the three nodes that constitute the element- and by the properties from the material assigned of the region it belongs to: steel tube, concrete, or steel profile. Therefore, the cross-section plastic resistance and flexural stiffness for major and minor axis bending at high temperatures (θ_i) can be obtained from all the mesh cells with the following equations:

$$N_{fi,pl,Rd} = \sum_{i=1}^{n} A_{a,i} \cdot k_{y_a,\theta_i} \cdot f_{y_a} + \sum_{i=1}^{n} A_{c,i} \cdot k_{c,\theta_i} \cdot f_c + \sum_{i=1}^{n} A_{p,i} \cdot k_{y_p,\theta_i} \cdot f_{y_p} \tag{6.1}$$

$$EI_{z,fi} = \sum_{i=1}^{n} A_{a,i} \cdot y_i^2 \cdot k_{E_a,\theta_i} \cdot E_a + \sum_{i=1}^{n} A_{c,i} \cdot y_i^2 \cdot E_{c,sec,\theta_i} + \sum_{i=1}^{n} A_{p,i} \cdot y_i^2 \cdot k_{E_p,\theta_i} \cdot E_p \tag{6.2}$$

$$EI_{y,fi} = \sum_{i=1}^{n} A_{a,i} \cdot z_i^2 \cdot k_{E_a,\theta_i} \cdot E_a + \sum_{i=1}^{n} A_{c,i} \cdot z_i^2 \cdot E_{c,sec,\theta_i} + \sum_{i=1}^{n} A_{p,i} \cdot z_i^2 \cdot k_{E_p,\theta_i} \cdot E_p \tag{6.3}$$

where subscripts *a*, *c*, and *p* correspond to the steel outer tube, the concrete core, and the embedded steel profile, respectively.

The reduction factors for the mechanical properties of concrete and steel at elevated temperatures ($k_{y,\theta}$, $k_{c,\theta}$, and $k_{E,\theta}$) were acquired from EN1994-1-2 (CEN, 2005c). While the concrete secant modulus (E_{c,sec,θ_i}) is not directly specified in the code, it can be obtained as:

$$E_{c,sec,\theta_i} = \frac{f_{c,\theta_i}}{\varepsilon_{cu,\theta_i}} = \frac{k_{c,\theta_i}}{\varepsilon_{cu,\theta_i}} \cdot f_c \tag{6.4}$$

A numerical integration procedure was implemented by means of a Python subroutine and applied to all the cases in the parametric study to obtain the plastic resistance and flexural stiffness of all the columns at different standard fire exposure times.

6.1.3. Analysis of results

In this section, the results obtained from the parametric study are discussed. Figure 6.1 to Figure 6.5 show the different parameters evaluated, most of them compared to the normalized cross-sectional plastic resistance of the columns at high temperatures, referred to their room temperature resistance ($N_{fi,pl,Rd}/N_{pl,Rd}$).

The outer shape, dimensions and thickness of the sections are studied with the cross-sectional slenderness (*D/t* or *B/t* for circular and square cases, respectively). The shape and dimensions of the sections are also analysed by the section factor (A_m/V). In this research, the section factor refers to the exposed perimeter of the section divided by its total cross-sectional area (eq. 6.5 and 6.6). Even though the SR-CFST sections are composite sections, the section factor can be defined with this approach as it is done for concrete-encased sections in Annex G of EN1994-1-2 (CEN, 2005c) and in the new method for CFST columns in Annex H of prEN1994-1-2:2021 (CEN, 2021).

Therefore, the section factor is defined for circular SR-CFST sections as:

$$\frac{A_m}{V} = \frac{P_m}{A} = \frac{\pi D}{\frac{\pi D^2}{4}} = \frac{4}{D} \tag{6.5}$$

and for SR-CFST square sections:

$$\frac{A_m}{V} = \frac{P_m}{A} = \frac{4B}{B^2} = \frac{4}{B} \tag{6.6}$$

The inner profile influence in the thermal behaviour of the SR-CFST columns are studied by a relation between the inner steel cross-sectional area, A_{sp}, and the concrete infill cross-sectional area, A_c. This quotient quantifies the amount of embedded steel in the concrete core of the section.

6.1.3.1. Influence of the outer section shape

Figure 6.1 shows the cross-sectional plastic resistance for the studied columns arranged by their total steel area (profile + steel tube).
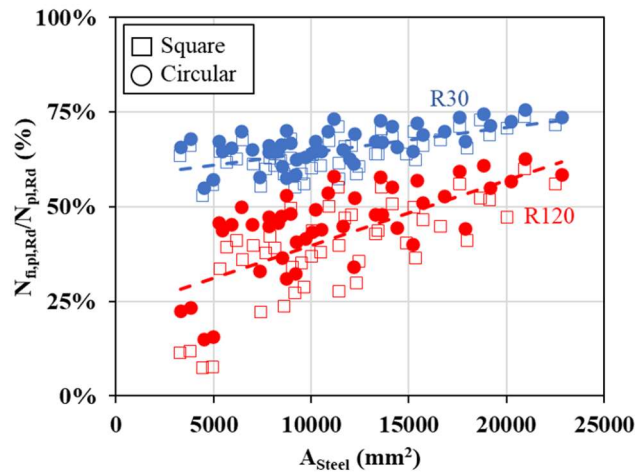
Figure 6.1   Influence of the steel sectional area vs. the cross-sectional plastic resistance of the columns for circular and square sections.

A linear trend can be observed in the graph, enhancing the mechanical capacity of the column as the steel usage is increased. This effect is accentuated as the exposure time is higher, which can be observed comparing the R30 cases against the R120, these last ones having a higher linear slope. Moreover, some differences can be observed between the circular and square geometries, as the circulars tend to have a better fire performance for the same steel usage. This phenomenon is also emphasized at higher fire exposure times.

There are two main reasons for this type of behaviour: first, the circular sections has a lower section factor (A_m/V) which have a positive effect on their thermal performance (i.e., slower temperature rise, therefore less degradation over time), and secondly, the distance between the steel profile and the exposed steel tube inner wall (concrete cover) is lower in the square cases, leading to a higher heating rate for the inner profile. These two particularities lead to a better performance of the circular columns over their square counterparts, increasing the effect as temperatures do.

6.1.3.2. Influence of the outer steel tube thickness

The relation between the cross-sectional slenderness of the columns (D/t) and their cross-sectional plastic resistance is included in Figure 6.2.
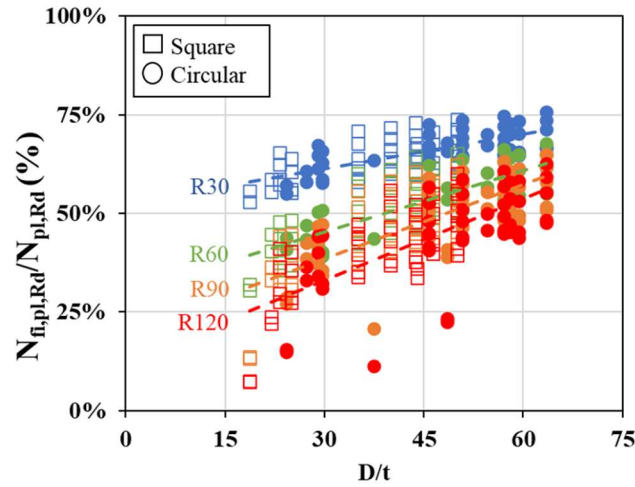
Figure 6.2   Influence of the cross-sectional slenderness (D/t) vs. the cross-sectional plastic resistance of the columns for circular and square sections.

For both circular and square geometries, the correlation is linearly positive, indicating that increasing the D/t parameter is beneficial in terms of fire performance of the columns. As the cross-sectional slenderness rises, the outer steel tube decreases as it gets thinner, allowing for most of the steel to be placed inside of the section at the inner steel profile. As the outer tube is directly exposed to fire without protection, its temperature elevates quickly, losing its load-bearing capacity rapidly. Consequently, reducing the amount of steel in that part and placing it embedded in the section where it is thermally protected both by the outer tube and the surrounding concrete boosts the cross-sectional capacity of the column.

6.1.3.3. Influence of the section factor

The influence of the section factor (A_m/V) is analysed to identify the effect of this geometrical parameter of the cross-sectional fire capacity of the columns (see Figure 6.3).
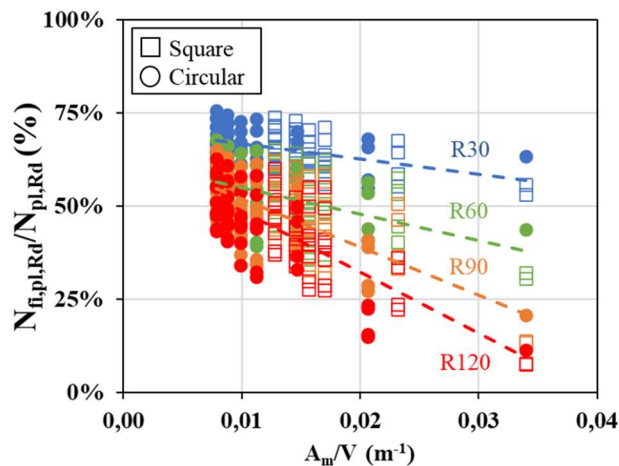
Figure 6.3   Influence of the section factor (A_m/V) vs. the cross-sectional plastic resistance of the columns for circular and square sections.

By definition, the section factor determines the area of the column exposed to the fire related to the heated volume. In this study, as the columns are studied sectionally, the parameter will define the exposed outer steel tube perimeter over the cross-sectional area of the column, providing a good indicator for the influence of the shape of the column in its thermal performance.

The relation between the two parameters is linearly negative. As the section factor increases, the exposed perimeter does so, increasing the heating rate of the column and thus degrading its mechanical properties at a quicker pace. This effect is incremented for higher heating times as the degradation becomes more intense in these scenarios. It is worth noting that, for the same steel usage, the section factor (A_m/V) of the circular columns is lower than that of their square counterparts, therefore clarifying the faster temperature and consequent mechanical degradation of the square specimens.

6.1.3.4. Influence of the dimensions of the inner profile

To analyze the influence of the inner profile steel content, the wider sections were considered as they were modelled with several steel profiles within. The circular 508 × 8 mm case and square 400 × 8 mm case were considered with inner profiles: HEA100, HEB100, HEA200, HEB200, HEA300 and HEB300 and compared in Figure 6.4.
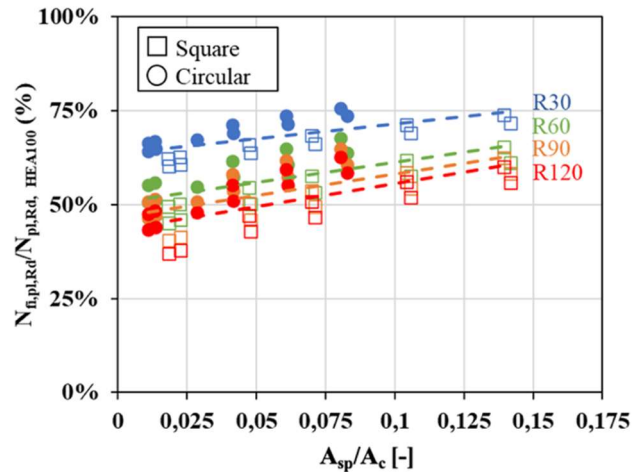
Figure 6.4   Influence of the A_{sp}/A_c ratio vs. the cross-sectional plastic resistance of the columns for sections CHS 508 × 8 mm and SHS 400 × 8 mm.

The results are compared in terms of an increase in the cross-sectional capacity of the specimens as compared to the case with the inner profile smaller area (HEA100). It can be observed that a higher A_{sp}/A_c ratio (therefore, a more significant embedded steel profile) provides enhanced fire resistance for both circular and square sections. Furthermore, the cross sections with an HEB section embedded inside show a better mechanical capacity than the HEA equivalents since the first sections have a higher steel area than the second ones, providing a higher load-bearing capacity than the initial case.

6.1.3.5. Influence of concrete moisture content

The moisture content effect was evaluated by its effect on the cross-sectional plastic resistance of the columns. Figure 6.5 shows this comparison over a circular case, with an outer tube dimension of 193 mm and an embedded HEA100 profile analysed with 4, 7 and 10% moisture content.
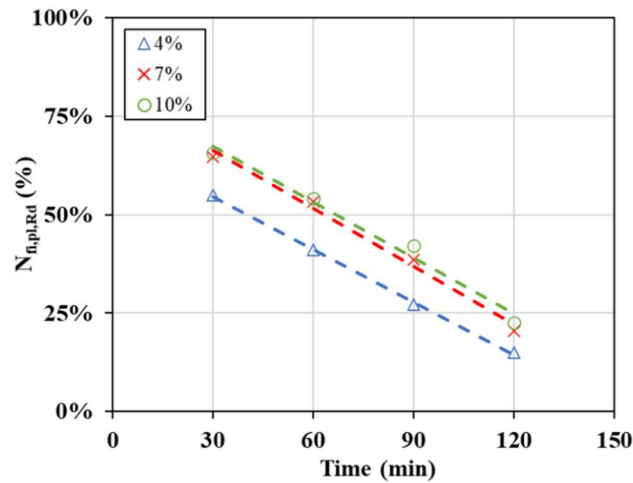
Figure 6.5   Influence of the concrete moisture content vs. the cross-sectional plastic resistance of the columns for circular and square sections.

The rise in moisture content positively affected the mechanical performance of the columns as it decreased the temperature rise in the cross-section. As the water content of the concrete evaporates, a plateau is generated in the temperatures as the thermal energy is used in the evaporation phase of water, which decreases the heating ratio of the inner column elements, slowing their degradation and thus increasing the mechanical capacity of the column. A notable difference can be observed between the 4 % and 7 % models, while at higher contents, the increase is less pronounced.

6.1.3.6. Summary of the parametric study results

Employing the results from the thermal parametric studies, insights about the thermal behaviour of SR-CFST sections were obtained. The circular columns appear to benefit from their shape in terms of thermal behaviour compared to their square counterparts. This is confirmed when analysing the section factor (A_m/V) effect on the section performance. Sections with lesser exposed areas have slower heating, keeping their mechanical properties unaffected for extended periods.

The cross-sectional slenderness (D/t or B/t) and the inner steel profile sectional area (A_{sp}/A_c) positively affect the heating of these sections, meaning that slender outer tubes and greater inner sections have better thermal performance. The moisture content also has a positive effect, delaying the temperature rise in the inner parts of the section due to the latent heat consumed by water evaporation.

These findings will be used in section 7.2 to develop a simplified temperature proposal for characterizing the temperature field of an SR-CFST section at a given standard fire exposure time.

6.2. THERMO-MECHANICAL PARAMETRIC STUDIES

This section conducts a series of parametric studies with the previously developed thermo-mechanical finite element model (Section 5.3). This study aims to analyse the influence of geometrical parameters and the use of high-strength materials on the fire performance of SR-CFST stub columns. The following section was developed during a research stay of the author of this thesis at the Faculty of Engineering and Information Technology of the University of Melbourne (Australia) in collaboration with Professor Tai Thai.

6.2.1. Cases of the parametric studies

An extensive three-dimensional thermo-mechanical parametric study was designed to study the influence of several geometrical and mechanical parameters in the behaviours of SR-CFST stub columns. These studied parameters were the outer dimensions of the SR-CFST section (D for the circular cases and B for the square ones), the thickness of the outer steel tube (t), the inner steel profile dimensions (accounted in terms of the cross-sectional inner steel area over the concrete fill area, A_{sp}/A_c), the load level (μ) and the mechanical properties of the inner concrete core (f_c) and the inner steel profile (f_y). The designed specimens for the parametric study were selected based on the commercially available sections, shapes, and materials. Table 6.2 shows the whole variation of the parameters that resulted in a total of 1440 numerical cases, 720 circular and 720 square shaped, respectively.

All the specimens selected for the parametric studies included slender sections (Class 4 sections) and for all the columns the relation between the area of the inner steel profile and the concrete core was $0.04 \leq A_{sp}/A_c \leq 0.13$. The minimum concrete cover of the steel section is defined to be the distance from the centre of an embedded element (i.e., web or flanges of the steel profile) to the concrete outer surface. It is decided to be $u_s \geq 35\ mm$. Both square and circular cases were designed to have a similar total sectional area of steel with a maximum difference of less than 4%. The boundary conditions of the parametric cases were set to Pinned – Pinned (P-P). The relation between the length of the columns and the outer dimension of the cross-section (L/D or L/B) was set to 1.5.

Regarding the material properties, the concrete core and inner steel profile were designed with multiple material strengths. For the concrete, three different compressive strengths were used in each case: 30, 60 and 90 MPa. Four yield strengths were introduced in each case for the inner steel profile: 275, 355, 460 and 690 MPa. The material combinations between the inner steel profile and the concrete infill are designed to meet the criteria established by Liew et al. (2021), except for the highest strength steel sections (690 MPa), which are incompatible with any concrete mix according to the recommendations of this author. It is worth mentioning that the recommendations are made for CFT sections and not for SR-CFST. The mechanical properties of the steel tube were set to a constant value of yield strength (355 MPa) in all cases.

Table 6.2   Combination of analysis cases for the parametric studies.

CIRCULAR CASES									
D (mm)	244.5		273		323.9		457		508	
t (mm) (D/t)	6.3 (39)	10 (24)	6.3 (43)	10 (27)	6.3 (51)	10 (32)	8 (57)	10 (46)	10 (51)	12.5 (41)
μ	0.3 – 0.5 – 0.7									
f_y (MPa)	275 - 355 – 460 – 690									
f_c (MPa)	C30/37 – C60/75– C90/105									
Profiles (A_{sp}/A_c)	HEB100 (0.07) HEB120 (0.09)	HEB100 (0.07) HEB120 (0.09)	HEB100 (0.05) HEB140 (0.09)	HEB100 (0.05) HEB140 (0.09)	HEB120 (0.05) HEB180 (0.09)	HEB120 (0.05) HEB180 (0.10)	HEB160 (0.04) HEB260 (0.08)	HEB160 (0.04) HEB260 (0.09)	HEB180 (0.04) HEB300 (0.09)	HEB180 (0.04) HEB300 (0.10)

SQUARE CASES									
B (mm)	200		220		260		350		400	
t (mm) (B/t)	6.3 (32)	10 (20)	6.3 (35)	10 (22)	6.3 (41)	10 (26)	8 (44)	10 (35)	10 (40)	12.5 (32)
μ	0.3 – 0.5 – 0.7									
f_y (MPa)	275 – 355 – 460 – 690									
f_c (MPa)	C30/37 – C60/75– C90/105									
Profiles (A_{sp}/A_c)	HEB100 (0.08) HEB120 (0.11)	HEB100 (0.09) HEB120 (0.12)	HEB100 (0.06) HEB140 (0.11)	HEB100 (0.07) HEB140 (0.12)	HEB120 (0.06) HEB180 (0.12)	HEB120 (0.06) HEB180 (0.13)	HEB160 (0.05) HEB260 (0.12)	HEB160 (0.05) HEB260 (0.12)	HEB180 (0.05) HEB300 (0.13)	HEB180 (0.05) HEB300 (0.13)

The moisture content of concrete was assumed to be 4% in all cases, as per Clause 3.3.2(7) of Eurocode 4 Part 1-2 (CEN, 2005c). This way, the comparison between all the cases is based purely on the mechanical differences of the mixtures.

6.2.2. Analysis of results

The parametric analysis results are shown in Figure 6.6 to Figure 6.11, portraying the effect of the studied parameters on the behaviours of the SR-CFST stub columns under fire. The graphs show the studied parameter variation in the horizontal axis compared to the numerically calculated failure time (FT) of the columns in minutes as the vertical axis. The following section describes the effect of the outer steel tube thickness (in terms of the cross-sectional slenderness, D/t or B/t), the section factor (A_m/V), the inner steel profile dimensions (through the A_{sp}/A_c ratio, and the concrete cover, u_s) and the material properties of the concrete and steel. For clarity purposes, the influence of the different parameters was analysed by subdividing the cases into sub-groups depending on their material properties. This way the influence of the studied variable can be isolated from the rest and conclusions can be drawn from the graphs.

6.2.2.1. Influence of the outer tube thickness

The influence of the outer tube thickness is analysed with the cross-sectional slenderness of the columns. As shown in Figure 6.6, this variable has a linearly positive influence on the failure time. This influence is notable at low load levels (30%), reduced in medium load levels (50%) and almost neglected for high-load scenarios (70%).

As the D/t (or B/t) value increases, the outer tube thickness is reduced, increasing the area of embedded concrete. The outer steel tube, directly exposed to the fire source, degrades promptly, losing a significant percentage of its load-bearing capacity. When reducing the area of the outer tube, the protecting

effect of this element still shields the section from heat, and more area of concrete can be introduced, resulting in a better behaviour of the column. This effect is reduced as the load level rises, as in higher load levels, the rapid loss of mechanical capacities of the outer tube transfers a considerable amount of load to the inner parts of the sections, which they cannot bear on their own, not taking advantage of the added thermal protection and failing prematurely.
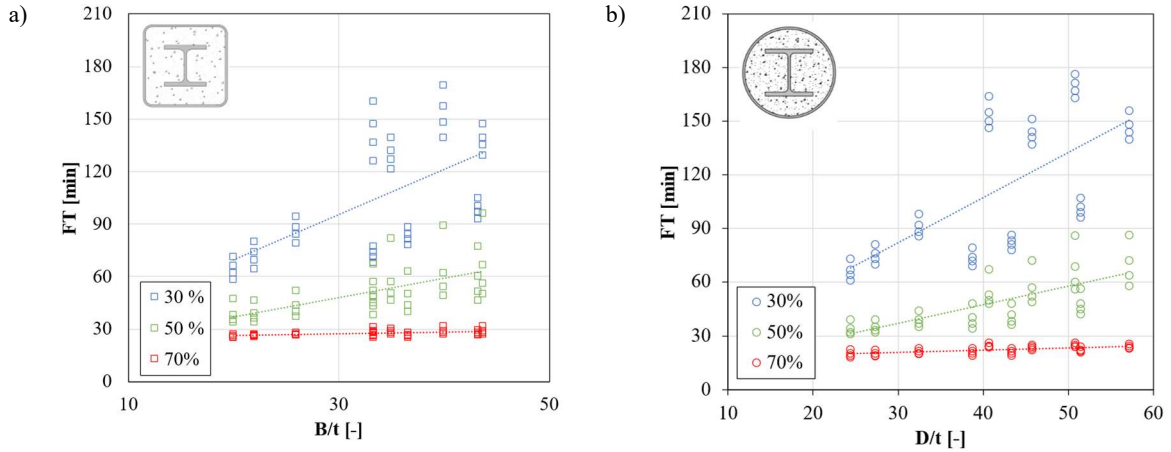
Figure 6.6   Influence of the cross-sectional slenderness (*D/t or B/t*) over the failure time of SR-CFST stub sections with both square and circular sections.

6.2.2.2. Influence of the section factor

The influence of the section factor (A_m/V) of the columns on the thermo-mechanical behaviour of the columns is included in Figure 6.7. The section factor determines the quantity of exposed steel area to the fire source compared to the volume of the member, and it is a good indicator of the influence of the outer shape and dimensions of columns on its fire behaviour. As expected, the relation is linearly negative, as a more exposed area means a higher thermal load and, therefore, a faster degradation of the elements of the column. The influence is heavily relevant at lower load levels (30%), and it decreases as the load level increases. The included graphs are filtered by concrete mixture (C60), but the same relation is obtained in any other combination. Note that, for circular columns, the section factors tend to be lower than their square counterparts, thus resulting in better fire performance and slower degradation of the columns.
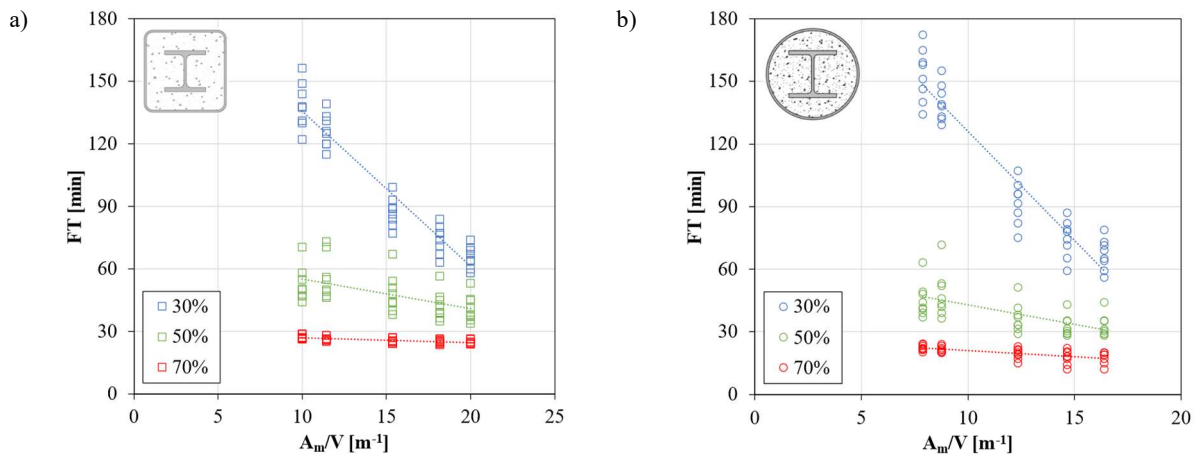
Figure 6.7   Influence of the section factor (*Am/V*) over the failure time of SR-CFST stub sections with both square and circular sections.

6.2.2.3. Influence of the dimensions of the inner profiles

The relation between the steel profile area and the concrete infill area studies the influence of the embedded steel profile dimensions compared to the dimensions of the column. To properly study the influence of this parameter, the cases are compared by filtering them steel profile yield strength (S460).

Figure 6.8 shows a comparison for both square and circular cases in which the A_{sp}/A_c ratio influence on the FT is analysed. When exposed to a fire source, the columns with a lower A_{sp}/A_c quotient appear to have a better behaviour as the inner steel profile is more protected by the surrounding concrete, thus remaining unaffected by thermal degradation for longer. This effect can be more clearly observed in Figure 6.9 in which the concrete cover (u_s) of the inner steel sections is plotted against the *FT* of the sections. As the cover increases, so does the *FT*, therefore improving the mechanical behaviour of SR-CFST stub columns under fire. This effect is enhanced at low load levels and loses importance as the load increases.
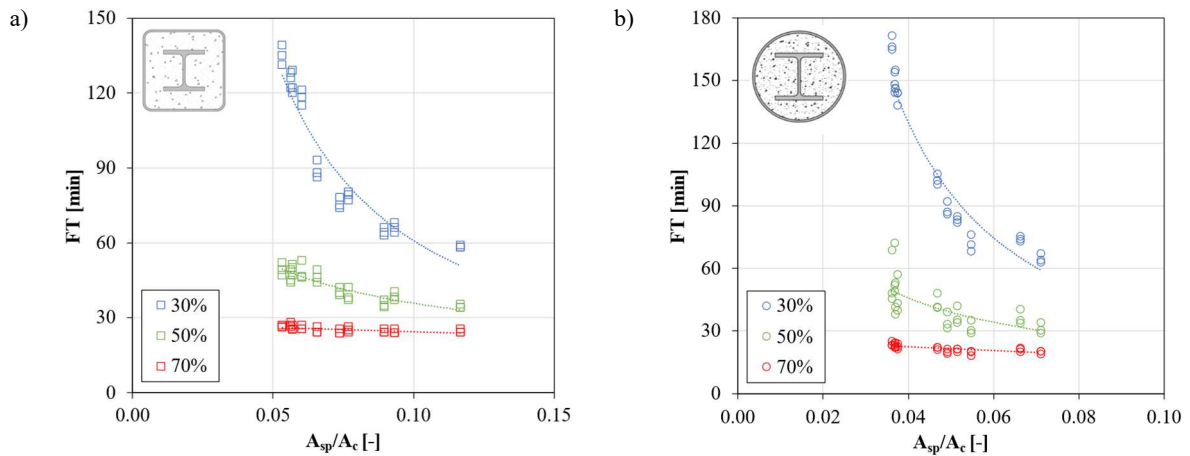
Figure 6.8   Influence of the A_{sp}/A_c ratio over the failure time of SR-CFST stub sections with both square and circular sections.
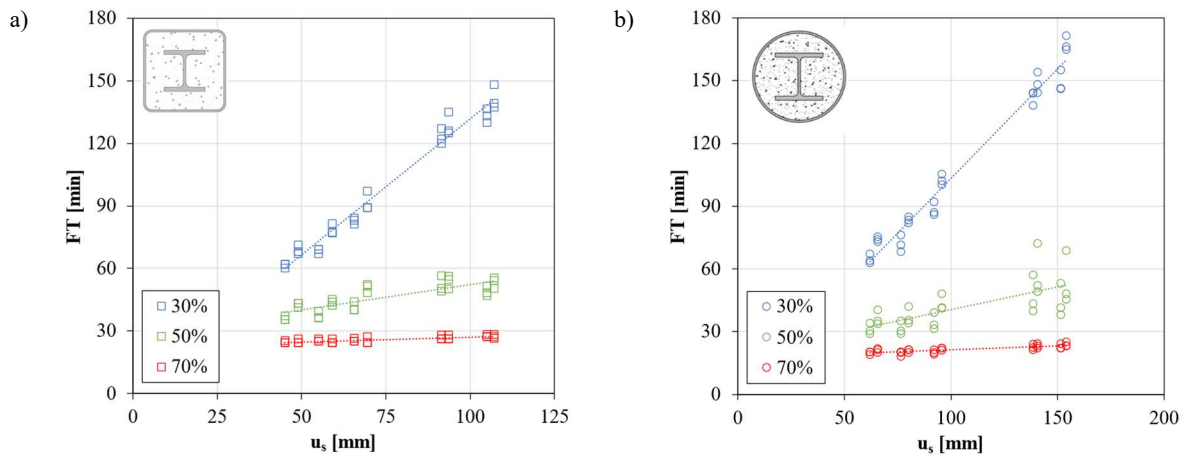
Figure 6.9   Influence of concrete cover (u_s) over the failure time of SR-CFST stub sections with both square and circular sections.

6.2.2.1. Influence of the mechanical properties of concrete

The compressive strength of concrete is studied through several specimens of different sizes and geometries (see Figure 6.10). The influence of this parameter must be analysed, considering the composition of the concrete mixtures and their compressive strength. High-strength concrete has a different mechanical behaviour than normal-strength concrete, having a faster reduction in their mechanical capacity (almost double) at high temperatures (> 600 ºC). Therefore, the added strength of the concrete is balanced by its worse thermal performance, reducing the influence of this parameter on the overall thermo-mechanical behaviour of the column. An example is the better performance of the lowest compressive strength (30 MPa) compared to the mixture with f_c = 60 MPa.

Mixed results are obtained from this analysis of the three studied concrete grades. While in the circular cases, a significant percentage of the C90 cases have a higher failure time than the C90 cases, the opposite happens when analysing the circular cases. This phenomenon may be caused by several factors, a significant one being the faster temperature evolution in the square cases due to a higher section factor than circular ones. This faster heating of the section causes rapid degradation of the concrete, therefore losing most of its load-bearing capacity. High-strength concrete loses its mechanical capacity quicker than normal-strength concrete at elevated temperatures, and this causes the premature failure of most square high-strength concrete sections. The process is reversed in circular columns: the temperature distribution is less aggressive, and the C90 concrete sustains its mechanical properties for longer, therefore bearing the load longer than the C30 concrete. The C60 grade was the least favourable option of the three as it loses capacity faster than the C30 grade, but the concrete strength is lower than the C90.
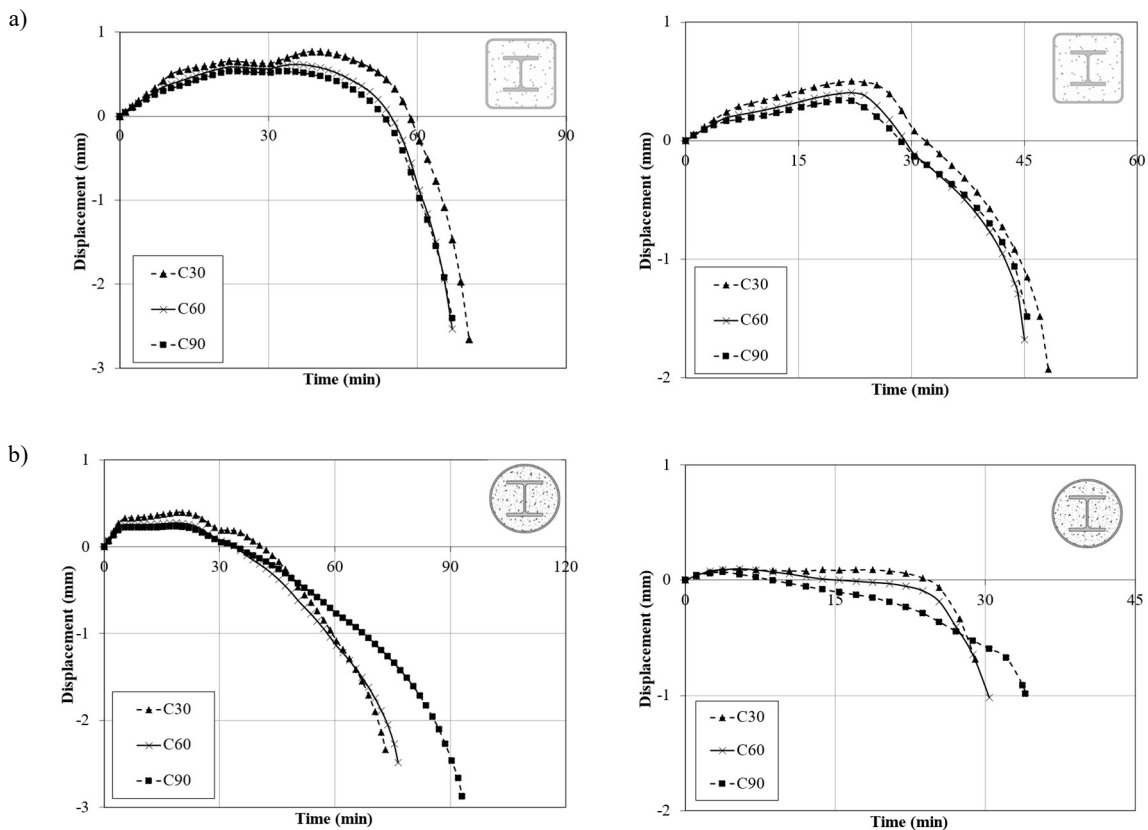
Figure 6.10   Displacement-time curves comparing the three studied concrete compressive strengths of SR-CFST stub sections with both a) square and b) circular sections.

Table 6.3   Influence of the concrete compressive strength on the failure time of the section under fire conditions.

	$FT_{C30} > FT_{C90}$	$FT_{C90} > FT_{C30}$
Square	83.33%	16.67%
Circular	27.08%	72.92%

6.2.2.1. Influence of the mechanical properties of steel

The influence of the steel profile yield strength (f_y) is studied with several sections of different geometries and sizes, as shown in Figure 6.11. The steel grade yield strength positively influences the mechanical performance of the columns, effectively increasing the load-bearing capacity of the SR-CFST columns in all cases. The inner profile is in the inner part of the section, resulting in thermally protected by the surrounding concrete and the outer steel tube. Henceforth, a stronger steel grade in this element provides a higher fire resistance as this profile remains below 400 ºC long, thus retaining all its mechanical capacities.

This effect is most noticeable at lower load ratios and less evident in high-load scenarios. As the application of load-level percentage depends on the room temperature capacity of the columns, the steel profile and its yield strength are an essential factor of the applied load. Therefore, the applied load for cases with high-strength steels is higher than for others. When the applied load is high, the load is transferred rapidly to the concrete and steel profile, rapidly failing, and not having time to benefit from this increase in the load-bearing capacity of the thermally protected section.
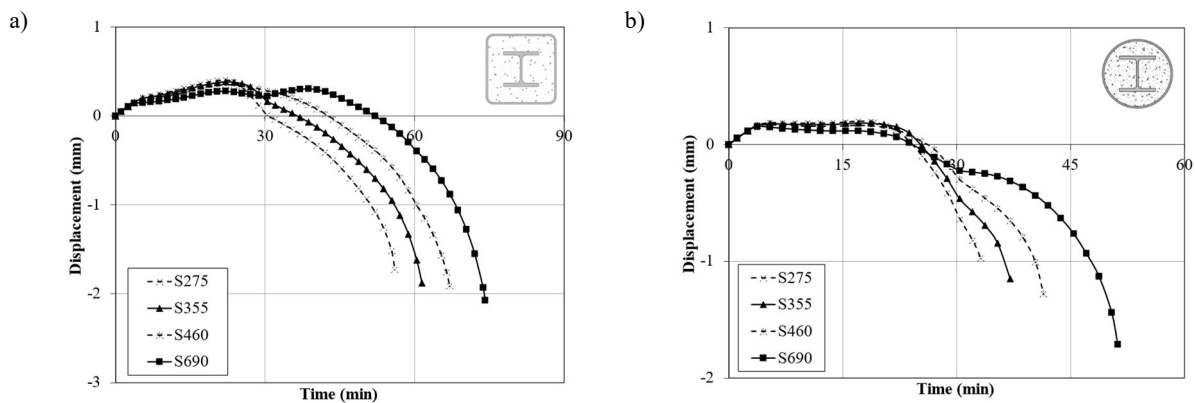
Figure 6.11   Displacement-time curves comparing the three studied concrete mixture compressive strengths of SR-CFST stub sections with both square and circular sections.

6.2.2.2. Summary of the parametric study results

Several conclusions can be drawn from this comprehensive analysis of the parametric study results. The section factor (A_m/V) accelerates the temperature evolution of the section, therefore leading to worse mechanical behaviour. By analysing the cross-sectional slenderness (D/t or B/t) of the columns, it is found that the most beneficial is to reduce the outer steel tube area (thinner tubes) in favour of more quantity of embedded concrete.

The inner profile dimensions affect the fire resistance of the SR-CFST stub columns. Smaller profiles have proven to be a better option in the fire scenario, as they remain unaffected longer and hold their mechanical properties undamaged for a more extended period. This is confirmed by the analysis of the concrete cover factor, having a positive influence in all cases analysed.

When considering the influence of the materials, the use of high-strength steel in the inner profile has been found to positively increase the failure time and the mechanical performance of the columns. The influence of concrete compressive strength is not so favourable, as it depends on the shape of the section. While a higher concrete strength can enhance the mechanical behaviour of the column, its faster degradation at high temperatures reduces its beneficial properties when exposed to fire. High-strength concrete appears to be the better option in the circular cases, while the opposite happens in the square cases.

All these findings will be used to develop a simplified method for predicting the cross-sectional plastic resistance of SR-CFST columns under fire conditions in section 7.3.

7.

DEVELOPMENT OF A SIMPLIFIED CALCULATION METHOD

This section presents the development of a simplified calculation method for obtaining the sectional plastic resistance of SR-CFST stub columns. Initially, an equivalent temperature proposal is developed based on the results obtained from the thermal model to characterize the temperature distribution of the composite section at a given fire exposure time. Next, a proposal is derived to calculate the cross-sectional plastic resistance of SR-CFST columns under fire conditions based on the existing formulation included in EN1994-1-2 (CEN, 2005c).

7.1. REVIEW OF EXISTING DESIGN GUIDANCE

As highlighted in the state of the art review, there is no established method for calculating the fire resistance of SR-CFST columns in the currently available design codes. Even so, the available normative for CFST and other composite sections will be presented hereafter.

The European design code for steel-concrete composite structures, EN 1994-1-2 (CEN, 2005c), includes in its Annex G a simplified temperature model to calculate the fire resistance of composite columns with partially encased steel sections uniformly exposed to fire. In this regard, the research group of the author of this thesis previously proposed an innovative design method (Albero et al., 2016), which was approved by the Technical Committee CEN/TC250/SC4 to be included in the new draft version of Eurocode 4 Part 1.2 (CEN, 2021) in replacement of the current Annex H for CFST sections.

The British design code, BS5950-8 (BSI, 2003), specifies an optional protection for concrete-filled sections depending on its section factor (A_m/V). Additional guidance on the design of these sections is not provided, and it advises following the works of Hicks et al. (2002) and Twilt et al. (1996).

The design code used for composite construction in Australia and New Zealand is the AS/NZS 2327 (Standards Australia & Standards New Zealand, 2014). The code includes tabulated data and a simplified method for concrete-filled hollow sections. It is worth mentioning that the available method in this code is based on the previously commented works by Espinós (2012) and Albero et al. (2016).

In Asia, the GB 50936-2014 (Chinese Standards, 2014) is the primary standard for CFST members. Additionally, a Fujian local standard for CFST, the DBJ 13-15-2003 (Construction Department of Fujian Province, 2003), incorporates expressions for calculating the strength index of unprotected columns in the fire situation or the thickness of the external fire protection, mandatory to achieve a given fire resistance value. The standard for CFT columns in Japan is given in the design guide manual published by the Architectural Institute of Japan (AIJ, 2008).

The AISC Design Guide 19 (AISC, 2003), the National Building Code of Canada (CCBFC, 2005) and the ACI 216 are the available design codes used in North America. The formulas proposed in these codes are based on the ones proposed by Kodur et al. (2000).

7.2. A NEW THERMAL CALCULATION METHOD FOR FIRE EXPOSED SR-CFST COLUMNS

As stated in the previous section, no international code regulations exist to obtain the fire resistance of SR-CFST columns. Based on the findings of the parametric studies exposed in section 6.1, a new method for evaluating the temperature field of an SR-CFST section in fire is developed.

7.2.1. Simplified cross-sectional temperature field proposal for SR-CFST columns

No specific procedure is included in EN1994-1-2 (CEN, 2005c) regarding the obtention of the temperature field in SR-CFST cross-sections, as they are relatively new and innovative solutions originated from CFST sections. In previous works by the research group (Albero et al., 2016; Espinós, 2012), a simplified method for the cross-sectional temperature evaluation was proposed for CFST columns, being approved by CEN/TC250/SC4 and included in the new version of prEN1994-1-2:2021 (CEN, 2021), broadening the application of the international code and providing a simple, yet effective, tool for practitioners. In their work, they proposed a uniform equivalent temperature for the concrete core and the outer steel tube that provided the same fire resistance of the column as using the real non-uniform temperature distribution. This approach was already used in Annex G of EN1994-1-2 (CEN, 2005c) for composite columns with partially encased steel sections.

Following the same approach as that in the new calculation method in prEN1994-1-2:2021 (CEN, 2021), this section aims to obtain a representative equivalent temperature for each element of the cross-section in SR-CFST columns: the steel tube ($\theta_{a,eq}$), the concrete core ($\theta_{c,eq}$) and the inner steel profile web ($\theta_{w,eq}$) and flanges ($\theta_{f,eq}$). The equivalent temperature distribution at their corresponding parts for both circular and square sections is included in Figure 7.1.
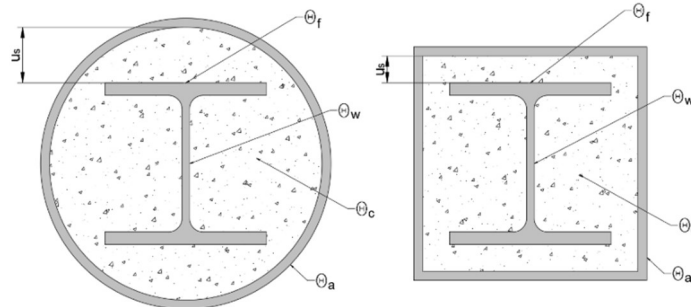
Figure 7.1.   Equivalent temperature distribution for the different parts of the SR-CFST section and geometrical definition of parameter u_s in circular and square columns.

With this approach, the fire resistance of the composite column can be assessed using a single value for the strength and for the stiffness of each component corresponding to the equivalent temperature, significantly simplifying the calculation process. The calculation procedure is conducted following the recommendations of Leskela (2009).

7.2.1.1. Calculation of the equivalent temperature for the outer steel tube

The equivalent temperature of the outer tube at elevated temperatures was obtained directly from the numerical analysis by computing the average value of the temperatures at the inner and outer surfaces, as the temperatures through the steel tube thickness were almost uniform for all standard fire exposure periods.

The previously proposed equation by the research group (Albero et al., 2016), as part of the design method for CFST columns, was tested here to obtain the equivalent temperature of the outer steel tube in the case of SR-CFST columns:

$$\theta_{a,eq} = -824.667 - 5.579R + 0.007R^2 - 0.009R \cdot A_m/V + 645.076 \cdot R^{0.269} \cdot (A_m/V)^{0017} \tag{7.1}$$

The application of this equation produced an average error value of 1.005 for circular specimens with 1.28% standard deviation and 1.021 with 1.26% standard deviation for square specimens. Figure 7.2 includes the predicted and numerically simulated temperatures at the outer steel tube. As can be observed, there is a high correlation between the compared values, which indicates that the formula is also valid for the SR-CFST typology.

In light of these results, the proposed formula is considered accurate in predicting the outer steel tube temperature for SR-CFST sections.
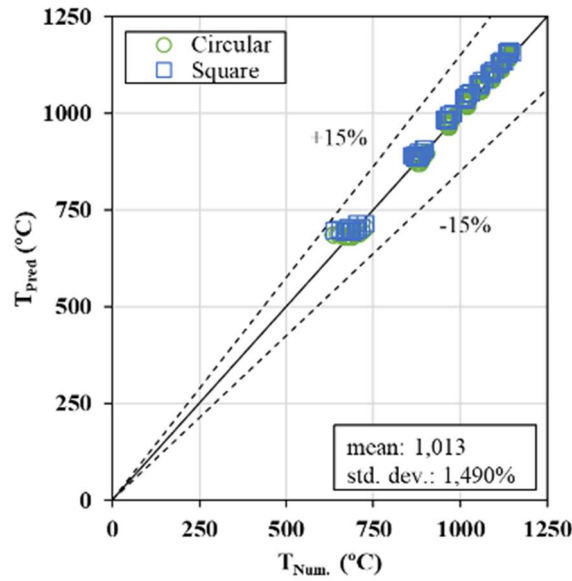
Figure 7.2.   Comparison of equivalent temperature and numerical temperature for the outer steel tube of SR-CFST sections.

7.2.1.2. Calculation of the equivalent temperature for the concrete infill

For the concrete infill equivalent temperature calculation, two approaches are taken: one based on the plastic resistance and the other based on the flexural stiffness of the concrete infill.

a)   Plastic resistance approach

The plastic resistance to axial compression of the concrete at elevated temperatures is defined by:

$$N_{fi,pl,Rd,c} = \sum_{i=1}^{n} A_{c,i} \cdot f_{c,\theta_i} = \sum_{i=1}^{n} A_{c,i} \cdot k_{c,\theta_i} \cdot f_c = f_c \cdot \sum_{i=1}^{n} A_{c,i} \cdot k_{c,\theta_i} \tag{7.2}$$

In order to obtain a single equivalent temperature that provides the same plastic resistance, the reduction factor is isolated:

$$N_{fi,pl,Rd,c} = f_c \cdot \sum_{i=1}^{n} A_{c,i} \cdot k_{c,\theta_i} = k_{c,\theta}(\theta_{c,eq1}) \cdot f_c \cdot A_c \rightarrow k_{c,\theta}(\theta_{c,eq1}) = \frac{\sum_{i=1}^{n}(A_{c,i} \cdot k_{c,i})}{A_c} \tag{7.3}$$

Once this factor is calculated, the equivalent temperature $\theta_{c,eq1}$ for the whole concrete can be obtained through linear interpolation in Table 3.3 of EN1994-1-2 (CEN, 2005c).

b) Flexural stiffness approach (major axis bending)

The flexural stiffness of the concrete core under a fire scenario is calculated as:

$$EI_{z,fi,c} = \sum_{i=1}^{n} I_{z,c,i} \cdot E_{c,sec,\theta_i} = \sum_{i=1}^{n} I_{z,c,i} \cdot \frac{f_{c,\theta,i}}{\varepsilon_{cu,\theta,i}} = \frac{f_c}{\varepsilon_{cu}} \cdot \sum_{i=1}^{n} I_{z,c,i} \cdot \frac{k_{c,\theta,i}}{\frac{\varepsilon_{cu,\theta,i}}{\varepsilon_{cu}}} = E_{c,sec} \cdot \sum_{i=1}^{n} I_{z,c,i} \cdot k_{Ec,\theta,i} \tag{7.4}$$

with $k_{Ec,\theta,i} = k_{c,\theta,i} \cdot \varepsilon_{cu}/\varepsilon_{cu,\theta,i}$.

The equivalent temperature that generates the same flexural stiffness is then obtained through the reduction factor applied to the whole concrete core:

$$EI_{z,fi,c} = E_{c,sec} \cdot \sum_{i=1}^{n} I_{z,c,i} \cdot k_{Ec,\theta,i} = k_{Ec,\theta}(\theta_{c,eq2}) \cdot E_{c,sec} \cdot I_{z,c} \rightarrow k_{Ec,\theta}(\theta_{c,eq2}) = \frac{\sum_{i=1}^{n}(I_{z,c,i} \cdot k_{Ec,\theta,i})}{I_{z,c}} \tag{7.5}$$

In the analysed SR-CFST columns, due to the embedded steel profile, the sections are not symmetric. That is why the same procedure described for the flexural stiffness in the major axis can be calculated for the minor axis following equations (7.4) and (7.5). Then, by linearly interpolating the obtained reduction factors $k_{Ec,\theta}(\theta_{c,eq})$ and $k_{Ec,\theta}(\theta_{c,eq})$ in Table 3.3 of EN1994-1-2 (CEN, 2005c), the equivalent temperatures for the concrete infill with the flexural stiffness procedure are obtained: $\theta_{c,eq}$ and $\theta_{c,eq}$.

Conservatively, the equivalent temperature of the concrete is taken as the maximum of the obtained temperatures with the procedures previously described:

$$\theta_{c,eq} = \max\{\theta_{c,eq1}, \theta_{c,eq2}, \theta_{c,eq3}\} \tag{7.6}$$

After applying this procedure to all the cases in the parametric study, a single temperature equation for the equivalent temperature of the concrete core valid for any standard fire resistance time was developed by means of a multiple nonlinear regression analysis. The main variables included in this examination are the standard fire time (R), the section factor (A_m/V) and the A_{sp}/A_c ratio. The developed equation is included hereafter:

$$\theta_{c,eq} = a_1 + b_1 R + b_2 R^2 + c_1\left(\frac{A_m}{V}\right) + c_2\left(\frac{A_m}{V}\right)^2 + d_1 R\left(\frac{A_m}{V}\right) + e_1 R^{f_1}\left(\frac{A_m}{V}\right)^{f_2} + g_1 R(\frac{A_{sp}}{A_c}) \tag{7.7}$$

where coefficients a_1 to g_1 are dependent on the column shape (circular or square) and are included in Table 7.1. The temperatures predicted by the equation were limited to a plateau of 1200 ºC due to the total loss of structural capacity of concrete beyond this value. As an alternative to the equation, two selection charts were developed as a simple tool for practitioners to use when designing an SR-CFST section and are included in Table 7.4 and Table 7.5. Intermediate values can be obtained via linear interpolation.

Table 7.1   Coefficients for the equivalent temperature of the concrete core $\theta_{c,eq}$(ºC).

	a_1	b_1	b_2	c_1	c_2	d_1	e_1	f_1	f_2	g_1
CIRC	1120,11	-10,14	7,80E-03	-145,94	4,05	1,30	-1,83E-05	1,91	2,84	5,17
SQUA	865,60	-23,88	2,91E-02	-93,38	1,55	5,88	-1,54	1,09	1,20	4,70

Figure 7.3 compares the calculated values with equation (7.7) and the numerically processed temperatures at the concrete core. As can be observed, there is a strong correlation between the two temperatures, proving this equation is valid in predicting concrete thermal behaviour.
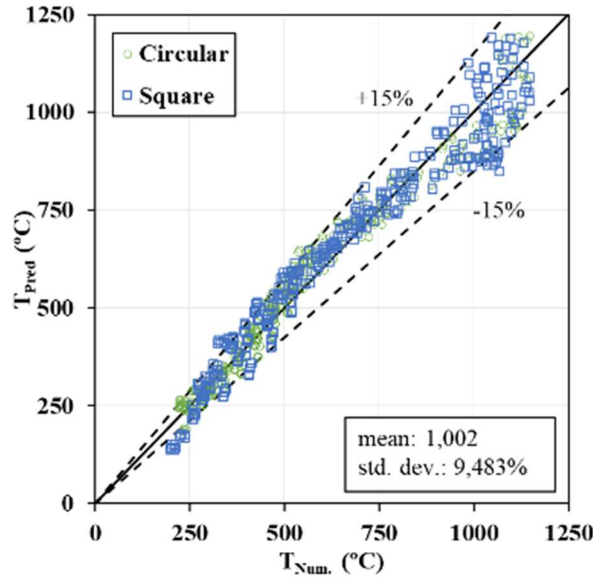
Figure 7.3.   Comparison of equivalent temperature and numerical temperature for the concrete core of SR-CFST sections.

7.2.1.3. Calculation of the equivalent temperature for the inner steel profile

Regarding the equivalent temperature of the inner profile, a significant difference was found between the flange and web temperature distribution. Therefore, two equivalent temperatures are proposed to adequately characterize the embedded steel section: one for the web and another for the flanges.

The procedure to obtain these equivalent temperatures is analogous to the process for deriving the equivalent temperature of the concrete infill. Both the web and the flanges are calculated separately by isolating the cells that correspond to each part of the section.

a)   Plastic resistance approach

The plastic resistance to compression for the inner steel section under the fire situation can be obtained by the following equations:

$$N_{fi,pl,Rd,f} = \sum_{i=1}^{n} A_{f,i} \cdot f_{s,\theta_i} = \sum_{i=1}^{n} A_{f,i} \cdot k_{s,\theta_i} \cdot f_s = f_s \cdot \sum_{i=1}^{n} A_{f,i} \cdot k_{s,\theta_i} \tag{7.8}$$

$$N_{fi,pl,Rd,w} = \sum_{i=1}^{n} A_{w,i} \cdot f_{s,\theta_i} = \sum_{i=1}^{n} A_{w,i} \cdot k_{s,\theta_i} \cdot f_s = f_s \cdot \sum_{i=1}^{n} A_{w,i} \cdot k_{s,\theta_i} \tag{7.9}$$

Then the reduction coefficient is isolated:

$$N_{fi,pl,Rd,f} = f_s \cdot \sum_{i=1}^{n} A_{f,i} \cdot k_{s,\theta_i} = k_{s,\theta}(\theta_{f,eq1}) \cdot f_s \cdot A_f \rightarrow k_{s,\theta}(\theta_{f,eq1}) = \frac{\sum_{i=1}^{n}(A_{f,i} \cdot k_{s,i})}{A_f} \qquad (7.10)$$

$$N_{fi,pl,Rd,w} = f_s \cdot \sum_{i=1}^{n} A_{w,i} \cdot k_{s,\theta_i} = k_{s,\theta}(\theta_{w,eq1}) \cdot f_s \cdot A_w \rightarrow k_{s,\theta}(\theta_{w,eq1}) = \frac{\sum_{i=1}^{n}(A_{w,i} \cdot k_{s,i})}{A_w} \qquad (7.11)$$

Subsequently, the equivalent temperatures of the steel flanges and web, $\theta_{f,eq1}$ and $\theta_{w,eq1}$, can be obtained by linear interpolation in Table 3.2 of EN1994-1-2 (CEN, 2005c).

b) Flexural stiffness approach (major axis bending)

The following equations are used to calculate the flexural stiffness for major axis bending of the inner profile section (flanges and web, respectively) exposed to elevated temperatures:

$$EI_{z,fi,f} = \sum_{i=1}^{n} I_{z,f,i} \cdot E_{a,\theta_i} = \sum_{i=1}^{n} I_{z,f,i} \cdot k_{E,\theta}(\theta_{f,eq2}) \cdot E_a = E_a \cdot \sum_{i=1}^{n} I_{z,f,i} \cdot k_{E,\theta}(\theta_{f,eq2}) \qquad (7.12)$$

$$EI_{z,fi,w} = \sum_{i=1}^{n} I_{z,w,i} \cdot E_{a,\theta_i} = \sum_{i=1}^{n} I_{z,w,i} \cdot k_{E,\theta}(\theta_{w,eq2}) \cdot E_a = E_a \cdot \sum_{i=1}^{n} I_{z,w,i} \cdot k_{E,\theta}(\theta_{w,eq2}) \qquad (7.13)$$

Next, the flexural stiffness reduction coefficient is isolated for both elements:

$$EI_{z,fi,f} = E_a \cdot \sum_{i=1}^{n} I_{z,f,i} \cdot k_{E,\theta}(\theta_{f,eq2}) = k_{E,\theta}(\theta_{f,eq2}) \cdot E_a \cdot I_{z,f} \rightarrow k_{E,\theta}(\theta_{f,eq2}) = \frac{\sum_{i=1}^{n}(I_{z,f,i} \cdot k_{E,\theta,i})}{I_{z,f}} \qquad (7.14)$$

$$EI_{z,fi,w} = E_a \cdot \sum_{i=1}^{n} I_{z,w,i} \cdot k_{E,\theta}(\theta_{w,eq2}) = k_{E,\theta}(\theta_{w,eq2}) \cdot E_a \cdot I_{z,w} \rightarrow k_{E,\theta}(\theta_{w,eq}) \qquad (7.15)$$
$$= \frac{\sum_{i=1}^{n}(I_{z,w,i} \cdot k_{E,\theta,i})}{I_{z,w}}$$

As with the concrete infill, this process is now replicated for the minor axis bending case, obtaining two sets of additional reduction coefficients: $k_{E,\theta}(\theta_{f,eq})$ and $k_{E,\theta}(\theta_{w,eq3})$. The equivalent temperatures $\theta_{f,eq}$, $\theta_{w,eq2}$, $\theta_{f,eq}$ and $\theta_{w,eq3}$ are then obtained by applying linear interpolation at Table 3.2 of EN1994-1-2 (CEN, 2005c).

The equivalent temperature for both the flanges and the web is obtained as the maximum of the three computed temperatures obtained in the previously explained procedure:

$$\theta_{f,eq} = \max\{\theta_{f,eq1}, \theta_{f,eq2}, \theta_{f,eq3}\} \qquad (7.16)$$

$$\theta_{w,eq} = \max\{\theta_{w,eq1}, \theta_{w,eq2}, \theta_{w,eq3}\} \qquad (7.17)$$

<u>Equivalent temperature for the flanges of the inner steel profile</u>
To develop a characteristic equation to predict the equivalent temperature of the steel profile flanges an additional parameter was described. The temperature of this part of the steel profile was heavily influenced by the amount of concrete cover (u_s) around them. This cover is defined as the distance between the flanges of the inner steel profile and the inner surface of the steel outer tube, as described in Figure 7.1.

By considering the concrete cover (u_s), as well as the effect of the standard fire time (R) and the section factor (A_m/V), an equation is obtained by multiple nonlinear regression analysis:

$$\theta_{f,eq} = a_1 + b_1 R + b_2 R^2 + c_1 \left(\frac{A_m}{V}\right) + c_2 \left(\frac{A_m}{V}\right)^2 + d_1 R \left(\frac{A_m}{V}\right) + e_1 R^{f_1} \left(\frac{A_m}{V}\right)^{f_2} + g_1 u_s \tag{7.18}$$

where coefficients a_1 to g_1 are dependent on the column shape (circular or square) and are exposed in Table 7.2.

Table 7.2   Coefficients for the equivalent temperature of the flanges of the embedded steel profile $\theta_{f,eq}$(ºC).

	a₁	b₁	b₂	c₁	c₂	d₁	e₁	f₁	f₂	g₁
CIRC	-1174,15	14,08	-2,03E-02	59,59	2,12E-02	-5,84E-02	9,53E-05	1,83	1,86	9,27
SQUA	794,25	-7,19	9,83E-03	-81,30	1,26	7,59	-4,51	1,05	1,06	-9,64

Additionally, two selection tables are provided in Table 7.6 and Table 7.7 (for circular and square columns, respectively) as an alternative calculation method for the steel profile flanges equivalent temperature. Linear interpolation can be used for intermediate values.

In Figure 7.4 a comparison between the predicted temperatures obtained with equation (7.18) and the numerically processed ones at the flanges of the inner profile.
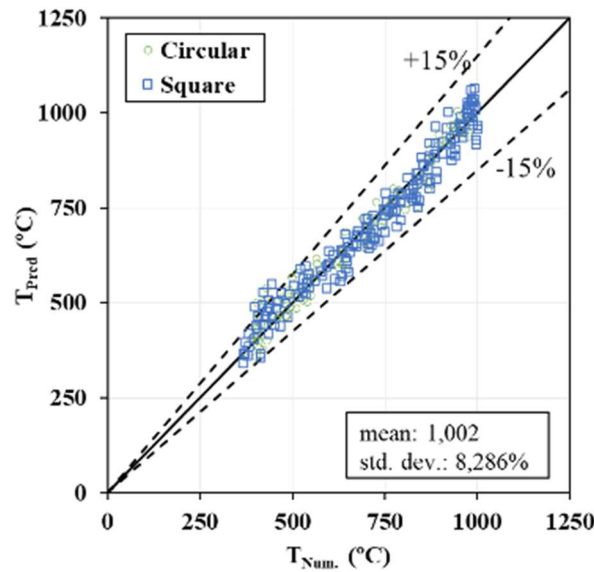
Figure 7.4.   Comparison of equivalent temperature and numerical temperature for the inner steel profile flanges of SR-CFST sections.

Equivalent temperature for the web of the inner steel profile

The relevant parameters when analyzing the web temperature history were the standard fire time (R), the section factor (A_m/V) and the A_{sp}/A_c ratio. Accordingly, a similar equation was obtained for the equivalent temperature of the steel profile web:

$$\theta_{w,eq} = a_1 + b_1 R + b_2 R^2 + c_1 \left(\frac{A_m}{V}\right) + c_2 \left(\frac{A_m}{V}\right)^2 + d_1 R \left(\frac{A_m}{V}\right) + e_1 R^{f_1} \left(\frac{A_m}{V}\right)^{f_2} + g_1 u_s \tag{7.19}$$

where coefficients a_1 to g_1 depend on the column shape (circular or square) and are included in Table 7.3.

Table 7.3   Coefficients for the equivalent temperature of the web of the embedded steel profile $\theta_{w,eq}$(ºC).

	a_1	b_1	b_2	c_1	c_2	d_1	e_1	f_1	f_2	g_1	g_2
CIRC	3267,34	3,24	0,01	184,79	-5,30	3,59	-1,29	1,18	1,01	10891,6	-55465,4
SQUA	-941,09	-5,32	6,62E-03	-22,25	0,36	3,41	-1,17	1,10	1,12	6939,91	-19679,4

Table 7.8 and Table 7.9 include two selection tables that provide an alternative method to obtain the steel profile web equivalent temperatures for circular and square sections, respectively. The temperatures obtained with Equation (7.19) are compared to the ones obtained with the numerical model and plotted in Figure 7.5.
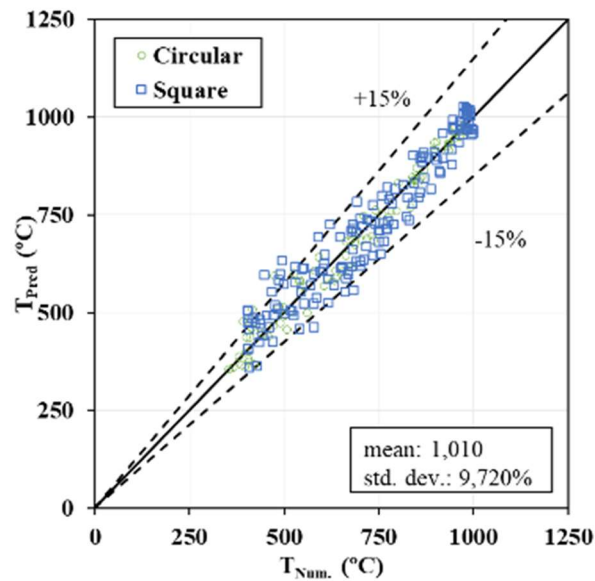
Figure 7.5.   Comparison of equivalent temperature and numerical temperature for the inner steel profile web of SR-CFST sections.

In both Figure 7.4 and Figure 7.5 it can be observed that equivalent equations for the steel profile are significantly accurate and have a good agreement between the calculated and numerically simulated data.

Table 7.4   Selection chart for the equivalent temperature of the concrete infill $\theta_{c,eq}$ (ºC) for circular sections.

A_{sp}/A_c		0,01						0,05						0,1					
		R30	R60	R90	R120	R180	R240	R30	R60	R90	R120	R180	R240	R30	R60	R90	R120	R180	R240
A_m/V (m^{-1})	10	<200	237	323	410	589	775	<200	249	341	435	626	825	<200	265	365	466	672	887
	15	<200	336	538	713	988	1165	<200	348	557	738	1025	>1200	<200	364	580	769	1072	>1200
	20	245	580	832	1005	1125	>1200	252	592	850	1030	1162	>1200	259	608	874	1061	>1200	

Table 7.5   Selection chart for the equivalent temperature of the concrete infill $\theta_{c,eq}$ (ºC) for square sections.

A_{sp}/A_c		0,02						0,1						0,2					
		R30	R60	R90	R120	R180	R240	R30	R60	R90	R120	R180	R240	R30	R60	R90	R120	R180	R240
A_m/V (m^{-1})	10		<200	<200	<200	<200	360		<200	<200	<200	239	450		<200	<200	213	324	563
	15	<200	275	381	477	690	979	<200	297	415	522	758	1069	<200	325	457	578	843	1182
	20	<200	392	572	715	966	>1200	<200	415	606	760	1034	>1200	<200	443	648	816	1119	>1200
	25	<200	512	722	868	1066	>1200	<200	534	755	913	1134	>1200	<200	562	798	969	>1200	
	30	278	645	850	962	>1200		289	667	884	1008	>1200		303	696	926	1064	>1200	

Table 7.6   Selection chart for the equivalent temperature of the flanges of the inner steel profile $\theta_{f,eq}$ (ºC) for circular sections.

A_m/V (m⁻¹)		10						20					
		R30	R60	R90	R120	R180	R240	R30	R60	R90	R120	R180	R240
u_s (mm)	15			<400	569	966	>1200	<400	544	791	986	>1200	>1200
	30			<400	430	827	1063	<400	405	652	847	1083	1117
	45				<400	688	924		<400	513	708	944	978
	60		<400		<400	549	785		<400	569	805	839
	75				<400	410	646	<400		<400	430	666	700
	90					<400	507				<400	527	561

Table 7.7   Selection chart for the equivalent temperature of the flanges of the inner steel profile $\theta_{f,eq}$ (ºC) for square sections.

A_m/V (m⁻¹)		15						30					
		R30	R60	R90	R120	R180	R240	R30	R60	R90	R120	R180	R240
u_s (mm)	15		<400	515	655	883	1079	<400	497	748	913	1077	1096
	30			<400	510	738	934		<400	604	769	932	952
	45				<400	594	789		<400	459	624	788	807
	60		<400		<400	449	645		<400	480	643	663
	75					<400	500	<400			<400	499	518
	90						<400					<400	<400

Table 7.8   Selection chart for the equivalent temperature of the inner steel profile web $\theta_{w,eq}$ (ºC) for circular sections.

A_{sp}/A_c		0,01						0,05						0,1					
		R30	R60	R90	R120	R180	R240	R30	R60	R90	R120	R180	R240	R30	R60	R90	R120	R180	R240
A_m/V (m⁻¹) 10							<400		<400			<400	<400		<400			<400	464
15			<400			<400	432				<400	552	734			<400	<400	681	863
20					<400	492	551			<400	552	795	853			<400	458	681	923	982

Table 7.9   Selection chart for the equivalent temperature of the inner steel profile web $\theta_{w,eq}$ (ºC) for square sections.

A_{sp}/A_c		0,02						0,1						0,2					
		R30	R60	R90	R120	R180	R240	R30	R60	R90	R120	R180	R240	R30	R60	R90	R120	R180	R240
A_m/V (m⁻¹) 10												<400	<400					<400	<400
15			<400				<400		<400		<400	418	606		<400		<400	522	710
20						<400	437				<400	634	803			<400	493	738	907
25					<400	413	530			<400	551	779	896			<400	479	654	882	1000
30					<400	502	541		<400	511	683	868	907		<400	614	787	972	1011

7.2.2. Applicability limits of the proposed method

The equations provided in section 7.2.1 of the present chapter should only be applied to SR-CFST sections that meet the following criteria:

- For circular SR-CFST columns:

$$8 \, m^{-1} \leq A_m/V \leq 20 \, m^{-1}$$

$$24 \leq D/t \leq 64$$

$$0{,}011 \leq A_{sp}/A_c \leq 0{,}108$$

- For square SR-CFST columns:

$$13 \, m^{-1} \leq A_m/V \leq 34 \, m^{-1}$$

$$19 \leq B/t \leq 50$$

$$0{,}018 \leq A_{sp}/A_c \leq 0{,}204$$

7.3. A NEW THERMO-MECHANICAL CALCULATION METHOD FOR AXIALLY LOADED SR-CFST STUB COLUMNS EXPOSED TO FIRE

A design proposal is developed in this section to facilitate the calculation of the cross-sectional plastic resistance of SR-CFST stub columns under fire conditions based on the previously proposed equivalent temperature equations (section 7.2) and the findings on the influence of the relevant parameters extracted from the thermo-mechanical parametric studies (section 6.2). The following section was developed during a research stay of the author of this thesis at the Faculty of Engineering and Information Technology of the University of Melbourne (Australia) in collaboration with Professor Tai Thai.

7.3.1. Simplified thermo-mechanical proposal for axially loaded SR-CFST columns

In assessing the capacity of steel-concrete composite structures under the fire action, the reference code in Europe is EN1994-1-2 (CEN, 2005c). Even though the code includes provisions for partially and totally-encased steel-concrete columns as well as CFST columns, there is no specific guidance for the SR-CFST columns studied in this investigation. This issue has been previously addressed in the thermal proposal of SR-CFST sections presented in section 7.2.1.

In this section, the previously proposed thermal method is used to calculate the simplified temperature distribution of the cross-sections, and the plastic resistance of the heated column at failure is subsequently obtained using a modified design formula. This way, the previous method is extended, and a comprehensive new procedure to obtain the plastic resistance of SR-CFST columns is developed, filling an existing gap in the European design code.

7.3.1.1. Application of the previous simplified method for the temperature field

Initially, the simplified cross-sectional temperature field method is applied to the sections of the present parametric study. This way, the equivalent temperatures of the outer tube, concrete infill and the flanges and web of the inner steel profile are obtained for each section at the numerically obtained failure time (see Figure 7.1).

Once the representative equivalent temperatures of each part of the section are known, the temperature-dependent mechanical degradation coefficients of steel and concrete corresponding to these equivalent temperatures are obtained. The steel reduction coefficients are extracted from Table 3.1 of EN1993-1-2 (CEN, 2005b) for both normal and high-strength steel. In turn, the coefficients for normal-strength concrete are extracted from Table 3.1 of EN1992-1-2 (CEN, 2004b), while the values for the high-strength concrete are obtained from Table 6.1 N of EN1992-1-2 (CEN, 2004b).

Once the mechanical properties of each component of the section have been reduced, the cross-sectional plastic resistance of the column at elevated temperature is computed as per Clause 4.3.5.1(4) of EN1994-1-2 (CEN, 2005c) by summing the contribution of the different parts:

$$N_{fi,pl,Rd} = A_a f_{y,\theta}(\theta_{a,eq})/\gamma_{M,fi,a} + A_c f_{c,\theta}(\theta_{c,eq})/\gamma_{M,fi,c} + A_f f_{y,\theta}(\theta_{f,eq})/\gamma_{M,fi,sp} \\ + A_w f_{y,\theta}(\theta_{w,eq})/\gamma_{M,fi,sp} \tag{7.20}$$

where:

A_i is the area of each element of the cross-section ($i = a$ or c or f or w) affected by fire, where a stands for "steel outer tube", c for "concrete", f for "steel inner profile flanges" and w for "steel inner profile web".

$f_{i,\theta}(\theta_{i,eq})$ is the design strength of part i at a temperature ($\theta_{i,eq}$) which can be calculated through the reduction factors from Table 3.2 and Table 3.3 of EN1994-1-2 (CEN, 2005c).

$\gamma_{M,fi,i}$ is the partial factor for the strength of a given material (i = a or c or sp) in the fire situation, where a stands for "steel outer tube", c for "concrete" and sp for "steel inner profile". As Clause 2.3(1) of EN1994-1-2 (CEN, 2005c) indicates, these coefficients are assumed to be 1,0.

7.3.1.2. Simplified plastic resistance proposal for SR-CFST sections under fire conditions

The computed plastic resistance by means of applying equation (7.20) (N_{pred}) is directly compared to the failure load of the sections from the numerical simulations (N_{num}). As can be observed in Figure 7.6, this tentative application of the plastic resistance equation provides unsafe predictions for most cases, especially for the columns with low load levels. Therefore, a correction is needed to obtain a robust equation that can be valid for different load levels.

a)   b)
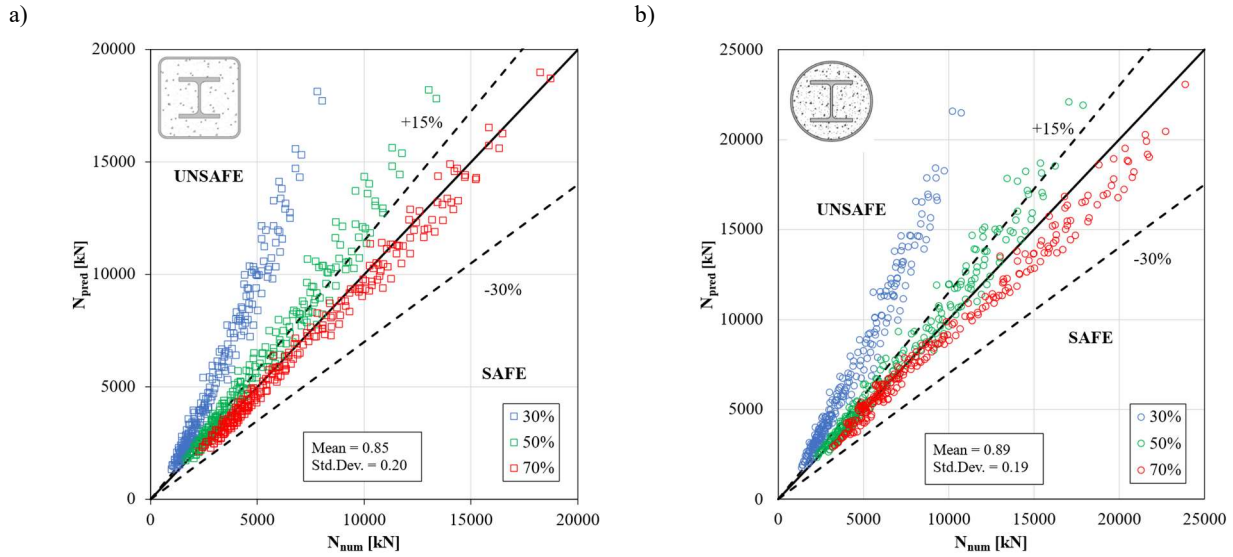
Figure 7.6.   Numerical vs. predicted fire plastic resistance obtained by directly applying the previous simplified temperature method for a) square and b) circular SR-CFST stub columns.

A simple modification of equation (7.20) is suggested, consisting of the addition of two homogenization coefficients to the concrete infill and the steel profile flanges. It should be mentioned that, when exposed to fire, the flanges of the steel profile and the inner concrete suffer a significant temperature gradient, therefore two coefficients need to be introduced here to "homogenise" this steep gradient and allow for a representation of these parts with a single equivalent temperature each. For the outer steel tube and web of the inner profile, however, this correction is not needed, as their temperature distribution is mostly uniform, therefore they can be easily represented with a single equivalent temperature, regardless the fire exposure time.

Therefore, a modified equation is proposed for evaluating the cross-sectional plastic resistance of SR-CFST columns in fire, by including the homogenization coefficients for the concrete infill and steel profile flanges:

$$N_{fi,pl,Rd} = A_a f_{y,\theta}(\theta_{a,eq})/\gamma_{M,fi,a} + k_{c,\theta} A_c f_{c,\theta}(\theta_{c,eq})/\gamma_{M,fi,c} + k_{f,\theta} A_f f_{y,\theta}(\theta_{f,eq})/\gamma_{M,fi,sp} \qquad (7.21)$$
$$+ A_w f_{y,\theta}(\theta_{w,eq})/\gamma_{M,fi,sp}$$

where:

$k_{f,\theta}$ and $k_{c,\theta}$ are the proposed homogenization factors for the steel profile flanges and concrete infill, respectively. Its values, which depend on the fire exposure time, are included in Table 7.10.

Table 7.10   Proposed homogenization factors for the steel profile flanges and concrete infill, for the evaluation of the plastic resistance of SR-CFST stub columns.

R (min)	$k_{c,\theta}$	$k_{f,\theta}$
30	1.00	1.00
60	0.70	0.70
90	0.6	0.5
120	0.5	0.4
180		

The proposed modification of the formula increases the accuracy of the method and provides conservative results. The proposed method is designed to meet the CEN TC 250 Horizontal Group Fire accuracy criteria (Kruppa, 1999):

-   The calculation result shall not be on the unsafe side by more than 15% of the reference result,
-   A maximum of 20% of individual calculation results shall be on the unsafe side,
-   The mean value of all percentage differences between calculation and reference results shall be safe.

Table 7.11 shows the results obtained for the accuracy parameters for both geometries, proving that the designed method complies with the reference accuracy criteria.

Table 7.11   Summary of the CEN TC 250 accuracy criteria (Kruppa, 1999) accomplishment with the proposed method.

	Maximum error	Unsafe results	Mean value
Square	14.90%	12.36%	1.10
Circular	12.06%	19.31%	1.09

Figure 7.7 shows the predicted results by applying the proposal in equation (7.21) in comparison with the numerically predicted plastic resistance under fire. A good agreement can be found between the two sets of data and most of the cases lay in the safe side. Therefore, the proposed method is proven to be reliable in predicting the axial capacity of SR-CFST stub columns at elevated temperature and being a useful tool for practitioners to easily obtain the plastic resistance in fire design.
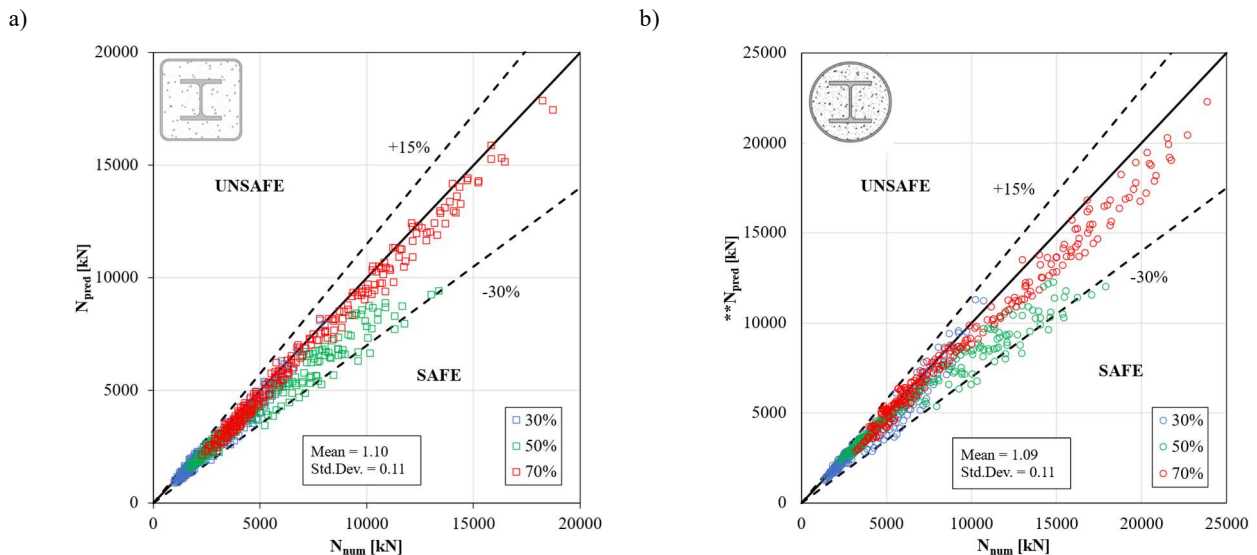
Figure 7.7.   Numerical vs. predicted fire plastic resistance obtained by applying the new method for a) square and b) circular SR-CFST stub columns.

7.3.2. Applicability limits of the proposed method

The exposed calculation method should only be applied to SR-CFST stub columns that meet the following criteria:

- For circular SR-CFST stub columns:

$$7.5 \leq A_m/V \leq 16.5$$

$$24.5 \leq D/t \leq 57$$

$$0.04 \leq A_p/A_c \leq 0.10$$

$$u_s \geq 52\ mm$$

- For square SR-CFST stub columns:

$$10 \leq A_m/V \leq 20$$

$$20 \leq B/t \leq 44$$

$$0.05 \leq A_p/A_c \leq 0.16$$

$$u_s \geq 30\ mm$$

- The method can be used for standard fire exposure times between 30 and 180 min.
- The method can be used for inner steel profile grades up to S690 and concrete grades up to C90.

8.

CONCLUSIONS

This final chapter presents the main conclusions obtained from the work developed in this thesis. Suggestions for future work are included at the end of the chapter.

8.1. SUMMARY AND GENERAL CONCLUSIONS

The present thesis analysed the fire performance of axially loaded SR-CFST stub columns of square and circular geometry through experimental tests and numerical simulations. The behaviour of SR-CFST stub columns at elevated temperature was studied through an experimental campaign consisting of two phases (post-fire tests and thermo-mechanical tests). In the post-fire campaign, thermal and mechanical tests were conducted to a set of six SR-CFST stub columns. Both tests were conducted according to the specified normative and relevant data about the thermal and post-fire mechanical response of the columns was obtained. Regarding the thermo-mechanical campaign, twelve tests were conducted to study the fire performance of SR-CFST columns. The temperature evolution of the sections and the vertical displacement of the columns were recorded.

A numerical model was developed to extend the experimental results: initially a thermal sectional finite element model was calibrated and subsequently expanded to a three-dimensional thermo-mechanical model. This numerical model was validated against available experimental data from the literature and by comparison with the results of the previously performed experimental campaign. Good agreement was found between the thermal response of the tests and the predicted temperature evolution obtained from the FE model. The model adequately reproduced the thermo-mechanical behaviour of the columns in terms of displacement-time response. Parametric studies comprising a total of 1440 cases were conducted by means of the FE model to study the effect of several geometrical parameters and the use of high-strength steel and concrete on the thermo-mechanical response of SR-CFST stub columns.

By reviewing the existing design guidance for steel-concrete composite columns, it was found that no specific formulation exists for the calculation of the fire performance of SR-CFST sections. Given the need to develop a specific and accurate method for predicting the thermal and mechanical behaviour of these columns in the fire scenario, a simplified calculation method was developed based on the results from the parametric studies.

In this method, a simplistic temperature proposal allows to evaluate the thermal behaviour of an SR-CFST section by using an equivalent temperature for each column part: outer steel tube, concrete infill and flanges and web of the embedded steel profile. A series of equations and design tables were presented to obtain the equivalent temperature of each part of the section. Subsequently, the cross-sectional plastic resistance of the SR-CFST column was calculated based on the previously obtained equivalent temperatures, by means of a proposed design equation which is in line with the provisions in Clause 4.3.5.1(4) of EN1994-1-2 (CEN, 2005c) adapted to SR-CFST sections with a set of "homogenization" factors. The method can be applied to a wide range of columns, square and circular geometries, with inner profiles using steel grades up to S690 and concrete grades up to C90 and standard fire exposure times ranging from 30 to 180 minutes. The developed method provides a simple tool for practitioners to obtain both the temperature field and the plastic resistance of SR-CFST stub columns with simple and direct calculation procedures.

8.2. SPECIFIC CONCLUSIONS

Through the work developed in this thesis, several specific conclusions were drawn, which are summarized in this section.

From the experimental investigation on the post-fire performance of SR-CFST columns, the following conclusions were obtained:

- The higher section factor (A_m/V) of square columns as compared with their circular counterparts caused a faster development of the temperature field, as observed in their shorter heating times.

- The concrete moisture content had a notable positive effect over the thermal behaviour of SR-CFST sections, as the heat transfer to the inner parts of the section is significantly delayed by the latent heat consumption in the evaporation stage. This effect was more significant as the water percentage was higher.

- The relatively low improvement in terms of residual post-fire strength denoted that the effect of including a larger steel profile in the SR-CFST sections is minor. The higher area of embedded steel profile is compensated by a faster heating of the section, therefore a greater loss of mechanical properties, as the steel profile is less protected by the surrounding concrete.

- The Residual Strength Index values for both square and circular columns were similar. As the load level of the circular columns was calculated assuming the concrete confinement, differently from the square cases (where no confinement was considered), it can be concluded that the effect of confinement seems to be still active in the post-fire scenario for the circular SR-CFST specimens, contributing to enhance their mechanical capacity after fire exposure.

- When comparing different material models from the literature for calculating the post-fire capacity of SR-CFST stub columns, it was found that the post-fire reduction coefficients proposed by Pons et al. (2022) yield the most accurate results.

From the thermo-mechanical experimental investigation of SR-CFST stub columns, several conclusions were obtained:

- The thermal evolution of the SR-CFST column specimens showed a delay in the heating of the inner profile because of the outer steel tube protection and the surrounding concrete.

- The use of high-strength materials (HSC and HSS) improved the thermo-mechanical behaviour of SR-CFST columns, enhancing their load-bearing capacity and failure time.

- The use of HSS at the inner profile was found to be the most beneficial strategy for a better thermo-mechanical performance of SR-CFST columns, as the concrete protects the inner steel profile, which can bear a higher amount of load while remaining undegraded for longer. In turn, HSC was found not to provide a significant improvement to the column fire resistance, as its superior mechanical properties are compensated by its lower moisture percentage and faster thermal degradation.

- The best results were obtained by combining HSS at the inner steel profile and NSC at the concrete infill. By combing the enhanced mechanical properties of HSS and the better thermal properties of NSC (due to its higher moisture content), the fire performance of SR-CFST stub columns can be maximized.

- The use of HSS at the outer tube was found not to be practical in fire design, as it losses its mechanical capacity fast by being directly exposed to the heat source and its advantageous mechanical properties cannot be then exploited.

The numerical investigation on the thermo-mechanical behaviour of SR-CFST stub columns allowed reaching a series of interesting conclusions:

- The constitutive material model for HSS at high temperatures proposed in EN1993-1-2 (CEN, 2005b) was found to provide the most accurate predictions for SR-CFST columns in fire. The formulation by Qiang et al. (2012) also had a good agreement with the experimental data.

- Regarding the constitutive models for HSC at high temperatures, the formulation proposed by Aslani and Bastami (2011) effectively predicted the thermo-mechanical behaviour of SR-CFST stub columns. However, as the reduction coefficients for HSC in EN1992-1-2 (CEN, 2004b) provided conservative and still accurate results, this model was deemed adequate for conducting the subsequent parametric studies.

- Circular sections presented a better thermal performance than their square counterparts. The reason behind this phenomenon was attributed to the greater section factor (A_m/V) of the square sections; as these shapes expose a higher amount of surface as related to their volume; therefore, they heat up faster, and their mechanical properties degrade at a higher rate.

- The use of thinner outer tubes had a positive effect over the thermal performance of SR-CFST sections. The outer steel tube quickly loses its mechanical properties but protects the inner parts of the section, therefore using a thinner tube (and thus a higher amount of concrete area) enhances the thermo-mechanical behaviour of the column.

- The beneficial effect of including an inner steel profile with greater dimensions is balanced by the higher temperatures that develop across these sections, which are less protected by concrete. Therefore, an intermediate solution should be obtained by embedding a profile with the maximum amount of steel area and an adequate concrete cover for each standard fire period.

In the last part of this thesis a simplified calculation method was developed. The main conclusions drawn from this process are as follows:

- The equivalent temperature proposal provided adequate results and a good agreement with the obtained data from the parametric studies, allowing to easily evaluate the thermal response of SR-CFST sections using a single temperature for each part (steel tube, concrete infill, steel profile web and flanges).

- The direct application of the cross-sectional plastic resistance formula for CFST sections adapted from EN1994-1-2 (CEN, 2005c) as a summation of the different parts of the section in combination with the equivalent temperatures led to unsafe predictions, therefore a set of homogenization factors were developed to extend its application to SR-CFST columns.

- The proposed design equation for evaluating the cross-sectional plastic resistance for SR-CFST columns showed good agreement when applied to the cases analysed in the parametric studies and was proven to be reliable in the design of SR-CFST columns at high temperatures.

8.3. FUTURE WORK

This investigation studied the fire behaviour of a novel composite column typology, which is a complex problem that includes many variables. Therefore, only some of the parameters have been considered in this dissertation. Hence, future lines and recommendations will be given next to expand this work.

As a future task, the numerical model should be expanded to analyse slender SR-CFST columns under fire conditions. This is the most immediate step, as the presented model and design proposal are only valid for stub columns and should be necessarily extended to longer columns. Several standard fire tests on slender SR-CFST columns were conducted within the scope of the HIFICOMP project at the time of writing this document. The results of these tests will serve to better understand the buckling behaviour of slender columns in fire and as a validation reference for the extended finite element model.

The presented simplified temperature field proposal might be further refined by proposing two different equivalent temperatures for the concrete infill: one for the highly confined concrete encased between the flanges of the steel profile and another one corresponding to the outer concrete ring. This way, the precision of the method could be increased, and more accurate results would be obtained both thermally and mechanically.

The load application is an essential factor for analysing the performance of composite columns. In this thesis, the effect of the load level was analysed through parametric studies. However, the load was always assumed to be concentrically applied. The analysis of the effect of the load eccentricity over the fire performance of SR-CFST columns is an aspect that should be considered in the future.

Using steel fibres in the concrete infill of the columns may be a possible line of study, as the fibres increase the strength of the material on the one hand but facilitate heat conduction on the other hand. The study of the effect of this type of material on the thermo-mechanical behaviour of SR-CFST could be an interesting contribution to the presented research.

It is also left for future work to extend this analysis to other types of cross-section geometries both for the outer steel tube (elliptical, rectangular, etc.) and for the inner steel profile (IPE profiles, cruciform sections, etc.), as well as other types of innovative composite cross-sections such as concrete-encased sections (CES).

Finally, the proposed calculation method for the cross-sectional plastic resistance of SR-CFST columns under fire should be extended to slender members, following the guidelines for the fire design of CFST columns included in the new prEN1994-1-2 (CEN, 2021). It is aimed to provide a comprehensive method for evaluating the capacity of SR-CFST columns in fire conditions, which will be transferred into the European design code through the participation of the advisors of this thesis in the CEN/TC250/SC4 Committee.

REFERENCES

ACI. (1989). ACI 216 R: Guide for determining the fire endurance of concrete elements. In *Concrete International*.

AIJ. (2008). *Recommendations for Design and Construction of Concrete Filled Steel Tubular Structures*. Architectural Institute of Japan (AIJ).

AISC. (2003). Design Guide 19: Fire Resistance of Structural Steel Framing. In *Steel Design Guide 19 AISC*.

Albero, V., Espinos, A., Romero, M. L., Hospitaler, A., Bihina, G., & Renaud, C. (2016). Proposal of a new method in EN1994-1-2 for the fire design of concrete-filled steel tubular columns. *Engineering Structures*, *128*. https://doi.org/10.1016/j.engstruct.2016.09.037

ASCE. (2003). *Standard Calculation Methods for Structural Fire Protection*. American Society of Civil Engineers. https://doi.org/10.1061/9780784406496

Aslani, F., & Bastami, M. (2011). Constitutive relationships for normal-and high-strength concrete at elevated temperatures. *ACI Materials Journal*, *108*(4). https://doi.org/10.14359/51683106

BSI. (2003a). BS 5950-8:2003 Structural use of steelwork in building. In *British Standards* (Vol. 8, Issue October).

BSI. (2003b). BS 5950-8:2003 Structural use of steelwork in building. *British Standards*, *8*(October).

Cai, J., Pan, J., & Wu, Y. (2015). Mechanical behavior of steel-reinforced concrete-filled steel tubular (SRCFST) columns under uniaxial compressive loading. *Thin-Walled Structures*, *97*. https://doi.org/10.1016/j.tws.2015.08.028

CCBFC. (2005). *National Building Code of Canada (NBCC)*. National Research Council of Canada (NRCC); .

CEN. (2002). *EN 1991-1-2, Eurocode 1: Actions on structures - Part 1-2: General actions - Actions on structures exposed to fire*. Comité Européen de Normalisation.

CEN. (2004a). *EN 1992-1-1, Eurocode 2: Design of concrete structures, Part 1.1: General rules and rules for buildings*. Comité Européen de Normalisation.

CEN. (2004b). *EN 1992-1-2, Eurocode 2: Design of concrete structures, Part 1.2: General rules – Structural fire design*. Comité Européen de Normalisation.

CEN. (2004c). *EN 1994-1-1, Eurocode 4: Design of composite steel and concrete structures. Part 1.1: General rules and rules for buildings*. Comité Européen de Normalisation.

CEN. (2005a). *EN 1993-1-1, Eurocode 3: Design of steel structures - Part 1-1: General rules and rules for buildings*. Comité Européen de Normalisation.

CEN. (2005b). *EN 1993-1-2, Eurocode 3: Design of steel structures, Part 1.2: General rules – Structural fire design*. Comité Européen de Normalisation.

CEN. (2005c). *EN 1994-1-2, Eurocode 4: Design of composite steel and concrete structures. Part 1.2: General rules - Structural fire design*. Comité Européen de Normalisation.

CEN. (2006). *EN 10025-1:2006. Hot rolled products of structural steels - Part 1: General technical delivery conditions*.

CEN. (2007). *EN 10219-1:2007. Cold formed welded structural hollow sections of non-alloy and fine grain steels - Part 1: Technical delivery conditions*.

CEN. (2015). EN 1993-1-12: Eurocode 3 - Design of steel structures - Part 1-12: Additional rules for the extension of EN 1993 up to steel grades S 700. *Design of Structural Elements*.

CEN. (2017). *TC250/SC4 N1836 - SC4.T4 Final Draft Annex H - Simple calculation model for concrete-filled hollow sections exposed to fire all around the column according to the standard temperature-time curve*. http://cen.iso.org/livelink/livelink/open/centc250sc4

CEN. (2020). *EN 1363-1 - Fire resistance tests General requirements*.

CEN. (2021). *TC250/SC4 N2192 - SC4.T7 Project Team final draft prEN 1994-1-2. Eurocode 4: Design of composite steel and concrete structures – Part 1-2: General – Structural fire design*.

Chen, B.-C., & Wang, T.-L. (2009). Overview of Concrete Filled Steel Tube Arch Bridges in China. *Practice Periodical on Structural Design and Construction*, *14*(2). https://doi.org/10.1061/(asce)1084-0680(2009)14:2(70)

Chen, Z., Ning, F., Song, C., & Liang, Y. (2022). Study on axial compression bearing capacity of novel concrete-filled square steel tube columns. *Journal of Building Engineering*, *51*. https://doi.org/10.1016/j.jobe.2022.104298

Chinese Standards. (2014). *GB 50936-2014, Technical code for concrete filled steel tubular structures*.

Chinese Standards. (2016). *GB/T706-2016. Hot rolled section steel.*

Chu, T. B. (2009). *Hollow steel section columns filled with self-compacting concrete under ordinary and fire conditions*. Université de Liège .

Chu, T. B., Gernay, T., Dotreppe, J.-C., & Franssen, J. (2016). Steel hollow columns with an internal profile filled with self-compacting concrete under fire conditions. *Proceedings of the Romanian Academy, Series A*, 152–159.

Construction Department of Fujian Province. (2003). *DBJ 13-51-2003 - Technical specification for concrete-filled steel tubular structures*.

Dassault Systèmes. (2021). Abaqus Unified FEA - SIMULIA^{TM} by Dassault Systèmes®. In *Dassault Systèmes Simulia*.

Ding, F. xing, Zhang, T., Liu, X. mei, Lu, Z. H., Guo, Q., & Jiang, G. shuai. (2017). Behavior of steel-reinforced concrete-filled square steel tubular stub columns under axial loading. *Thin-Walled Structures*, *119*. https://doi.org/10.1016/j.tws.2017.07.021

Dotreppe, C. J., Binh Chu, T., Eng, R., & Marc Franssen, J. (2010). Steel hollow columns filled with self-compacting concrete under fire conditions. In *Proceedigns of the 3rd fib International Congress*.

Du, Y., Qi, H., Jiang, J., Richard Liew, J. Y., & Li, S. (2021). Thermo-mechanical behaviour of ultra-high strength concrete encased steel columns in standard fires. *Engineering Structures*, *231*, 111757. https://doi.org/10.1016/j.engstruct.2020.111757

Elchalakani, M., Zhao, X. L., & Grzebieta, R. (2002). Tests on concrete filled double-skin (CHS outer and SHS inner) composite short columns under axial compression. *Thin-Walled Structures*, *40*(5). https://doi.org/10.1016/S0263-8231(02)00009-5

Endo, F., Yamanaka, M., Watnabe, T., Kageyama, M., Yoshida, O., Katsumata, H., & Sano, T. (2011). Advanced technologies applied at the new 'Techno Station' building in Tokyo, Japan. *Structural Engineering International: Journal of the International Association for Bridge and Structural Engineering (IABSE)*, *21*(4). https://doi.org/10.2749/101686611X13049248220609

Espinós Capilla, A. (2012). *Numerical analysis of the fire resistance of circular and elliptical slender concrete filled tubular columns* [Universitat Politècnica de València]. https://doi.org/10.4995/Thesis/10251/17579

Espinos, A., Romero, M. L., & Hospitaler, A. (2010). Advanced model for predicting the fire response of concrete filled tubular columns. *Journal of Constructional Steel Research*, *66*(8–9). https://doi.org/10.1016/j.jcsr.2010.03.002

Espinos, A., Romero, M. L., & Hospitaler, A. (2012). Simple calculation model for evaluating the fire resistance of unreinforced concrete filled tubular columns. *Engineering Structures*, *42*. https://doi.org/10.1016/j.engstruct.2012.04.022

Espinos, A., Romero, M. L., & Hospitaler, A. (2013). Fire design method for bar-reinforced circular and elliptical concrete filled tubular columns. *Engineering Structures*, *56*. https://doi.org/10.1016/j.engstruct.2013.05.026

Espinos, A., Romero, M. L., & Lam, D. (2016). Fire performance of innovative steel-concrete composite columns using high strength steels. *Thin-Walled Structures*, *106*, 113–128. https://doi.org/10.1016/j.tws.2016.04.014

Espinos, A., Romero, M. L., Serra, E., & Hospitaler, A. (2015). Circular and square slender concrete-filled tubular columns under large eccentricities and fire. *Journal of Constructional Steel Research*, *110*. https://doi.org/10.1016/j.jcsr.2015.03.011

Essopjee, Y., & Dundu, M. (2015). Performance of concrete-filled double-skin circular tubes in compression. *Composite Structures*, *133*. https://doi.org/10.1016/j.compstruct.2015.08.033

Fang, X., Wei, H., Jiang, Y., Chen, F., Zeng, X., & Lai, H. (2010). Seismic design of the Guangzhou West Tower. *Jianzhu Jiegou Xuebao/Journal of Building Structures*, *31*(1).

Ghojel, J. (2004). Experimental and analytical technique for estimating interface thermal conductance in composite structural elements under simulated fire conditions. *Experimental Thermal and Fluid Science*, *28*(4). https://doi.org/10.1016/S0894-1777(03)00113-4

Han, L. H., & An, Y. F. (2014). Performance of concrete-encased CFST stub columns under axial compression. *Journal of Constructional Steel Research*, *93*. https://doi.org/10.1016/j.jcsr.2013.10.019

Han, L. H., Huo, J. S., & Wang, Y. C. (2005). Compressive and flexural behaviour of concrete filled steel tubes after exposure to standard fire. *Journal of Constructional Steel Research*, *61*(7). https://doi.org/10.1016/j.jcsr.2004.12.005

Han, L. H., Li, W., & Bjorhovde, R. (2014). Developments and advanced applications of concrete-filled steel tubular (CFST) structures: Members. *Journal of Constructional Steel Research*, *100*. https://doi.org/10.1016/j.jcsr.2014.04.016

Han, L. H., Liao, F. Y., Tao, Z., & Hong, Z. (2009). Performance of concrete filled steel tube reinforced concrete columns subjected to cyclic bending. *Journal of Constructional Steel Research*, *65*(8–9). https://doi.org/10.1016/j.jcsr.2009.03.013

Han, L. H., Tao, Z., Huang, H., & Zhao, X. L. (2004). Concrete-filled double skin (SHS outer and CHS inner) steel tubular beam-columns. *Thin-Walled Structures*, *42*(9). https://doi.org/10.1016/j.tws.2004.03.017

Han, L.-H. (2024). *Theory of Concrete-Filled Steel Tubular Structures*. Springer Nature Singapore. https://doi.org/10.1007/978-981-99-2170-6

Han, L.-H., & Huo, J. (2003). Concrete-Filled Hollow Structural Steel Columns after Exposure to ISO-834 Fire Standard. *Journal of Structural Engineering*, *129*(1). https://doi.org/10.1061/(asce)0733-9445(2003)129:1(68)

Han, L.-H., Yang, Y. F., & Xu, L. (2003). An experimental study and calculation on the fire resistance of concrete-filled SHS and RHS columns. *Journal of Constructional Steel Research*, *59*(4). https://doi.org/10.1016/S0143-974X(02)00041-X

Han, L.-H., & Yang, Y.-F. (2007). *Modern Technology of Concrete-Filled Steel Tubular Structures* (2nd ed.). China Architecture and Building Press.

Han, L.-H., Zhao, X.-L., Yang, Y.-F., & Feng, J.-B. (2003). Experimental Study and Calculation of Fire Resistance of Concrete-Filled Hollow Steel Columns. *Journal of Structural Engineering*, *129*(3). https://doi.org/10.1061/(asce)0733-9445(2003)129:3(346)

Hanswille, G., & Lippes, M. (2008). Einsatz von hochfesten Stählen und Betonen bei Hohlprofil-Verbundstützen. *Stahlbau*, *77*(4). https://doi.org/10.1002/stab.200810041

Hassanein, M. F., Patel, V. I., & Bock, M. (2017). Behaviour and design of hexagonal concrete-filled steel tubular short columns under axial compression. *Engineering Structures*, *153*. https://doi.org/10.1016/j.engstruct.2017.10.010

He, Y. Bin, Xiao, A. L., Guo, J., & Zhou, H. B. (2010). Bearing capacity of stub columns composed of structural steel and self-compacting high-strength concrete-filled steel tube: Experimental research. *Journal of Natural Disasters*, *19*(4).

Hicks, S. J., Newman, G. M., Edwards, M., & Orton, A. (2002). *Design guide for SHS concrete filled columns*. Corus Tubes Structural & Conveyance Business   Stephen James Hicks.

Hu, X., Guo, H., & Yao, Y. (2015). Interaction approach for concrete filled steel tube columns under fire conditions. *Journal of Building Engineering*, *3*. https://doi.org/10.1016/j.jobe.2015.07.006

Huang, C. S., Yeh, Y.-K., Liu, G.-Y., Hu, H.-T., Tsai, K. C., Weng, Y. T., Wang, S. H., & Wu, M.-H. (2002). Axial Load Behavior of Stiffened Concrete-Filled Steel Columns. *Journal of Structural Engineering*, *128*(9). https://doi.org/10.1061/(asce)0733-9445(2002)128:9(1222)

Huang, Z.-F., Tan, K.-H., Toh, W.-S., & Phng, G.-H. (2008). Fire resistance of composite columns with embedded I-section steel - Effects of section size and load level. *Journal of Constructional Steel Research*, *64*(3), 312–325. https://doi.org/10.1016/j.jcsr.2007.07.002

Ibañez, C., Romero, M. L., Espinos, A., Portolés, J. M., & Albero, V. (2017). Ultra-high Strength Concrete on Eccentrically Loaded Slender Circular Concrete-filled Dual Steel Columns. *Structures*, *12*. https://doi.org/10.1016/j.istruc.2017.07.005

ISO. (2000). *ISO 12570:2000. Hygrothermal performance of building materials and products. Determination of moisture content by drying at elevated temperature*.

ISO. (2014). ISO 834-11 - Fire resistance tests — Elements of building construction. In *International Organization for Standardization: Geneva, Switzerland* (Vol. 2014).

Johansson, M. (2002). Composite action and confinement effects in tubular steel-concrete columns. *Doktorsavhandlingar Vid Chalmers Tekniska Hogskola*, *1912*.

Karasaki, H., Hitomi, Y., & Takahashi, H. (2015). Structural design of a high-rise building above a motorway. *IABSE Conference, Nara 2015: Elegance in Structures - Report*. https://doi.org/10.2749/222137815815774241

Kodur, V. K. R. (1999). Performance-based fire resistance design of concrete-filled steel columns. *Journal of Constructional Steel Research*, *51*(1). https://doi.org/10.1016/S0143-974X(99)00003-6

Kodur, V. K. R. (2007). Guidelines for Fire Resistant Design of Concrete-Filled Steel HSS Columns - State-of-the-Art and Research Needs. *Steel Structures*, *7*.

Kodur, V. K. R., & Mackinnon, D. H. (2000). Design of concrete-filled hollow structural steel columns for fire endurance. *Engineering Journal*, *37*(1).

Kodur, V. K. R., Wang, T. C., & Cheng, F. P. (2004). Predicting the fire resistance behaviour of high strength concrete columns. *Cement and Concrete Composites*, *26*(2). https://doi.org/10.1016/S0958-9465(03)00089-1

Kruppa, J. (1999). *CEN TC 250 Horizontal Group Fire. Document n° 99/130. Proposal for a Methodology to check the Accuracy of Assessment Methods*.

Leskela, M. V. (2009). Inconsistencies in the fire design rules of composite columns to EN 1994-1-2. *Steel Concrete Composite and Hybrid Structures*, 489–494.

Li, G. Q., & Song, L. X. (2020). Mechanical properties of TMCP Q690 high strength structural steel at elevated temperatures. *Fire Safety Journal*, *116*. https://doi.org/10.1016/j.firesaf.2020.103190

Li, G., Zhan, Z., Yang, Z., Fang, C., & Yang, Y. (2020). Behavior of concrete-filled square steel tubular stub columns stiffened with encased I-section CFRP profile under biaxial bending. *Journal of Constructional Steel Research*, *169*. https://doi.org/10.1016/j.jcsr.2020.106065

Li, H. T., & Young, B. (2017). Material properties of cold-formed high strength steel at elevated temperatures. *Thin-Walled Structures*, *115*. https://doi.org/10.1016/j.tws.2017.02.019

Lie, T. T. (1984). A procedure to calculate fire resistance of structural members. *Fire and Materials*, *8*(1). https://doi.org/10.1002/fam.810080108

Lie, T. T. (1994). Fire Resistance of Circular Steel Columns Filled with Bar-Reinforced Concrete. *Journal of Structural Engineering*, *120*(5). https://doi.org/10.1061/(asce)0733-9445(1994)120:5(1489)

Lie, T. T., & Chabot, M. (1990). Method to predict the fire resistance of circular concrete filled hollow steel columns. *Journal of Fire Protection Engineering*, *2*(4). https://doi.org/10.1177/104239159000200402

Lie, T. T., & Irwin, R. J. (1995). Fire Resistance of Rectangular Steel Columns Filled with Bar-Reinforced Concrete. *Journal of Structural Engineering*, *121*(5). https://doi.org/10.1061/(asce)0733-9445(1995)121:5(797)

Liew, J. Y. R., & Xiong, D. X. (2010). Experimental investigation on tubular columns infilled with ultra-high strength concrete. *Tubular Structures XIII - Proceedings of the 13th International Symposium on Tubular Structures*. https://doi.org/10.1201/b10564-88

Liew, J. Y. R., Xiong, M. X., & Lai, B. L. (2021). Design of Steel-Concrete Composite Structures Using High-Strength Materials. In *Design of Steel-Concrete Composite Structures Using High-Strength Materials*. https://doi.org/10.1016/B978-0-12-823396-2.00041-1

Lin-Hai, H., Qing-Hua, T., & Tian-Yi, S. (2015). Fire Performance of Steel Reinforced Concrete Columns. *Journal of Structural Engineering*, *141*(4), 04014128. https://doi.org/10.1061/(ASCE)ST.1943-541X.0001081

Ma, H., Dong, J., Hu, G., & Liu, Y. (2019). Axial compression performance of composite short columns composed of RAC-filled square steel tube and profile steel. *Journal of Constructional Steel Research*, *153*. https://doi.org/10.1016/j.jcsr.2018.10.018

Mao, W. J., Wang, W. Da, & Zhou, K. (2022). Fire performance on steel-reinforced concrete-filled steel tubular columns with fire protection. *Journal of Constructional Steel Research*, *199*, 107580. https://doi.org/10.1016/J.JCSR.2022.107580

Mao, W. J., Wang, W. Da, Zhou, K., & Du, E. F. (2021). Experimental study on steel-reinforced concrete-filled steel tubular columns under the fire. *Journal of Constructional Steel Research*, *185*, 106867. https://doi.org/10.1016/J.JCSR.2021.106867

Mao, W. J., Zhou, K., & Wang, W. Da. (2023). Investigation on fire resistance of steel-reinforced concrete-filled steel tubular columns subjected to non-uniform fire. *Engineering Structures*, *280*, 115653. https://doi.org/10.1016/J.ENGSTRUCT.2023.115653

Mao, W.-J., Wang, W.-D., & Xian, W. (2020). Numerical analysis on fire performance of steel-reinforced concrete-filled steel tubular columns with square cross-section. *Structures*, *28*, 1–16. https://doi.org/10.1016/j.istruc.2020.08.043

Mao, X., & Kodur, V. K. R. (2011). Fire resistance of concrete encased steel columns under 3- and 4-side standard heating. *Journal of Constructional Steel Research*, *67*(3), 270–280. https://doi.org/10.1016/j.jcsr.2010.11.006

Matsudo, M., Nishida, H., Ohtsuka, T., Hirashima, T., & Abe, T. (2008). Mechanical properties of high strength concrete at high temperatures. *Journal of Structural and Construction Engineering (Transactions of AIJ)*, *73*(624). https://doi.org/10.3130/aijs.73.341

Matsumoto, S., Hosozawa, O., Narihara, H., Komuro, T., & Kawamoto, S. (2014). Structural Design of an Ultra High-rise Building Using Concrete Filled Tubular Column with 780 N/㎟ Class High-strength Steel and Fc150 N/㎟ High-strength Concrete. *International Journal of High-Rise Buildings*, *3*(1).

Meng, F.-Q., Zhu, M.-C., Clifton, G. C., Ukanwa, K.U. & Lim, J. B. P. (2021). Fire performance of edge and interior circular steel-reinforced concrete-filled steel tubular stub columns. *Steel and Composite Structures*, *41*(1), 115–122.

Meng, F.-Q., Zhu, M.-C., Mou, B., & He, B. (2019). Residual Strength of Steel-Reinforced Concrete-Filled Square Steel Tubular (SRCFST) Stub Columns After Exposure to ISO-834 Standard Fire. *International Journal of Steel Structures*, *19*(3), 850–866. https://doi.org/10.1007/s13296-018-0174-z

Meng, F.-Q., Zhu, M.-C., Clifton, G. C., Ukanwa, K. U., & Lim, J. B. P. (2020). Performance of square steel-reinforced concrete-filled steel tubular columns subject to non-uniform fire. *Journal of Constructional Steel Research*, *166*. https://doi.org/10.1016/j.jcsr.2019.105909

Molkens, T., Cashell, K. A., & Rossi, B. (2021). Post-fire mechanical properties of carbon steel and safety factors for the reinstatement of steel structures. *Engineering Structures*, *234*, 111975. https://doi.org/10.1016/J.ENGSTRUCT.2021.111975

Neuenschwander, M., Knobloch, M., & Fontana, M. (2010). Fire behavior of concrete filled circular hollow section columns with massive steel core. *Proceedings of SDSS' Rio 2010: International Colloquium Stability and Ductility of Steel Structures*, *1*.

Neuenschwander, M., Knobloch, M., & Fontana, M. (2013). Fire Tests of Concrete-Filled Circular Hollow Section Columns with a Solid Steel Core. *Composite Construction in Steel and Concrete VII - Proceedings of the 2013 International Conference on Composite Construction in Steel and Concrete*. https://doi.org/10.1061/9780784479735.039

Okada, K., Sekkei, N., Okada, K., & Yoshida, S. (2014). Structural Design of Nakanoshima Festival Tower. *International Journal of High-Rise Buildings*, *Vol 3*(No 3).

Park, S. H., Choi, S. M., & Chung, K. S. (2008). A study on the fire-resistance of concrete-filled steel square tube columns without fire protection under constant central axial loads. *Steel and Composite Structures*, *8*(6). https://doi.org/10.12989/scs.2008.8.6.491

Park, S. H., Chung, K. S., & Choi, S. M. (2007). A study on failure prediction and design equation of concrete filled square steel tube columns under fire condition. *International Journal of Steel Structures*, *7*(3).

Phan, L. T., & Carino, N. J. (2003). Code provisions for high strength concrete strength-temperature relationship at elevated temperatures. *Materials and Structures/Materiaux et Constructions*, *36*(256). https://doi.org/10.1617/13811

Pons, D., Lapuebla-Ferri, A., & Romero, M. L. (2022). Post-fire Residual Strength and Ductility of Structural Steels from Hollow Sections. *Ce/Papers*, *5*(4), 458–466. https://doi.org/https://doi.org/10.1002/cepa.1777

Qiang, X., Bijlaard, F., & Kolstein, H. (2012). Dependence of mechanical properties of high strength steel S690 on elevated temperatures. *Construction and Building Materials*, *30*, 73–79. https://doi.org/10.1016/j.conbuildmat.2011.12.018

Romero, M. L., Espinós, A., Renaud, C., Bihina, G., Schaumann, P., Kleiboemer, I., Gardner, L., Rodrigues, J. P., Laim, L., Lozano, C., & Iglesias, G. (2016). *Fire resistance of innovative and slender concrete filled tubular composite columns (FRISCC)* .

Romero, M. L., Ibañez, C., Espinos, A., Portolés, J. M., & Hospitaler, A. (2017). Influence of Ultra-high Strength Concrete on Circular Concrete-filled Dual Steel Columns. *Structures*, *9*. https://doi.org/10.1016/j.istruc.2016.07.001

Samarakkody, D. I., Thambiratnam, D. P., Chan, T. H. T., & Moragaspitiya, P. H. N. (2017). Differential axial shortening and its effects in high rise buildings with composite concrete filled tube columns. *Construction and Building Materials*, *143*. https://doi.org/10.1016/j.conbuildmat.2016.11.091

Schaumann, P., & Kleibömer, I. (2015). Thermal and structural response of concrete-filled tubular columns with massive steel core in case of fire. *Bautechnik*, *92*(5). https://doi.org/10.1002/bate.201500003

Shakil, S., Lu, W., & Puttonen, J. (2020). Experimental studies on mechanical properties of S700 MC steel at elevated temperatures. *Fire Safety Journal*, *116*, 103157. https://doi.org/10.1016/J.FIRESAF.2020.103157

Shao, Z., Zha, X., & Wan, C. (2022). Design method of fire-resistance capacity of reinforced-concrete-filled steel tube column under axial compression. *Fire Safety Journal*, *129*. https://doi.org/10.1016/j.firesaf.2022.103572

Shi, Y. L., Xian, W., Wang, W. Da, & Li, H. W. (2019). Experimental performance of circular concrete-filled steel tubular members with inner profiled steel under lateral shear load. *Engineering Structures*, *201*. https://doi.org/10.1016/j.engstruct.2019.109746

Standards Australia, & Standards New Zealand. (2014). AS/NZS 2327 - Composite Structures. *Proceedings of the Australasian Structural Engineering Conference 2014 (ASEC 2014)*, *July*.

Sun, J. (2023). Experimental investigation on residual capacity of square steel-reinforced concrete-filled steel tubular columns after fire. *Journal of Structural Fire Engineering*. https://doi.org/10.1108/JSFE-03-2023-0021

Tan, K. H., & Tang, C. Y. (2004a). Interaction Formula for Reinforced Concrete Columns in Fire Conditions. *ACI Structural Journal*, *101*(1). https://doi.org/10.14359/12994

Tan, K. H., & Tang, C. Y. (2004b). Interaction Model for Unprotected Concrete Filled Steel Columns Under Standard Fire Conditions. *Journal of Structural Engineering*, *130*(9). https://doi.org/10.1061/(asce)0733-9445(2004)130:9(1405)

Tan, Q.-H., Gardner, L., & Han, L.-H. (2019). Performance of Steel-Reinforced Concrete-Filled Stainless Steel Tubular Columns at Elevated Temperature. *International Journal of Structural Stability and Dynamics*, *19*(1). https://doi.org/10.1142/S0219455419400029

Tan, Q.-H., Gardner, L., Han, L.-H., & Song, T.-Y. (2019). Fire performance of steel reinforced concrete-filled stainless steel tubular (CFSST) columns with square cross-sections. *Thin-Walled Structures*, *143*. https://doi.org/10.1016/j.tws.2019.106197

Tang, C. Y., & Tan, K. H. (2001). Basis and Application of Simple Interaction Formula for Steel Frames under Fire Conditions. *Journal of Structural Engineering*, *127*(10). https://doi.org/10.1061/(asce)0733-9445(2001)127:10(1214)

Tao, Z., & Ghannam, M. (2013). Heat transfer in concrete-filled carbon and stainless steel tubes exposed to fire. *Fire Safety Journal*, *61*, 1–11. https://doi.org/10.1016/J.FIRESAF.2013.07.004

Tao, Z., & Han, L. H. (2006). Behaviour of concrete-filled double skin rectangular steel tubular beam-columns. *Journal of Constructional Steel Research*, *62*(7). https://doi.org/10.1016/j.jcsr.2005.11.008

Tao, Z., Han, L. H., & Wang, Z. Bin. (2005). Experimental behaviour of stiffened concrete-filled thin-walled hollow steel structural (HSS) stub columns. *Journal of Constructional Steel Research*, *61*(7). https://doi.org/10.1016/j.jcsr.2004.12.003

Tao, Z., Han, L. H., & Wang, D. Y. (2007). Experimental behaviour of concrete-filled stiffened thin-walled steel tubular columns. *Thin-Walled Structures*, *45*(5). https://doi.org/10.1016/j.tws.2007.04.003

Tao, Z., Han, L. H., & Wang, D. Y. (2008). Strength and ductility of stiffened thin-walled hollow steel structural stub columns filled with concrete. *Thin-Walled Structures*, *46*(10). https://doi.org/10.1016/j.tws.2008.01.007

Tao, Z., Han, L. H., & Zhao, X. L. (2004). Behaviour of concrete-filled double skin (CHS inner and CHS outer) steel tubular stub columns and beam-columns. *Journal of Constructional Steel Research*, *60*(8). https://doi.org/10.1016/j.jcsr.2003.11.008

Tao, Z., Wang, X.-Q., & Uy, B. (2013). Stress-Strain Curves of Structural and Reinforcing Steels after Exposure to Elevated Temperatures. *Journal of Materials in Civil Engineering*, *25*(9), 1306–1316. https://doi.org/10.1061/(ASCE)MT.1943-5533.0000676

Twilt, L., Hass, R., Klingsch, W., Edwards, M., & Dutta, D. (1996). *Design guide for structural hollow section columns exposed to fire*. Verlag TÜV Rheinland.

Uenaka, K., Kitoh, H., & Sonoda, K. (2010). Concrete filled double skin circular stub columns under compression. *Thin-Walled Structures*, *48*(1). https://doi.org/10.1016/j.tws.2009.08.001

Wang, W. Da, Jia, Z. L., Xian, W., & Shi, Y. L. (2023). Performance of SRCFST member under long-term loading and preload on steel tube. *Journal of Building Engineering*, *73*. https://doi.org/10.1016/j.jobe.2023.106700

Wang, W. Da, Mao, W. J., & Zhou, K. (2024). Experimental investigation on residual capacity of steel-reinforced concrete-filled thin-walled steel tubular columns subjected to combined loading and temperature. *Thin-Walled Structures*, *197*. https://doi.org/10.1016/j.tws.2024.111557

Wang, F., Liu, F., Yang, H., & Sheng, H. (2023). Axial compressive performances of thin-walled steel tube confined steel-reinforced concrete columns after fire exposure. *Thin-Walled Structures*, *190*. https://doi.org/10.1016/j.tws.2023.110919

Wang, Q. X., Zhu, M. C., & Wang, H. D. (2006). Experimental research on square steel tubular columns filled with steel-reinforced self-consolidating high-strength concrete under axial load. *American Concrete Institute, ACI Special Publication*, *SP-235*. https://doi.org/10.14359/15857

Wang, Q., Zhao, D., & Guan, P. (2003). Study on the mechanical properties of axially loaded steel tubular columns filled with steel-reinforced high-strength concrete. *Jianzhu Jiegou Xuebao/Journal of Building Structures*, *24*(6).

Wang, Q., Zhao, D., & Guan, P. (2004). Experimental study on the strength and ductility of steel tubular columns filled with steel-reinforced concrete. *Engineering Structures*, *26*(7). https://doi.org/10.1016/j.engstruct.2004.02.009

Wang, Y. C. (2000). A simple method for calculating the fire resistance of concrete-filled CHS columns. *Journal of Constructional Steel Research*, *54*(3). https://doi.org/10.1016/S0143-974X(99)00061-9

Wang, Y. C., & Kodur, V. K. R. (1999). An approach for calculating the failure loads of unprotected concrete filled steel columns exposed to fire. *Structural Engineering and Mechanics*, *7*(2). https://doi.org/10.12989/sem.1999.7.2.127

Wang, Z. H., & Tan, K. H. (2006). Green's function solution for transient heat conduction in concrete-filled CHS subjected to fire. *Engineering Structures*, *28*(11). https://doi.org/10.1016/j.engstruct.2006.02.007

Xian, W., Wang, W. Da, Wang, R., Chen, W., & Hao, H. (2020). Dynamic response of steel-reinforced concrete-filled circular steel tubular members under lateral impact loads. *Thin-Walled Structures*, *151*. https://doi.org/10.1016/j.tws.2020.106736

Yang, H., Liu, F., & Gardner, L. (2013). Performance of concrete-filled RHS columns exposed to fire on 3 sides. *Engineering Structures*, *56*. https://doi.org/10.1016/j.engstruct.2013.08.019

Yang, X., Tang, C., Chen, Y., & Qiao, T.-Y. (2020). Compressive behavior of steel-reinforced concrete-filled square steel tubular stub columns after exposure to elevated temperature. *Engineering Structures*, *204*, 110048. https://doi.org/https://doi.org/10.1016/j.engstruct.2019.110048

Yu, M., Hu, X., Xu, L., & Cheng, S. S. (2022). A general unified method for calculating fire resistance of CFST columns considering various types of steel and concrete. *Journal of Building Engineering*, *59*. https://doi.org/10.1016/j.jobe.2022.105125

Yu, M., Pei, X., Xu, L., & Ye, J. (2018). A unified formula for calculating bending capacity of solid and hollow concrete-filled steel tubes under normal and elevated temperature. *Journal of Constructional Steel Research*, *141*. https://doi.org/10.1016/j.jcsr.2017.11.017

Yu, M., Xu, H., Ye, J., & Chi, Y. (2018). A unified interaction equation for strength and global stability of solid and hollow concrete-filled steel tube columns under room and elevated temperatures. *Journal of Constructional Steel Research*, *148*. https://doi.org/10.1016/j.jcsr.2018.05.026

Yu, M., Zha, X., Ye, J., & Li, Y. (2013). A unified formulation for circle and polygon concrete-filled steel tube columns under axial compression. *Engineering Structures*, *49*. https://doi.org/10.1016/j.engstruct.2012.10.018

Yu, M., Zha, X., Ye, J., & Wang, B. (2014). A unified method for calculating fire resistance of solid and hollow concrete-filled steel tube columns based on average temperature. *Engineering Structures*, *71*. https://doi.org/10.1016/j.engstruct.2014.03.038

Zhang, S., Guo, L., Ye, Z., & Wang, Y. (2005). Behavior of steel tube and confined high strength concrete for concrete-filled RHS tubes. *Advances in Structural Engineering*, *8*(2). https://doi.org/10.1260/1369433054037976

Zhao, T. (2020). Bearing Capacity Studies on Square Steel Tube Confined Steel Reinforced Concrete Column under Eccentric Load. *Advances in Civil Engineering*, *2020*. https://doi.org/10.1155/2020/4212049

Zhao, X. L., & Grzebieta, R. (2002). Strength and ductility of concrete filled double skin (SHS inner and SHS outer) tubes. *Thin-Walled Structures*, *40*(2). https://doi.org/10.1016/S0263-8231(01)00060-X

Zhao, X.-L., Han, L.-H., & Lu, H. (2010). Concrete-filled Tubular Members and Connections. In *Concrete-filled Tubular Members and Connections*. https://doi.org/10.1201/9781482266085

Zheng, J., & Wang, J. (2018). Concrete-Filled Steel Tube Arch Bridges in China. *Engineering*, *4*(1), 143–155. https://doi.org/10.1016/j.eng.2017.12.003

Zheng, X. Z., Cai, J., & Zheng, X. H. (2013). Axial compressive behavior of stiffened square concrete-filled steel tubular stub columns under axial load. *Huanan Ligong Daxue Xuebao/Journal of South China University of Technology (Natural Science)*, *41*(10). https://doi.org/10.3969/j.issn.1000-565X.2013.10.020

Zhong, S. tong, & Zhang, S. (1999). Application and development of concrete-filled steel tubes (CFST) in high rise buildings. *Advances in Structural Engineering*, *2*(2). https://doi.org/10.1177/136943329900200207

Zhou, G., Luo, C., Chen, C., Dong, X., Chen, X., & Liu, X. (2014). The Structural Design of the Haiyi Hotel in Jiangmen. *Guangdong Architecture Civil Engineering*, *8*, 3–7.

Zhou, P., & Zhu, Z. (1997). Concrete-Filled Tubular Arch Bridges in China. *Structural Engineering International*, *7*(3). https://doi.org/10.2749/101686697780494699

Zhu, M.-C., Liu, J. X., Wang, Q. X., & Feng, X. F. (2010). Experimental research on square steel tubular columns filled with steel-reinforced self-consolidating high-strength concrete under axial load. *Engineering Structures*, *32*(8). https://doi.org/10.1016/j.engstruct.2010.04.002

Zhu M.-C., Meng F.-Q., & He B. (2016). Experimental research on fire resistance of steel tubular columns filled with steel reinforced concrete. *Journal of Building Structures*, *37*(3), 36–43.

ANNEX I. COMPENDIUM OF PUBLICATIONS
ARTICLE 1
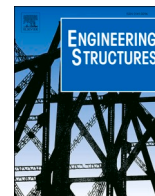
Simplified proposal for the temperature field of steel-reinforced CFST columns exposed to fire

David Medall [a], Ana Espinós [a],[*], Vicente Albero [b], Manuel L. Romero [a]

[a] *ICITECH, Universitat Politècnica de València, Valencia, Spain*
[b] *Department of Mechanical Engineering and Construction, Universitat Jaume I, Castellón, Spain*

ARTICLE INFO

ABSTRACT

Concrete-filled steel tubular (CFST) columns are composite sections that may contribute to reduce the environmental impact in construction through a more efficient use of resources. By embedding a steel profile inside a CFST section, a new typology is generated, the so-called steel-reinforced concrete-filled steel tubular (SR-CFST) columns, which may enhance not only the structural capacity of these composite columns at room temperature but also their fire performance. This paper focuses on studying the thermal behaviour of SR-CFST columns under fire conditions, for which purpose a two-dimensional finite element model was developed by the authors and validated by comparing the temperature distribution results with experimental tests available in the literature. Subsequently, parametric studies were carried out to analyse the influence of the relevant parameters – cross-section shape, outer tube thickness, inner steel profile dimensions, section factor – over the cross-sectional capacity of SR-CFST columns exposed to a standard ISO 834 fire. Using the data obtained from the parametric studies, a simplified temperature distribution proposal was derived. In the presented proposal, the composite section was divided onto four components (hollow steel tube, concrete infill, inner steel profile web and flanges) and simplified equations and tables were developed through statistical data processing in order to find the representative equivalent temperature of each part of the section. By doing so, the reduced cross-sectional capacity of a SR-CFST column at a given fire resistance period can be easily evaluated by using a single strength and stiffness value for each component of the section corresponding to its assigned equivalent temperature. This simplified approach may be helpful for practitioners in the fire design process of SR-CFST columns, for which the current provisions in Eurocode 4 Part 1.2 do not provide guidance in predicting the temperature field.

1. Introduction

The premature failure of slender concrete-filled steel tubular (CFST) columns when exposed to fire has been highlighted in previous investigations by the authors [1]. Given these limitations, solutions are sought for improving the fire performance of this typology of composite columns. In recent years, innovative solutions have been developed to increase both the load-bearing capacity and fire resistance of CFST columns [2]. One of these solutions consists of embedding an open steel profile within the concrete infill of the CFST section, generating the so-called steel-reinforced CFST section (SR-CFST), see Fig. 1. In this configuration, the inner steel profile results thermally protected by the surrounding concrete and therefore, its degradation at elevated temperatures is delayed, which may thus help resist the applied load for a more extended period of fire exposure time. This composite section combines the advantages of CFST columns and steel-reinforced concrete (SRC) columns.

Numerous public buildings in China have adopted SR-CFCST columns as the main load-bearing structural members. A successful example of a high-rise building using SR-CFST sections is the Haiyi Hotel in Jiangmen (China), described by Zhou et al. [3].

These types of composite sections are also being gradually introduced in Europe. An example of the use of this solution is the Millennium Tower in Wien (Austria) [4]. It is a fifty-five storey (202 m high) with CFST columns made of outer S355 CHS tubes with a C40–C60 concrete infill. The internal columns of the building have been provided with embedded H profiles to increase their load-bearing capacity. More recent studies covered the use of CFST sections for other innovative applications, such as retaining wall systems [5,6] and massive steel–concrete composite columns and beams [7].

Amongst the scarce experimental investigations found on SR-CFST

Nomenclature

A_i	Cross-sectional area of a cell of the finite element mesh
$A_{a,i}$	Cross-sectional area of a cell of the outer steel tube
$A_{c,i}$	Cross-sectional area of a cell of the concrete infill
$A_{p,i}$	Cross-sectional area of a cell of the inner steel profile
A_m/V	Section factor
B	Outer dimension of the square section
c_p	Specific heat
CES	Concrete encased sections
CFST	Concrete-filled steel tube
D	Outer diameter of the circular section
E_a	Elastic modulus of the steel of the outer tube at room temperature
$E_{a,\theta}$	Elastic modulus of the steel of the outer tube at the temperature θ
$E_{c,sec}$	Secant modulus of concrete at room temperature
$E_{c,sec,\theta}$	Secant modulus of concrete at the temperature θ
E_p	Elastic modulus of the steel of the inner profile at room temperature
$E_{p,\theta}$	Elastic modulus of the steel of the inner profile at the temperature θ
$EI_{y,fi}$	Flexural stiffness of the composite section in the fire situation (minor axis)
$EI_{y,fi,c}$	Flexural stiffness of the concrete infill in the fire situation (minor axis)
$EI_{y,fi,f}$	Flexural stiffness of the steel profile flanges in the fire situation (minor axis)
$EI_{y,fi,w}$	Flexural stiffness of the steel profile web in the fire situation (minor axis)
$EI_{z,fi}$	Flexural stiffness of the composite section in the fire situation (major axis)
$EI_{z,fi,c}$	Flexural stiffness of the concrete infill in the fire situation (major axis)
$EI_{z,fi,f}$	Flexural stiffness of the steel profile flanges in the fire situation (major axis)
$EI_{z,fi,w}$	Flexural stiffness of the steel profile web in the fire situation (major axis)
F	View factor
FE	Finite element
f_c	Compressive cylinder strength of concrete at room temperature
$f_{c,\theta}$	Compressive cylinder strength of concrete at the temperature θ
$f_{y,a}$	Yield strength of the steel of the outer tube at room temperature
$f_{y,a,\theta}$	Yield strength of the steel of the outer tube at the temperature θ
$f_{y,p}$	Yield strength of the steel of the inner profile at room temperature
$f_{y,p,\theta}$	Yield strength of the steel of the inner profile at the temperature θ

h_j	Joint contact conductance
ISCR	Inner Steel Contribution Ratio
$I_{a,i}$	Second moment of area of a cell of the outer steel tube
$I_{c,i}$	Second moment of area of a cell of the concrete infill
$I_{f,i}$	Second moment of area of a cell of the inner steel profile flange
$I_{w,i}$	Second moment of area of a cell of the inner steel profile web
k	Thermal conductivity
$k_{i,\theta}$	Reduction factor for a material property at elevated temperature
$N_{pl,Rd}$	Design cross-sectional plastic resistance to axial compression
$N_{fi,pl,Rd}$	Design cross-sectional plastic resistance to axial compression in fire
$N_{fi,pl,Rd,a}$	Outer steel tube plastic resistance to axial compression in fire
$N_{fi,pl,Rd,c}$	Concrete plastic resistance to axial compression in fire
$N_{fi,pl,Rd,f}$	Steel profile flanges plastic resistance to axial compression in fire
$N_{fi,pl,Rd,w}$	Steel profile web plastic resistance to axial compression in fire
n	Normal direction to a surface
P_m	Perimeter of the exposed surface
q	Heat flux
R	Standard fire exposure time
SR-CFST	Steel-reinforced concrete-filled steel tube
t	Thickness of the outer steel tube
u_s	Concrete cover
y_i	Coordinate of the centroid of a cell of the FE mesh (perpendicular to major axis)
z_i	Coordinate of the centroid of a cell of the FE mesh (perpendicular to minor axis)
α_c	Convective coefficient
ε	Emissivity
ε_{cu}	Concrete strain at room temperature
$\varepsilon_{cu,\theta}$	Concrete strain at the temperature θ
θ	Temperature
θ_i	Temperature of the centroid of a cell of the FE mesh
θ_a	Temperature of the outer steel tube surface
$\theta_{a,eq}$	Equivalent temperature of the outer steel tube
$\theta_{c,eq}$	Equivalent temperature of the concrete infill
$\theta_{f,eq}$	Equivalent temperature of the flanges of the inner steel profile
$\theta_{w,eq}$	Equivalent temperature of the web of the inner steel profile
θ_g	Gas temperature in the vicinity of the fire exposed member
θ_m	Surface temperature of the exposed member
θ_r	Effective radiation temperature of the fire environment
θ_{exp}	Experimentally measured temperature
θ_{num}	Numerically calculated temperature
ρ	Density
σ	Stephan-Boltzmann constant

columns exposed to fire conditions, the works from Chu et al. [8–10], Zhu et al. [11] and Meng et al. [12] can be cited. The first authors tested at elevated temperature ten columns filled with self-compacting concrete embedding another steel profile. Four of the column specimens used an embedded HEB profile - two of which were protected by intumescent coating- and were tested with time resistance times ranging between 39 and 79 min. The experimental results were completed through a numerical model developed by the authors using the SAFIR computer code. Regarding the studies by Zhu et al. [11], eight fire resistance tests were carried out on SR-CFST columns filled with normal

strength concrete under non-uniform fire conditions. Five square and three circular SR-CFST columns were tested. More details of these fire tests can be found in [13] for the square SR-CFST sections and [14] for the circular SR-CFST sections. In the same research framework, Meng et al. [12] studied experimentally the residual strength of SR-CFST stub columns after exposure to iSO-834 fire. Three square SR-CFST columns composed of an outer SHS and an inner steel profile were exposed from 2, 3 and 4 sides inside a small electric furnace. Once cooled down, the column specimens were loaded incrementally until failure to obtain their residual strength. Based on the results of parametric studies

conducted by the authors, formulae were proposed for predicting the residual strength of SR-CFST columns after different types of fire exposure.

In light of the review of the experimental programmes published in the literature, it can be seen that the number of available fire test results on SR-CFST columns is still scarce. Given the lack of sufficient experimental evidence, researchers worldwide have focused on studying the fire performance of SR-CFST sections through analytical or numerical models.

The first work which can be found in the literature on the analytical resolution of the transient heat conduction in concrete filled steel hollow sections exposed to fire is that from Lie [15]. Based on the finite differences method [16], Lie and co-workers derived expressions which allow to calculate the temperature of the concrete core and steel tube by subdividing the cross-sectional area of the column in a number of layers for CHS columns [17,18] or elements in the case of RHS columns [19].

Later investigations by Tan & Tang [20] extended the Rankine method to the analyses of plain and reinforced concrete filled tubular columns at elevated temperatures.

Wang & Tan [21] presented a theoretical approach for the heat transfer analysis of concrete filled steel circular hollow sections subjected to fire based on an analytical Green's function solution. This approach can be used to predict the temperature field inside the composite domain and the heat flux at the fire and steel–concrete interfaces.

Despite the analytical solution of CFST sections with different geometries (circular, square) has been widely covered by researchers in the last decades, when it comes to SR-CFST sections, the multiple steel–concrete interfaces and the complex thermal gradient generated within the inner profile make it difficult to derive analytical equations, reason that has motivated researchers to the development of numerical models that facilitate this task.

The numerical investigation conducted by Espinós et al. [22] compared the fire performance of different types of innovative steel––concrete composite columns – SR-CFST columns among them – and proposed strategies for enhancing the fire resistance of traditional CFST columns by using inner steel profiles. The numerical model was developed in ABAQUS using three-dimensional eight-noded solid elements for the steel tube and concrete core and four-noded three-dimensional bilinear rigid quadrilateral elements with a maximum finite element size of 20 mm. The thermal resistance at the steel–concrete interface was assumed via a constant value for the gap conductance parameter. The error obtained with this model (test/prediction) was 1.08 with a standard deviation equal to 0.19. It was observed that by "splitting" the outer steel tube into two profiles and moving most of the amount of steel towards the inner part of the section, the resisting profile resulted "internally" protected by the surrounding concrete. Thus its degradation at elevated temperatures was delayed, lengthening the fire endurance of

the column. It was also found that the fire performance of SR-CFST columns might be significantly enhanced by using high strength steel at the inner profiles.

Tan et al. [23,24] developed a numerical model for SR-CFST columns using stainless steel at the outer tube. These authors carried out additional parametric studies in order to assess and optimise the performance of these composite sections and quantify the increase in terms of fire resistance when introducing an inner steel profile in CFST sections with carbon steel or stainless-steel outer tube. The model was meshed setting a maximum finite element size of 20 mm. Solid elements were used for the in-filled concrete, while shell elements were used for the steel tube and profile. The model had a mean error value of 1.048 and a coefficient of variation of 0.071 for the circular columns and 1.055 and 0.072 respectively for the square columns. It was found that the SR-CFST columns with stainless steel outer tube exhibited an enhanced fire resistance over the corresponding CFST and CFSST columns with the same cross-sectional area or load-bearing capacity at room temperature.

Mao et al. [25] presented a numerical study on the fire performance of SR-CFST columns with square cross-sections. The influence of parameters such as the column slenderness, concrete and steel strength and the steel ratio of the outer tube and inner profile were assessed through numerical simulations. The mesh of the model used in this study employed 8-node brick elements (DC3D8) for all components and a maximum finite element size of 20 mm. A constant value of 0.01 m^2 $°C/W$ was assumed for the thermal resistance at the steel–concrete interface. The mean value and standard deviation values obtained were 1.083 and 0.076 respectively. It was found that the proportions of the steel used at the outer tube and inner profile have a notable influence on the fire resistance of SR-CFST columns. The authors also highlighted the potential of using high strength steel at the inner profile for enhancing the fire resistance, which was in line with the findings by Espinós et al. [22].

A finite element model for SR-CFST columns subjected to non-uniform fire was developed by Meng et al. [13,14] and validated against the tests previously reported in Zhu et al. [11]. Four-noded shell elements, S4R, were used in this study. The interaction between the outer steel tube and the inner concrete core was introduced via a constant value of 200 W/m^2 for the gap conductance. An average ratio of experimental ultimate bearing capacity N_{cr} to the simulated results N'_{cr} was 0.98 and the standard deviation was 0.015. Parametric studies were carried out employing the numerical model in order to assess the application of the existing fire design methods of CFST columns to SR-CFST columns. Regarding the design guidance, at present, there is no specific method in the literature or international design codes that cover this type of sections. In the absence of a specific calculation method, the fire design approach for CFST sections developed by the authors of this paper in previous investigations [26] – which is currently used in Europe
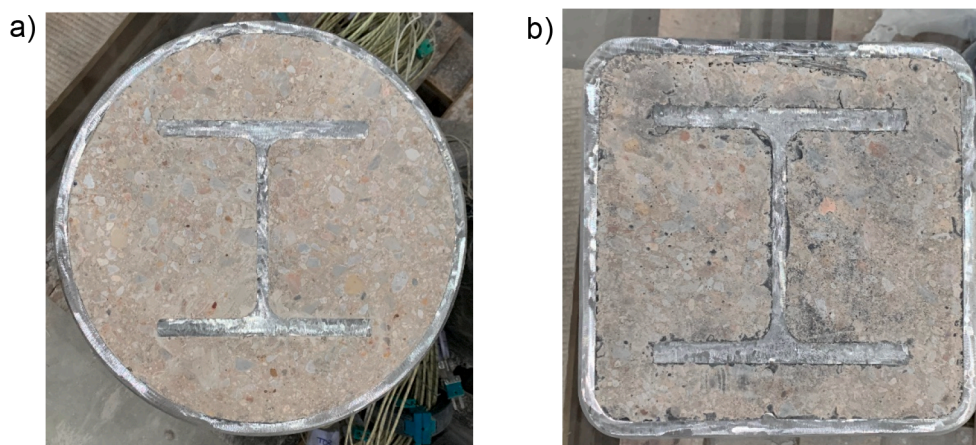
Fig. 1. SR-CFST sections studied in this paper: (a) circular; (b) square.

in replacement of the Annex H method of EN1994-1-2 – was tentatively applied to SR-CFST columns. The method produced conservative results in predicting the fire resistance of axially loaded SR-CFST columns under uniform fire exposure conditions. However, it was concluded that further research is needed to provide accurate predictions for different types of loading (i.e. eccentricities) and fire exposure conditions (i.e. non-uniform fire). It should be pointed out that, since SR-CFST sections are beyond the scope of the new Annex H method, fixed "equivalent" values for in certain parameters (i.e. reinforcement ratio and member slenderness) were assumed by Meng et al. as an intend to apply the method to SR-CFST sections, assimilating the inner steel profile of the SR-CFST section to a reinforcement in a CFST section. This may be a possible source of the deviations found in the predictions; therefore, further research is needed to develop a specific design method for the fire evaluation of SR-CFST columns.

In light of the revision of state of the art, where the scarce number of investigations available on SR-CFST sections has been evidenced, as well as the lack of guidance in Eurocode 4 Part 1.2 [27] for this type of sections, it can be seen that there is a need for developing design equations that allow predicting the temperature distribution in SR-CFST sections in order to evaluate the axial capacity of the columns when subjected to fire. This will be one of the aims of this paper, where a finite element thermal model will be developed and generalized through parametric studies to develop a simplified design proposal that will provide practitioners with a practical tool to easily predict the cross-sectional capacity of SR-CFST sections under fire conditions.

2. Development of the finite element model

A two-dimensional (2D) finite element model was developed utilizing the general-purpose nonlinear finite element analysis package ABAQUS [28]. As this research focuses on the thermal behaviour of SR-CFST columns exposed to a standard fire, a 2D model is enough to analyse the temperature development within the section, assuming that the columns are uniformly exposed in all their length. The use of a 2D model is suitable in this scenario, since the primary goal of the numerical model is to evaluate the cross-sectional plastic resistance and flexural stiffness values at the critical section of the columns. This decision may provide conservative results in the case of a non-uniform fire exposure. Moreover, as this thermal model does not take into account the situation of localized fires but a generalized fire at the compartment (post-flash-over), the assumption of considering the column uniformly exposed along its full length can be made. The main characteristics of the developed numerical model are described in the following subsections.

2.1. Geometry and finite element mesh

The geometry of the model is composed of an assembly of three different parts: outer steel tube, concrete encasement and inner steel profile.

These parts are meshed using 3-node linear heat transfer triangles (DC2D3) with nodal temperature degree of freedom. Based on the results of a mesh sensitivity study (see the following subsection), a maximum finite element (FE) size of 10 mm was used. An example of the FE mesh for a circular SR-CFST section can be seen in Fig. 2.

2.1.1. Mesh sensitivity study

A mesh sensitivity study was performed to select the optimal size of the finite elements in the thermal model. Three different FE sizes were considered: 5, 10 and 20 mm.

Specimens 3A and 4A tested by Chu et al. [8–10] were numerically simulated to evaluate the appropriate mesh density. As shown in Fig. 3, a coarser mesh (20 mm FE) produced considerable deviations when comparing the numerically predicted temperatures with the measured temperatures at the selected thermocouple locations. In turn, FE sizes of 5 and 10 mm provided more accurate predictions in terms of
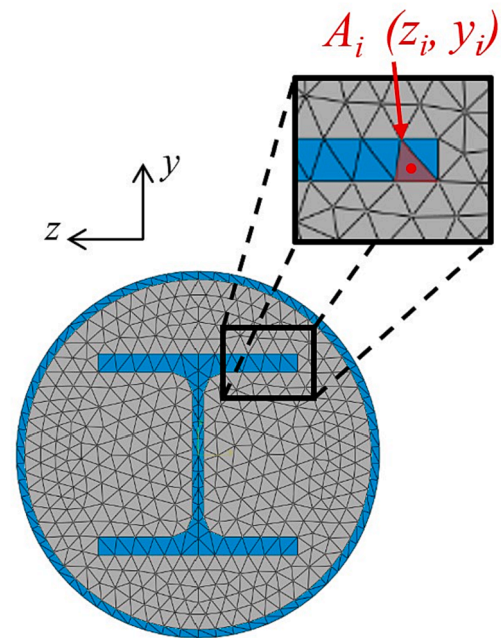
Fig. 2. Detail of the centroid position (z_i, y_i) and area (A_i) of a given triangular *i*-element of the mesh.
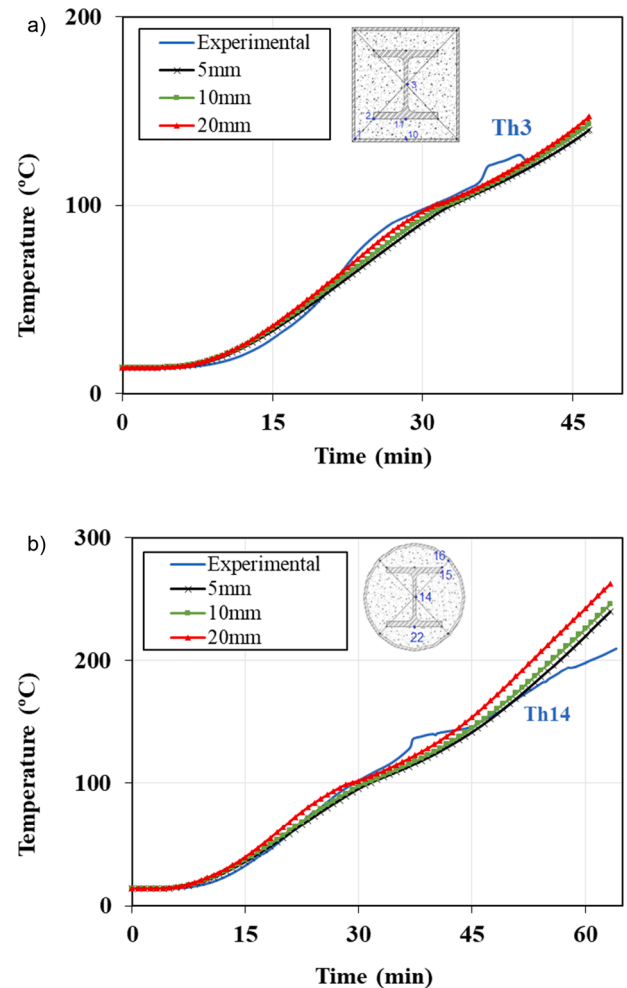
Fig. 3. Mesh sensitivity analysis. Comparison with the case specimens tested Chu et al. [5]: (a) 3A, (b) 4A.

temperature, being relatively close to the experimental results. Given the similarity in the temperature predictions obtained with 5 and 10 mm, the second FE size (10 mm) was chosen, as a more refined mesh (5 mm) does not result in a greater precision while it would lead to a higher computational cost.

Therefore, the suitable element size which provided accurate results with reasonable computational times was found to be 10 mm for the sectional dimensions covered in this paper.

2.2. Thermal analysis and boundary conditions

A nonlinear heat transfer analysis was conducted in ABAQUS for computing the temperature field of the studied SR-CFST sections subjected to fire conditions. The heat balance equation given in (1), based on the Fourier's law of heat conduction, was implemented in the numerical model. The fire action was applied in the model to the exposed surface of the SR-CFST section as a thermal load through the convection and radiation heat transfer mechanisms, which are driven by the equations given in (2).

$$\nabla(\boldsymbol{k} \bullet \nabla\theta) = \rho c_p \frac{\partial\theta}{\partial t} \tag{1}$$

$$-\boldsymbol{n} \bullet \boldsymbol{k} \bullet \nabla\theta = \alpha_c (\theta_m - \theta_g) + F \bullet \varepsilon \bullet \sigma\left(\theta_r^4 - \theta_g^4\right) \tag{2}$$

where θ_m is the surface temperature of the exposed member and θ_g and θ_r are the gas temperature in the vicinity of the fire exposed member and the effective radiation temperature of the fire environment,

respectively.

The evolution of the fire temperature in the model was assumed to follow the standard iSO-834 curve, for the cases analysed in the parametric studies. In those cases used for validation, where the temperature history of the real fire curve applied at the test was known, the average temperature–time curve measured inside the furnace was used, since this can be an important source of error when validating the model.

The values recommended in EN 1991-1-2 [29] were adopted for the governing parameters of the heat transfer problem. For the heat transfer portion by convection, a convective coefficient $\alpha_c = 25$ W/m^{2}K was assumed at the exposed steel surface.

For the radiative portion of heat transfer, an emissivity value $\varepsilon = 0.7$ was adopted at the exposed steel surface, while the emissivity of the fire was taken as $\varepsilon = 1$ and the Stephan-Boltzmann constant $\sigma = 5.67 \cdot 10^{-8}$ W/m^{2}K^4.

The nonlinear heat transfer analysis results consisted of the time evolution of the nodal temperatures (NT11) at the different nodes of the FE mesh. For example, Fig. 4 shows a plot of the numerically predicted cross-sectional temperature field for specimens 3A and 4A tested by Chu et al. [9] at two standard fire periods (30 and 60 min).

2.3. Steel-concrete interface

When exposed to elevated temperatures, the outer steel tube separates transversely from the concrete infill due to the different thermal expansion coefficients of steel and concrete. This phenomenon causes the opening of physical space at the interface between the steel tube and
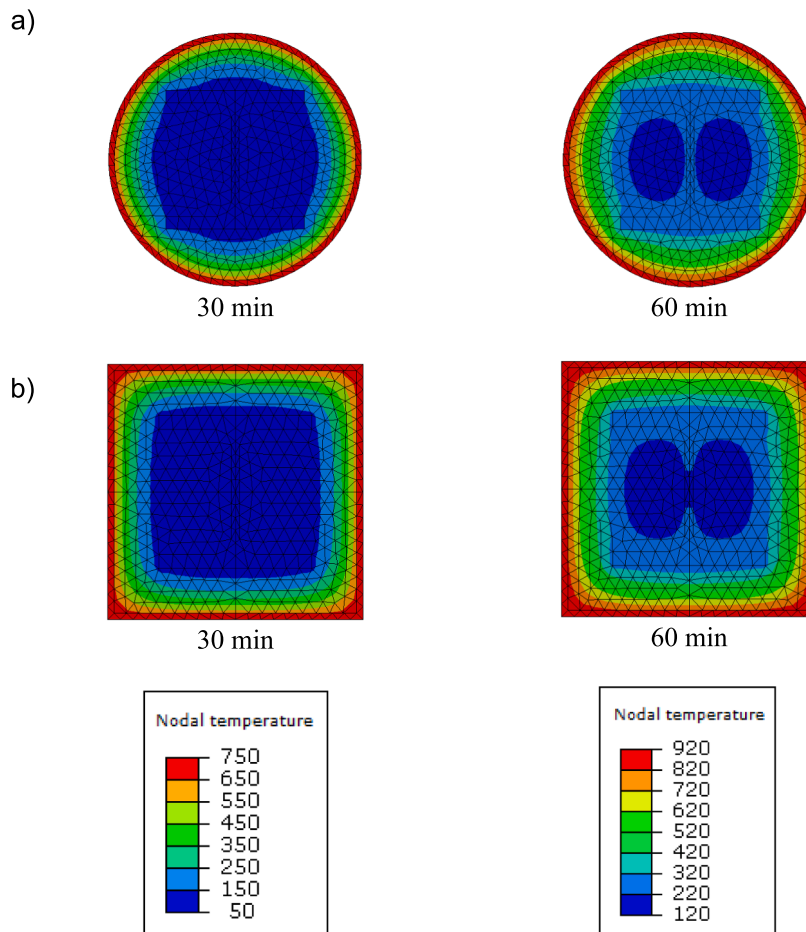
Fig. 4. Temperature field of the SR-CFST sections tested by Chu et al. [5] obtained from the numerical simulations: (a) 3A, (b) 4A.

the concrete infill, which can be considered an "air gap".

This resistance to heat flow is known as the contact thermal resistance and is usually expressed in terms of a joint contact conductance (h_j), defined as:

$$q = h_j \bullet \Delta\theta \qquad (3)$$

where $\Delta\theta$ is the temperature difference between the two contacting surfaces at the interface.

The effect of this "air gap" in CFST sections was studied by Ghojel [30], proving that this effect causes a thermal resistance at the boundary between steel and concrete and thus a temperature difference between the outer steel tube and the concrete core. Based on experimental measurements, Ghojel proposed an expression for estimating the interface thermal conductance in circular and square CFST sections as a function of the temperature:

$$h_j = 160.5 - 63.8 \bullet \exp\left(-339.9 \bullet \theta_a^{-1.4}\right) W/m^2 \bullet K \qquad (4)$$

where θ_a is the temperature of the outer steel tube surface in degrees Celsius.

Tao and Ghannam [31] proposed a new expression to evaluate the thermal contact conductance, as a function of the sectional dimensions:

$$\text{Circular columns}: \; h_j = 516 \bullet (D/100)^{-2.373} W/m^2 \bullet K \qquad (5)$$

$$\text{Square/rectangular columns}: \; h_j = 115 \bullet (B/100)^{-0.85} W/m^2 \bullet K \qquad (6)$$

where D is the diameter of the circular tube and B is the side length of a square or rectangular tube (in mm).

This model tends to stabilise around a constant value for massive sections (over 300 mm outer dimension), equal to 38.1 W/m^{2}K for circular columns and 45.2 W/m^{2}K for rectangular columns. Therefore, the influence of the outer dimension in the contact conductance value predicted by this model is more noticeable for reduced sectional dimensions, more pronounced for circular sections.

The described thermal resistance at the boundary between the outer steel tube and the concrete encasement was considered in the numerical model through the "gap conductance" option in ABAQUS [28]. Based on the sensitivity study results (presented in the following sub-section), a constant gap conductance value of 200 W/m^{2}K was used to model the thermal resistance at this interface.

However, for modelling the thermal contact between the concrete infill and the inner steel profile, a "perfect thermal contact" was considered – i.e., the temperatures of the steel profile and concrete are coupled at the interface – due to the reduced temperatures that can be reached at the inner parts of the composite section, no transversal separation is expected between the profile and the surrounding concrete encasement. Therefore, these surfaces are considered to remain in perfect contact during all the fire exposure. Other researchers already used this assumption with enough accuracy [24,25].

2.3.1. Sensitivity analysis for the gap conductance model at the outer steel tube-concrete interface

Three different options for modelling the "gap conductance" at the interface between the outer steel tube and the concrete core were studied. On a first assumption, a constant value of $h_j = 200$ W/m^{2}K was employed, as used by the authors in previous investigations [32]. The second option considered the gap conductance model as a function of the steel temperature suggested by Ghojel [18]. The third option used the model by Tao and Ghannam [31], dependent on the outer sectional dimensions.

The sensitivity analysis results on the gap conductance value can be seen in Fig. 5, where the prediction of temperatures at different points of the section are compared with the measured temperatures under the three models studied. As it can be seen, the computed temperatures at the outer steel tube are similar under the three models. However, at the monitored point of the concrete infill – located close to the interface -the

a)

b)
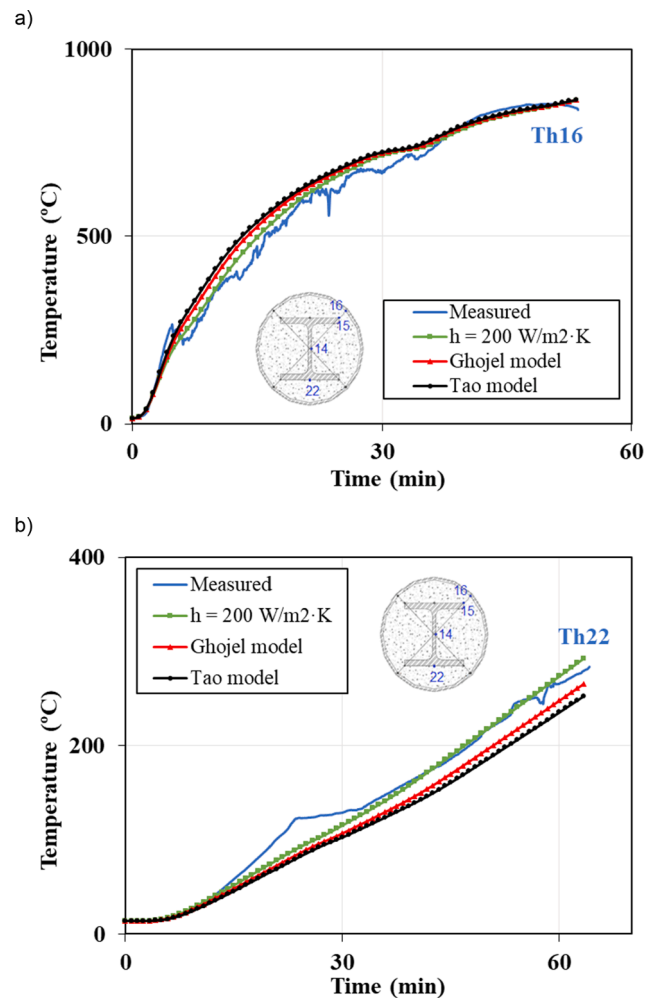
Fig. 5. Sensitivity analysis on the "gap conductance" model. Comparison with case 3A tested by Chu et al. [5].

best prediction was obtained assuming a constant gap conductance value. This observation was similar for other case specimens used to validate the numerical model from the tests available in the literature, although these results have not been included here for extension reasons.

It is worth noting that the model from Ghojel [30], dependent on the temperature of the outer steel tube is more time consuming, as it requires updating the gap conductance value at each calculation step as the temperature of the steel tube increases during the fire exposure. Therefore, assuming a constant value of $h_j = 200$ W/m^{2}K does not mean a loss of accuracy, while it allows for a more economical computing strategy in view of the parametric studies to be carried out in the framework of this research.

2.4. Material properties at elevated temperatures

The temperature-dependent thermal properties of the materials were accounted for in the numerical model.

For steel, the temperature-dependent thermal properties – specific heat (c_p) and thermal conductivity (k) – given in EN 1993-1-2 [33] were adopted.

The thermal properties for concrete at elevated temperatures were obtained from EN 1992-1-2 [34]. However, for modelling the thermal conductivity (k), the new model proposed in the draft version of prEN 1992-1-2:2021 [35] was adopted, which recommends using a transition between the upper and lower limit in the range of temperatures between

140 and 160 °C.

The latent heat of water vaporisation was taken into account through a peak value in the specific heat (c_p) formulation of concrete between 100 and 200 °C, as per Clause 3.3.2(8) in EN 1994-1-2 [27]. When no test data was available, a moisture content equal to 4 % of the concrete weight was assumed in the numerical model by default, as recommended in Clause 3.3.2(7) of EN 1994-1-2 [27], which was modelled through a peak value of 5577.9 J/Kg·K in the specific heat formulation.

3. Validation of the thermal model

In this section, the described numerical model is validated by comparing the temperature distribution results with experimental tests on SR-CFST columns available in the literature.

3.1. Validation of the thermal response of steel-reinforced CFST sections

The main characteristics of the SR-CFST case specimens used for validation are given in Table 1.

In the first validation stage, the experimental results from Chu et al. [9] were used. Specimens 3A and 4A were selected from the reported tests, the former consisted of a circular hollow steel tube of 219.1 × 5 mm with an embedded HEB 120 profile and the latter was a square hollow steel tube of 200 × 5 mm with the same embedded profile. A 6 % moisture value was considered, as reported in the experimental campaign, which equals to a specific heat peak value of 8518.6 J/Kg·K.

Tests 3B and 4B, protected with intumescent paint, were also tentatively compared for extending the validation, although fire-protected sections are out of the scope of this research.

The results of comparing the temperature evolution at the relevant points between the numerical simulations and the experimental thermocouple measurements reported by Chu et al. [9] can be seen in Fig. 6.

Additionally, four square and two circular SR-CFST sections from the experimental programme carried out by Zhu et al. [11] were numerically simulated. The cross-sectional dimensions of the outer square hollow sections (specimens S1H, S2H, S3H and S4H) were 300 mm × 300 mm × 6 mm, while the dimensions of the outer circular hollow sections (specimens C2H and C4H) were 300 mm × 8 mm. The inner steel profile was, in all cases, an H-section HW 150 × 150 (150 mm × 150 mm × 7 mm × 10 mm) according to the Chinese standard GB706-2008. The actual non-uniform fire exposure conditions of these tests

Fig. 6. Comparison between measured and computed temperature–time curves for the case specimens tested Chu et al. [5]: (a) 3A, (b) 4A.

Table 1
Summary of the geometrical and material properties of the column specimens used for validation.

Specimen	D (mm) B (mm)	t (mm)	$f_{y,tube}$ (MPa)	Inner profile	$f_{y,profile}$ (MPa)	f_c (MPa)	Exposure type	Fire protection	Moisture
SR-CFST sections									
3A [5]	219.1	5	420	HEB120	375	35	4-side	–	6 %
3B [5]	219.1	5	420	HEB120	375	35	4-side	Intumescent coating	6 %
4A [5]	200	5	510	HEB120	375	35	4-side	–	6 %
4B [5]	200	5	510	HEB120	375	35	4-side	Intumescent coating	6 %
C4H [7]	300	8	360	HW 150 × 150	345	55	4-side	–	5 %
C2H [7]	300	8	360	HW 150 × 150	345	55	½-section	–	5 %
S4H [7]	300	6	360	HW 150 × 150	345	55	4-side	–	5 %
S3H [7]	300	6	360	HW 150 × 150	345	55	3-side	–	5 %
S2H [7]	300	6	360	HW 150 × 150	345	55	2-side	–	5 %
S1H [7]	300	6	360	HW 150 × 150	345	55	1-side	–	5 %
CES sections									
RCC03 [25]	300 × 300			UC152 × 152 × 37	320	43	460	4-side	4 %
SZCC03 [20]	350 × 350			UC254 × 254 × 73	320	44	460	4-side	4 %
SZCC04 [20]	400 × 400			UC305 × 305 × 97	400	44	460	4-side	4 %
FR4S06 [21]	300 × 300			175 × 175 × 7.5 × 11	242.3–281.3	40	335	4-side	5.79 %
FR4S38 [21]	350 × 250			200 × 150 × 6 × 9	242.3–281.3	40	335	4-side	5.79 %
FR3S37 [21]	350 × 250			200 × 150 × 6 × 9	242.3–281.3	40	335	3-side	5.79 %
FR3S65 [21]	350 × 250			200 × 150 × 6 × 9	242.3–281.3	40	335	3-side	5.79 %
SRC1-1 [22]	300 × 300			150 × 150 × 10 × 10	307	38	383	4-side	4 %
SRHSC-1 [29]	300 × 300			200 × 200 × 8 × 12	380	121.1[a]	504	4-side	< 3 %

[a] Ultra-high-strength concrete with 0.5% steel fibers and 0.15% polypropylene fibers in volume.

were reproduced by the numerical model, with some of the columns being subjected to one, two, three or four-side fire exposure. Ceramic fibre blankets with thermal conductivity of 0.1–0.2 W/m°C were used for materialising the thermal insulation of the specimens subjected to non-uniform fire exposure. A 5 % moisture value was considered for simulating these case specimens, which was introduced via a specific heat peak value of 7048.2 J/Kg·K, as reported in the experimental campaign.

The results of comparing temperatures between the numerical model and the experimental test reported by Zhu et al. [11] are given in Fig. 7.

3.2. Validation of the thermal response of concrete-encased sections

Given the lack of sufficient experimental evidence on the thermal behaviour of SR-CFST sections, the validation of the numerical model was complemented by comparison with experimental test results of Concrete Encased Sections (CES) subjected to elevated temperatures. These sections consist of a reinforced concrete section with an embedded open steel profile; therefore, the information on the temperature field results helpful in verifying the thermal response of the numerical model, with the only particularity of the absence of the outer steel tube. A summary of the main characteristics of the CES sections used in this complementary validation is given in Table 1.

The tested specimens for validation of CES sections were taken from the experimental campaigns carried out by Huang et al. [36,37], Mao & Kodur [38], Han et al. [39] and Du et al. [40].

Test RCC03 was selected from Huang et al. [36], consisting of a square section of dimensions 300 × 300 mm. In turn, tests SZCC03 and SZCC04 were taken from Huang et al. [26], with outer dimensions 350 × 350 mm and 400 × 400 mm, respectively, to extend the validation to a wide range of sectional dimensions. In the absence of test data on the measured moisture content of these experimental programmes, a value of 4 % was considered. The results of comparing the numerical simulations with the cases tested by Huang et al. are given in Fig. 8 (test RCC03) and Fig. 9 (tests SZCC03, SZCC04).

Additionally, four test specimens from Mao & Kodur [38] were considered, as given in Table 1. These cases included three rectangular sections of dimensions 350 × 250 mm and one square section of 300 × 300 mm. The average moisture content at the time of the fire test (120 days) reported by the authors was considered in the numerical simulations, with a value of 5.79 %. This was modelled by a peak value of 8209.8 J/Kg·K in the specific heat formulation. The comparison of the temperature evolution at the relevant points of the section for two of the analysed specimens (FR4S06 and FR4S38) can be seen in Fig. 10.

Case specimen SRC1-1 from Han et al. [39] was used in this validation, consisting of a square section of dimensions 300 × 300 mm. Again, in the absence of test data on the measured moisture content of these experimental programmes, a value of 4 % was considered. The comparison of the evolution of temperatures between the numerical simulation and test for this case specimen can be seen in Fig. 11.

Finally, the validation was completed with one particular test specimen from Du et al. [40], made of ultra-high-strength concrete. Steel fibres with a dosage of 0.5 % in volume were added to the concrete mix to improve its ductility, while 0.15 % of polypropylene fibres were added to prevent spalling at elevated temperatures. The moisture content of concrete was measured during the tests, lower than 3 %, which was introduced by a specific heat peak value of 4107.5 J/Kg·K. The temperature evolution can be seen in Fig. 12.

3.3. Summary of the validation

A summary of the validation of the numerical model is presented in Fig. 13, where for each case specimen used for validation, the predicted and measured temperatures at the location of the thermocouples are plotted for different fire exposure times (30, 60, 90, 120 min). A good agreement is observed, with most points within the ±15 % boundaries.

The mean and standard deviation values of the temperature predictions have been summarised in Table 2, where the prediction errors have been calculated as $\theta_{num}/\theta_{exp}$, a mean value higher than 1 meaning that the thermal model is conservative (i.e., higher temperature predicted by the numerical model in comparison with the experimental
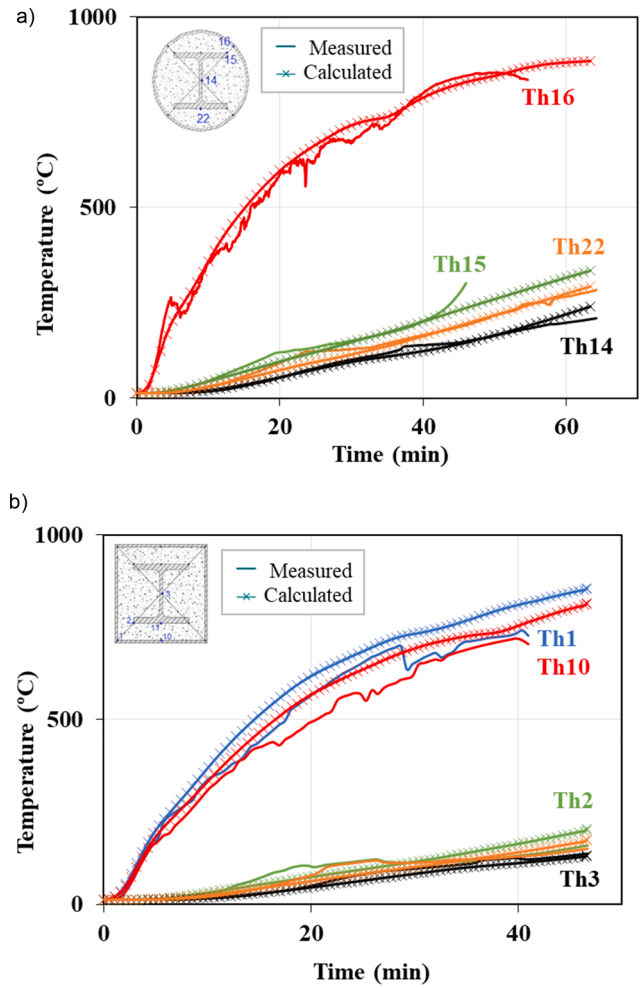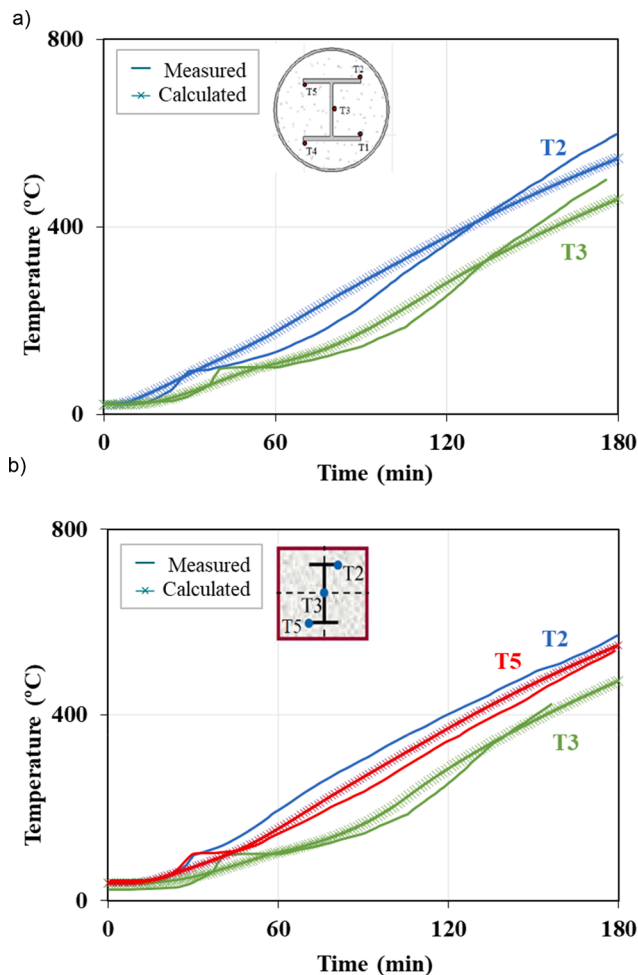

Fig. 7. Comparison between measured and computed temperature–time curves for the case specimens tested by Zhu et al. [7]: (a) C4H, (b) S4H.
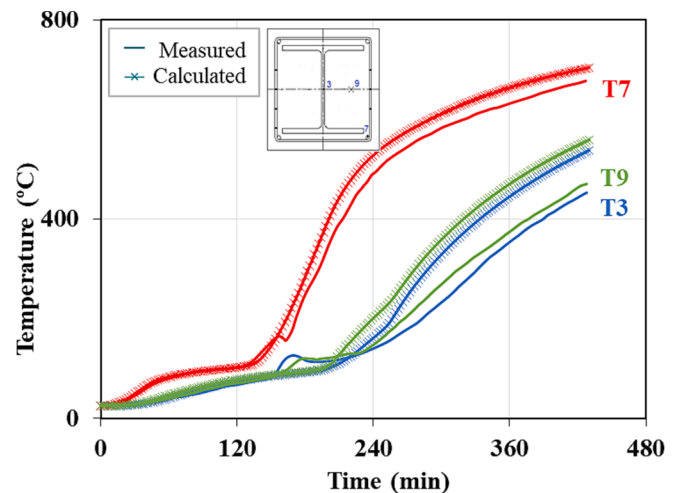
Fig. 8. Comparison between measured and computed temperature–time curves at the relevant points of the section for case RCC03 from Huang et al. [25].
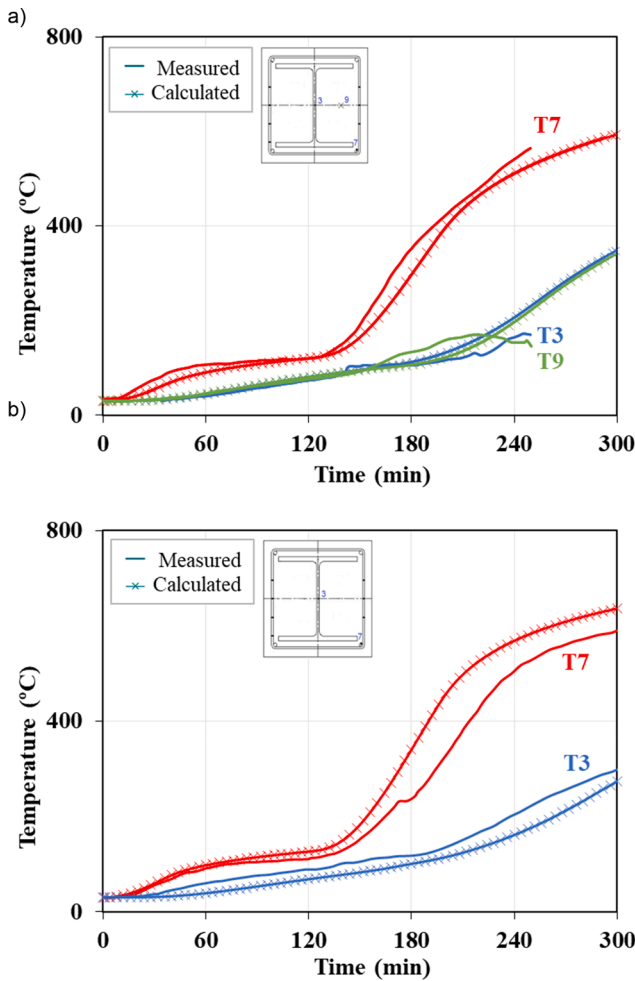
Fig. 9. Comparison between measured and computed temperature–time curves for the case specimens from Huang et al. [26]: (a) SZCC03, (b) SZCC04.

Fig. 10. Comparison between measured and computed temperature–time curves for the case specimens from Mao & Kodur [27]: (a) FR4S06, (b) FR4S38.

value). The average value of the prediction errors accounting for all the columns analysed is 1.03 with a standard deviation of 0.20. Thus, the model can be considered accurate and slightly conservative. It can also be seen in Table 2 that the thermal model predictions are more accurate for temperatures higher than 300 °C, with an average value of 0.99 and a narrower dispersion (0.08 standard deviation). The reason is that in the range of temperatures between 100 °C and 200 °C, the evaporation of the moisture content in concrete occurs, which produces a plateau in the temperature–time curves that is difficult to predict by the numerical model. It is worth reminding that the water vaporisation in concrete has been implicitly accounted for through the specific heat formulation, which causes this deviation at low temperatures. However, when the evaporation phenomena finish and the concrete temperature skips this plateau, the model can predict the evolution of temperatures with reasonable accuracy.

In view of this comparison, and given the variety of sections studied, the different experimental sources compared, and the lack of further details on parameters such as the concrete moisture content, the accuracy of the temperature predictions is considered appropriate. Therefore, the numerical model is judged reliable for conducting parametric studies on the thermal behaviour of SR-CFST sections, which will be carried out in the following section.

Fig. 11. Comparison between numerical and experimental temperature–time curves at the relevant points of the section for case SRC1-1 from Han et al. [28].

Fig. 12. Comparison between numerical and experimental temperature–time curves at the relevant points of the section for case SRHSC-1 from Du et al. [29].
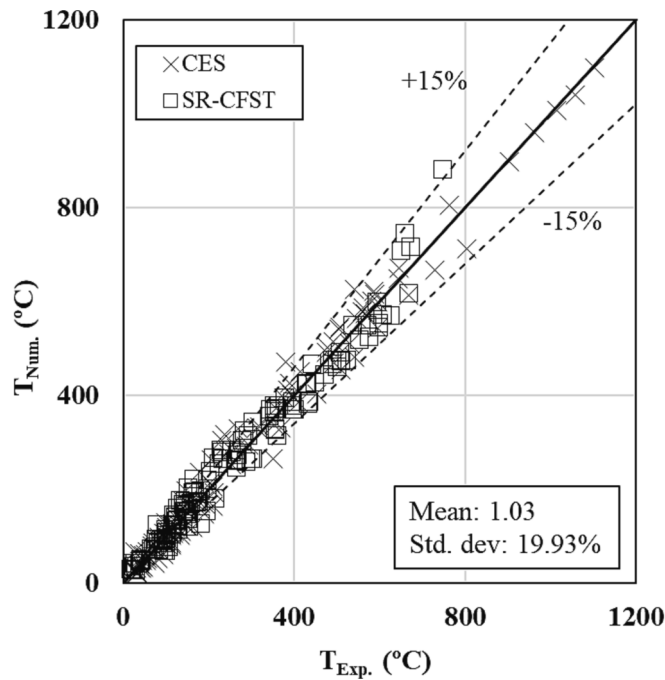
Fig. 13. Numerically predicted temperatures versus experimental temperatures at the available thermocouple locations for the different cases used for validation.

Table 2
Summary of the prediction errors in the validation of the thermal model ($\theta_{num}/\theta_{exp}$).

Section type	$\theta < 300\ °C$		$\theta \geq 300\ °C$		All range of θ	
	Mean	Std. dev.	Mean	Std. dev.	Mean	Std. dev.
All	1.06	0.24	0.99	0.08	1.03	0.20
SR-CFST	1.06	0.30	1.04	0.17	1.06	0.26
CES	1.03	0.26	1.01	0.08	1.02	0.21

4. Parametric studies on the thermo-mechanical response of SR-CFST columns

4.1. Composite sections used in the parametric study

A parametric study was carried out to analyse the influence of the different factors affecting the cross-sectional capacity of SR-CFST columns when subjected to fire. Table 3 shows the different column specimens studied.

The parameters varied were the outer dimension of the steel tube (*D* or *B* in the case of circular and square columns, respectively), the steel tube wall thickness (*t*) and the inner profile dimensions.

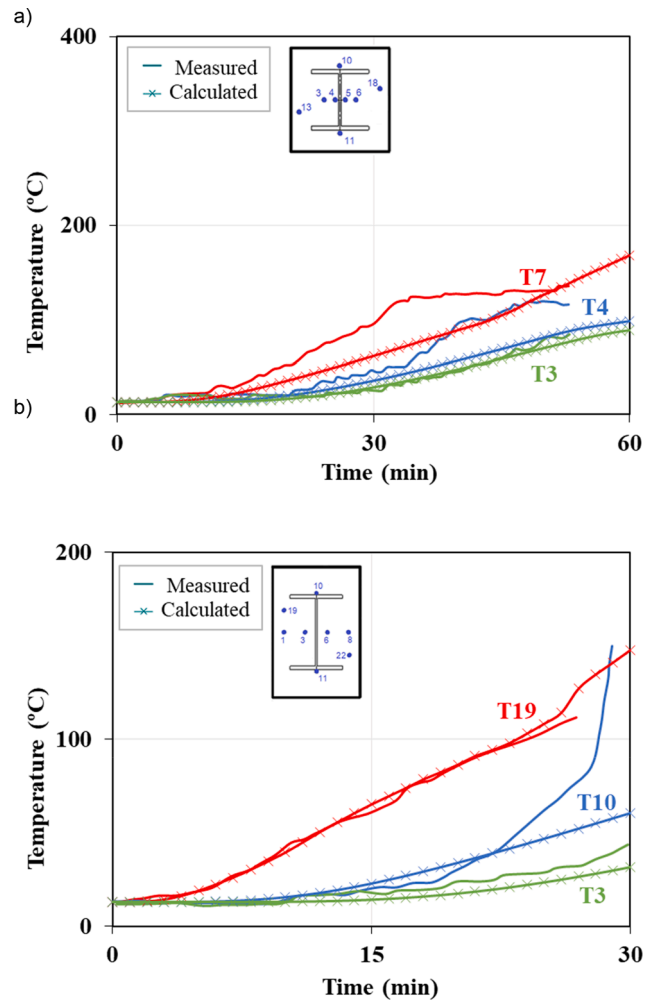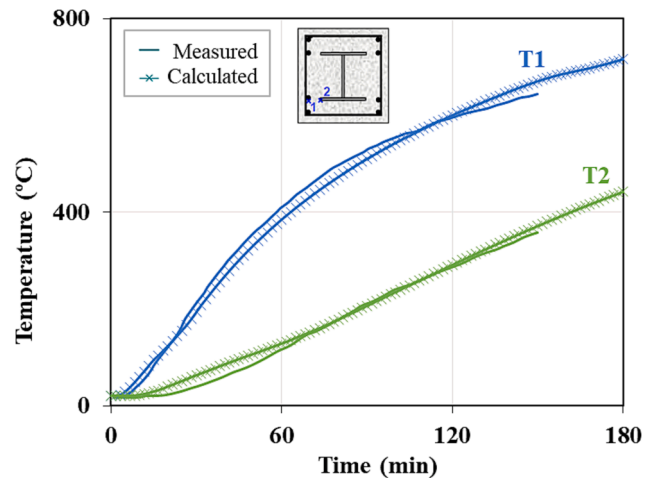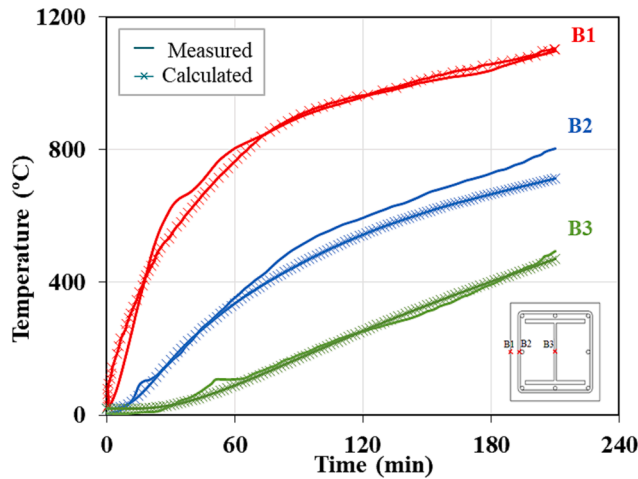Two sets of cross-sections were analysed, the first set comprising 8 circular geometries and the second set including their 8 square counterparts. For comparison purposes, the outer tube dimensions were chosen so that all the circular/square pairs had approximately the same amount of steel area – from a catalogue range of commercially available sections, with differences below 2 % –. Two wall thicknesses were studied for each of the selected outer dimensions (thin and thick outer tube). It is worth noting that the hollow steel sections were designed to meet the criteria of non-slender sections, according to EN1993-1-1 [41], except for specimen CHS 508 × 8, which was not able to meet this criterion and was therefore classified as class 4. For each steel tube, different inner profiles were considered from the European vast flange beams catalogue. HEA and HEB sections were used, increasing their dimensions progressively. Two or three different inner profiles were studied for the wider hollow tubes, while for the narrower tubes, a single inner profile was chosen, given the spacing limitations within the section. In total, 120 case analyses were generated in these parametric studies: 60 column specimens with circular sections and other 60 with square sections.

Additionally, the influence of the concrete moisture content was studied in this investigation, covering three different values of moisture content: 4 %, 7 % and 10 %, so the total number of numerical simulations conducted amounts $120 \times 3 = 360$.

The nominal values of the steel yield strength and concrete compressive strength were assumed to be 355 MPa and 30 MPa, respectively (calcareous aggregates being considered for concrete). The steel and concrete grades were not varied in this analysis, since the main goal was to focus on the thermal response of the columns, rather than on the mechanical effects. The recommended values in EN 1994-1-2 [27] for steel and concrete thermal properties at elevated temperatures were used, except for the thermal conductivity of concrete, where the new proposal in prEN 1992-1-2:2021 [35] was adopted instead. Based on the previous sensitivity study results, a value of 200 W/m²K for the gap conductance at the steel–concrete interface was considered, while a perfect thermal contact was assumed at the inner profile-concrete interface.

4.2. Sectional integration for computing plastic resistance and stiffness

The SR-CFST sections had been previously discretised using a triangular mesh to carry out the thermal analysis (see Section 2.1). Therefore, the temperatures at the nodes of the FE mesh were known from the computed cross-sectional temperature field. As shown in Fig. 2, each triangular i-element of this mesh can be characterised by its position (z_i, y_i), area (A_i) and temperature (θ_i) – obtained by linear interpolation from nodal temperatures – and by the corresponding material properties for steel tube, concrete or inner profile. Thus, the cross-section plastic resistance and flexural stiffness for both major and minor axis bending at elevated temperatures can be integrated from cells using the following formulae:

$$N_{fi,pl,Rd} = \sum_{i=1}^{n} A_{a,i} \bullet k_{y_a,\theta_i} \bullet f_{y_a} + \sum_{i=1}^{n} A_{c,i} \bullet k_{c,\theta_i} \bullet f_c + \sum_{i=1}^{n} A_{p,i} \bullet k_{y_p,\theta_i} \bullet f_{y_p} \quad (7)$$

Table 3
Summary of the analysis cases in the parametric studies.

(a) Circular Sections			(b) Square Sections		
D (mm)	t (mm)	Inner profile	B (mm)	t (mm)	Inner profile
193.7	4	HE100B	150	4	HE100B
	8			8	
219.1	4	HE120B	175	4	HE120B
	8			8	
273	5	HE140B	220	5	HE140B
	10			10	
323.9	6	HE140B–HE180B	260	6	HE140B – HE180B
	10			10	
355.6	6	HE100B–HE200B	300	6	HE100B–HE200B
	12.5			12.5	
406.4	7	HE120B–HE220B	325	7	HE120B–HE220B
	14.2			14.2	
457	8	HE100B–HE180B–HE280B	350	8	HE100–HE180B–HE280B
	10			10	
508	8	HE100B–HE200B–HE300B	400	8	HE100–HE200B–HE300B
	10			10	

Note: Same combinations repeated with inner HEA profiles.

$$EI_{z,fi} = \sum_{i=1}^{n} A_{a,i} \bullet y_i^2 \bullet k_{E_a,\theta_i} \bullet E_a + \sum_{i=1}^{n} A_{c,i} \bullet y_i^2 \bullet E_{c,sec,\theta_i} + \sum_{i=1}^{n} A_{p,i} \bullet y_i^2 \bullet k_{E_p,\theta_i} \bullet E_p \quad (8)$$

$$EI_{y,fi} = \sum_{i=1}^{n} A_{a,i} \bullet z_i^2 \bullet k_{E_a,\theta_i} \bullet E_a + \sum_{i=1}^{n} A_{c,i} \bullet z_i^2 \bullet E_{c,sec,\theta_i} + \sum_{i=1}^{n} A_{p,i} \bullet z_i^2 \bullet k_{E_p,\theta_i} \bullet E_p \quad (9)$$

where subscripts a, c and p correspond to the steel tube, concrete infill, and inner steel profile, respectively.

A numerical integration procedure was implemented through a Python subroutine and applied recurrently to all the analysed composite sections to compute their plastic resistance and flexural stiffness, as explained above.

The reduction factors for the mechanical properties of concrete and steel at their corresponding temperatures ($k_{y,\theta}$, $k_{c,\theta}$, $k_{E,\theta}$) were obtained from EN1994-1-2 [27]. It is worthy to note that the reduction factor for the concrete secant modulus (E_{c,sec,θ_i}) is not directly given in EN1994-1-2, nonetheless, it can be derived as follows:

$$E_{c,sec,\theta_i} = \frac{f_{c,\theta_i}}{\varepsilon_{cu,\theta_i}} = \frac{k_{c,\theta_i}}{\varepsilon_{cu,\theta_i}} \bullet f_c \quad (10)$$

In summary, once the nodal temperature was captured from the thermal FE analysis, the cross-sectional plastic resistance and stiffness were computed from eq. (7), (8) and (9) in order to carry out the comparisons in terms of mechanical capacity between the different column configurations in the parametric study.

4.3. Analysis of results of the parametric study

Fig. 14 to Fig. 17 present the evaluation of the parametric study results. Henceforth, the vertical axis represents the normalised cross-sectional plastic resistance of the columns at elevated temperature, referred to their room temperature value ($N_{fi,pl,Rd}/N_{pl,Rd}$).

The influence of the outer section shape (circular versus square), the outer hollow steel tube thickness (expressed in terms of the cross-sectional slenderness, D/t or B/t), the section factor (A_m/V) and the inner steel profile dimensions (measured through the "Inner Steel Contribution Ratio") is analysed in the following subsections.

Note that, in steel structures, the section factor (A_m/V) is defined as the fire exposed perimeter of the section divided by the total steel area. In this case, although the section is composite, the section factor can be defined as the fire exposed perimeter divided by the total area of the section (steel plus concrete), as already done for composite columns with partially encased steel sections in Annex G of EN 1994-1-2 [27] and

in the new method for CFST columns in Annex H of prEN 1994-1-2:2021 [42]. Henceforth, for a circular SR-CFST section it results $A_m/V = P_m/A = \pi D/(\pi D^2/4) = 4/D$, while for a square SR-CFST section it is equal to $A_m/V = P_m/A = 4B/B^2 = 4/B$.
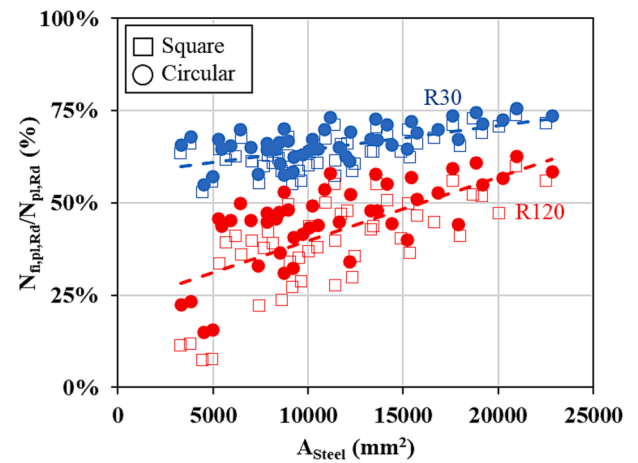

Fig. 14. Influence of the total steel area over the cross-sectional plastic resistance of the columns for both circular and square sections.
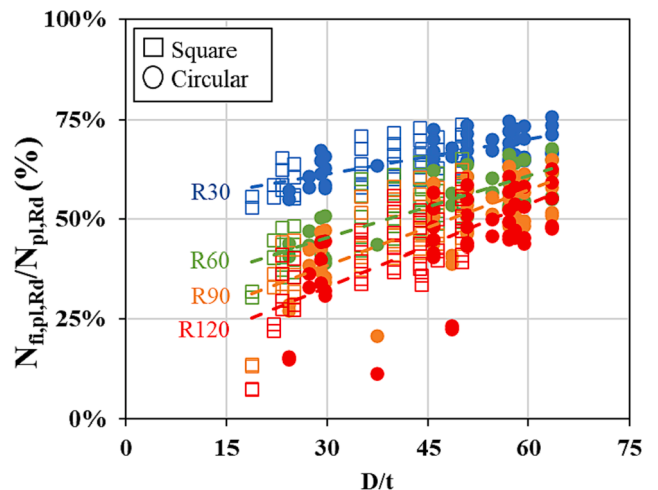

Fig. 15. Influence of the cross-sectional slenderness (D/t) over the plastic resistance of the columns, for both circular and square sections.
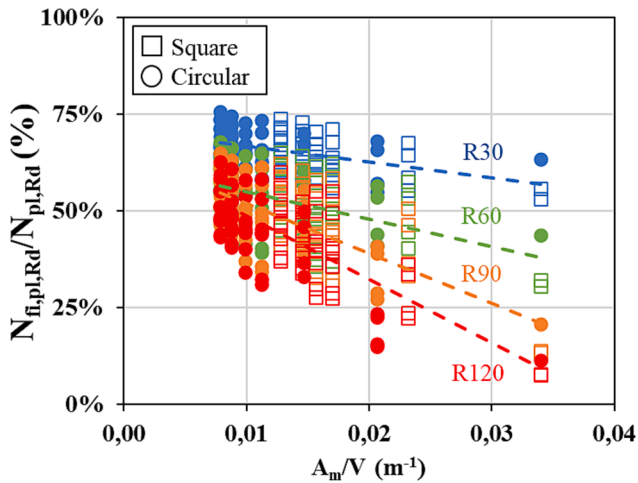
Fig. 16. Influence of the section factor (A_m/V) over the cross-sectional plastic resistance of the columns for both circular and square sections.
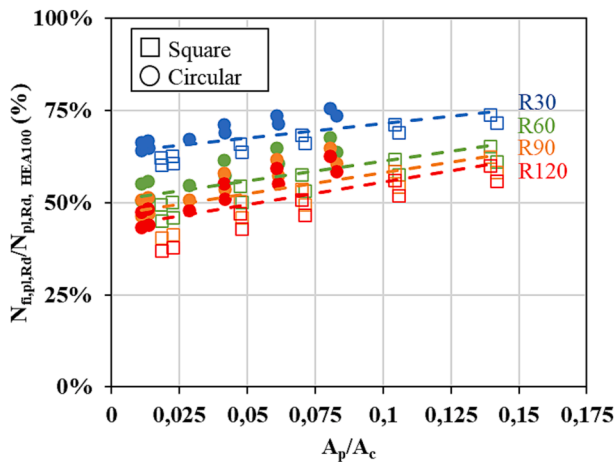

Fig. 17. Influence of the Inner Steel Contribution Ratio (ISCR) over the cross-sectional plastic resistance of the columns for sections CHS 508 mm × 8 mm and SHS 400 mm × 8 mm.

In turn, the "Inner Steel Contribution Ratio" (ISCR) has been defined by the authors as A_p/A_c (inner steel profile area divided by the concrete infill area) in order to quantify the amount of steel embedded in the concrete mass.

4.3.1. Influence of the outer section shape

Fig. 14 plots the results in terms of cross-sectional plastic resistance for the different series of columns studied, arranged by increasing the total steel area (steel tube + inner profile). It can be observed that the trend is positively linear, meaning that as the steel usage is increased, the mechanical capacity of the column rises. Additionally, this figure exhibits the differences between the circular and square cross-section shapes with the same steel usage, showing that the circular columns perform better under the effect of fire exposure. The reason for this behaviour is twofold: firstly, the lower section factor (A_m/V) of the circular columns provides them with a better thermal behaviour – i.e. slower temperature rise –, and secondly, the shortest distance between the inner face of the outer steel tube and the inner steel profile corner – i. e. concrete cover – is smaller in the square sections, which causes the heat to reach the steel H-section faster, which in turn explains its faster reduction in terms of load-bearing capacity.

The effect of the geometry becomes more pronounced as the fire exposure time is increased, resulting in a higher difference in axial

capacity between the circular and square sections (note the difference for R120 as compared to R30).

4.3.2. Influence of the outer steel tube thickness

As shown in Fig. 15, the relationship between the cross-sectional slenderness (D/t) and the cross-sectional plastic resistance of the column is linearly positive for both square and circular sections. This effect can be explained by the fact that, as the D/t value is incremented, the area of steel at the outer surface is reduced (thinner hollow section), thus allowing for a more considerable amount of concrete infill and higher dimensions of the inner steel profile. Since it is directly exposed to fire, the outer steel tube is heavily affected by the temperature increase and rapidly loses its load-bearing capacity; therefore, the reduction of the amount of steel used in the outer tube and the increase in the dimensions of the inner profile – thermally protected by the concrete infill – enhances the cross-sectional capacity of the column.

4.3.3. Influence of the section factor

Fig. 16 shows the influence of the section factor (A_m/V) over the cross-sectional capacity of the columns. This parameter measures the amount of steel area exposed to the fire in relation to the heated volume and thus gives an idea of the influence of the outer sectional shape and dimensions over the thermal response of the columns. The section factor value affected the cross-sectional plastic resistance in a negative linear trend. As the A_m/V increases, the fire exposed perimeter of the cross-section also rises, causing the column to heat up faster, thus losing its mechanical properties at a faster pace than sections exposing a reduced perimeter to the fire. Note that for the same steel usage, the section factor (A_m/V) of the square columns is higher than that of their circular counterparts, thus explaining the faster temperature rise and mechanical deterioration of the square columns.

4.3.4. Influence of the dimensions of the inner profiles

The influence of the amount of steel used at the inner profiles was studied by varying the H-steel profile dimensions for a fixed size of the outer steel tube. Fig. 17 compares the different inner profiles analysed for the CHS 508 mm × 8 mm and the SHS 400 mm × 8 mm (inner profiles HE100A, HE200A, HE300A, HE100B, HE200B, HE300B). The results in terms of cross-sectional capacity are referred to the case with HE100A inner profile. They show the potential benefit of using an encased profile of higher dimensions, increasing the so-called "Inner Steel Contribution Ratio" (ISCR). Given these results, it becomes clear that the cross-sectional capacity of the columns, for any fire exposure time, is enhanced by the progressive increase in the ISCR for both circular and square sections.

Additionally, cross-sections with an HEB embedded profile have shown to have a higher mechanical capacity when compared to their HEA counterparts. This phenomenon is mainly due to the higher area of steel in HEB sections than HEA, which allows for a higher load-bearing capacity for the column.

4.3.5. Influence of the concrete moisture content

An analysis of the effect of the concrete moisture content over the cross-sectional plastic resistance of the columns was additionally conducted. Fig. 18 shows this effect for the case with outer CHS of diameter 194 mm and HEA100 inner profile, which was studied under three different values of moisture content: 4 %, 7 % and 10 %. As it was expected, the concrete moisture content has a favourable effect over the performance of the columns when exposed to fire, in the sense that as the moisture content increases, the temperature rise within the cross-section becomes slower and thus the mechanical capacity is increased. It can be observed that the increase in terms of cross-sectional plastic resistance capacity between the 4 % and 7 % models is remarkable, while for higher moisture contents this effect is less pronounced.
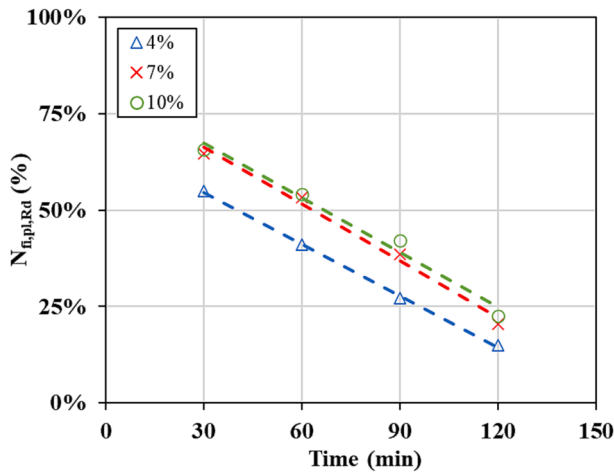
Fig. 18. Influence of the concrete moisture content over the cross-sectional plastic resistance of the columns for both circular and square sections.

4.3.6. Summary of the analysis results

Through this analysis, it was found that the development of temperatures across the section is highly affected by the section factor value (A_m/V), with a faster increase of temperatures for those columns with higher section factors (i.e. small diameters), which expose a relatively high surface to the fire for the same volume and thus heat up faster. This effect ultimately affects the cross-sectional plastic resistance of the columns, leading to higher capacities for the columns with lower section factors. The variation of the inner steel profile dimensions also influenced positively the thermal behaviour of the column as the ISCR parameter was increased (i.e. higher dimensions of the inner steel profile). It was also observed that a change in the steel tube wall thickness influenced the thermal response of the columns, in the sense that a lower steel tube wall thickness benefits the mechanical capacity of the composite section, provided that the amount of steel removed from the outer tube is introduced at the inner steel profile.

Finally, regarding the influence of the concrete moisture content, it was observed that a higher value of this parameter was beneficial for the thermal response of the section. Therefore, the most conservative concrete moisture content value of 4 % will be assumed in the subsequent design proposal, as recommended in Clause 3.3.2(7) of EN1994-1-2 [27].

All these findings will be used in the following section for developing a simplified proposal for predicting the temperature field in SR-CFST columns.

5. Development of a simplified temperature distribution proposal for Steel-reinforced CFST sections

In evaluating a steel–concrete composite section under fire based on the provisions of EN 1994-1-2 [27], it is required to compute the cross-sectional temperature field after a given duration of fire exposure. However, the code does not provide any simplified process to obtain the temperature field of the cross-section quickly. This chapter presents a simple method to evaluate the temperature field within an SR-CFST column, which may help practitioners in this task.

It is intended to obtain a uniform equivalent temperature for the whole concrete core ($\theta_{c,eq}$), the web and the flanges of the embedded steel profile ($\theta_{w,eq}$ and $\theta_{f,eq}$) and the outer steel tube ($\theta_{a,eq}$) to get the exact fire resistance of the column which would be obtained by using the actual non-uniform temperature distribution. The benefit of this approach is that the designer can evaluate the fire resistance of the cross-section by using a single strength and stiffness value for each component of the composite cross-section corresponding to its temperature. The authors previously used this approach for developing a temperature

distribution proposal for CFST columns [26] which has been recently included in the draft version of the new Eurocode 4 Part 1.2 (prEN 1994-1-2:2021) [42]. The calculation procedure is described hereafter.

5.1. Previous simplified methods for predicting the temperature field of composite sections

Annex G of EN 1994-1-2 [27] presents a simplified temperature model to calculate the fire resistance of composite columns with partially encased steel sections uniformly exposed to fire. This method shows four different temperatures corresponding to the concrete area, the reinforcing bars, steel profile web and flanges. The concrete core and steel profile flanges temperature correlate with the standard fire resistance time (R) and the column section factor (A_m/V). For the reinforcing bars, the method provides the reduction factors for the steel yield strength and modulus of elasticity directly, depending on the standard fire resistance time (R) and the geometrical average of the axis distance of the reinforcement to the outer concrete surface (u_s).

The method used on the web of the embedded steel profile is significantly different from that used at the flanges. EN 1994-1-2 Annex G [27] states that, to consider the effect of temperature on the material properties, a part of the web may be neglected, thus reducing the material properties of the flange itself. Therefore, the height reduction of the profile web is given as a function of the standard fire resistance time; thus, the design plastic resistance and flexural stiffness can be worked out after removing this part of the web.

This approach was tentatively applied to the inner profiles and concrete infill of the SR-CFST sections studied in this paper by introducing some adaptations. However, as the method is developed explicitly for partially encased sections (i.e. without outer steel tube and with the inner steel profile flanges directly exposed to the fire), the predicted temperature distributions were far from realistic, as shown in Fig. 19.

Regarding the fire design of CFST columns, the authors of this paper previously proposed an innovative design method [26] which was approved by the Technical Committee CEN/TC250/SC4 [43] to be included in the new version of Eurocode 4 Part 1.2 (prEN 1994-1-2:2021) [41] in replacement of the current Annex H. This method presents three different equations to obtain the equivalent temperatures of
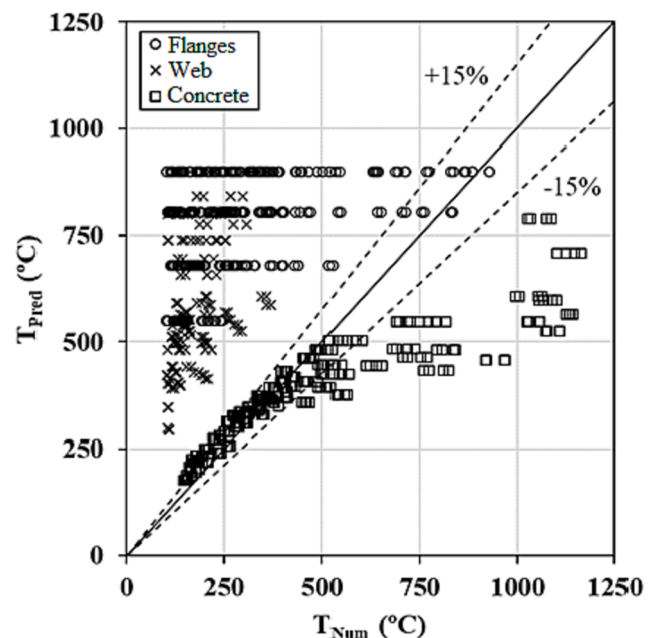

Fig. 19. Comparison between predicted and numerical temperatures at the different parts of the composite section using the equations from Annex G of EN 1994-1-2 [24].

the main components of the cross-section: the concrete core, the outer steel tube and the reinforcement bars. According to the proposed equations, the concrete infill and the outer steel tube equivalent temperatures were highly associated with the standard fire exposure time (R) and the section factor (A_m/V).

On the other hand, a different approach was adopted to obtain the equivalent temperature of the reinforcing bars, based on previous works on the development of temperature fields in concrete structures subjected to fire by Wickström [44]. The reinforcing bars' temperature was strongly correlated to the parameter R/u_s^2, being u_s the concrete cover, measured from the axis distance of the reinforcing bars to the exposed surface of the concrete.

Some parts of the existing temperature proposal for CFST columns developed by the authors [26] will be adapted here to SR-CFST sections, such as the equivalent temperature equation for the outer steel tube or the shape of the function for the concrete infill, as the temperature field in these parts of the section is similar.

5.2. Simplified cross-sectional temperature field proposal for SR-CFST sections

A multivariant regression analysis was performed, based on the results of the previously presented study on the influence of specific parameters.

This section aims to characterise the SR-CFST cross-section temperature field in a simple but practical way by obtaining an equivalent temperature for each part of the composite cross-section: the outer steel tube ($\theta_{a,eq}$), the concrete infill ($\theta_{c,eq}$), the inner steel profile web ($\theta_{w,eq}$) and flanges ($\theta_{f,eq}$). Fig. 20 shows the definition of the equivalent temperatures associated with their corresponding parts.

5.2.1. Calculation of the equivalent temperature for the outer steel tube

For the outer steel tube, the equivalent temperature at each standard fire time was directly obtained from the numerical analyses by calculating the average value of the temperatures at both inner and outer surfaces. This temperature was almost uniform through the steel tube wall thickness for each standard fire period.

The equation previously proposed by the authors in the design method for CFST columns [26] to obtain the equivalent temperature of the outer steel tube was tested in this study, producing an average error of 1.005 for the circular specimens with a 1.28 % standard deviation and an average error of 1.021 with 1.26 % standard deviation for the square ones, therefore considering it accurate enough to be applied to SR-CFST columns. The specified formula is given hereafter:

$$\theta_{a,eq} = -824.667 - 5.579R + 0.007R^2 - 0.009R \bullet A_m/V + 645.076$$
$$\bullet R^{0.269} \bullet (A_m/V)^{0.017} \tag{11}$$

Alternatively, a selection chart is given in Table 5 to obtain directly the outer steel tube temperature.

Fig. 21 compares the calculated and numerically predicted temperatures at the outer steel tube. Since the temperatures obtained with the equation are highly correlated with those extracted from the parametric study, the formula is considered valid for the column typologies analysed in this study.

5.2.2. Calculation of the equivalent temperature for the concrete infill

The equivalent temperature representing the concrete infill can be derived through two different approaches, by using either the plastic resistance or the flexural stiffness of the whole concrete part:

a) Plastic resistance approach.

The plastic resistance to axial compression of the concrete infill in the fire situation is equal to:

$$N_{fi,pl,Rd,c} = \sum_{i=1}^{n}(A_{c,i} \bullet f_{c,\theta_i}) = \sum_{i=1}^{n}(A_{c,i} \bullet k_{c,\theta_i} \bullet f_c) = f_c \bullet \sum_{i=1}^{n}(A_{c,i} \bullet k_{c,\theta_i}) \tag{12}$$

A single equivalent temperature is needed, which produces the same plastic resistance through its corresponding reduction factor when applied to the whole concrete infill:

$$N_{fi,pl,Rd,c} = f_c \bullet \sum_{i=1}^{n}(A_{c,i} \bullet k_{c,\theta_i}) = k_{c,\theta}(\theta_{c,eq1}) \bullet f_c \bullet A_c \rightarrow k_{c,\theta}(\theta_{c,eq1})$$
$$= \frac{\sum_{i=1}^{n}(A_{c,i} \bullet k_{c,\theta_i})}{A_c} \tag{13}$$

Once this reduction coefficient is calculated, the equivalent temperature $\theta_{c,eq1}$ representing the whole concrete part can be found in Table 3.3 in EN 1994-1-2 [27] using linear interpolation.

b) Flexural stiffness approach (major axis bending).

The flexural stiffness of the concrete infill in the fire situation for major axis bending is equal to:
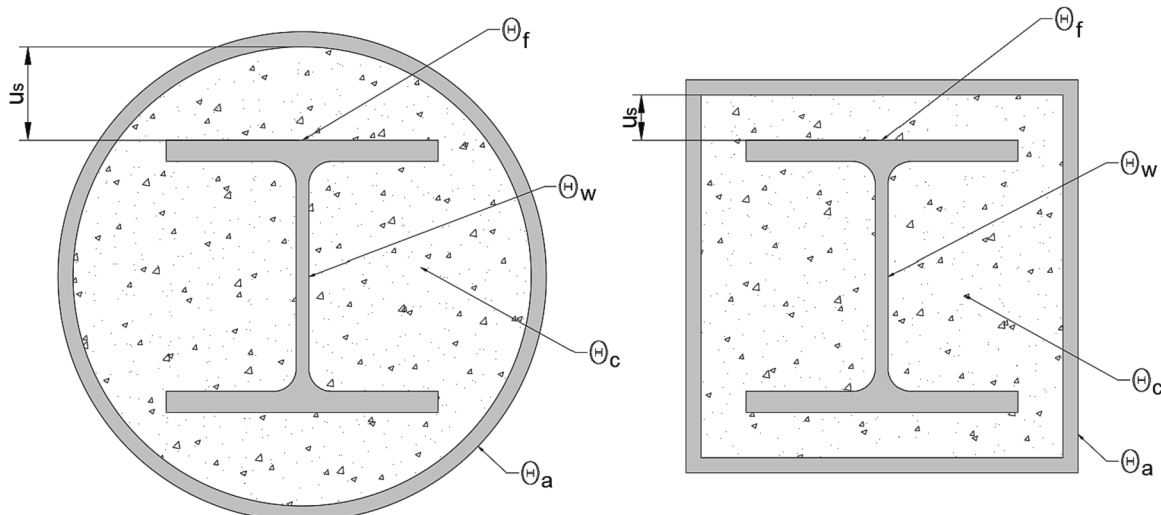
Fig. 20. Equivalent temperatures of the different parts of the composite section and definition of the parameter us in circular and square SR-CFST columns.
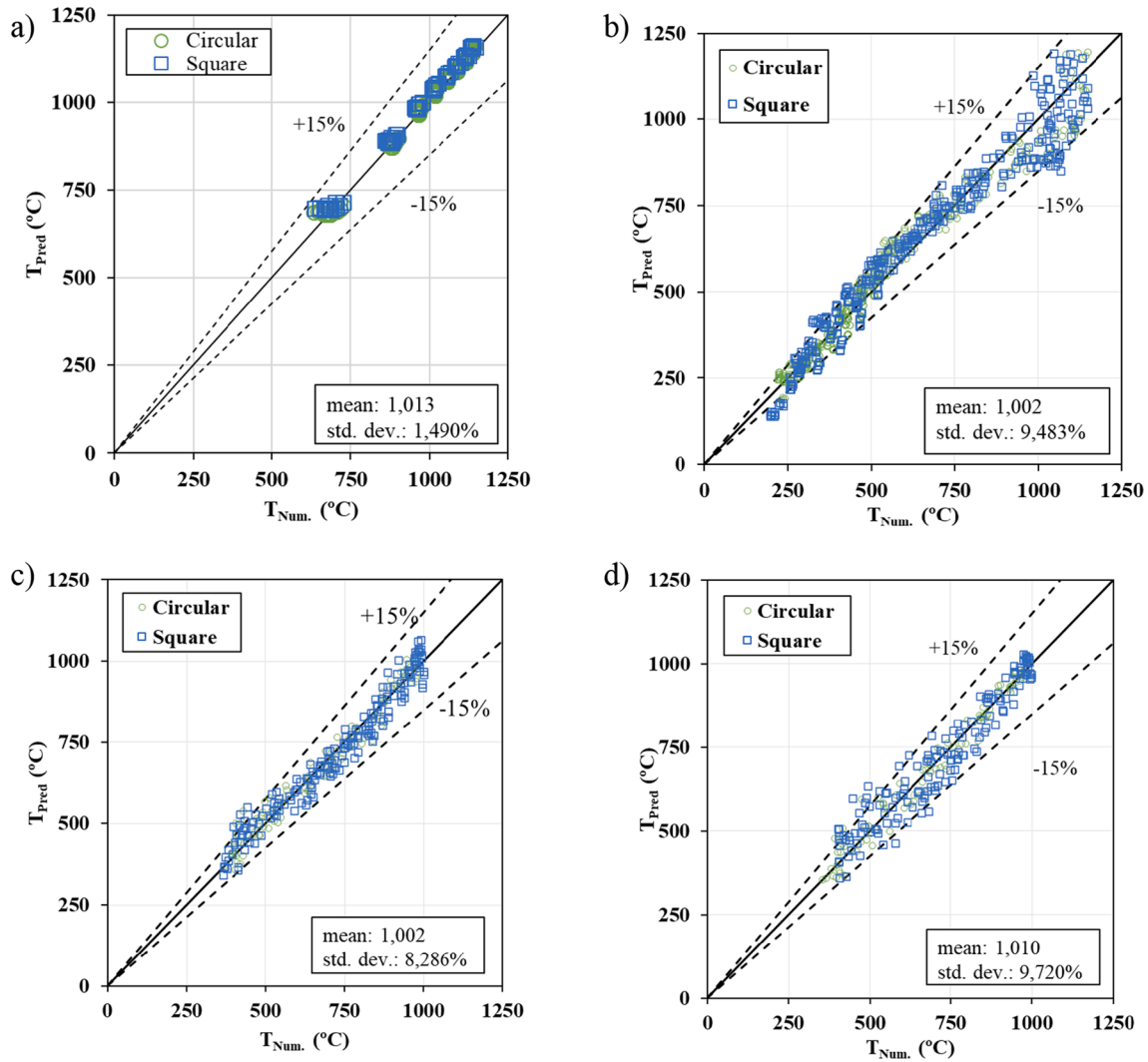
Fig. 21. Comparison between predicted equivalent temperature and numerical temperature: (a) outer steel tube, (b) concrete infill, (c) inner steel profile flanges and (d) inner steel profile web.

$$EI_{z,fi,c} = \sum_{i=1}^{n} (I_{z,c,i} \bullet E_{c,sec,\theta_i}) = \sum_{i=1}^{n} \left(I_{z,c,i} \bullet \frac{f_{c,\theta,i}}{\varepsilon_{cu,\theta,i}}\right) = \frac{f_c}{\varepsilon_{cu}} \bullet \sum_{i=1}^{n} \left(I_{z,c,i} \bullet \frac{k_{c,\theta,i}}{\frac{\varepsilon_{cu,\theta,i}}{\varepsilon_{cu}}}\right)$$

$$= E_{c,sec} \bullet \sum_{i=1}^{n} (I_{z,c,i} \bullet k_{Ec,\theta,i}) \tag{14}$$

with $k_{Ec,\theta,i} = k_{c,\theta,i} \bullet \varepsilon_{cu}/\varepsilon_{cu,\theta,i}$.

It is required to obtain an equivalent temperature that produces the same flexural stiffness through its corresponding reduction factor when applied to the whole concrete part:

$$EI_{z,fi,c} = E_{c,sec} \bullet \sum_{i=1}^{n} (I_{z,c,i} \bullet k_{Ec,\theta,i}) = k_{Ec,\theta}(\theta_{c,eq2}) \bullet E_{c,sec} \bullet I_{z,c} \rightarrow k_{Ec,\theta}(\theta_{c,eq2})$$

$$= \frac{\sum_{i=1}^{n} (I_{z,c,i} \bullet k_{Ec,\theta,i})}{I_{z,c}} \tag{15}$$

In this type of geometry, the column section is not symmetric. As a result, the flexural stiffness of the concrete must be calculated for both axes using the same method for the minor axis bending. The equivalent temperatures for the concrete infill resulting from applying this procedure to both axes are $\theta_{c,eq2}$ and $\theta_{c,eq3}$, which can be obtained through Table 3.3 in EN 1994-1-2 [27] by using linear interpolation and considering $k_{Ec,\theta} = k_{c,\theta} \bullet \varepsilon_{cu}/\varepsilon_{cu,\theta}$.

Conservatively, the equivalent temperature of the concrete infill will be defined as the maximum of the temperatures obtained through the three approaches described above:

$$\theta_{c,eq} = max\{\theta_{c,eq1}, \theta_{c,eq2}, \theta_{,eq3}\} \tag{16}$$

A single equation for the equivalent temperature of concrete valid for any fire resistance period was developed by using a multiple nonlinear regression analysis, which includes the effect of A_m/V, A_{sp}/A_c, and R:

$$\theta_{c,eq} = a_1 + b_1R + b_2R^2 + c_1(A_m/V) + c_2\left(\frac{A_m}{V}\right)^2 + d_1R(A_m/V) + e_1R^{f1}\left(\frac{A_m}{V}\right)^{f2}$$

$$+ g_1R(A_{sp}/A_c)$$

$$\leq 1200°C \tag{17}$$

where coefficients a_1 to g_1 depend on the shape of the section (circular or square) and are given in Table 4. A temperature plateau was set at 1200 °C due to the loss of structural capacity of concrete above this value. This equation can be used as an alternative to the selection chart .

A comparison between calculated and numerically predicted temperatures at the concrete infill can be observed in Fig. 21(a).

Alternatively, a selection chart is given in Table 6 for circular sections and Table 7 for square sections to facilitate designers in obtaining the equivalent temperature of the concrete infill for a particular fire

Table 4
Coefficients for the equivalent temperature of the concrete infill $\theta_{c,eq}$ (°C), flanges $\theta_{f,eq}$ (°C) and web $\theta_{w,eq}$ (°C) of the inner steel profile.

		a₁	b₁	b₂	c₁	c₂	d₁	e₁	f₁	f₂	g₁	g₂
CONCRETE	CIRC	1120,11	−10,14	7,80E−03	−145,94	4,05	1,30	−1,83E−05	1,91	2,84	5,17	–
	SQUA	865,60	−23,88	2,91E−02	−93,38	1,55	5,88	−1,54	1,09	1,20	4,70	–
FLANGES	CIRC	−1174,15	14,08	−2,03E−02	59,59	2,12E−02	−5,84E−02	9,53E−05	1,83	1,86	9,27	–
	SQUA	794,25	−7,19	9,83E−03	−81,30	1,26	7,59	−4,51	1,05	1,06	−9,64	–
WEB	CIRC	3267,34	3,24	0,01	184,79	−5,30	3,59	−1,29	1,18	1,01	10891,6	−55465,4
	SQUA	−941,09	−5,32	6,62E−03	−22,25	0,36	3,41	−1,17	1,10	1,12	6939,91	−19679,4

Table 5
Selection chart for the equivalent temperature of the outer steel tube $\theta_{a,eq}$ (°C) (extracted from [15]).

		R30	R60	R90	R120	R180	R240
A_m/V (m⁻¹)	5	669	858	951	1005	1070	1125
	10	687	879	973	1028	1094	1149
	15	697	890	984	1039	1105	1158
	20	704	897	992	1046	1110	1162
	25	709	903	996	1050	1112	1162
	30	713	906	999	1052	1113	1162
	35	716	909	1001	1053	1113	1162
	40	719	911	1002	1054	1113	1162
	45	721	912	1003	1054	1113	1162

period directly from the value of the section factor of the column. For intermediate values of the section factor and the inner steel contribution ratio, linear interpolation can be used.

5.2.3. Calculation of the equivalent temperature for the inner steel profile

Concerning the temperature of the inner steel profile, it has been observed that the temperatures obtained at the flanges differ significantly from the ones obtained on the web. Thus, two equivalent temperatures will be proposed in this study: one for the web and another one for the flanges.

The procedure to obtain the equivalent temperature at the flanges and the web of the steel profile was like that applied for deriving the equivalent temperature of the concrete infill. Both parts (flanges and web) were calculated separately by isolating the cells corresponding to

each zone and processing them individually.

a) Plastic resistance approach.

The plastic resistance to axial compression of the inner steel profile parts under elevated temperature conditions can be obtained by using the following formulae:

$$N_{fi,pl,Rd,f} = \sum_{i=1}^{n}(A_{f,i} \bullet f_{s,\theta_i}) = \sum_{i=1}^{n}(A_{f,i} \bullet k_{s,\theta_i} \bullet f_s) = f_s \bullet \sum_{i=1}^{n}(A_{f,i} \bullet k_{s,\theta_i}) \qquad (18)$$

$$N_{fi,pl,Rd,w} = \sum_{i=1}^{n}(A_{w,i} \bullet f_{s,\theta_i}) = \sum_{i=1}^{n}(A_{w,i} \bullet k_{s,\theta_i} \bullet f_s) = f_s \bullet \sum_{i=1}^{n}(A_{w,i} \bullet k_{s,\theta_i}) \qquad (19)$$

By isolating the reduction factor in this equation, it can be derived by performing a sectional integration process:

$$N_{fi,pl,Rd,f} = f_s \bullet \sum_{i=1}^{n}(A_{f,i} \bullet k_{s,\theta_i}) = k_{s,\theta}(\theta_{f,eq1}) \bullet f_s \bullet A_f \rightarrow k_{s,\theta}(\theta_{f,eq1})$$
$$= \frac{\sum_{i=1}^{n}(A_{f,i} \bullet k_{s,\theta_i})}{A_f} \qquad (20)$$

$$N_{fi,pl,Rd,w} = f_s \bullet \sum_{i=1}^{n}(A_{w,i} \bullet k_{s,\theta_i}) = k_{s,\theta}(\theta_{w,eq1}) \bullet f_s \bullet A_w \rightarrow k_{s,\theta}(\theta_{w,eq1})$$
$$= \frac{\sum_{i=1}^{n}(A_{w,i} \bullet k_{s,\theta_i})}{A_w} \qquad (21)$$

The equivalent temperatures of the steel profile flanges and web, $\theta_{f,eq1}$ and $\theta_{w,eq1}$, respectively, can be obtained using linear interpolation in

Table 6
Selection chart for the equivalent temperature of the concrete infill $\theta_{c,eq}$ (°C) for circular sections.

A_p/A_c		0,01						0,05						0,1					
		R30	R60	R90	R120	R180	R240	R30	R60	R90	R120	R180	R240	R30	R60	R90	R120	R180	R240
A_m/V (m⁻¹)	10	<200	237	323	410	589	775	<200	249	341	435	626	825	<200	265	365	466	672	887
	15	<200	336	538	713	988	1165	<200	348	557	738	1025	>1200	<200	364	580	769	1072	>1200
	20	245	580	832	1005	1125	>1200	252	592	850	1030	1162	>1200	259	608	874	1061	>1200	

Table 7
Selection chart for the equivalent temperature of the concrete infill $\theta_{c,eq}$ (°C) for square sections.

A_p/A_c		0,02						0,1						0,2					
		R30	R60	R90	R120	R180	R240	R30	R60	R90	R120	R180	R240	R30	R60	R90	R120	R180	R240
A_m/V (m⁻¹)	10		<200	<200	<200	<200	360		<200	<200	<200	239	450		<200	<200	213	324	563
	15	<200	275	381	477	690	979	<200	297	415	522	758	1069	<200	325	457	578	843	1182
	20	<200	392	572	715	966	>1200	<200	415	606	760	1034	>1200	<200	443	648	816	1119	>1200
	25	<200	512	722	868	1066	>1200	<200	534	755	913	1134	>1200	<200	562	798	969	>1200	
	30	278	645	850	962	>1200		289	667	884	1008	>1200		303	696	926	1064	>1200	

Table 3.2 in EN 1994-1-2 [27].

b) Flexural stiffness approach.

The flexural stiffness of the inner steel profile parts under fire conditions for major axis bending can be calculated through the following equation:

$$EI_{z,fi,f} = \sum_{i=1}^{n}(I_{z,f,i} \bullet E_{a,\theta}) = \sum_{i=1}^{n}(I_{z,f,i} \bullet k_{E,\theta}(\theta_{f,eq2}) \bullet E_a)$$
$$= E_a \bullet \sum_{i=1}^{n}(I_{z,f,i} \bullet k_{E,\theta}(\theta_{f,eq2})) \tag{22}$$

$$EI_{z,fi,w} = \sum_{i=1}^{n}(I_{z,w,i} \bullet E_{a,\theta}) = \sum_{i=1}^{n}(I_{z,w,i} \bullet k_{E,\theta}(\theta_{w,eq2}) \bullet E_a)$$
$$= E_a \bullet \sum_{i=1}^{n}(I_{z,w,i} \bullet k_{E,\theta}(\theta_{w,eq2})) \tag{23}$$

Subsequently, the flexural stiffness reduction coefficient is obtained:

$$EI_{z,fi,f} = E_a \bullet \sum_{i=1}^{n}(I_{z,f,i} \bullet k_{E,\theta}(\theta_{f,eq2})) = k_{E,\theta}(\theta_{f,eq2}) \bullet E_a \bullet I_{z,f} \rightarrow k_{E,\theta}(\theta_{f,eq2})$$
$$= \frac{\sum_{i=1}^{n}(I_{z,f,i} \bullet k_{E,\theta,i})}{I_{z,f}} \tag{24}$$

$$EI_{z,fi,w} = E_a \bullet \sum_{i=1}^{n}(I_{z,w,i} \bullet k_{E,\theta}(\theta_{w,eq2})) = k_{E,\theta}(\theta_{w,eq2}) \bullet E_a \bullet I_{z,w} \rightarrow k_{E,\theta}(\theta_{w,eq2})$$
$$= \frac{\sum_{i=1}^{n}(I_{z,w,i} \bullet k_{E,\theta,i})}{I_{z,w}} \tag{25}$$

This procedure is replicated for minor axis bending, given the asymmetric cross-section distribution, thus obtaining another two sets of equivalent temperatures corresponding to each part of the steel profile: $\theta_{f,eq3}$, and $\theta_{w,eq3}$. Equivalent temperatures $\theta_{f,eq2}$, $\theta_{w,eq2}$, $\theta_{f,eq3}$ and $\theta_{w,eq3}$ can be extracted from Table 3.2 in EN 1994-1-2 [27] by applying linear interpolation.

The representative equivalent temperature for the flange and the web is taken as the maximum of the three temperatures obtained from the described procedure:

$$\theta_{f,eq} = max\{\theta_{f,eq1}, \theta_{f,eq2}, \theta_{f,eq3}\} \tag{26}$$

$$\theta_{w,eq} = max\{\theta_{w,eq1}, \theta_{w,eq2}, \theta_{w,eq3}\} \tag{27}$$

Equivalent temperature for the flanges of the inner steel profile

An additional parameter was introduced to quantify the concrete cover around the flanges of the inner steel profile, which was found to influence their temperature strongly. This parameter, defined as u_s, measures the distance between the flanges of the embedded steel profile and the inner surface of the hollow steel tube, as defined in Fig. 220.

The equivalent temperature of the inner steel profile flanges is obtained by using multiple nonlinear regression analyses, including the effect of A_m/V, u_s, and R:

$$\theta_{f,eq} = a_1 + b_1 R + b_2 R^2 + c_1(A_m/V) + c_2(A_m/V)^2 + d_1 R(A_m/V) + e_1 R^{f1}(A_m/V)^{f2} + g_1 u_s \tag{28}$$

where coefficients a_1 to g_1 depend on the section shape (circular or square), see Table 4.

Fig. 21(b) shows the comparison between the calculated and numerically predicted temperatures at the flanges of the inner profile.

Additionally, two equivalent temperature tables are presented in Table 8 and Table 9 (for circular and square sections, respectively), which can be an alternative to applying the previously presented equations. For the section factor (A_m/V) and concrete cover (u_s), linear interpolation can be used on intermediate values.

Equivalent temperature for the web of the inner steel profile

Besides the standard fire time (R) and the section factor (A_m/V), the ISCR parameter was relevant when analysing the web temperature. Thus, a similar formula was obtained for the equivalent temperature of the steel profile web, which includes the effect of A_m/V, A_{sp}/A_c, and R:

$$\theta_{w,eq} = a_1 + b_1 R + b_2 R^2 + c_1(A_m/V) + c_2(A_m/V)^2 + d_1 R(A_m/V) + e_1 R^{f1}(A_m/V)^{f2} + g_1(A_{sp}/A_c) + g_2(A_{sp}/A_c)^2 \tag{29}$$

where coefficients a_1 to g_2 depend on the cross-section shape (circular or square), see Table 4.

A comparison between the calculated and numerically predicted temperatures at the web of the steel profile can be observed in Fig. 21(c).

Two equivalent temperature tables are also given (Table 10 for circular and Table 11 for square sections), which can serve as an alternative design method. Linear interpolation can be used for intermediate values of the section factor and the ISCR.

5.3. Applicability limits of the proposed method

The previously given equivalent temperature equations should only be applied for SR-CFST columns which meet the following requirements:

- For circular SR-CFST columns:

$$8m^{-1} \leq A_m/V \leq 20m^{-1}$$

$$24 \leq D/t \leq 64$$

$$0,011 \leq A_p/A_c \leq 0,108$$

- For square SR-CFST columns:

$$13m^{-1} \leq A_m/V \leq 34m^{-1}$$

Table 8

Selection chart for the equivalent temperature of the flanges of the inner steel profile $\theta_{f,eq}$ (°C) for circular sections.

A_m/V (m⁻¹)		10						20					
		R30	R60	R90	R120	R180	R240	R30	R60	R90	R120	R180	R240
	15			<400	569	966	>1200	<400	544	791	986	>1200	>1200
	30			<400	430	827	1063	<400	405	652	847	1083	1117
	45				<400	688	924		<400	513	708	944	978
u_s (mm)	60		<400		<400	549	785			<400	569	805	839
	75				<400	410	646	<400	<400		430	666	700
	90					<400	507				<400	527	561

Table 9

Selection chart for the equivalent temperature of the flanges of the inner steel profile $\theta_{f,eq}$ (°C) for square sections.

A_m/V (m⁻¹)		15						30					
		R30	R60	R90	R120	R180	R240	R30	R60	R90	R120	R180	R240
	15		<400	515	655	883	1079	<400	497	748	913	1077	1096
	30			<400	510	738	934		<400	604	769	932	952
	45				<400	594	789		<400	459	624	788	807
u_s (mm)	60		<400		<400	449	645			<400	480	643	663
	75					<400	500	<400			<400	499	518
	90						<400				<400	<400	<400

Table 10

Selection chart for the equivalent temperature of the inner steel profile web $\theta_{w,eq}$ (°C) for circular sections.

A_p/A_c		0,01						0,05						0,1					
		R30	R60	R90	R120	R180	R240	R30	R60	R90	R120	R180	R240	R30	R60	R90	R120	R180	R240
	10						<400					<400	<400		<400			<400	464
A_m/V (m⁻¹)	15		<400			<400	432		<400		<400	<400	552	734			<400	<400	681	863
	20				<400	492	551			<400	552	795	853		<400	458	681	923	982

(Note: in the 0,05 group, values 552 and 734 fall in columns R180 and R240 for row 15; in the 0,1 group, row 15 shows <400 in R120 and values 681, 863 in R180, R240.)

Table 11

Selection chart for the equivalent temperature of the inner steel profile web $\theta_{w,eq}$ (°C) for square sections.

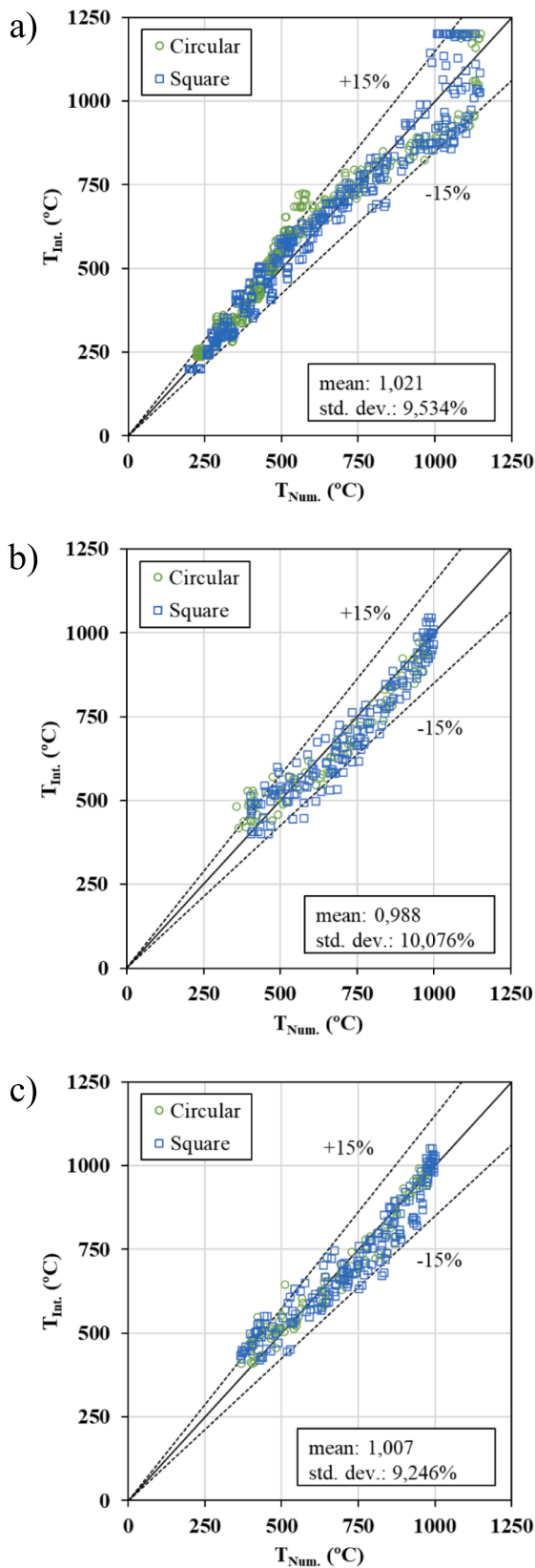| A_p/A_c		0,02						0,1						0,2					
		R30	R60	R90	R120	R180	R240	R30	R60	R90	R120	R180	R240	R30	R60	R90	R120	R180	R240
	10											<400	<400					<400	<400
A_m/V (m⁻¹)	15		<400				<400		<400		<400	418	606		<400		<400	522	710
	20				<400	437					<400	634	803			<400	493	738	907
	25				<400	413	530			<400	551	779	896		<400	479	654	882	1000
	30				<400	502	541		<400	511	683	868	907		<400	614	787	972	1011

Fig. 22. Comparison between predicted and linearly interpolated temperature:
(a) concrete infill, (b) inner steel profile flanges and (c) inner steel profile web.

$$19 \leq B/t \leq 50$$

$$0,018 \leq A_p/A_c \leq 0,204$$

- The method can be used for standard fire exposure times ranging between 30 and 240 min.

5.4. Verification of the proposed design method

A final verification step was conducted to check the accuracy of the presented method in predicting the temperature field of SR-CFST. Several analysis cases selected from the parametric study database were used as check points for the model, and the equivalent temperatures for the different parts of the composite section were obtained by linearly interpolating in the presented design tables. Fig. 22 shows the comparison between the interpolated temperatures and the numerically computed ones at certain locations of the cross-section. The mean and standard deviation values of the prediction errors obtained for the concrete core, inner steel profile flanges and web are also given in the figure.

As can be seen, the method provides a good prediction accuracy within its applicability boundaries. It covers and extensive range of application, considering long fire exposure times (up to 240 min) and a wide range of cross-sectional dimensions.

6. Summary and conclusions

This paper presented a numerical investigation of the thermal behaviour of SR-CFST columns exposed to fire. The authors developed a sectional FE model using the nonlinear analysis software package ABAQUS and validated against several SR-CFST and CES specimens from experimental campaigns available in the literature.

Once validated, the numerical model was used to conduct a parametric study comprising 120 analysis cases. An evaluation of the influence of several parameters on the cross-sectional plastic resistance of the SR-CFST columns was performed. These parameters were the section shape (circular or square), the outer steel tube thickness, the section factor, and the Inner Steel Contribution Ratio (ISCR). A numerical integration procedure was developed by the authors through a Python subroutine and recurrently applied to compute the plastic resistance and flexural stiffness of all the analysed composite sections as a summation of the cells of the FE mesh, taking into account the degraded properties of steel and concrete at elevated temperature, which were assigned to the different cells from the previously computed cross-sectional temperature field at each standard fire period.

The parametric analyses found that the circular columns performed better under the effect of fire exposure, and this effect was more pronounced as the fire exposure time increased. For the same steel usage, the section factor of the square columns was higher than that of their circular counterparts, thus explaining their faster temperature rise and mechanical deterioration. It was also found that the reduction of the outer steel tube thickness and the increase in the dimensions of the inner steel profile incremented the mechanical capacity of the columns at elevated temperatures. Moreover, the cross-sectional capacity of the columns was enhanced by the progressive increase in the ISCR for both circular and square sections.

An innovative design method for determining the cross-sectional temperature field of unprotected SR-CFST columns under iSO-834 standard fire conditions was also presented in this paper. The developed equivalent temperature equations cover an existing limitation in EN 1994-1-2 regarding the lack of a temperature distribution proposal for specific steel–concrete composite sections, such as SR-CFST. The

proposed method provides designers with a user-friendly tool to quickly calculate the cross-sectional temperature field of these composite sections for the subsequent application of the reduction coefficients of the steel and concrete parts degraded by their temperatures. A single equivalent temperature representing the outer steel tube, concrete infill, inner steel profile web and flanges can be obtained through the proposed equations and tables. This way, the sectional capacity of a SR-CFST column exposed to fire can be easily computed as at room temperature (i.e. by adding the contribution of each component of the section) but simply reducing the capacity of each part according to its assigned equivalent temperature.

This proposal can be very helpful in the fire design process of steel–concrete composite structures, providing an accessible and simple tool for practitioners, while it has the potential to be further expanded for considering other cross-section types and geometries.

CRediT authorship contribution statement

David Medall: Conceptualization, Methodology, Validation, Formal analysis, Investigation, Writing – original draft. **Ana Espinós:** Conceptualization, Methodology, Investigation, Writing – review & editing, Funding acquisition, Project administration. **Vicente Albero:** Conceptualization, Methodology, Investigation, Writing – review & editing. **Manuel L. Romero** Conceptualization, Supervision, Funding acquisition, Project administration, Investigation.

Declaration of Competing Interest

The authors declare that they have no known competing financial interests or personal relationships that could have appeared to influence the work reported in this paper.

Data availability

Data will be made available on request.

References

[1] Espinos A, Romero ML, Serra E, Hospitaler A. Circular and square slender concrete-filled tubular columns under large eccentricities and fire. J Constr Steel Res 2015; 110:90–100. https://doi.org/10.1016/j.jcsr.2015.03.011.

[2] Romero ML, Espinós A, Lapuebla-Ferri A, Albero V, Hospitaler A. Recent developments and fire design provisions for CFST columns and slim-floor beams. J Constr Steel Res 2020;172:106159. https://doi.org/10.1016/j.jcsr.2020.106159.

[3] Zhou G, Luo C, Chen C, Dong X, Chen X, Liu X. The structural design of the Haiyi Hotel in Jiangmen. Guangdong Architect Civ Eng 2014:3–7.

[4] Romero ML, Espinós A, Renaud C, Bihina G, Schaumann P, Kleiboemer I et al. Fire resistance of innovative and slender concrete filled tubular composite columns (FRISCC). Final Report. Catalogue Number KI-NA-28082-EN-N. Brussels: RFCS Publications; 2016.

[5] Ferdous W, Bai Y, Almutairi AD, Satasivam S, Jeske J. Modular assembly of water-retaining walls using GFRP hollow profiles: components and connection performance. Compos Struct 2018;194. doi: 10.1016/j.compstruct.2018.03.074.

[6] Ferdous W, Almutairi AD, Huang Y, Bai Y. Short-term flexural behaviour of concrete filled pultruded GFRP cellular and tubular sections with pin-eye connections for modular retaining wall construction. Compos Struct 2018;206. doi: 10.1016/j.compstruct.2018.08.025.

[7] Ferdous W, Manalo A, Alajarmeh OS, Zhuge Y, Mohammed AA, Bai Y, et al. Bending and shear behaviour of waste rubber concrete-filled frp tubes with external flanges. Polymers (Basel) 2021;13. doi: 10.3390/polym13152500.

[8] Chu TB, Gernay T, Dotreppe JC, Franssen JM. Steel hollow columns with an internal profile filled with self-compacting concrete under fire conditions. Proc Roman Acad 2016;17(2):152–9.

[9] Chu TB. Hollow steel section columns filled with self-compacting concrete under ordinary and fire conditions. PhD thesis. University of Liege, Belgium; 2009.

[10] Dotreppe JC, Chu TB, Franssen JM. Steel hollow columns filled with self-compacting concrete under fire conditions. In: 3rd FIB international congress; 2010.

[11] Zhu MC, Meng FQ, He B. Experimental research on fire resistance of steel tubular columns filled with steel reinforced concrete. J Build Struct 2016;37:36–43.

[12] Meng FQ, Zhu MC, Mou B, He B. Residual strength of steel-reinforced concrete-filled square steel tubular (SRCFST) stub columns after exposure to ISO-834 standard fire. Int J Steel Struct 2019;19:850–66. https://doi.org/10.1007/s13296-018-0174-z.

[13] Meng FQ, Zhu MC, Clifton GC, Ukanwa KU, Lim JBP. Performance of square steel-reinforced concrete-filled steel tubular columns subject to non-uniform fire. J Constr Steel Res 2020;166. doi: 10.1016/j.jcsr.2019.105909.

[14] Meng FQ, Zhu MC, Clifton GC, Ukanwa KU, Lim JBP. Fire performance of edge and interior circular steel-reinforced concrete-filled steel tubular stub columns. Steel Compos Struct 2021;41:115–22.

[15] Lie TT. A procedure to calculate fire resistance of structural members. Fire Mater 1984;8(1):40–8.

[16] Dusinberre GM. Heat transfer calculations by finite differences. Scranton, PA: International Textbook Company; 1961.

[17] Lie TT. A method to predict the fire resistance of circular concrete filled hollow steel columns. J Fire Prot Eng 1990;2(4):111–26.

[18] Lie TT. Fire resistance of circular steel columns filled with bar-reinforced concrete. J Struct Eng (ASCE) 1994;120(5):1489–509.

[19] Lie TT, Irwin RJ. Fire resistance of rectangular steel columns filled with bar-reinforced concrete. J Struct Eng (ASCE) 1995;121(5):797–805.

[20] Tan KH, Tang CY. Interaction model for unprotected concrete filled steel columns under standard fire conditions. J Struct Eng (ASCE) 2004;130(9):1405–13.

[21] Wang ZH, Tan KH. Green's function solution for transient heat conduction in concrete-filled CHS subjected to fire. Eng Struct 2006;28(11):1574–85.

[22] Espinos A, Romero ML, Lam D. Fire performance of innovative steel-concrete composite columns using high strength steels. Thin-Walled Struct 2016;106: 113–28. https://doi.org/10.1016/j.tws.2016.04.014.

[23] Tan QH, Gardner L, Han LH. Performance of steel-reinforced concrete-filled stainless steel tubular columns at elevated temperature. Int J Struct Stability Dyn 2019;19. doi: 10.1142/S0219455419400029.

[24] Tan QH, Gardner L, Han LH, Song TY. Fire performance of steel reinforced concrete-filled stainless steel tubular (CFSST) columns with square cross-sections. Thin-Walled Struct 2019;143. doi: 10.1016/j.tws.2019.106197.

[25] Mao WJ, Wang WD, Xian W. Numerical analysis on fire performance of steel-reinforced concrete-filled steel tubular columns with square cross-section. Structures 2020;28:1–16. https://doi.org/10.1016/j.istruc.2020.08.043.

[26] Albero V, Espinos A, Romero ML, Hospitaler A, Bihina G, Renaud C. Proposal of a new method in EN1994-1-2 for the fire design of concrete-filled steel tubular columns. Eng Struct 2016;128:237–55. https://doi.org/10.1016/j.engstruct.2016.09.037.

[27] CEN. EN 1994-1-2, Eurocode 4: design of composite steel and concrete structures. Part 1.2: general rules - structural fire design; 2005.

[28] Abaqus/CAE user's guide. Version 2019. Dassault Systèmes; 2019.

[29] CEN. EN 1991-1-2, Eurocode 1: actions on structures - Part 1-2: general rules - actions on structures exposed to fire; 2002.

[30] Ghojel J. Experimental and analytical technique for estimating interface thermal conductance in composite structural elements under simulated fire conditions. Exp Therm Fluid Sci 2004;28:347–54.

[31] Tao Z, Ghannam M. Heat transfer in concrete-filled carbon and stainless steel tubes exposed to fire. Fire Saf J 2013;61:1–11. https://doi.org/10.1016/J.FIRESAF.2013.07.004.

[32] Espinos A, Romero ML, Hospitaler A. Advanced model for predicting the fire response of concrete filled tubular columns. J Constr Steel Res 2010;66(8–9): 1030–46. https://doi.org/10.1016/j.jcsr.2010.03.002.

[33] CEN. EN 1993-1-2, Eurocode 3: design of steel structures, Part 1.2: general rules – structural fire design; 2005.

[34] CEN. EN 1992-1-2, Eurocode 2: design of concrete structures, Part 1.2: general rules – structural fire design; 2004.

[35] CEN/TC250/SC2 N1897 - stable version prEN 1992-1-2:2021-09. Eurocode 2: design of concrete structures - Part 1-2: general rules - structural fire design; 2021.

[36] Huang ZF, Tan KH, Phng GH. Axial restraint effects on the fire resistance of composite columns encasing I-section steel. J Constr Steel Res 2007;63:437–47. https://doi.org/10.1016/j.jcsr.2006.07.001.

[37] Huang ZF, Tan KH, Toh WS, Phng GH. Fire resistance of composite columns with embedded I-section steel - effects of section size and load level. J Constr Steel Res 2008;64:312–25. https://doi.org/10.1016/j.jcsr.2007.07.002.

[38] Mao X, Kodur VKR. Fire resistance of concrete encased steel columns under 3- and 4-side standard heating. J Constr Steel Res 2011;67:270–80. https://doi.org/10.1016/j.jcsr.2010.11.006.

[39] Han LH, Tan QH, Song TY. Fire performance of steel reinforced concrete columns. J Struct Eng 2015;141:04014128. https://doi.org/10.1061/(ASCE)ST.1943-541X.0001081.

[40] Du Y, Qi H, Jiang J, Liew JYR, Li S. Thermo-mechanical behaviour of ultra-high strength concrete encased steel columns in standard fires. Eng Struct 2021;231:111757. https://doi.org/10.1016/j.engstruct.2020.111757.

[41] CEN. EN 1993-1-1, Eurocode 3: design of steel structures - Part 1-1: general rules and rules for buildings; 2005.

[42] CEN/TC250/SC4 N2192 - SC4.T7 Project Team final draft prEN 1994-1-2. Eurocode 4: design of composite steel and concrete structures – Part 1-2: general – structural fire design; 2021.

[43] CEN/TC250/SC4 N1836 - SC4.T4 Final Draft Annex H - simple calculation model for concrete filled hollow sections exposed to fire all around the column according to the standard temperature-time curve; 2017.

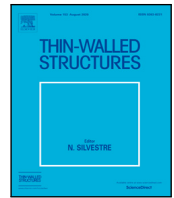[44] Wickström U. A very simple method for estimating temperature in fire exposed concrete structures. Sweden; 1986.

ANNEX I. COMPENDIUM OF PUBLICATIONS
ARTICLE 2

Full length article

Experimental residual capacity of steel-reinforced concrete-filled steel tubular stub columns after fire exposure

D. Medall [a], C. Ibáñez [a],*, V. Albero [b], A. Espinós [a], M.L. Romero [a]

[a] *ICITECH, Universitat Politècnica de València, Valencia, Spain*
[b] *Department of Mechanical Engineering and Construction, Universitat Jaume I, Castellón, Spain*

ARTICLE INFO

ABSTRACT

Technological advances in the development of steel–concrete composite structures have led to the introduction of novel types of sections in the sought of higher load-bearing capacities. Particularly for composite columns, the axial capacity of concrete-filled steel tubular (CFST) sections may be enhanced by the introduction of an open steel profile embedded within the concrete infill, forming the so-called steel-reinforced concrete-filled steel tubular (SR-CFST) columns. An important aspect that should be revised, in order to safely use these sections in design, is their performance after a fire. In this experimental program, six SR-CFST stub columns are tested in the post-fire situation. Two series of columns comprising three circular and three square sections with the same steel usage are tested for comparison purposes. The size of the inner steel profile is varied in order to investigate its effect over the post-fire capacity of the columns. The specimens were initially exposed to elevated temperatures inside an electric furnace, and then cooled to ambient temperature; afterwards compressive axial load was applied gradually until failure, to ascertain their residual capacity. The experimental results show the high ductility of the SR-CFST stub columns after heating, with the circular specimens reaching higher post-fire peak loads than their square counterparts. This load increases with the size of the embedded steel profile. The post-fire capacities of the columns are evaluated through the Residual Strength Index, showing similar values for both circular and square SR-CFST columns. Finally, a design equation is proposed to facilitate the evaluation of the post-fire compression resistance of SR-CFST columns, as an extension of the existing room temperature design equation in Eurocode 4 Part 1–2 for CFST columns, accounting for the degradation of the steel and concrete after fire exposure through the corresponding residual factors.

1. Introduction

In recent years, innovative solutions have been developed to increase both the load-bearing capacity and fire resistance of steel–concrete composite columns, as it is the case of steel-reinforced concrete-filled steel tubular (SR-CFST) sections, where an open steel profile is embedded within the concrete infill of the well-known concrete-filled steel tubular (CFST) section. Examples of high-rise buildings which use these types of composite sections for the main load-bearing compression members are spreading around the world [1,2], in sought of higher capacities with minimum cross-sectional dimensions.

In a fire situation, this form of construction also enhances the performance of the composite columns, since the inner steel profile is thermally protected by the surrounding concrete, thus delaying its degradation at high temperatures [3]. Therefore, SR-CFST columns may be a good alternative to improve the fire resistance of CFST columns, which is limited by the direct exposure of the outer steel tube to the heat source.

Although the many advantages of the application of SR-CFST columns are making their study appealing for the research community, investigations on their fire and post-fire structural response are particularly scarce, especially those that consider the post-heating phase.

A better understanding of the behaviour of SR-CFST columns after a fire, which is dominated by the maximum temperature achieved by the different components of the composite cross-section, is required to properly estimate the residual capacity of this typology and to adopt a reasonable reinstatement strategy with minimum post-fire repair.

Revising the available literature, it is worth drawing attention to the tests performed at the University of Liège [4], those carried out in Shanghai [5,6] and the experiments conducted at Southeast University [7]. In the first experimental program, the fire resistance of ten slender composite columns was tested using self-compacting concrete. Four of the ten sections were SR-CFST (with an embedded HEB120 steel profile), combining circular and square shapes for the outer steel tube.

---

* Corresponding author.
    E-mail address: caribus@upv.es (C. Ibáñez).

Notations

b	Flange dimension of the open steel profile
f_c	Compressive concrete cylinder strength (test date)
f_{ui}	Ultimate strength of steel for the embedded steel profile
f_{uo}	Ultimate strength of steel for the outer steel tube
$f_{ui,post}$	Ultimate strength of steel for the embedded steel profile after fire exposure
$f_{uo,post}$	Ultimate strength of steel for the outer steel tube after fire exposure
f_{yo}	Yield strength of steel for the hollow steel tube
f_{yi}	Yield strength of steel for the embedded steel profile
h	Height of the open steel profile
t	Outer steel tube thickness
t_f	Flange thickness of the open steel profile
t_w	Web thickness of the open steel profile
A_a	Cross-sectional area of the outer steel tube
A_a	Cross-sectional area of the outer steel tube
A_a/A_{tot}	Steel ratio for the outer steel tube
A_c	Cross-sectional area of the concrete core
$A_{c,i}$	Cross-sectional area of the -i concrete ring or layer
A_f	Cross-sectional area of the flanges of the embedded steel profile
A_{tot}	Total cross-sectional area of the column
A_{sp}	Cross-sectional area of the embedded steel profile
A_{sp}/A_{tot}	Steel ratio for the embedded steel profile
A_w	Cross-sectional area of the web of the embedded steel profile
B	Outer dimension for square sections
D	Outer diameter for circular sections
E_s	Elastic modulus of steel
$N_{calc,j}$	Residual plastic resistance calculated for approach –j
$N_{post,exp}$	Experimental residual load at post-fire
$N_{post,exp}/N_{calc,j}$	Prediction error for approach –j in comparison with $N_{post,exp}$
$N_{u,0}$	Ultimate load at room temperature
RSI	Residual Strength Index
ε_v	Longitudinal strain
ε_h	Transverse strain
η_a, η_c	Factors related to the confinement of concrete
v_s	Poisson's ratio of steel at the elastic range
$\overline{\lambda}$	Relative slenderness
σ_v	Longitudinal stress at the outer steel tube surface
σ_h	Transverse stress at the outer steel tube surface
$\theta_{a,max}$	Maximum temperature reached in the outer steel tube
$\theta_{c,i,max}$	Maximum temperature reached in the -i concrete ring or layer
$\theta_{f,max}$	Maximum temperature reached in the flanges of the embedded steel profile
$\theta_{w,max}$	Maximum temperature reached in the web of the embedded steel profile

Due to the application of intumescent paint in some specimens, the fire resistance times ranged from 39 up to 79 min for a load level of 0.4 and a maximum external dimension of 219.1 mm. For outer dimensions greater than 219.1 mm, a complementary numerical study was carried by means of the software SAFIR.

In the experimental programs by Meng et al. [5,6], fire resistance tests on eight SR-CFST columns were conducted. The effect of non-uniform heating was taken into consideration and, in this case, again square and circular geometries were considered. The SR-CFST columns had an embedded HW150×150 and were 1800 mm long although only the central 1200 mm were heated. The experiments revealed that the inner steel profile considerably enhanced the fire behaviour of the specimens, exceeding 240 min for the 1-side and 2-sides exposed columns. Lately, Mao et al. [7] also investigated the fire performance of SR-CFST columns but with cruciform section profiled steel. The specimens were tested under the ISO-834 standard fire curve and parameters including the shape of the outer steel tube (circular or square) or the load ratio were considered. Once more, it was found that the fire resistance of SR-CFST columns had substantial improvement compared with CFST columns.

Recently, the residual strength of SR-CFST stub columns after exposure to ISO-834 standard fire curve was assessed by Meng et al. [8] through tests on three non-uniformly heated 600 mm long square columns. The specimens were composed of an outer square steel tube of dimensions 300×300×6 mm and an inner steel profile HW150×150. The study focused on the influence of the number of sides exposed to the heating source, so the columns were 2, 3 and 4-sides exposed inside a small electric furnace, where a hysteretic pre-heat process was initially applied in order to approach the standard fire curve. Once cooled down, the columns were tested to failure to obtain their residual strength. As presumed, the residual strength of the columns decreased with the fire exposure time and a high ductility level was generally observed for the stub SR-CFST columns, since they maintained their load bearing capacity reasonably constant after reaching the peak point instead of showing a sharp drop. Expressions for the residual strength after different types of fire exposure were presented based on parametric studies.

The most recent research found in relation with the post-fire behaviour of SR-CFST columns is the work presented by Yang et al. [9] where the results of an extensive experimental program on 135 square SR-CFST columns are presented. In the research, 108 SR-CFST specimens were tested after being heated for different times and 27 kept unheated for reference. Among the conclusions drawn by the authors it may be highlighted that the inner steel section ratio is the parameter with the highest influence in the post-peak behaviour of the columns whereas the maximum temperature reached has the greatest effect on the residual bearing capacity of the columns. In their work, the authors also proposed a set of equations for the evaluation of the ultimate strength of square SR-CFST both at room temperature and after fire exposure. Despite the high number of tests performed, it must be noted that the range of geometrical variation was narrow since all of the tested specimens had the same outer dimension (B = 200 mm) with minor variations in the thickness of the outer tube (2.94 to 4.78 mm) and only three different embedded steel profiles.

Thus, the literature analysis confirms that the number of available fire and post-fire test results on SR-CFST columns is scarce. Therefore, in this paper, the results of a series of experiments on the behaviour of SR-CFST columns after exposure to elevated temperature are presented. The history of sectional temperatures is analysed as well as the response in terms of axial load–displacement. The failure mode of the

Table 1
Details of the specimens and test results.

Specimen	D or B (mm)	t (mm)	$\frac{A_a}{A_{tot}}$ (%)	f_{yo} (MPa)	f_{uo} (MPa)	Inner section	$\frac{A_{sp}}{A_{tot}}$ (%)	f_{yi} (MPa)	f_{ui} (MPa)	f_c (MPa)	$N_{post,exp}$ (kN)
SR-CFST-C-T1	273	10	14.1	451	504	HEB100	12.0	315	445	24.3	4799
SR-CFST-C-T2	273	10	14.1	451	504	HEB120	14.6	308	437	24.3	>5000
SR-CFST-C-T3	273	10	14.1	451	504	HEB140	17.1	315	441	24.3	>5000
SR-CFST-S-T1	220	10	16.8	560	680	HEB100	12.2	315	445	24.3	4153
SR-CFST-S-T2	220	10	16.8	560	680	HEB120	14.8	308	437	24.3	4615
SR-CFST-S-T3	220	10	16.8	560	680	HEB140	17.4	315	441	24.3	4896

Note: D and B are the outer diameter or dimension for circular and square sections respectively; t is the outer steel tube thickness; f_{yo} and f_{yi} are the yield strength of steel for the outer steel tube and inner embedded section respectively; f_{uo} and f_{ui} are the ultimate strength of steel for the outer steel tube and inner embedded section respectively; f_c is the concrete cylinder compressive strength; A_a/A_{tot} is the steel ratio for the outer steel tube (where A_a is the cross-sectional area of the outer steel tube and A_{tot} is the total cross-sectional area of the column); and A_{sp}/A_{tot} is the steel ratio for the embedded steel profile (where A_{sp} is the cross-sectional area of the embedded steel profile).
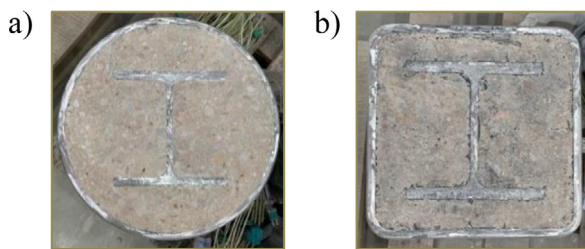

Fig. 1. SR-CFST configurations analysed: (a) circular; (b) square.

columns is investigated together with the stress state at the outer steel tube, derived from the measured strains. Finally, the suitable residual factors for steel after fire exposure are assessed, and a proposal of a design equation for the evaluation of the residual cross-sectional axial compression capacity of SR-CFST columns, based on an extension of the room temperature equations in Eurocode 4 Part 1–1, is presented.

2. Experimental investigation

2.1. Column specimens

Within the framework of this investigation, six SR-CFST specimens, consisting of three specimens with circular sections and three specimens with square sections, were fabricated to conduct axial compression loading tests after exposure to elevated temperatures (see Fig. 1a and Fig. 1b). For the sake of comparison, the selected circular and square steel tubes had the same cross-sectional steel area with a maximum difference of a 2.51%. Three different open steel sections with wide flanges are embedded inside the concrete core of both series: HEB100, HEB120 and HEB140.

Table 1 presents the cross-sectional characteristics and mechanical properties of the materials of all the specimens, and also summarizes the values of the experimental residual loads at post-fire ($N_{post,exp}$) which will be analysed in Section 2. For convenience, the test specimens were named SR-CFST-S-Ti, where S stands for the cross-sectional outer tube shape (C for circular and S for square) and Ti refers to the inner embedded steel profile dimensions, where T1 stands for HEB100, T2 for HEB120 and T3 for HEB140. As summarized in Table 1, for the circular columns, ϕ273×10 hollow steel tubes were employed, while the hollow square steel tubes were #220×10 with a maximum difference of a 2.51% in cross-sectional steel area.

Note that the embedded open steel section HEB100 has an outer dimension of $h = b = 100$ mm ($t_f = 10$ mm, $t_w = 6$ mm); the HEB120 has $h = b = 120$ mm ($t_f = 11$ mm, $t_w = 6.5$ mm), and the HEB140 has $h = b = 140$ mm ($t_f = 12$ mm, $t_w = 7$ mm).

The thermal test was the first step of the experiments, where each SR-CFST specimen was uniformly exposed to high temperatures inside the furnace. Next, after cooling at room temperature, the post-fire test to evaluate the resistance of the columns subjected to increasing axial load was conducted in a vertical frame. Test procedure is further explained in Section 2.5.

2.2. Material properties

Steel

In this experimental plan, all of the steel tubes were cold formed welded structural hollow sections in accordance with EN 10219-1 [10] and had a nominal yield strength of S355. Regarding the embedded open steel profiles, all of them were hot rolled in conformity with EN 10025-1 [11] and had a nominal yield strength of S275. To ensure getting enough material for the coupon tests, extra material than strictly needed was supplied. For all of the hollow steel tubes and embedded steel profiles that were used, the actual values of the yield strength (f_{yo} and f_{yi}, respectively) and the ultimate strength (f_{uo} and f_{ui}, respectively) are summarized in Table 1 For the steel tubes and the embedded steel profiles, the values were obtained through the corresponding coupon tests. According to the European standards, the modulus of elasticity of steel was set to 210 GPa.

Concrete

The pertinent standard tests were carried out on the 100 mm cube to obtain the actual compressive strength of concrete (f_c). Therefore, the equivalent cylinder compressive strength was obtained from the values of the strength of the cubic samples according to Eurocode 2 Part 1–1 [12], and is shown in Table 1. Concrete moisture concrete was 7.952% weight measured at the beginning of the experimental program. The sets of concrete samples were prepared in a planetary mixer and cured in standard conditions during 28 days. To be consistent, the corresponding concrete samples were tested the day when the experiment was conducted.

2.3. Preparation of specimens

The preparation of all of the columns as well as the tests took place at the facilities of ICITECH, Universitat Politècnica de València (Spain). To perfect the load application conditions during the post-fire test, steel plates with dimensions 300x300x10 mm were placed at both ends of each specimen. First, a steel plate was welded to the bottom of the embedded steel profile (Fig. 2a). Next, the thermocouples were positioned together with the hollow steel tube in order to correctly place the thermocouples wires (Fig. 2b and Fig. 2c). For that purpose, a hole was drilled at the top end of the columns which ultimately also allowed vapour ventilation during heating. Later, the bottom of the hollow steel tube was welded to the steel plate. Once the concrete was poured into the column and settled with the help of a needle vibrator (Fig. 2d), the specimen was covered with a plastic film. Finally, the second plate was welded to the top end of the column (Fig. 2e) right after smoothing the top surface in order to assure planarity and the contact of the steel plate with all of the components.
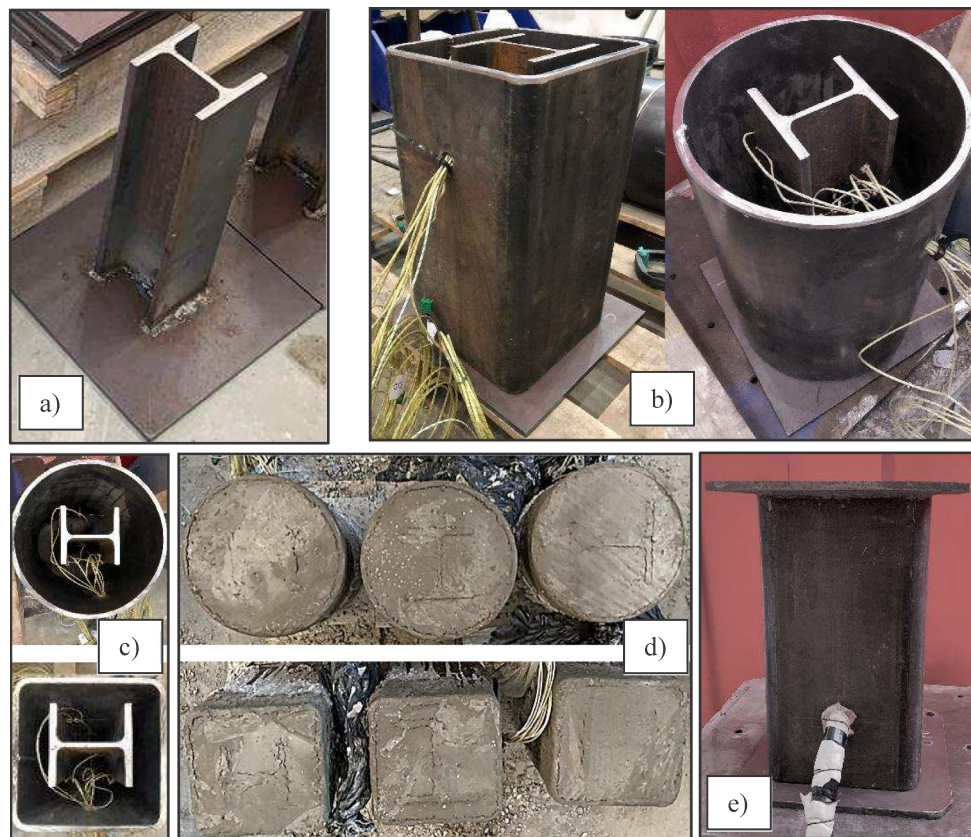
Fig. 2. Columns preparation: (a) Steel plate welded at bottom end of the embedded profile; (b) Positioning of hollow steel tube; (c) Positioning of thermocouples; (d) Columns after casting; (e) Column finished.
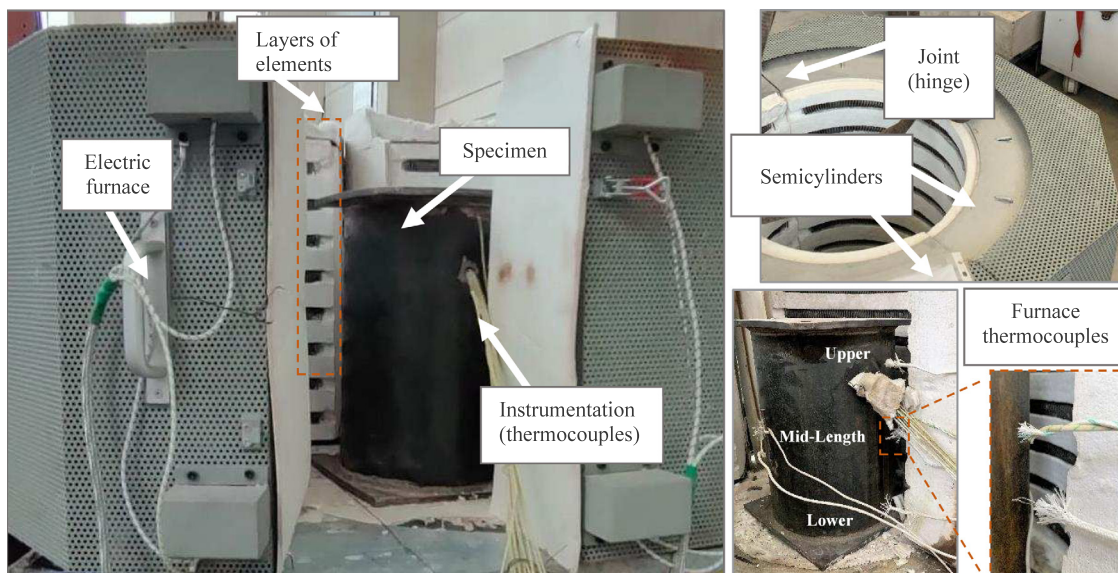

Fig. 3. Thermal test setup.

2.4. Thermal test setup

The heating of the specimens was conducted by a small vertical electric furnace of 10 kW power. The furnace consisted of two semi-cylinders joined by a hinge and had an inner diameter of 400 mm. As displayed in Fig. 3, on the inner refractory wall of the semicylinders, the electric elements are distributed evenly in parallel layers through the whole length for both sides.

The furnace temperature was controlled by five thermocouples located close to the refractory walls at different levels of the furnace as follow: one at the upper level, three at mid-length level and one at the lower level (see Fig. 3). For each specimen, the thermal response was registered by 12 thermocouples located at specific points of interest at the mid-length cross-section of the column, according to the layout presented in Fig. 4. Thermocouples 1 and 6 were welded to the outer surface of the steel tube whereas thermocouples 11 and 12 were welded
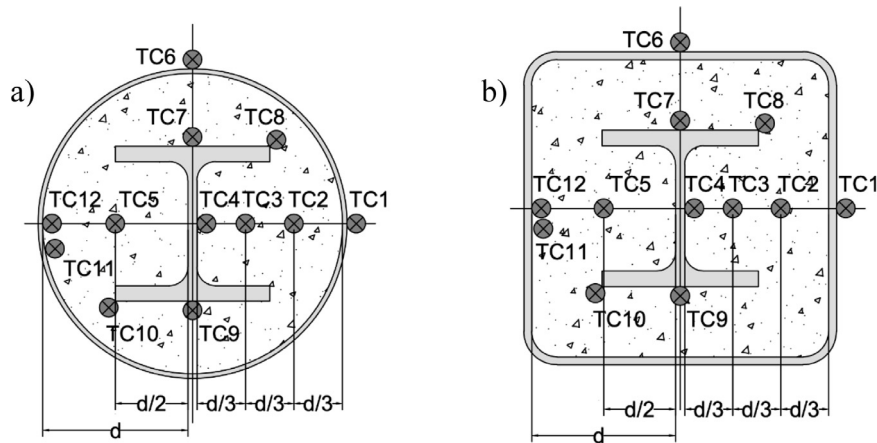
Fig. 4. Thermocouples layout: (a) circular sections; (b) square sections.
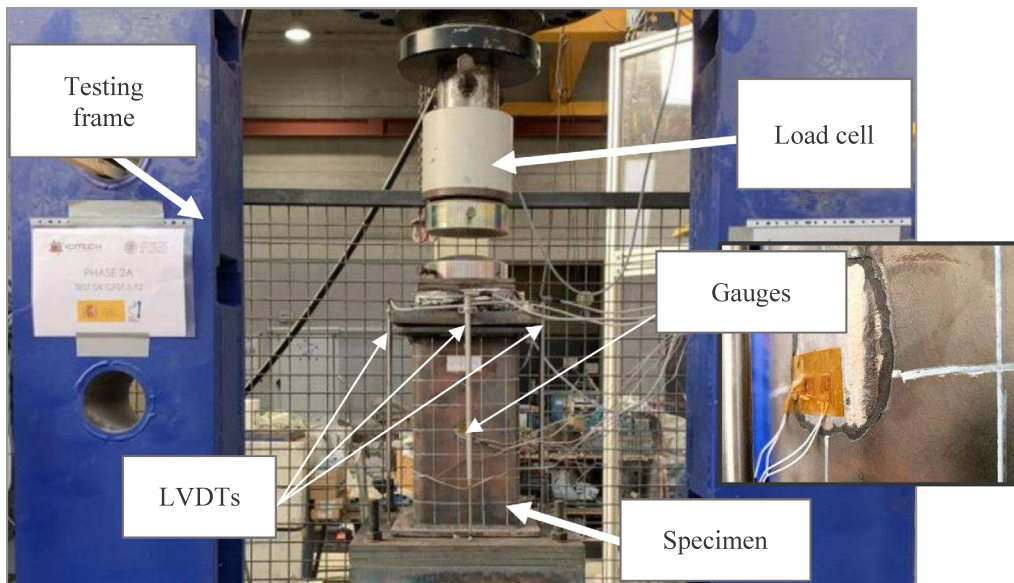

Fig. 5. Post-fire test setup.

to the inner surface. At the embedded HEB steel profile, thermocouples 7 to 10 were welded at different points of flanges and web. Thermocouples 2 to 5 were embedded in the concrete core: number 2 to 4 were placed equidistantly with a separation of 1/6 of the section width; and number 5 was positioned at 1/4 of the section width.

2.5. Test procedure

The circular and square SR-CFST columns were first heated unloaded in the described electric furnace, since this condition is considered to be more conservative in the evaluation of the residual strength of concrete after heating [13–15]. For the thermal tests, both top and bottom surfaces were protected with fibre blankets to prevent heat loss. To guarantee that the embedded steel profile, in all of the tested specimens, had a significant reduction in its mechanical properties, the furnace temperature target was set to 1000 °C. As a result, due to the electric furnace power specifications, the heating times for all of the specimens were higher than 240 min. Once the target temperature was attained, the electric furnace was switched off and opened so that

the column cooled at ambient temperature. The time histories of the furnace and cross-sectional temperatures were registered during the heating and also part of the cooling process.

After the specimen had cooled down, the investigation continued with the compression test to obtain the residual strength of the SR-CFST column after heating. As presented in Fig. 5, a vertical testing frame with a hydraulic jack with capacity of 5000 kN was employed for that purpose. In Fig. 5, the setup of this mechanical test for one of the square SR-CFST columns is shown. The boundary conditions during the experiments for all of the tested stub columns were pinned–fixed (P–F) with a length of 400 mm. The mechanical response of each column was monitored by means of four LVDTs placed at the four sides of the column to register the top end axial displacement as well as to control slight deviations that may occur during loading. Additionally, two sets of strain gauges were attached to the four sides of the column in the longitudinal and transversal directions (see Fig. 5).

At the start of each experiment and right after the correct positioning of the specimen, the pertinent displacement control test was conducted. Thus, data from the four LVDTs were monitored to assure
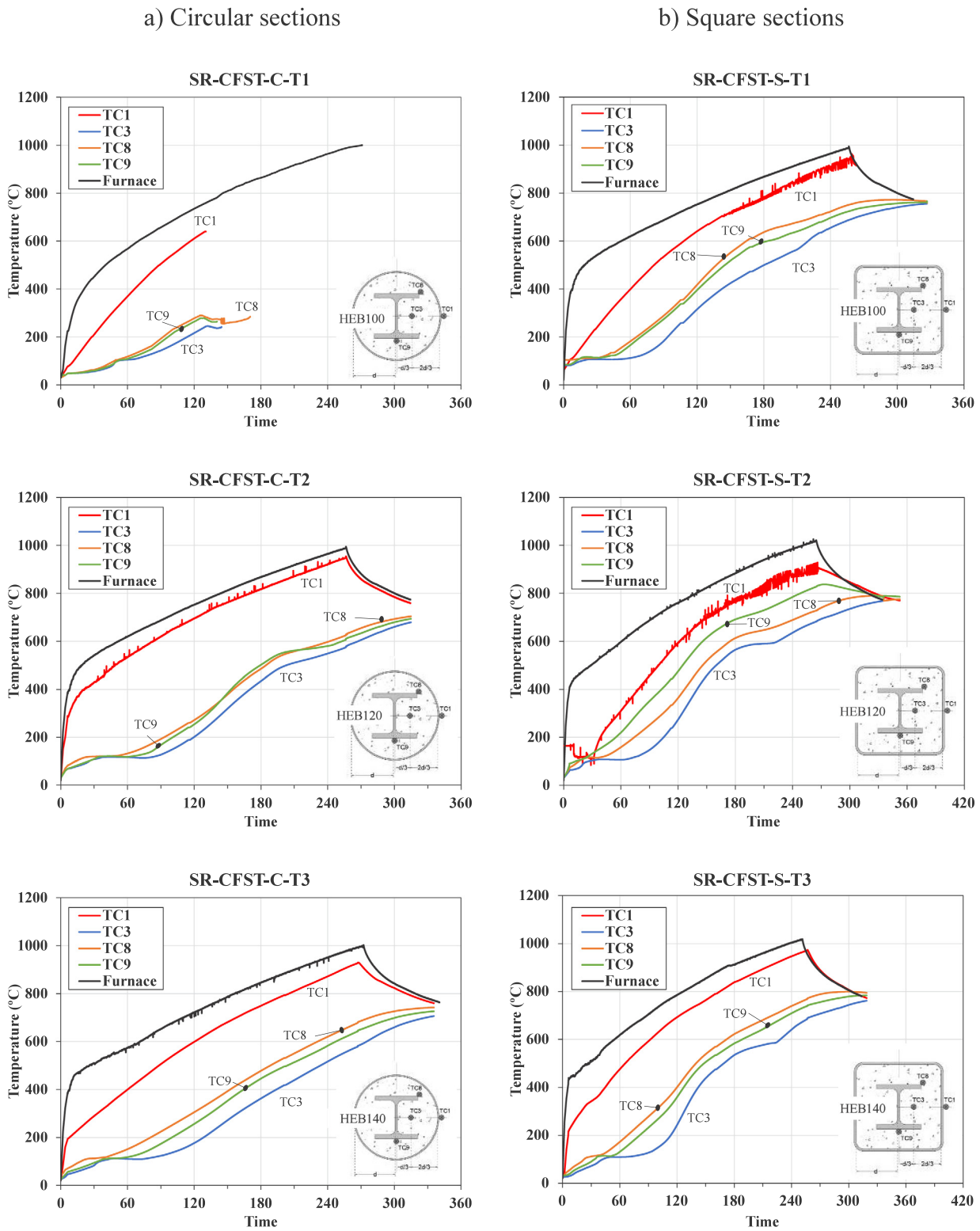
a) Circular sections

b) Square sections

Fig. 6. Cross-sectional temperatures.

that the columns were, in fact, axially loaded and that the compression was uniformly applied. A displacement-controlled test was conducted with a loading rate of 0.1 mm/min. The load cell allowed to measure the applied load during the test which was recorded together with the evolution of the axial displacement of the columns, showing its shortening due to the applied load. From the data acquisition system, the time histories of the load and displacement rate were also recorded.

3. Analysis of experimental results

3.1. Cross-sectional temperatures

The time history of the cross-sectional temperatures monitored during the heating and part of the cooling process are shown in Fig. 6. Although data from the 12 thermocouples installed were recorded, for

Fig. 7. External surface of the columns after heating: (a) SR-CFST-C-T2; (b) SR-CFST-S-T2.

the sake of clarity only the temperatures of four of the thermocouples are displayed together with the evolution of the furnace temperature.

Due to a failure in the connection of some thermocouples to the data acquisition system when specimen SR-CFST-C-T1 was tested, temperatures are missing from 120 min on for TC1; from 150 min on for TC3 and TC9; and from approximately 180 min on for TC9.

As presented in Fig. 6, the effect of the thermal protection provided by the outer steel tube and the low thermal diffusivity of concrete can be perceived in the delay of temperature rise in the concrete core for both series. In general, temperatures are higher for the square SR-CFST columns than for the corresponding circular columns, which may be due to the effect of the section factor, since for the same cross-sectional area, the square sections present a higher exposed perimeter.

It can be seen that in the specimens SR-CFST-C-T3 and SR-CFST-S-T3, the embedded steel profile (HEB140) reaches higher temperatures than the other two types of sections. For the same external dimensions, the greater the embedded steel profile, the less the concrete cover that protects the profile.

The external surface of the steel tubes became dark burgundy and the characteristic orangey rust that usually covers the steel surface

disappeared. A close up of specimens SR-CFST-C-T2 and SR-CFST-S-T2 is shown in Fig. 7, where it can also be seen that part of the degraded outer thin layer of the steel tube sloughed off during heating. In Fig. 8a, the state of all of the tested columns after the heating is presented.

To illustrate the final state of all of the components of the columns after the tests, specimens SR-CFST-C-T1 and SR-CFST-S-T1 were selected for further examination and were cut longitudinally to analyse the embedded profile and the concrete core (see Fig. 9). It can be seen that the degraded concrete has a yellow colour in contrast to the undamaged concrete which still possess its original grey colour. With a dashed red line, the limit of the degradation area has been marked. As expected, this area includes the outer part of the concrete core and part of the concrete at the top of the column, due to the heat travelling to the upper part of the furnace during the heating. As can be seen in Fig. 6b for specimen SR-CFST-S-T1, the temperatures achieved at the last part of the heating test are between 600 °C and 800 °C. For temperatures higher than 600 °C a change in the concrete microstructure occurs producing the abovementioned change of colour.

3.2. Failure modes

In Fig. 8 the columns of the circular and the square series are shown after both the thermal (Fig. 8a) and the post-fire test (Fig. 8b) to have a general view of the state of the columns after the tests and directly visualize the changes in their physical state.

After the post-fire mechanical tests, the columns were highly damaged and cracked due to the high level of compression achieved during the test (see Fig. 8b). The columns at failure developed the characteristic elephant foot due to local buckling of the outer steel tube, especially the square specimens. As pointed out by Meng et al. [8], this phenomenon is caused by the different thermal expansion of the different materials and the uneven temperature field, which enables the steel tube to support the increasing axial load and yield. In the case of the tested columns, the outward bulges appeared near the top end of the columns, which may be due to the fact that it is on this end where the hole for water evaporation was drilled. Also, the ball joint of the load cell was located at this side, facilitating the folding of the steel tube closer to the top end.
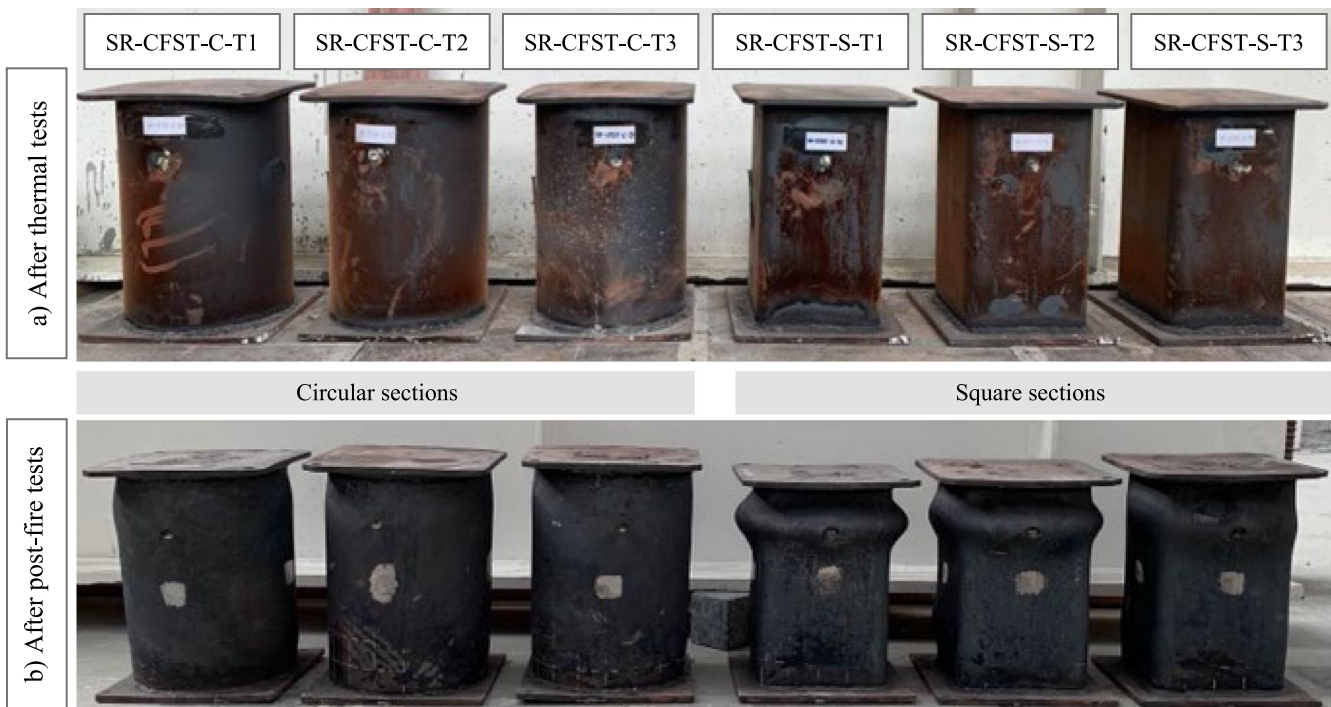

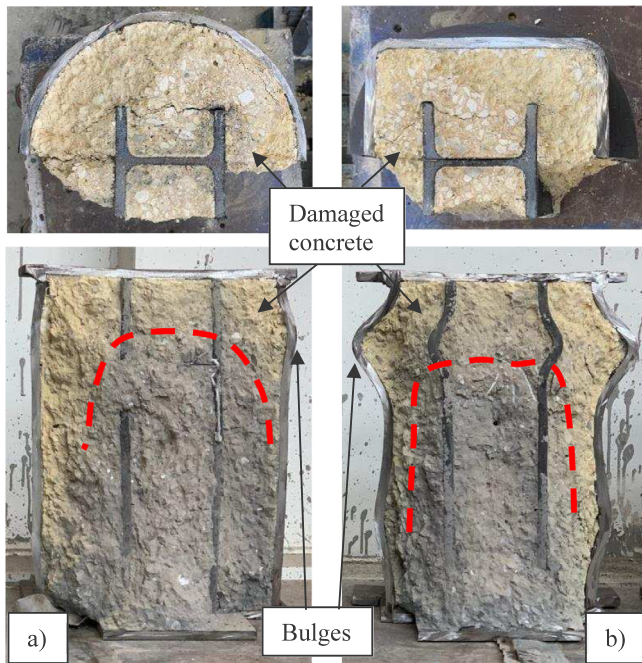**Fig. 8.** Columns after the thermal and the post-fire mechanical test.

Fig. 9. Failure mode: (a) SR-CFST-C-T1; (b) SR-CFST-S-T1.

In general, the occurrence of the bulges was symmetrical and took place at the same location over the column length for the whole perimeter in both types of geometries (see Fig. 8b and Fig. 9). Right on the bulges, a gap appeared between the folded steel tube and the damaged concrete (see Fig. 9). Due to the maximum temperatures reached by the concrete, the bonding capacity of concrete was significantly reduced so the degraded concrete crumbled to the touch. This was also observed by Yang et al. [9] in their investigation since no plates were welded at the end of the tested columns so when the surfaces were being prepared for the mechanical test after the heating, it was observed that small bits and coarse aggregates scattered from the concrete. However, in this

experimental program, thanks to the welded steel plates, the concrete surface at the top end of the columns was practically intact and kept the planarity.

Another phenomenon observed in the tests was the apparition of shear slippage lines (see Fig. 10) that describe the plane of maximum tangential stress, with an angle of 45° with respect to the main compression stress direction (longitudinal axis). These lines appeared and generally started to grow when the applied load reached about 3000 kN (60%–75% of the maximum load), corresponding to the point when the outer steel tube entered the plastic stage, as will be later confirmed in the stress analysis presented in Section 3.3. The shear slippage lines continued to develop during the last part of the test and became greater until eventually the ultimate capacity of the columns was attained.

In Fig. 10 it can also be observed how a very thin superficial layer of the outer steel tube sloughs off. This is the mill scale (also known as calamine), a surface oxidation layer that is generated during the hot rolling process. This layer initially protects the steel tube when is in storage, but it is not very stable and eventually it peels off. In addition, its thermal expansion coefficient is smaller than that of the rest of the steel so it is very affected by the temperature gradients. Given that after heating it is more fragile, during the post-fire tests it sloughs off.

3.3. Stress analysis of the outer steel tube

The stress state of the outer steel tube during the load tests was measured using strain gauges, vertical and horizontal, at 0°, 90°, 180° and 270°, as shown in Fig. 11.

The strain gauge measurements registered during the load tests are provided in Fig. 12. For comparison purposes, only the results for the square specimens are shown. It is worth noting that in these graphs, positive strain implies contraction, while negative strain means elongation.

From these strain readings, the vertical (σ_v) and hoop (σ_h) stresses at the linear elastic range can be directly obtained by assuming a state of plane stress at the outer surface of the steel tube, based on Hooke's law:

$$\sigma_v = \frac{E_s}{1-v_s^2}\left(\varepsilon_v + v_s\varepsilon_h\right)$$
$$\sigma_h = \frac{E_s}{1-v_s^2}\left(\varepsilon_h + v_s\varepsilon_v\right)$$

(1)

Fig. 10. Shear slippage lines: (a) SR-CFST-C-T1 during the test; (b) SR-CFST-C-T2 bottom end close up.
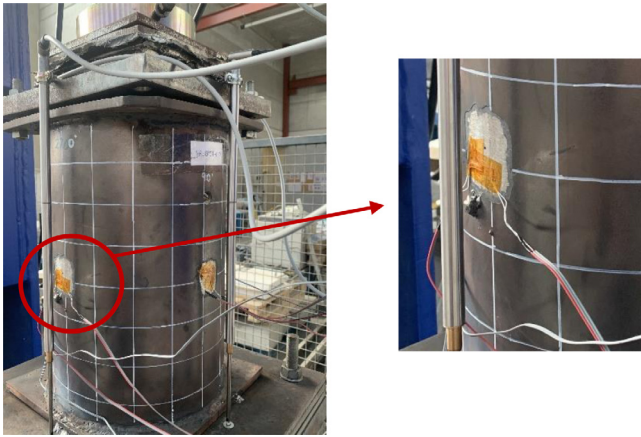
Fig. 11. Detailed view of the strain gauges attached to the outer steel tube surface.

where ε_v and ε_h are the longitudinal and transverse strain, respectively, v_s is the Poisson's ratio of steel at the elastic range and E_s is the elastic modulus of steel.

Based on the elastic–plastic theory, the Von Misses equivalent stress can be computed, as given by:

$$\sigma_{eq,VM} = \frac{\sqrt{2}}{2}\sqrt{\left(\sigma_h - \sigma_v\right)^2 + \sigma_v^2 + \sigma_h^2} \tag{2}$$

where σ_v and σ_h are the longitudinal and transverse stress at the outer steel tube surface, respectively.

In the elastic–plastic range, however, the expressions given in Eq. (1) are not valid, thus the relevant stress–strain relations may be obtained based on an incremental procedure, as given in [16], where the tangent modulus of steel (E_s^t) may be updated at each strain increment:

$$E_s^t = \frac{(f_y - \sigma_{eq,VM})\sigma_{eq,VM}}{(f_y - f_p)f_p}E_s \tag{3}$$

as well as the Poisson's ratio:

$$v_{sp} = 0.217\frac{\sigma_{eq,VM} - f_p}{f_y - f_p} + v_s \tag{4}$$

By applying the described procedure, the stress state of the outer steel tube during loading at the post-fire tests was obtained for the stub columns. It is worth mentioning that the referred mechanical properties of steel were assumed to be affected by the maximum temperature reached at the heating phase, that is, the corresponding post-fire residual factors were applied to f_p, f_y and E_s based on the maximum temperatures registered at the outer steel tube for each specimen.

Fig. 13 displays the evolution of the vertical (V) and hoop (H) stresses at the four studied orientations (0°, 90°, 180° and 270°) for specimen SR-CFST-S-T3. It is worth noting that in these graphs, positive stresses are compression stresses, while negative stresses refer to tensile stresses.

As it can be seen, at the initial stage of loading (elastic range), the vertical stresses increase linearly, while the transverse (hoop) stresses remain with a small value, increasing at a slower pace. As the axial load increases, the material enters into an elastic–plastic regime, where the slope of the load versus stress curves gradually reduces leading to the plastic stage, where both the vertical and horizontal stresses show a rapid development, indicating a possible effect of the lateral confinement stresses between the outer steel tube and the concrete core. This point occurs once the load level corresponding to a 60%–75% of the ultimate load (about 3000 kN) is reached. This is coincident with the visual observation of the development of the shear slippage lines at 45° relative to the longitudinal direction that was highlighted in Section 3.2, indicative of plastic failure in pure compression. In this

plastic stage, the stresses continue developing without a significant load increase, as it can be seen in the horizontal plateau in Fig. 14. A strain hardening stage can be recognized between 200 and 400 MPa, at the end of which the stresses tend to stabilize again, point where the steel tube failure takes hold. By computing the Von Misses equivalent stress at this point (see Fig. 14), values close to the post-fire ultimate strength of steel corresponding to the maximum temperature reached by the outer tube at the heating tests can be found.

As an example, specimen SR-CFST-S-T3 attained a maximum temperature at the outer tube of 989 °C, what according to [17] corresponds to a post-fire reduction coefficient of the ultimate strength of steel equal to 0.577, therefore $f_{uo,post} = 0.577 \times f_{uo,20} = 0.577 \times 680$ MPa = 392 MPa. From this point on, the outer steel tube is not capable to sustain the load anymore, thus being primarily sustained by the concrete core and the inner steel profile, until eventually the failure of the column occurs.

3.4. Force–displacement response

As can be seen in Fig. 15, the initial response was mostly linear elastic up to approximately 65%–70% of the peak load ($N_{post,exp}$), which is in concordance to the response observed by other authors [8]. The columns then entered the plastic range and the stiffness of the columns decreased gradually. Finally, the specimens achieved the peak load which kept constant for a significant period instead of presenting a sharp drop, showing the high ductility of the columns. Table 1 shows the values of the peak load registered during the experiments for all of the tested columns.

Note that in Fig. 15, for columns SR-CFST-C-T2 and SR-CFST-C-T3, the tests were manually paused due to the technical limitations of the vertical frame (5000 kN) and this fact did not allow to register the maximum load experimentally (see column $N_{post,exp}$ in Table 1).

In general, circular SR-CFST columns had higher peak loads than their square counterparts. For each series, the peak load at post-fire increased as the size of the embedded steel profile did, being the maximum values for the specimens with and embedded HEB140 (see Fig. 16).

3.5. Residual strength index

To quantify the loss of load bearing capacity experienced by the columns after being exposed to high temperatures, the Residual Strength Index (RSI) is calculated. The approach proposed by Han et al. [18] has been adopted, where RSI is defined as:

$$RSI = \frac{N_{post,exp}}{N_{u,0}} \tag{5}$$

where $N_{u,0}$ and $N_{post,exp}$ are the room temperature and experimental post-fire ultimate load respectively.

For the calculation of $N_{u,0}$, the equations given in Clause 6.7.3.2 of Eurocode 4 Part 1–1 [19] for evaluating the plastic resistance to compression of CFST sections are used and adapted to SR-CFST sections. Account for the inner steel profile will be done by adding its contribution to the plastic resistance of the composite cross-section in the summation of components, as previously proposed by Liew et al. [2].

In the case of square SR-CFST sections, confinement at room temperature is neglected. Therefore, $N_{u,0}$ may be calculated by adding the plastic resistances of its components, as given in Clause 6.7.3.2(1) of Eurocode 4 Part 1–1 [19]:

$$N_{u,0} = A_a f_{uo} + A_c f_c + A_{sp} f_{ui} \tag{6}$$

where A_a and f_{uo} are the cross-sectional area and the ultimate strength of the steel tube; A_c and f_c are the cross-sectional concrete area and the compressive cylinder strength of concrete; and A_{sp} and f_{ui} are the cross-sectional area and the ultimate strength of the embedded steel profile.
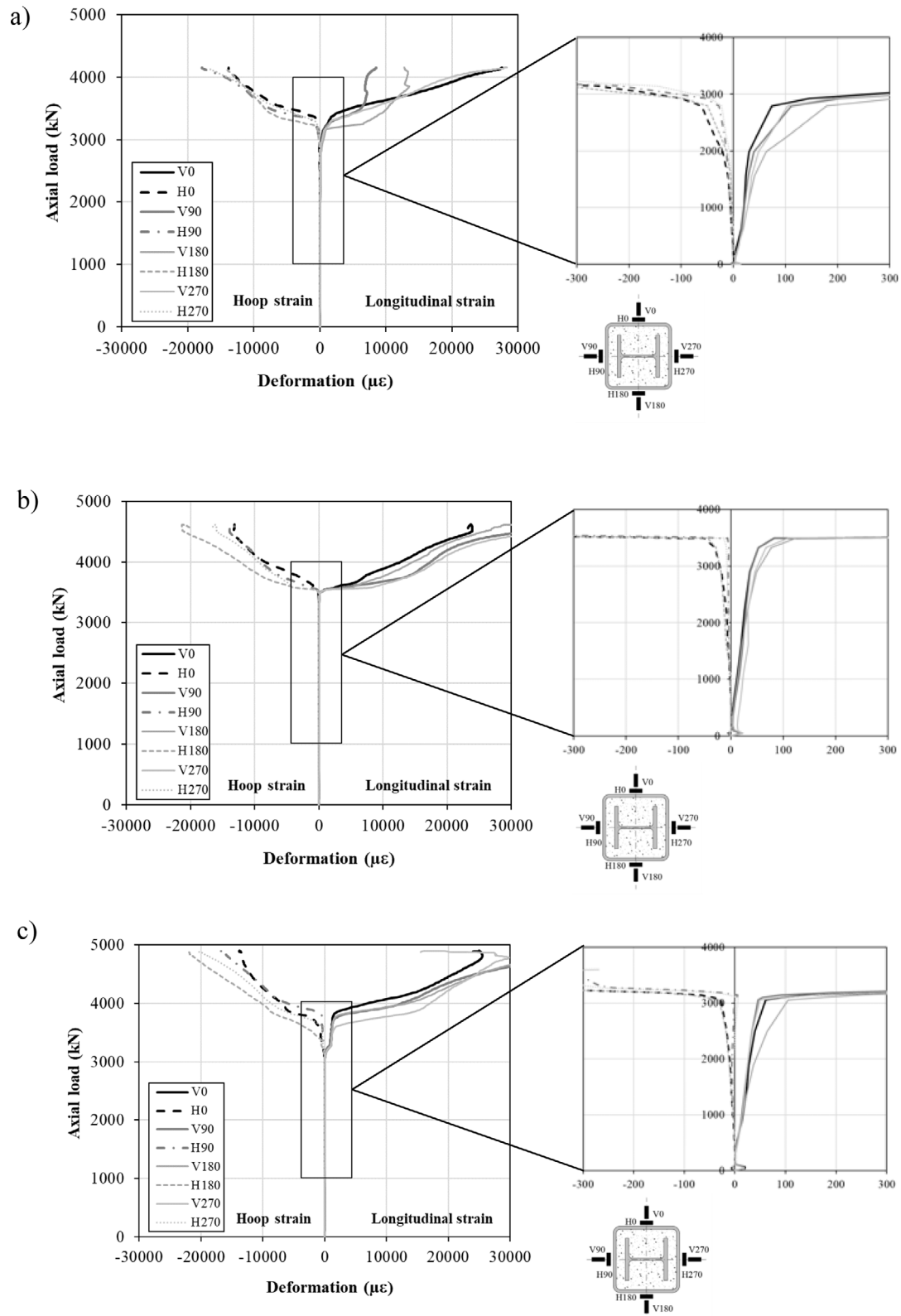
Fig. 12. Deformation state at the outer steel tube surface for the square columns: (a) SR-CFST-S-T1; (b) SR-CFST-S-T2; (c) SR-CFST-S-T3.

For circular columns, account may be taken of the increase in strength of concrete caused by confinement as stated in Clause 6.7.3.2 (6) of Eurocode 4 Part 1–1 [19], provided that the relative slenderness does not exceed 0.5 ($\bar{\lambda} < 0.5$) and a load eccentricity to diameter ratio less than 0.1 — what is the case of the studied columns. This is given by:

$$N_{u,0} = \eta_a A_a f_{uo} + A_c f_c \left(1 + \eta_c \frac{t}{D} \frac{f_{uo}}{f_c}\right) + A_{sp} f_{ui} \tag{7}$$

where t is the wall thickness of the steel tube; D refers to the external diameter of the column; and η_a and η_c are the factors related to the
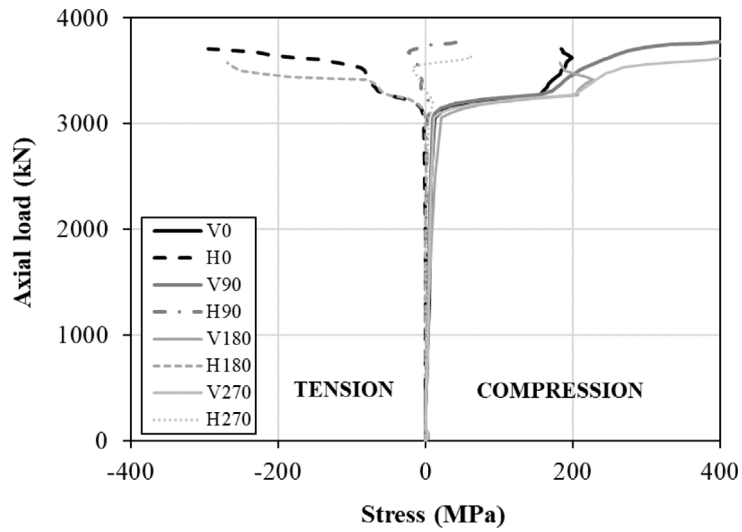
Fig. 13. Development of stresses at the outer steel tube surface for specimen SR-CFST-S-T3.
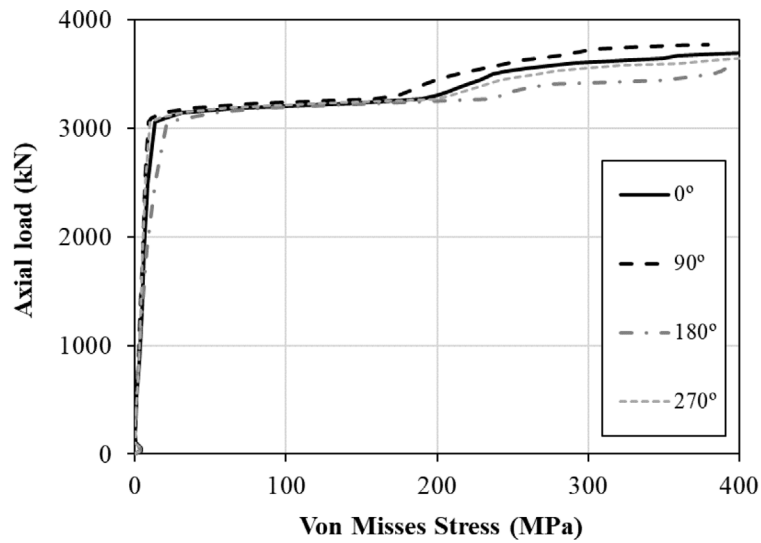

Fig. 14. Axial load versus Von Misses equivalent stress for specimen SR-CFST-S-T3.
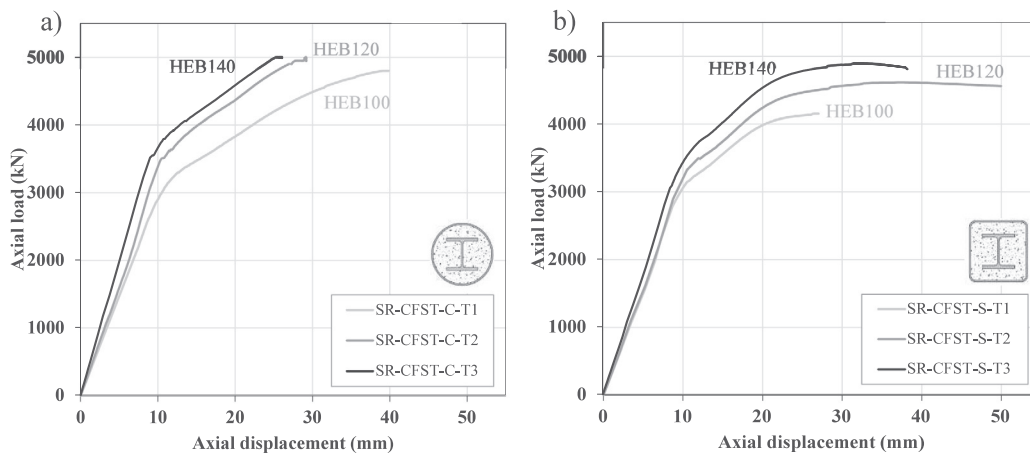

Fig. 15. Axial load–displacement curves: (a) circular sections; (b) square sections.
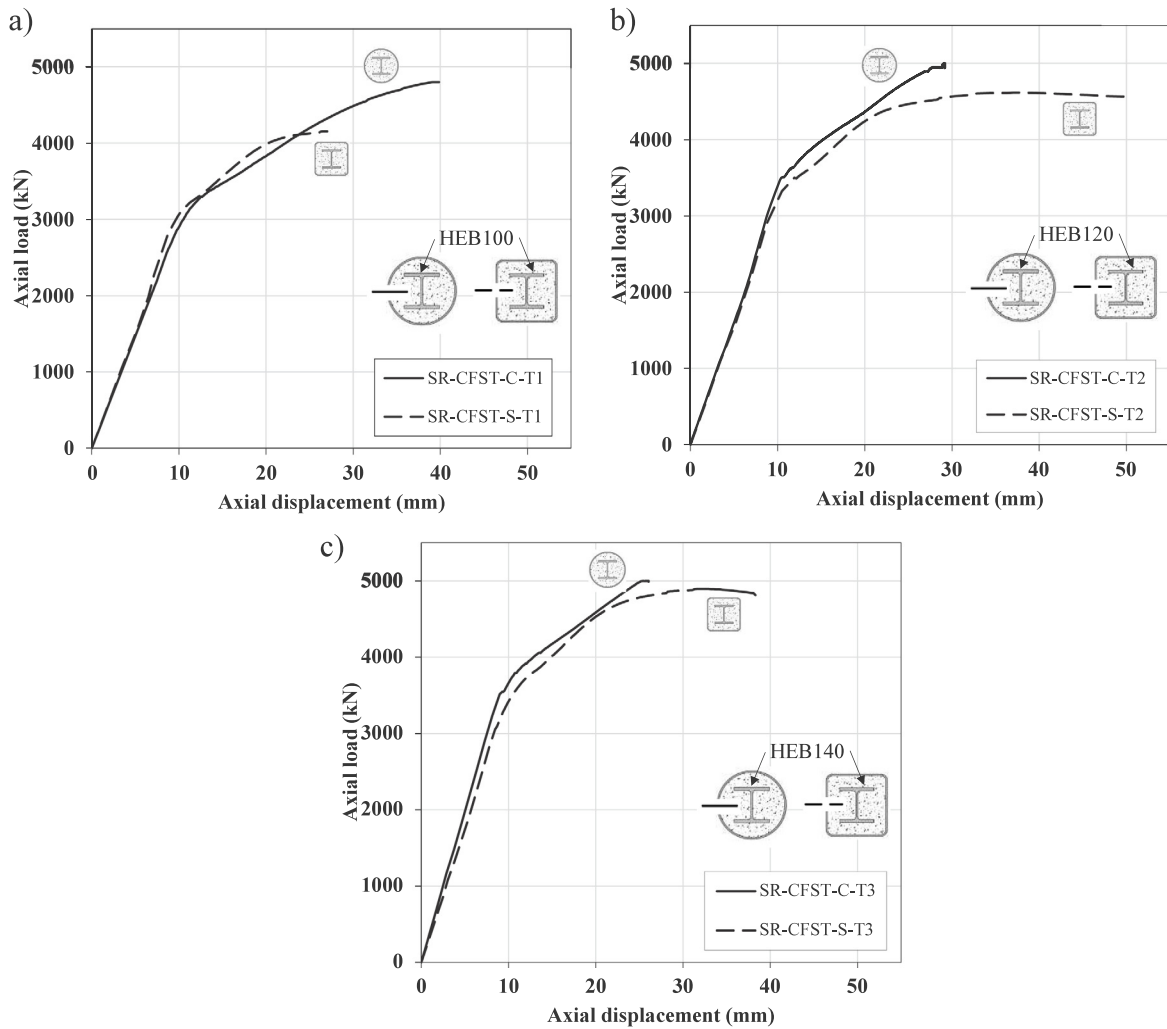
Fig. 16. Axial load–displacement curves for different embedded profiles: (a) HEB100; (b) HEB120; (c) HEB140.

confinement of concrete. For axially loaded members, these factors are given by:

$$\eta_a = 0.25\left(3 + 2\overline{\lambda}\right) \tag{8}$$

$$\eta_c = 4.9 - 18.5\overline{\lambda} + 17\overline{\lambda}^2 \tag{9}$$

Note that Eurocode 4 Part 1–1 uses in these equations the design value for the yield strength of steel and for the concrete compressive strength, which in this investigation have been replaced for the actual values of the ultimate strength of steel and the actual concrete cylinder compressive strength derived from the material tests and reported in Table 1, as the aim is to obtain the ultimate capacity of the columns.

The calculated values for $N_{u,0}$ are presented in Table 2, together with the experimental values for the $N_{post,exp}$, which are shown again for comparison purposes.

For all of the tested columns, the values of the *RSI* are calculated as given in Eq. (5) and summarized in Table 2. For the circular SR-CFST columns, account for the confinement has been made. Note that for columns SR-CFST-C-T2 and SR-CFST-C-T3, the values of the *RSI* in Table 2 appear marked with * since they have been calculated assuming a $N_{post,exp}$ of 5000 kN, but the real values for those *RSI* would be slightly higher.

Fig. 17 illustrates the *RSI* values for both series. Generally, the *RSI* has the same order of magnitude for both circular and square columns, all of them around 0.55–0.60. The fact that the loss of capacity is similar for both shapes, implies that confinement, which

Table 2
Post-fire test results and RSI.

	Specimen	$N_{u,0}$ (kN)	$N_{post,exp}$ (kN)	*RSI*
	SR-CFST-C-T1	8774	4799	0.547
	SR-CFST-C-T2	9016	>5000	0.554*
	SR-CFST-C-T3	9331	>5000	0.536*
	SR-CFST-S-T1	7547	4153	0.550
	SR-CFST-S-T2	7856	4615	0.587
	SR-CFST-S-T3	8245	4896	0.594

has been considered for the calculation of $N_{u,0}$ in circular columns, is still active at the post-fire situation. For the square SR-CFST columns, the difference between the *RSI* values of all of the tested columns is not very important (7.4% and 1.2% with respect to the lowest value of 0.55 corresponding to SR-CFST-S-T1). This can be due to the fact that the higher degradation of the larger inner steel profiles (less concrete cover to protect them from fire) compensates somehow with the greater cross-sectional area of the profile, thus leading to values of *RSI* quite similar for all of the tested specimens.

Note that the results analysed and the conclusions that may be drawn from them are valid for a heating time of 240 min to the t-T curve applied during these experiments. Further tests and the subsequent analyses should be conducted to evaluate the post-heating response and *RSI* under different fire models and heating times.
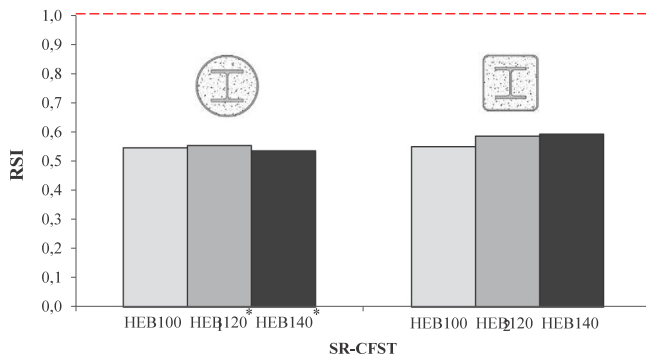
Fig. 17. Residual Strength Index (*RSI*).

4. Evaluation of the current design guidelines

In this section, an attempt to evaluate the residual load-bearing capacity of SR-CFST columns by means of the currently available design guidelines and considering the residual capacity of the materials after fire exposure is presented. For the residual factors of the materials, different proposals found in the literature are assessed.

At present, Eurocode 4 Part 1–2 [20] does not include any design recommendations to calculate the residual plastic resistance to compression of steel–concrete composite columns after being exposed to high temperatures. Therefore, in the absence of an established formula to do so, the expressions available in Clause 6.7.3.2 of Eurocode 4 Part 1–1 [19] for room temperature design will be used to evaluate the residual plastic resistance of SR-CFST columns, adapted to post-fire conditions by utilizing the residual material properties after fire exposure. Again, account for the inner steel profile will be done by adding its contribution in the summation of components in the post-fire situation, as already done for the room temperature evaluation of the plastic resistance of the composite cross-section [2]. Depending on the geometry of the sections (circular or square), effect of confinement will or will not be included in the calculations, which will be discussed at the end of this section.

Thus, following the same approach as Section 3.5 for the room temperature plastic resistance to compression of the cross-sections, Eqs. (6) and (7) will be adapted to post-fire conditions for evaluating the residual capacity of square and circular specimens.

Regarding the material properties, even though Eurocode 4 Part 1–2 [20] includes a formula in its Annex C to calculate the residual strength of concrete after fire exposure — available also in the last draft version of Eurocode 2 Part 1–2 (pr EN1992-1-2:2021-09) [21] —, there is still a lack of guidance regarding this matter for structural steel in the design codes.

Therefore, efforts have been made by several researchers to quantify the properties of structural steel after being affected by fire conditions. The different formulae available in the literature are assessed to test their level of accuracy in the prediction of the residual capacity of SR-CFST columns in contrast to the experimental results obtained in the present investigation.

The British Standard 5950-8:2003 [22] in its Annex B "re-use of steel after a fire", Clause B.2.1, states that the mechanical properties of structural steels are not significantly affected until they reach temperatures higher than 600 °C. For micro-alloyed steels of grade S355 in particular, the British code states that it can be assumed that at least 75% of the strength is regained on cooling from temperatures above 600 °C.

In turn, Tao et al. [23] proposed a series of formulae to calculate the residual strength of both structural and reinforcing steel based on a statistical analysis of data from the literature. More recently, Molkens et al. [24] reviewed the post-fire tests for structural steel

available in the literature (718 tests in total). After the corresponding statistical analysis, these authors recommended a set of residual factors for normal, high-strength and very high-strength steel after exposure to elevated temperatures, which generally showed a sharp drop in the mechanical properties around 500–600 °C.

Finally, as part of the overarching project that encompasses this investigation, the post-fire residual strength of structural steel was also investigated [17]. In particular, coupons from different steel hollow sections were tested, obtaining the corresponding post-fire residual factors for varying temperatures, ranging from 20 to 1000 °C.

For the calculation of the residual plastic resistance, the cross-section discretization scheme presented in Fig. 18 is followed, with a clear differentiation of the three components of the section. The key parameter in this calculation is the maximum temperature reached by each material. For that reason, the embedded steel profile has been divided into two parts: flanges (more exposed to the heat source) and web (protected by the surrounding concrete). Also, given the non-uniform temperature field obtained in the concrete core when exposed to high temperatures, it has been divided in four concentric rings or layers as shown in Fig. 18. A representative temperature is assigned to each component or division of the cross-section. The values for these representative temperatures are the maximum values measured during the experiments presented in Section 3.2. The steel outer tube is assigned a temperature (θ_a) which ranges between 920 and 970 °C, depending on the experimental test. The temperatures for the flanges (θ_f) and the web (θ_w) of the inner steel profile range between 700 and 800 °C. For the concrete core, each ring or layer has its own representative temperature ($\theta_{c,i}$), which is associated to the peak temperature of the corresponding thermocouple (see Fig. 18).

Therefore, the plastic resistance to compression of the SR-CFST cross-sections after exposed to high temperatures will be obtained as follows:

Square sections (no confinement considered):

$$N_{u,post} = A_a f_{uo,post}(\theta_{a,max}) + \sum_{i=1}^{4} A_{c,i} f_{c,post}(\theta_{c,i,max})$$
$$+ A_w f_{ui,post}(\theta_{w,max}) + A_f f_{ui,post}(\theta_{f,max}) \qquad (10)$$

where $A_{c,i}$ is the cross-sectional area of the $-i$ concrete ring or layer; $f_{c,post}$ is the ultimate concrete compressive strength affected by the corresponding residual factor for a maximum temperature $\theta_{c,i,max}$; A_w and A_f are the cross-sectional areas of the web and the flanges of the embedded steel profile; and $f_{uo,post}$ and $f_{ui,post}$ are the ultimate strength of the outer steel tube and the embedded steel profile affected by the corresponding residual factors for the maximum temperatures $\theta_{a,max}$, $\theta_{f,max}$ and $\theta_{w,max}$ respectively.

Circular sections (confinement effect included):

$$N_{u,post} = \eta_a A_a f_{uo,post}(\theta_{a,max})$$
$$+ \sum_{i=1}^{4} A_{c,i} f_{c,post}(\theta_{c,i,max}) \left(1 + \eta_c \frac{t}{D} \frac{f_{uo,post}(\theta_{a,max})}{f_{c,post}} \right)$$
$$+ A_w f_{ui,post}(\theta_{w,max}) + A_f f_{ui,post}(\theta_{f,max}) \qquad (11)$$

where the average compressive strength of the concrete core after fire exposure to account for the confinement effect in the post-fire situation can be represented as:

$$\overline{f_{c,post}} = \frac{\sum_{i=1}^{4} A_{c,i} f_{c,post}(\theta_{c,i,max})}{A_c} \qquad (12)$$

By applying the procedure explained above, the residual axial capacity of the six tested specimens is calculated and compared against the experimental values. The formula provided in Annex C of Eurocode 4 Part 1–2 [20] will be used to obtain the residual compressive strength of concrete after heating and cooling back to ambient temperature. In turn, for the steel parts (i.e. outer steel tube and embedded profile),
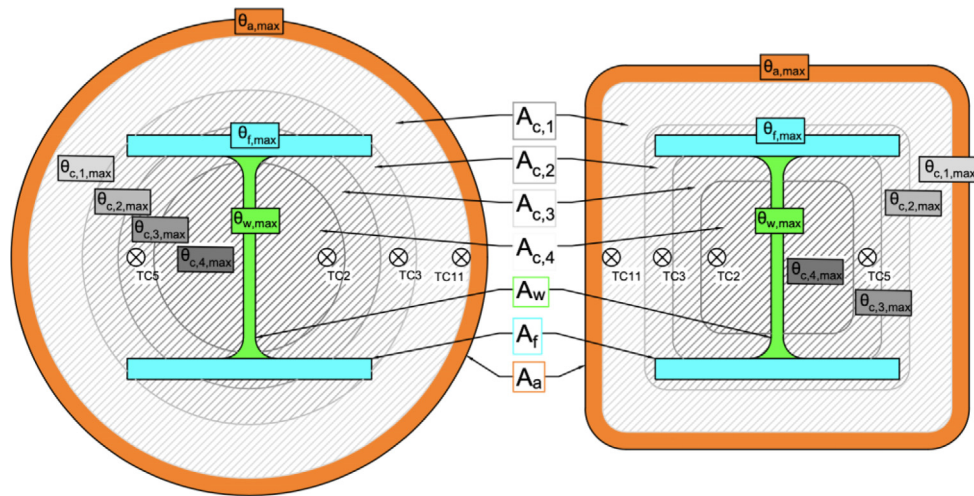
Fig. 18. Zones division of the cross-section.

Table 3
Post-fire residual plastic resistance for the SR-CFST columns calculated under different approaches for evaluating the residual factors.

	Specimen	$N_{post,exp}$ (kN)	$N_{calc,1}$ (kN)	$N_{calc,2}$ (kN)	$N_{calc,3}$ (kN)	$N_{calc,4}$ (kN)
	SR-CFST-C-T1	4799	5785,9	6724,9	5118,1	4821,3
	SR-CFST-C-T2	>5000*	6077,3	7054,5	5446,3	5163,4
	SR-CFST-C-T3	>5000*	6447,0	7422,0	5632,4	5383,1
	SR-CFST-S-T1	4153	5255.6	6202.1	4639.3	4368.2
	SR-CFST-S-T2	4615	5530.0	6483.9	4837.3	4556.4
	SR-CFST-S-T3	4896	5902.8	6831.2	4951.4	4726.9

Note: 1, British Standard [22]; 2, Tao et al. [23]; 3, Molkens et al. [24]; and 4, Pons et al. [17].

Table 4
$N_{post,exp}/N_{calc,j}$ for the different approaches compared.

	Specimen	$\dfrac{N_{post,exp}}{N_{calc,1}}$	$\dfrac{N_{post,exp}}{N_{calc,2}}$	$\dfrac{N_{post,exp}}{N_{calc,3}}$	$\dfrac{N_{post,exp}}{N_{calc,4}}$
	SR-CFST-C-T1	0.83	0.71	0.94	1.00
	SR-CFST-C-T2	0.82*	0.71*	0.92*	0.97*
	SR-CFST-C-T3	0.78*	0.67*	0.89*	0.93*
	SR-CFST-S-T1	0.79	0.67	0.90	0.95
	SR-CFST-S-T2	0.83	0.71	0.95	1.01
	SR-CFST-S-T3	0.83	0.72	0.99	1.04
	Mean	**0.82**	**0.70**	**0.94**	**1.00**
	SD	**0.02**	**0.02**	**0.04**	**0.04**

the four different approaches presented in this section (formulae and residual factors proposed by different authors) are assessed.

Therefore, in Table 3, the different calculated values for the post-fire residual plastic resistance of the tested columns are presented ($N_{calc,j}$), where the numbers at the subscripts j correspond to: 1, British Standard [22]; 2, Tao et al. [23]; 3, Molkens et al. [24]; and 4, Pons et al. [17]. Column $N_{post,exp}$ in Table 3 displays the values of the experimental capacity of the specimens after fire exposure (taken from Section 3.4), which is used as a reference for the assessment of the different approaches.

In Table 4, the calculated values are compared with the experimental results using the relation $N_{post,exp}/N_{calc,j}$. Note that a value greater than one for the error indicates a conservative prediction, while a value lower than one stands for a no conservative prediction. The mean error and the standard deviation (SD) obtained for each approach are also summarized in Table 4. Note that, once more, the values of columns SR-CFST-C-T2 and SR-CFST-C-T3 appear marked with * in Table 4 since they have been calculated assuming a $N_{post,exp}$ of 5000 kN. These values have also been neglected in the calculation of the mean and SD of the prediction errors.

Although all of the studied proposals only consider a significant reduction of the steel mechanical properties after being exposed to temperatures higher than 500–600 °C, some differences can be found in their predictions. It can be seen that both the British Standard [22] approach ($N_{post,exp}/N_{calc,1}$) and the residual factors proposed by Tao et al. [23] ($N_{post,exp}/N_{calc,2}$) greatly overestimate the residual plastic resistance (average error well below 1), being the second one the least accurate of all of the studied approaches with a mean error of 0.70 (30% overestimation). In turn, the set of residual factors proposed by Molkens et al. [24] provides a better agreement between the experimental and the theoretical values ($N_{post,exp}/N_{calc,3}$) with a mean

error of 0.94. The comparison shows that the set of residual factors proposed by Pons et al. [17] ($N_{post,exp}/N_{calc,4}$) gives the most accurate predictions, with an average value of the prediction error equal to 1.00 and a reduced scatter (standard deviation 0.04). This proposal assumes in fact a more accurate and progressive loss of capacity of steel, in contrast with other approaches that basically discriminate between temperatures above or below 500–600 °C. Therefore, the set of residual factors proposed by Pons et al. [17] is recommended to be used in combination with Eq. (11) for the calculation of the post-fire residual compression resistance of SR-CFST columns. It should be noted that the proposal described in this section it is just a preliminary approach developed with a very limited number of experiments. Given the reduced number of experimental results, the conclusions of this analysis cannot be considered to be definitive. For the development and validation of a solid proposal, more data will be needed, from both experiments and validated numerical models able to capture the response of the columns. Therefore, the predictions should then be taken with caution.

It should also be highlighted that the calculated values for the circular specimens include the effect of confinement, which has been considered in the contribution of the concrete part to the cross-sectional capacity as given in Eq. (11). If confinement would have been neglected for the circular specimens, the results would arise very low predictions of the ultimate load: as an example, for column specimen SR-CFST-C-T1 the predicted value would be 3743.4 kN with the proposed set of residual factors from Pons et al. [17] (leading to a 28% error). This result seems to confirm that confinement is still active at the post-fire situation and contributes to increase the ultimate load of the circular columns to a certain extent, conclusion which should be further confirmed by means of a deeper study through parametric studies.

5. Summary and conclusions

In this experimental investigation, the residual axial compression capacity of stub SR-CFST columns in a post-fire situation has been studied. For that purpose, a series of six SR-CFST specimens were tested, three of them with circular section and another three with square section. For comparison purposes, the circular and square steel tubes were selected so that the amount of steel used at the outer tube was similar (with a maximum difference of a 2.51%). In order to reproduce the situation of a post-fire event, the columns were in a first stage uniformly heated inside an electric furnace and, after cooling down to ambient, they were tested to failure in a vertical frame by applying an increasing axial load. The evolution of the temperatures at the relevant points of the cross-section was registered during the thermal tests by means of an arrangement of thermocouples, while the axial load versus displacement histories and strain measurements at the outer steel tube surface were captured during the loading tests, which were analysed to understand the stress development and the failure patterns at the post-fire situation. The analysis of the experimental results allowed reaching some relevant conclusions on the post-fire behaviour of SR-CFST columns:

• Temperatures registered during the heating tests were generally higher for the square SR-CFST sections than for their circular counterparts, which are attributed to the higher section factor of square columns. This causes a faster degradation of the square columns, leading to lower ultimate loads after fire exposure.

• For the same external dimensions, specimens with a larger embedded steel profile experienced a higher temperature rise at the inner parts of the section, as the amount of concrete cover protecting the steel profile from the heat source is lower. However, this effect compensates with the higher dimensions of the inner profile and thus higher axial capacity.

• The SR-CFST stub columns showed a high ductility after heating, with the circular specimens reaching higher peak loads than their square counterparts. For each series, the peak load at post-fire increased with the size of the embedded steel profile.

• The evaluation of the *RSI* showed that the loss of capacity after fire was similar for circular and square SR-CFST columns, and that the influence of the size of the embedded steel profile was not significant in the rate of capacity loss. This analysis also pointed out that, for circular columns, confinement may still be active at the post-fire situation, contributing to increase their ultimate load.

The currently available design rules were revised, finding that there is still a lack on guidance regarding the post-fire evaluation of steel–concrete composite columns and in particular for SR-CFST sections. In the absence of a method to do so, the equations for evaluating the axial capacity of CFST sections at room temperature in Eurocode 4 Part 1–1 were adapted to account for the residual capacity of the materials after fire exposure. Different proposals found in the literature for the residual factors of steel and concrete after fire exposure were assessed, being the proposal from Pons et al. [17] the one that aroused the best predictions. The results of this comparison seemed also to confirm that confinement is still active at the post-fire situation in the circular SR-CFST sections and therefore its effect should be accounted for in the evaluation of its residual capacity after fire exposure. The proposed post-fire design equations and residual factors showed a good agreement with the experimental results, although given the limited number of available tests, further parametric studies should be conducted in order to strengthen these conclusions.

CRediT authorship contribution statement

D. Medall: Writing – original draft, Methodology, Investigation, Formal analysis, Conceptualization. **C. Ibáñez:** Writing – original draft, Methodology, Investigation, Formal analysis, Conceptualization. **V. Albero:** Methodology, Investigation, Conceptualization. **A. Espinós:** Writing – original draft, Project administration, Methodology, Investigation, Funding acquisition, Conceptualization. **M.L. Romero:** Supervision, Project administration, Investigation, Funding acquisition, Conceptualization.

Declaration of competing interest

The authors declare the following financial interests/personal relationships which may be considered as potential competing interests: Ana Espinos reports financial support was provided by Agencia Estatal de Investgación. David Medall reports financial support was provided by Agencia Estatal de Investgación.

Data availability

Data will be made available on request.

References

[1] M.L. Romero, A. Espinós, C. Renaud, G. Bihina, P. Schaumann, I. Kleiboemer, Fire Resistance of Innovative and Slender Concrete Filled Tubular Composite Columns (FRISCC). Final Report. Catalogue Number KI-NA-28082-EN-N, RFCS Publications, Brussels, 2016.

[2] J. Liew, M. Xiong, Design Guide for Concrete Filled Tubular Members with High Strength Materials To Eurocode 4, Research Publishing, Singapur, 2015.

[3] D. Medall, A. Espinós, V. Albero, M.L. Romero, Simplified proposal for the temperature field of steel-reinforced CFST columns exposed to fire, Eng. Struct. 273 (2022) 115083, http://dx.doi.org/10.1016/J.ENGSTRUCT.2022.115083.

[4] Dotreppe J. Claude, Chu T. Binh, R. Eng, Franssen J. Marc, Steel hollow columns filled with self-compacting concrete under fire conditions, 2010.

[5] F.-Q. Meng, M.-C. Zhu, G.C. Clifton, K.U. Ukanwa, JBP Lim, Performance of square steel-reinforced concrete-filled steel tubular columns subject to non-uniform fire, J. Constr. Steel Res. 166 (2020) http://dx.doi.org/10.1016/j.jcsr.2019.105909.

[6] Meng Fan-Qin, Zhu Mei-Chun, G. Charles Clifton, Kingsley U. Ukanwa, James B.P. Lim, Fire performance of edge and interior circular steel-reinforced concrete-filled steel tubular stub columns, Steel Compos. Struct. 41 (2021) 115–122.

[7] W.J. Mao, W. da Wang, K. Zhou, E.F. Du, Experimental study on steel-reinforced concrete-filled steel tubular columns under the fire, J. Constr. Steel Res. 185 (2021) 106867, http://dx.doi.org/10.1016/J.JCSR.2021.106867.

[8] F. Meng, M.-C. Zhu, B. Mou, B. He, Residual strength of steel-reinforced concrete-filled square steel tubular (SRCFST) stub columns after exposure to ISO-834 standard fire, Int. J. Steel Struct. 19 (2019) 850–866, http://dx.doi.org/10.1007/s13296-018-0174-z.

[9] X. Yang, C. Tang, Y. Chen, T.-Y. Qiao, Compressive behavior of steel-reinforced concrete-filled square steel tubular stub columns after exposure to elevated temperature, Eng. Struct. 204 (2020) 110048, http://dx.doi.org/10.1016/j.engstruct.2019.110048.

[10] EN 10219-1:2007, Cold formed welded structural hollow sections of non-alloy and fine grain steels - part 1: Technical delivery conditions, 2007.

[11] EN 10025-1:2006, Hot rolled products of structural steels - part 1: General technical delivery conditions, 2006.

[12] CEN. EN. 1992-1-1, Eurocode 2: Design of Concrete Structures, Part 1.1: General Rules and Rules for Buildings, Comité Européen de Normalisation, Brussels, Belgium, 2004.

[13] K.D. Hertz, Concrete strength for fire safety design, Mag. Concr. Res. 57 (2005) 445–453, http://dx.doi.org/10.1680/macr.2005.57.8.445.

[14] J. Huo, G. Huang, Y. Xiao, Effects of sustained axial load and cooling phase on post-fire behaviour of concrete-filled steel tubular stub columns, J. Constr. Steel. Res. 65 (2009) 1664–1676, http://dx.doi.org/10.1016/j.jcsr.2009.04.022.

[15] F. Liu, L. Gardner, H. Yang, Post-fire behaviour of reinforced concrete stub columns confined by circular steel tubes, J. Constr. Steel. Res. 102 (2014) 82–103, http://dx.doi.org/10.1016/J.JCSR.2014.06.015.

[16] S. Zhang, L. Guo, Z. Ye, Y. Wang, Behavior of steel tube and confined high strength concrete for concrete-filled RHS tubes, Adv. Struct. Eng. 8 (2005) 101–116, http://dx.doi.org/10.1260/1369433054037976.

[17] D. Pons, A. Lapuebla-Ferri, M.L. Romero, Post-fire residual strength and ductility of structural steels from hollow sections, Ce/Papers 5 (2022) 458–466, http://dx.doi.org/10.1002/cepa.1777.

[18] L.H. Han, J.S. Huo, Y.C. Wang, Compressive and flexural behaviour of concrete filled steel tubes after exposure to standard fire, J. Constr. Steel. Res. 61 (2005) 882–901, http://dx.doi.org/10.1016/j.jcsr.2004.12.005.

[19] CEN. EN 1994-1-1, Eurocode 4: Design of Composite Steel and Concrete Structures. Part 1.1: General Rules and Rules for Buildings. Brussels, Comité Européen de Normalisation, Belgium, 2004.

[20] CEN. EN 1994-1-2, Eurocode 4: Design of Composite Steel and Concrete Structures. Part 1.2: General Rules - Structural Fire Design, Comité Européen de Normalisation, Brussels, Belgium, 2005.

[21] CEN/TC250/SC2 N1897, Stable version pren 1992-1-2:2021-09. Eurocode 2: Design of concrete structures - part 1-2: General rules - structural fire design, 2021.

[22] British Standards Institution (BSI), BS 5950-8:2003 structural use of steelwork in building. British standards, 2003, p. 8.

[23] Z. Tao, X.-Q. Wang, B. Uy, Stress-strain curves of structural and reinforcing steels after exposure to elevated temperatures, J. Mater. Civ. Eng. 25 (2013) 1306–1316, http://dx.doi.org/10.1061/(ASCE)MT.1943-5533.0000676.

[24] T. Molkens, K.A. Cashell, B. Rossi, Post-fire mechanical properties of carbon steel and safety factors for the reinstatement of steel structures, Eng. Struct. 234 (2021) 111975, http://dx.doi.org/10.1016/J.ENGSTRUCT.2021.111975.

ANNEX I. COMPENDIUM OF PUBLICATIONS

ARTICLE 3

Thermo-mechanical compression tests on steel-reinforced concrete-filled steel tubular stub columns with high performance materials

David Medall, Carmen Ibáñez*, Ana Espinós and Manuel L. Romero

ICITECH, Universitat Politècnica de València, Valencia, Spain

Abstract.   Cost-effective solutions provided by composite construction are gaining popularity which, in turn, promotes the appearance on the market of new types of composite sections that allow not only to take advantage of the synergy of steel and concrete working together at room temperature, but also to improve their behaviour at high temperatures. When combined with high performance materials, significant load-bearing capacities can be achieved even with reduced cross-sectional dimensions. Steel-reinforced concrete-filled steel tubular (SR-CFST) columns are one of these innovative composite sections, where an open steel profile is embedded into a CFST section. Besides the renowned benefits of these typologies at room temperature, the fire protection offered by the surrounding concrete to the inner steel profile, gives them an enhanced fire performance which delays its loss of mechanical capacity in a fire scenario. The experimental evidence on the fire behaviour of SR-CFST columns is still scarce, particularly when combined with high performance materials. However, it is being much needed for the development of specific design provisions that consider the use of the inner steel profile in CFST columns. In this work, a new experimental program on the thermo-mechanical behaviour of SR-CFST columns is presented to extend the available experimental database. Ten SR-CFST stub columns, with circular and square geometries, combining high strength steel and concrete were tested. It was seen that the circular specimens reached higher failure times than the square columns, with the failure time increasing both when high strength steel was used at the embedded steel profile and high strength concrete was used as infill. Finally, different proposals for the reduction coefficients of high performance materials were assessed in the prediction of the cross-sectional fire resistance of the SR-CFST columns.

Keywords: concrete-filled steel tubular columns; embedded steel profile; fire reduction factors; fire resistance; high strength concrete; high strength steel

1. Introduction

The use of high performance materials (i.e., high strength steel and high strength concrete) in composite sections allows to achieve a significant load bearing capacity with reduced cross-sectional dimensions. Given the increased popularity of composite construction all over the word, technological developments in this field are constant and are allowing the appearance of new types of composite sections. With these innovative sections, the benefits of steel and concrete working together are still exploited but, at the same time, improvements are made in other aspects. This is the case of the so-called steel-reinforced concrete-filled steel tubular (SR-CFST) columns, where an open steel profile is embedded into a CFST section. Apart from the well-known advantages of these typologies at room temperature, they show an enhanced fire performance due to the inherent fire protection offered by the surrounding concrete to the inner steel profile, which delays its loss of mechanical capacity at elevated temperatures (Espinós *et al.* 2016). Hence, combined with high performance materials, the column may resist the applied load for an extended fire exposure time.

In light of the review of the experimental programmes published in the literature, it can be seen that the number of available fire test results on SR-CFST columns is still limited. One of the first works published on SR-CFST columns exposed to fire conditions were the tests performed at the University of Liège by Dotreppe *et al.* (2010). Using self-compacting concrete as infill, the fire resistance of ten slender composite columns was tested. Circular and square shapes for the outer steel tube were combined. Only four of the ten sections were SR-CFST (with an embedded HEB120 steel profile). For a load level of 0.4 and a maximum external dimension of 219.1 mm, the fire resistance times ranged from 39 up to 79 min thanks to the application of intumescent paint in some specimens.

The experiments carried out in Shanghai (Meng *et al.* 2020, 2021) revealed that the inner steel profile considerably enhanced the fire behaviour of the specimens, exceeding 240 min in some cases. The fire resistance of eight SR-CFST columns was tested considering the effect of non-uniform heating in both square and circular geometries. The SR-CFST columns had an embedded HW150 × 150 and a length of 1800 mm although only the central 1200 mm were heated.

More recently, and particularly on SR-CFST columns with a cruciform steel section embedded in the concrete, experiments were conducted at Southeast University (Mao

---

*Corresponding author, Lecturer
 E-mail: caribus@upv.es

et al. 2021, 2022, 2023). In those experiments the columns were tested subjected to uniform and non-uniform heating and with and without fire protection. Once again, circular and square specimens were tested under the ISO-834 standard fire curve and different load ratios. Although high performance materials were not used, it was found that the fire resistance of SR-CFST columns had substantial improvement compared with CFST columns.

The lack of experiments on SR-CFST columns with innovative materials at elevated temperatures was also pointed out by Tan *et al.* (2019a, 2019b) in their works on SR-CFST columns with stainless steel. The authors focused their research on the FE analysis of these columns but the validation of the models was accomplished by parts using experiments on CFST columns with stainless steel since there are not available test data in the published literature that can be used to that end.

With the aim of extending the available experimental data, and based on the conclusions from previous research, this work presents a series of thermo-mechanical tests performed on stub SR-CFST columns. New features, which have not been investigated in the previous experimental campaigns, such as the use of high strength steel (with yield strength over 460 MPa) for the embedded profile and high strength concrete (with cylinder compressive strength over 50 MPa) as infill are covered here to ease the understanding of the performance of these columns in a fire situation. The history of sectional temperatures is analysed as well as the response in terms of axial load–displacement. In total ten SR-CFST stub columns with high performance materials are tested, four circular and six square sections. The tests results are analysed and the influence of the high performance materials in the failure times of the columns under fire are evaluated by means of the High Performance Ratio. Finally, the suitable reduction factors for the materials are assessed with a proposed design equation for the evaluation of the load bearing capacity of SR-CFST stub columns at elevated temperatures.

2. Experimental program

2.1 Definition of tests specimens

Within the framework of this research, in total 12 stub columns were tested under compression at elevated temperatures, combining circular and square shapes. Two of the columns were a circular and square hollow tubes which served as reference and ten were SR-CFST specimens grouped into two series comprising circular and square geometries respectively (see Fig. 1).

The cross-sectional properties of all tested specimens and more data related to each series are summarized in Table 1. For clarity, the test specimens were named as follows: SR-CFST-**X-TMi** (i.e., SR-CFST-C-TM1), where **X** stands for the cross-sectional shape of the outer steel tube (**C** for circular and **S** for square), **TM** stands for "Thermo-Mechanical" and **i** represents the number of test, each of them with a different combination of grades for the embedded steel profile and the concrete infill. For the

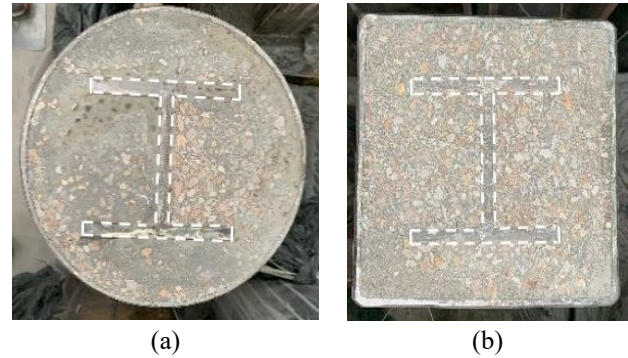(a)   (b)

Fig. 1 SR-CFST shapes tested: (a) circular; (b) square

hollow steel tube tests, designation CHS and SHS followed by the label TM0 indicative of a reference case was used

For the circular columns, $\phi 273 \times 6.3$ mm hollow steel tubes were used for all the specimens, from C-TM0 to C-TM4. For the square specimens, S-TM0 to S-TM4, the selected hollow steel tubes were #220 × 6.3 mm, in an intend that the steel usage of the two groups of circular and square specimens was very similar, with a difference of only 0.57% in terms of outer steel tube area. Normal and high strength steel for the embedded profile and also normal and high strength concrete for the infill were combined. As an addition to the square series, specimens S-TM5 and S-TM6 in particular had a #250 × 10 mm hollow tube made of high strength steel. The results from these last two test specimens will serve to assess the effect of increasing both the thickness and the strength of the outer steel tube. For the embedded steel profiles, HEB140 sections were used in all the cases, with dimensions $h=b=140$ mm ($t_f=12$ mm, $t_w=7$ mm). All the columns had a length of 600 mm.

2.2 Material properties

Steel

In this experimental program, cold-formed hollow steel tubes with grade S355 were used for specimens TM0 to TM4. For square specimens TM5 and TM6, hot-rolled quenched and tempered hollow steel tubes with steel grade S770 were used. Regarding the embedded steel profiles, in five of the SR-CFST columns hot-rolled sections with steel grade S275 were used, while for the other five SR-CFST columns, the inner profiles were fabricated from welded high strength steel plates of grade S700MC. For all the hollow steel tubes and embedded steel profiles, the actual values of the yield strength (f_{yo} and f_{yi}, respectively) and the ultimate strength (f_{uo} and f_{ui}, respectively) were determined through the corresponding coupon tests (three coupons per sample), the average measured value being shown in Table 1.

Concrete

Normal and high strength concrete mixes of 30 and 90 MPa characteristic cylinder compressive strength, respectively, were prepared in a planetary mixer and cured in standard conditions for 28 days at the laboratories of the Concrete Science and Technology Institute (ICITECH), Universitat Politècnica de València, using the experience

Table 1 Details of the tested specimens

Specimen	D or B (mm)	t_o (mm)	f_{yo} (MPa)	f_{uo} (MPa)	f_{yi} (MPa)	f_{ui} (MPa)	f_c (MPa)	Moisture (%)	μ (%)	N_{exp} (kN)	FT (min)
CHS-TM0	273	6.3	413.33	483.28	-	-	-		40	1020.7	63
SR-CFST-C-TM1	273	6.3	413.33	483.28	315	441	29.73	6.28	40	2812.3	267
SR-CFST-C-TM2	273	6.3	413.33	483.28	777.2	853.68	29.73	6.28	40	3488.9	405
SR-CFST-C-TM3	273	6.3	413.33	483.28	315	441	86.16	2.11	40	3936.8	317
SR-CFST-C-TM4	273	6.3	413.33	483.28	777.2	853.68	86.16	2.11	40	4624.3	383
SHS-TM0	220	6.3	495.84	549.65	-	-	-		40	1154.3	43
SR-CFST-S-TM1	220	6.3	495.84	549.65	315	441	29.73	6.28	40	2377.4	239
SR-CFST-S-TM2	220	6.3	495.84	549.65	777.2	853.68	29.73	6.28	40	3097.9	308
SR-CFST-S-TM3	220	6.3	495.84	549.65	315	441	86.16	2.11	40	3306.5	285
SR-CFST-S-TM4	220	6.3	495.84	549.65	777.2	853.68	86.16	2.11	40	4027.0	294
SR-CFST-S-TM5	250	10	824	864	315	441	29.73	6.28	30	3406.5	274
SR-CFST-S-TM6	250	10	824	864	777.2	853.68	86.16	2.11	30	4821.7	395

*Note: D and B are the outer diameter or dimension for circular and square sections respectively; t_o is the outer steel tube thickness; f_{yo} and f_{yi} are the yield strength of steel for the outer steel tube and inner embedded section respectively; f_{uo} and f_{ui} are the ultimate strength of steel for the outer steel tube and inner embedded section respectively; f_c is the concrete cylinder compressive strength; μ is the load level; N_{exp} is the applied load; and FT is the failure time.

acquired in precious experimental campaigns with high strength concrete (Pons *et al.* 2018).

Sets of three cylindrical and three cubic samples for each type of concrete mix used for filling the column specimens were also prepared. Before the start of the experimental program, the pertinent uniaxial compression tests were performed in order to obtain the actual concrete compressive strength (f_c), which is given in Table 1. The moisture content values displayed in the same table were obtained for the different concrete batches by following a standard procedure, according to ISO 12570:2000 (ISO 2000). Before drying, the concrete samples obtained from each batch were weighed and afterwards introduced inside a heat chamber for drying at a constant temperature of 105 ºC. After 48 h, the samples were extracted from the chamber and let to cool down until reaching 30-40 ºC (to minimise re-absorption of moisture) and weighed again until the change of mass was less than 0.1% of the total mass. The moisture content mass by mass was then obtained by relating the mass difference of the test specimen before and after drying to the final mass value.

2.3 Specimens preparation

In this experimental campaign, all the columns were prepared and tested at the Concrete Science and Technology Institute (ICITECH), at Universitat Politècnica de València (Spain). At both ends of each specimen, steel plates with dimensions 300 × 300 × 10 mm were placed to ensure that the load application conditions were optimal. The steel plate at the bottom of the embedded steel profile was the first one to be welded (Fig. 2(a)). Before placing the hollow steel tube concentrically with the embedded steel profile, a hole was drilled at the lower part of the steel tube to allow vapour ventilation during heating. This hole was then also used to allow the wires of the thermocouples to pass

through once they were positioned at the cross-section (Fig. 2(b)). Next, the bottom of the hollow steel tube was welded to the steel plate (Fig. 2(c)). Once the column was filled with concrete and it was settled with the help of a needle vibrator, the specimen was covered with a plastic film. Finally, once the top surface was smooth to guarantee planarity and the contact of the steel plate with all the components, the second plate was welded to the top end of the column. Figs. 3-5 show the cross-sections of all the tested specimens.

In Fig. 6 the layout of the set of ten thermocouples positioned at the mid-length of the column is presented. In order to register the complete evolution of the cross-sectional temperatures during the tests, the thermocouples were placed as described next. In the steel components the arrangement was as follows: to the outer steel tube surface, thermocouples number 1 and 6 were welded; and thermocouples number 7, 8, 9 and 10 were welded at different points of the embedded steel profile. At the concrete infill, thermocouples were distributed so that thermocouples number 2, 3 and 4 were placed equidistantly, with a separation of 1/6 of the section width, being thermocouple number 4 in contact with the web of the embedded steel profile. Thermocouple number 5 was also embedded and positioned at 1/4 of the section width.

2.4 Test setup and procedure

For the experiments, a thermo-mechanical testing protocol was designed, where a sustained load was applied to the stub SR-CFST columns, being simultaneously heated inside an electrical furnace. For that purpose, a vertical testing frame equipped with a hydraulic jack of 5000 kN capacity was employed as shown in Fig. 7. The applied load was calculated as a 40% of the theoretical ultimate capacity of the columns at room temperature, using the measured
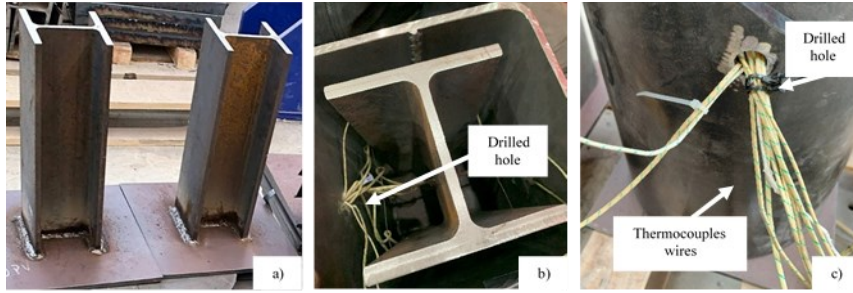
Fig. 2 Columns preparation: a) Steel plate welded at bottom end of the embedded profile; b) Positioning of thermocouples; c) Positioning of hollow steel tube
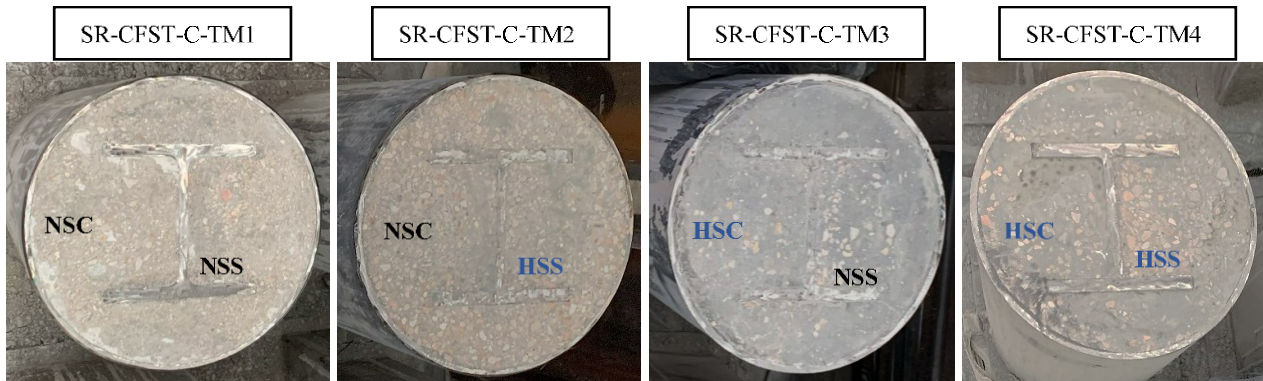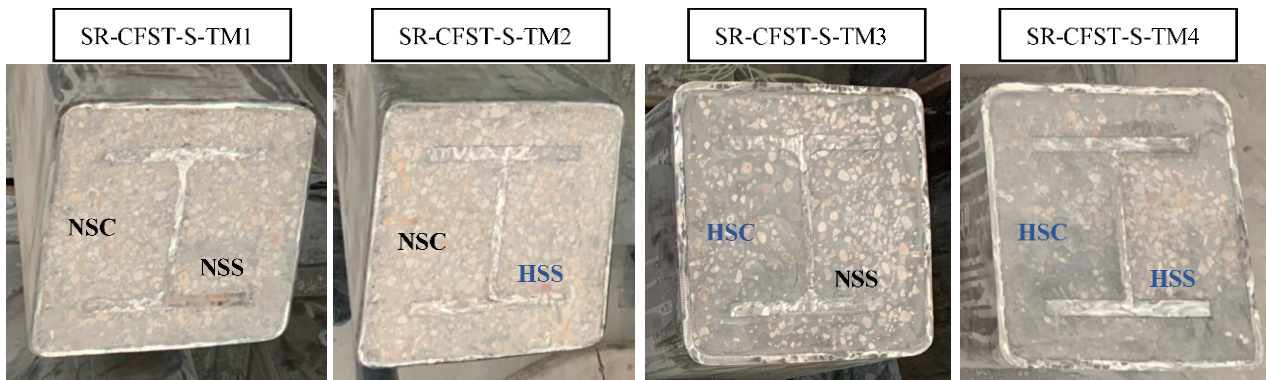

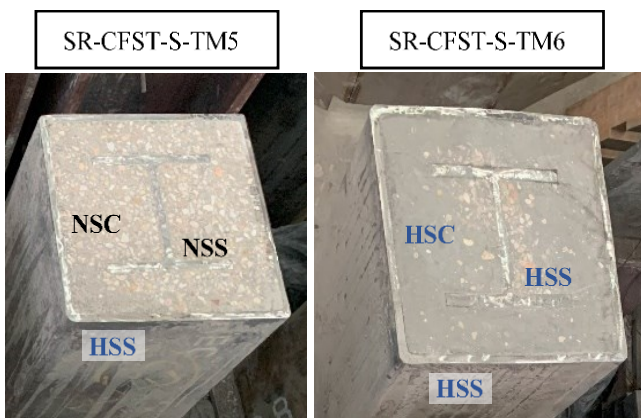Fig. 3 Circular specimens φ273 × 6.3 mm

Fig. 4 Square specimens #220 × 6.3 mm

Fig. 5 Square specimens #250 × 10 mm (Note: NSC and HSC stand for Normal and High Strength Concrete respectively; NSS and HSS stand for Normal and High Strength Steel respectively)

material strengths, except for specimens S-TM5 and S-TM6, which presented a higher ultimate load, and thus a 30% load level was applied to them, in order not to exceed the capacity of the hydraulic jack, see values of load level (μ) and applied load (N_{exp}) in Table 1.

The ultimate capacity of the columns at room temperature necessary to obtain the applied load value was calculated as given in Clause 6.7.3.2 of EN1994-1-1 (CEN 2004) by adding the plastic resistances of the three components of the cross-section (i.e., outer steel tube, concrete infill and inner steel profile).

The load was applied concentrically to the top end of the columns through a spherical bearing, while the bottom end of the columns was attached to the testing rig through a bolted plate. Once the desired load was applied, it was kept constant and the heating of the specimen started, with unrestrained column elongation.
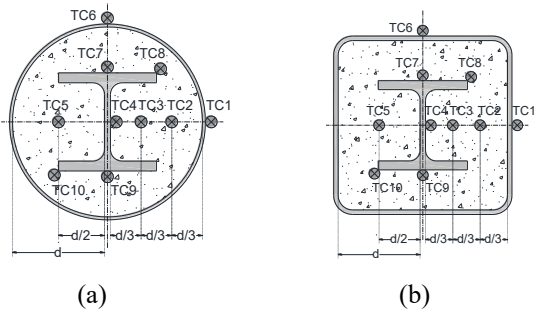
(a)   (b)

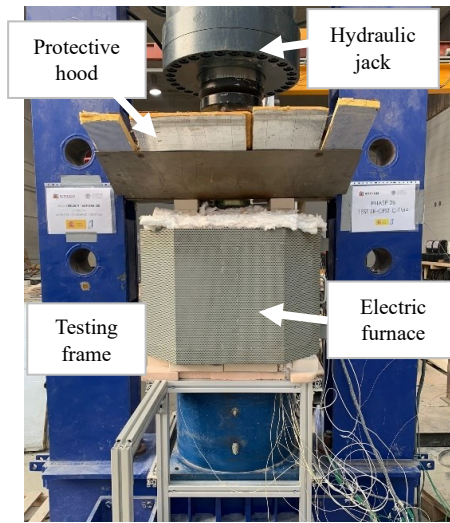Fig. 6 Layout of thermocouples: a) circular sections; b) square sections

Fig. 7 General view of the test setup

For the heating of the column specimens, an *ad-hoc* manufactured electric furnace of 10000 W power was coupled to the testing rig, see Fig. 7. The furnace had an inner diameter of ϕ400 mm, consisting of two semicylinders joined by a hinge. As can be seen in Fig. 8, the electric elements of the refractory wall of each semicylinder were distributed evenly in parallel layers through the whole length for both sides. To guarantee the uniformity of the heating through measurements of the furnace inner temperature, three thermocouples were evenly distributed inside the furnace chamber along its height.

Fibre blanket was used to cover the open cavities at the top and bottom ends of the furnace once the furnace was closed and the specimen was ready for testing, in order to minimise the heat loss. As can be also seen in Fig. 7, a purpose-made protective hood was attached to the top end of the column to prevent the load cell from receiving the convective heat flow. Additionally, the contacting plates at the top end of the column were thermally insulated with layers of fibre blanket to avoid the possible heat conduction towards the load cell.

A transient heating regime was applied in the thermo-mechanical tests, with a non-constant heating rate. The electric furnace power target was set to its maximum according to the manufacturer specifications, although due to its high inertia at the first stages of heating and the massive size of the tested stub column specimens, the
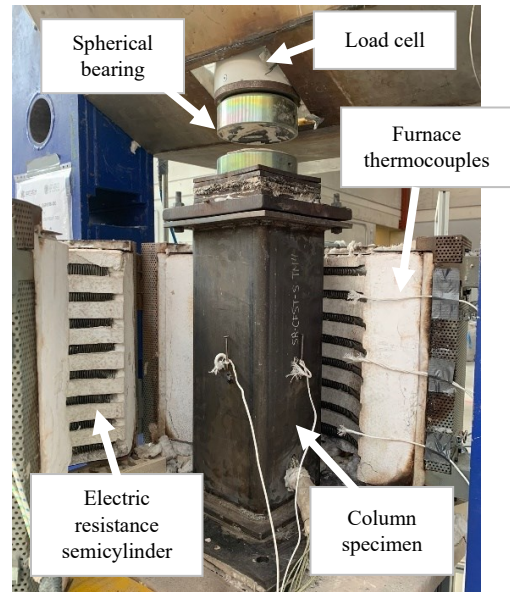

Fig. 8 Specimen prepared for testing inside the electric furnace
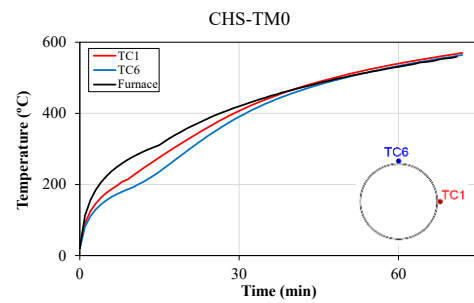
(a)
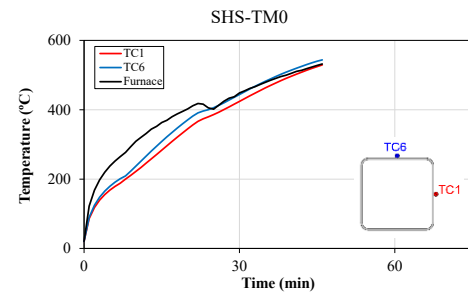
(b)

Fig. 9 Cross-sectional temperatures for hollow specimens CHS-TM0 (a) and SHS-TM0 (b)

standard ISO-834 temperature-time curve was not followed in the tests. This fact justifies that all the comparisons and discussion of results presented in this work refers to "failure times", rather than "standard fire resistance times".

3. Analysis of test results

3.1 Cross-sectional temperatures

In Figs. 9-11 the evolution of the cross-sectional

Fig. 10 Cross-sectional temperatures for specimens TM1-TM4; a) circular sections; b) square sections

temperatures is shown for the tested columns but, for the sake of clarity only the data of five of the thermocouples are displayed together with the evolution of the furnace temperature.

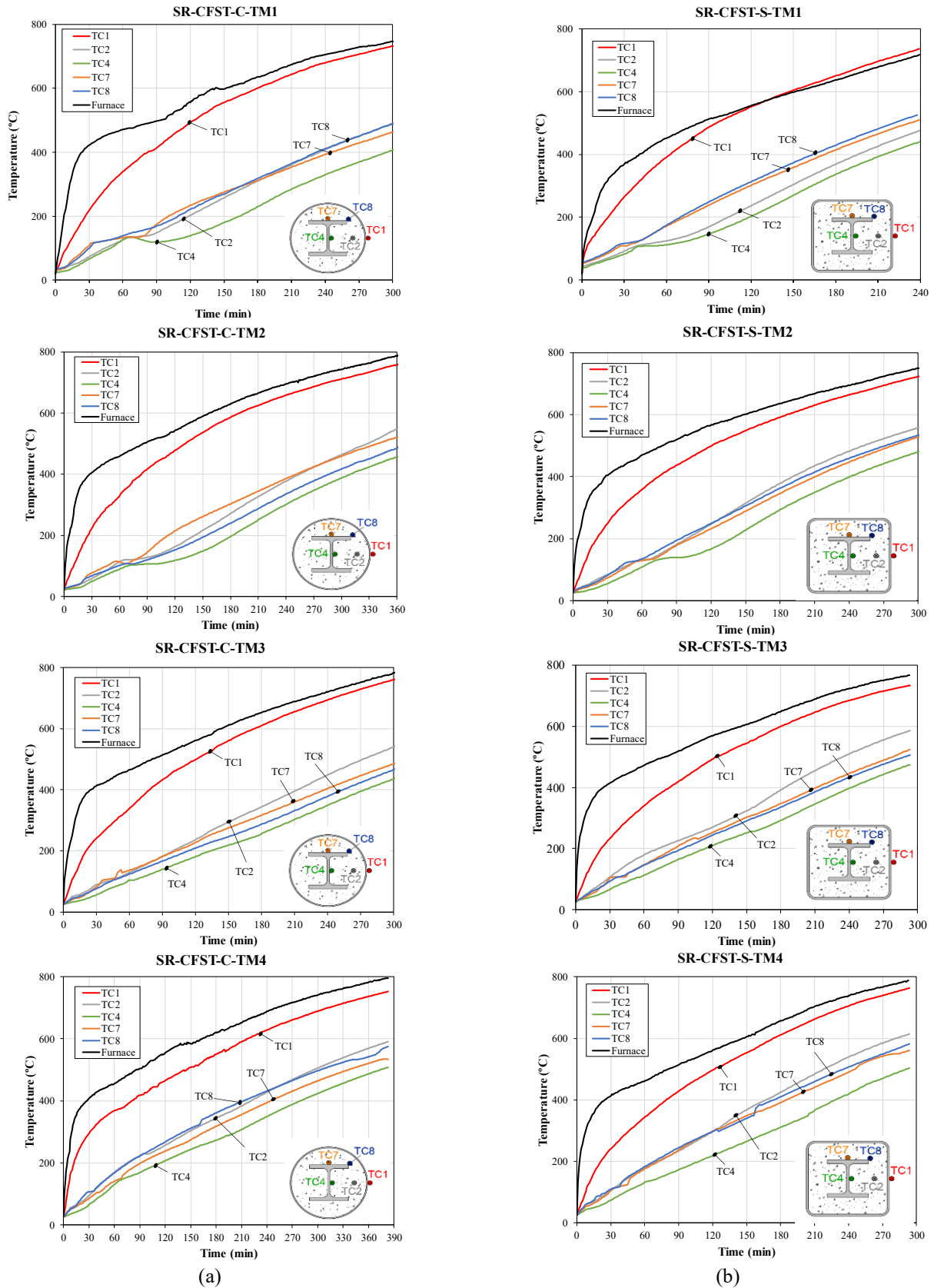For circular and square specimens of series TM1-TM4 the registered temperatures during the heating process are

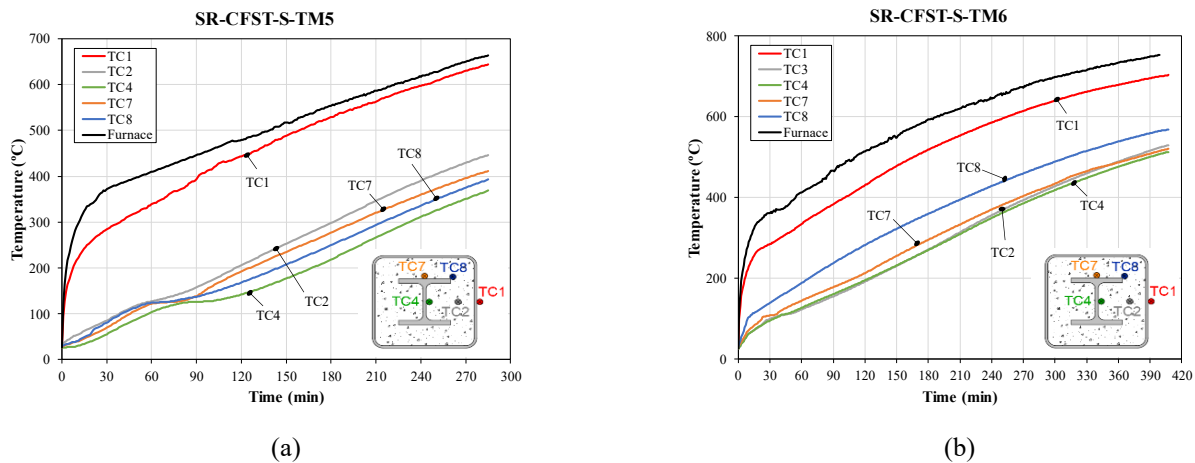(a)   (b)

Fig. 11 Cross-sectional temperatures for square specimens S-TM5 (a) and S-TM6 (b)

shown in Fig. 10. For the square SR-CFST columns temperatures were generally higher than for the corresponding circular columns, which may be explained with the effect of the section factor, i.e., for the same cross-sectional area, the square sections present a higher exposed perimeter. For both geometries, the delay of temperature rise at the inner steel profile can be observed. The thermal protection provided by the outer steel tube together with the low thermal diffusivity of concrete are responsible for this effect. In Fig. 9 the evolution of the outer steel tube temperatures is shown for specimens CHS-TM0 and SHS-TM0. In comparison with the composite columns with concrete core and embedded steel profile, it is clear that the steel tube heats much quicker leading to much higher temperatures. For example, in the CHS-TM0, at 30 min the steel tube has achieved 400ºC, whereas in the SR-CSFT-C series, it is almost after 90 min of heating when this temperature is reached. The same happens with the SHS-TM0 specimen and the SR-CFST-S series.

In Fig. 11 the history of temperatures at cross-section is shown for square specimens SR-CFST-S-TM5 and SR-CFST-S-TM6, which have a #250x10 mm outer tube made of high strength steel. Both the increase in the sectional dimension and the increase in the outer steel tube thickness evidence much more the delay in the heating of the inner concrete and embedded steel profile. Once more, the outer steel tube provides an inherent thermal protection, enhanced by the increment in the tube thickness (10 mm vs. 6.3 mm).

3.2 Failure modes

In Figs. 12-13 photographs of the state of all the columns after the thermo-mechanical tests are displayed. As shown in these figures, the outer steel tubes experienced local buckling around their mid-sections, which was more evident for the hollow tubes. In the SR-CFST columns, the local buckling was more notable for the square specimens.

In Figs. 14-15, the graphs show the evolution along the heating time of the axial displacement at the top end of the column for all the tested columns which was monitored and recorded by means of the load cell, showing a first stage dominated by the expansion of the outer tube; a second

Fig. 12 Hollow columns after the tests

stage with a gradual shortening of the column after the degradation of the outer tube; and the end of the test when eventually the defined failure criterion is met.

Based on EN1363-1 Section 11.1(b) (CEN 2020), a homogenous criterion was defined for determining the failure time of the columns where, for vertical members in compression, failure is established when one of the following two criteria is met:

- Vertical contraction limit: h/100 mm
- Contraction velocity limit: 3h/1000 mm

where h is the initial length of the column. Therefore, the maximum contraction allowed for the tested columns was set to 600/100=6 mm and the maximum contraction velocity was set to 3 × 600/1000=1.8 mm/min. For all the SR-CFST tests, the first criterion was met earlier, while for the hollow tube tests, the second criterion was reached sooner.

From the graphs of Figs. 14-15 the evolution of the response can be analysed. At the first stage of the heating, due to the direct exposure to the heat source and the higher thermal expansion of steel as compared to the concrete infill, the outer steel tube supports alone the applied load for a certain amount of time until yielding. After its loss of capacity, the load is transferred to the inner parts of the section, which owing to the higher thermal capacity of the concrete infill, heat up slower and are in turn are able to sustain the load for a significant period of time, until
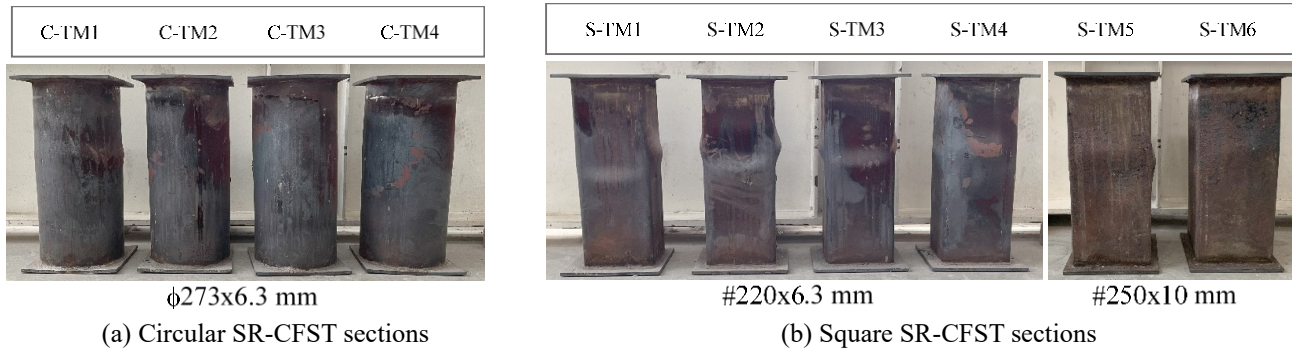
(a) Circular SR-CFST sections (b) Square SR-CFST sections

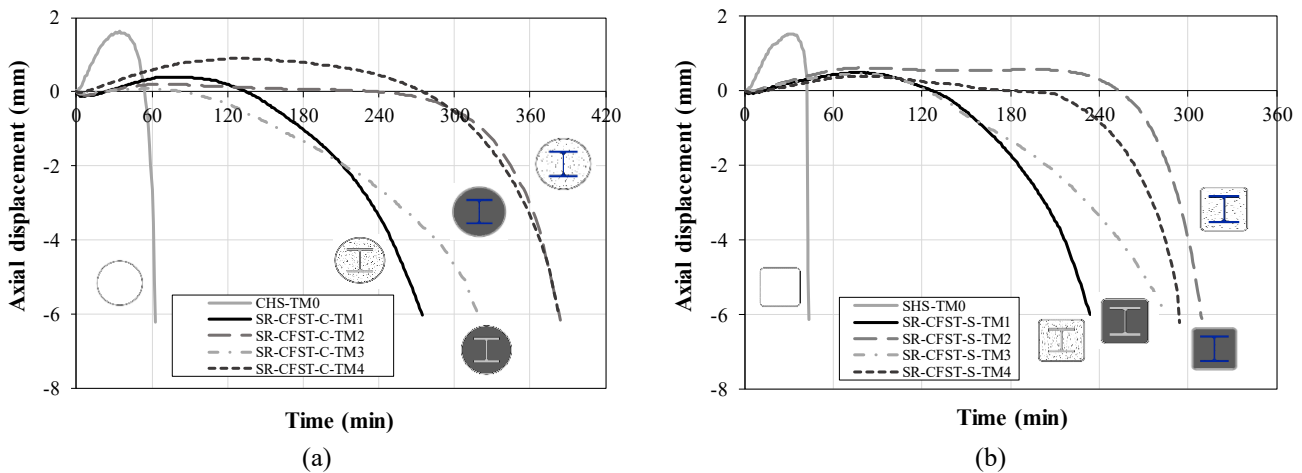Fig. 13 SR-CFST stub columns after the tests

(a) (b)

Fig. 14 Axial displacement versus time curves for specimens TM0-TM4 : (a) circular sections; (b) square sections

eventually the degradation of concrete and the inner steel profile occurs, stage where the column axial displacement gradually decreases, as a sign of capacity loss.

3.3 Comparison of the thermo-mechanical performance of the different cases analysed

In general, the circular SR-CFST specimens were able to sustain the applied load for a longer heating time than their square counterparts. For each series TM0-TM4, the failure time significantly increased when using high strength steel at the inner profile, and a certain enhancement was also obtained with the use of high strength concrete (HSC).

A much lower failure time was observed for the hollow tubes than for the SR-CFST columns. Their premature failure is due not only to the reduced mechanical capacity triggered by the local buckling of the tube wall, but also to the extremely fast heating of the section. Given the lack of concrete filling, the phenomenon of heat dissipation that benefits the SR-CFST columns does not occur, leading to the sharp increase of temperatures in the steel tube that can be perceived in Fig. 10.

Special mention should be made of the response observed for specimens SR-CFST-S-TM5 and SR-CFST-S-TM6. These specimens have bigger dimensions than their counterparts of the square series and also, the thickness of the steel tube is higher (10 mm vs. 6.3 mm). Although the
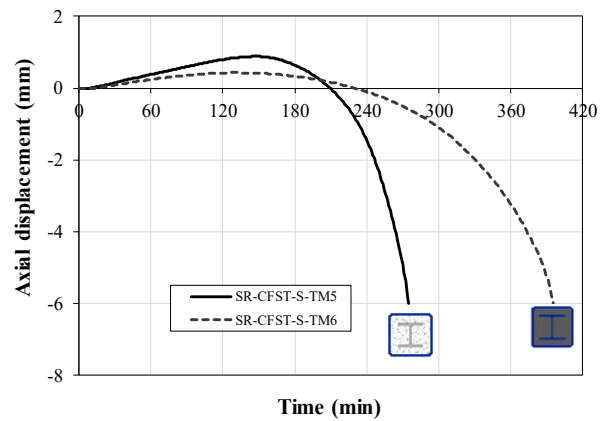
Fig. 15 Axial displacement versus time curves for specimens S-TM5 and S-TM6

failure times (FT) registered were higher, these are lower than expected, even more considering that in these cases high strength steel was used in the outer tube. FT for specimens SR-CFST-S-TM1 and SR-CFST-S-TM4 were 239 min and 294 min correspondingly whereas columns SR-CFST-S-TM5 and SR-CFST-S-TM6 reached 275 and 396 min respectively. As observed previously in Fig. 11, the heating is delayed but the limited improvement leads to think that the outer steel tube acts only as a thermal barrier. It degrades with high temperatures protecting the inner parts

but, at the same time, this does not allow to take advantage of its potential as a high performance material.

This tendency for composite columns with two steel components was already observed by the authors (Romero *et al.* 2015) after conducting a series of tests on double-tube concrete-filled steel tubular columns (DT-CFST) under fire. One of the main conclusions drawn was that in case of fire, a good design strategy for composite columns could be placing the highest amount of steel at the inner part of the section, so as to be thermally protected. Specifically, for SR-CFST this fact was also observed by the authors in a numerical study (Medall *et al.* 2022).

4. Assessment of the failure time of SR-CFST stub columns under fire

In this section, an analysis of the mechanical contribution of the different configurations of materials obtained from the experimental results is conducted. By means of this analysis one of the objectives of this work would be covered: the assessment of the influence that the high performance materials have on the failure time of the SR-CFST columns.

In the investigations related to CFST columns it is common to talk about ratios when conducting these analyses. Thus, taking as a basis the same concept, a new mechanical ratio can be defined: the high performance ratio (HPR).

Considering that the expected enhanced mechanical behaviour of a SR-CFST column with high performance materials with respect to a SR-CFST column with normal strength materials is due precisely to the presence of high strength concrete or high strength steel, the HPR is calculated as the ratio between the failure time achieved by a column of each series (FT_{C-TMi} or FT_{S-TMi}) with respect to the failure time measured for the TM1 column of the corresponding series, which will serve as reference (FT_{C-TM1} or FT_{S-TM1}). Therefore, a value greater than unity means that the contribution of the high performance materials is positive. The HPR ratio will be calculated only for specimens TM2 to TM4, both circular and square, since are the ones that have the same cross-sectional area of steel as the corresponding specimen TM1.

For circular SR-CFST columns, Eq. (1) will be used:

$$HPR_{Ci} = \frac{FT_{C-TMi}}{FT_{C-TM1}} \qquad (1)$$

And for square SR-CFST columns, Eq. (2) will apply:

$$HPR_{Si} = \frac{FT_{S-TMi}}{FT_{S-TM1}} \qquad (2)$$

The values obtained for this ratio may help to quantify the trend observed previously through the load-deflection curves. The HPR values are shown in Table 2 and represented in Fig. 16.

In view of the values of the HPR, it is clear that using high strength steel in the inner steel section is the most effective strategy to enhance the fire response of SR-CFST stub columns, especially in circular columns. This may be explained because the circular shape offers the columns a

Table 2 HPR for the different tested specimens

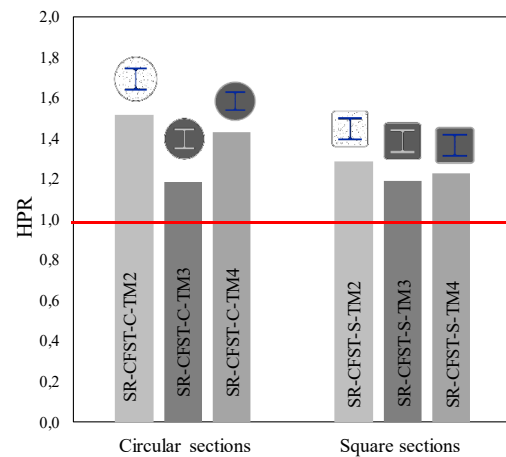| Specimen	FT (min)	HPR
SR-CFST-C-TM1	267	-
SR-CFST-C-TM2	405	1.52
SR-CFST-C-TM3	317	1.19
SR-CFST-C-TM4	383	1.43
SR-CFST-S-TM1	239	-
SR-CFST-S-TM2	308	1.29
SR-CFST-S-TM3	285	1.19
SR-CFST-S-TM4	294	1.23

Fig. 16 HPR for both series of tested SR-CFST columns

better thermal behaviour (lower section factor) and also, due to the effect of partial confinement, which should be confirmed by means of further numerical investigations.

However, in both TM3 specimens, the response is mainly controlled by the concrete infill, highly influenced by its moisture content, which according to the measured values was slightly lower for the high strength concrete mixture as compared to the normal strength one, therefore producing a faster heating of the section. Note that with the same moisture content the benefits of filling the SR-CFST columns with high strength concrete would have been even more notable.

For square specimens SR-CFST-S-TM5 and SR-CFST-S-TM6, which had high strength steel outer tubes, improvement ratios had been calculated with respect to specimens SR-CFST-S-TM1 and SR-CFST-S-TM4, which had the same combination of materials for the inner components, i.e., normal strength concrete and steel for the concrete infill and the embedded steel profile respectively in specimen SR-CFST-S-TM1; and high strength concrete and steel in the case of specimen SR-CFST-S-TM4.

Note that specimens S-TM5 and S-TM6 have an increment of 76.38% in the cross-sectional area of steel and 25.53% in the cross-sectional area of concrete. The improvement ratios obtained for each pair are 1.15 for S-TM5 vs. S-TM1 and 1.35 for S-TM6 vs. S-TM4. Considering the greater section dimensions of specimens S-TM5 and S-TM6 and the lower load level applied to them

(30% vs. 40%), the enhancement in terms of failure time obtained by using high strength steel at the outer tube is lower than expected. This corroborates the concept that using more area of steel of a higher grade at the outer tube does not lead to a notable gain in the fire performance of these type of composite columns.

5. Assessment of the reduction factors of high-performance materials for SR-CFST stub columns

This section evaluates the current design provisions for the cross-sectional plastic resistance of SR-CFST columns at elevated temperatures and the applicability of the currently available proposed reduction coefficients. These coefficients are taken from international codes as well as from the proposals of different authors. Their accuracy for estimating the cross-sectional plastic resistance of SR-CFST columns under high temperatures is obtained by comparing their predictions with the values registered during the described experiments.

5.1 HSS reduction coefficients

Currently, only few design codes incorporate reduction coefficients specifically developed for high strength steels in fire conditions. In the case of EN1993-1-2 (CEN 2005), although the scope of application is limited to steel grades up to S460, it is stated in Clause 2.2 of EN1993-1-12 (CEN 2015) that it can be extended to steels up to grade S700 without further adjustments. The Australian standard AS/NZ 2327 (2017) has also extended its applicability to steels with yield strength up to 690 MPa, referring to AS 4100 (2020) for the variation of the mechanical properties of steel with temperature. Although the range of steel grades is enlarged in ANSI/AISC 360-16 (AISC 2010), its reduction factors apply only to steels up to grade S450. The field of application of the reduction coefficients provided by British Standards BS590-8:2003 (BSI 2003) which is limited to structural steels between grades S275 and S355 is even more restrictive, making them unsuitable for their application to high strength steels assessment in fire conditions.

A deep literature analysis revealed several studies on reduction coefficients at high temperatures involving high strength steels of different grades such as S690 (Qiang *et al.* 2012), Q690 (Li and Song 2020), S700 (Shakil *et al.* 2020) and steels with nominal yield stresses between 700 and 900 MPa (Li and Young 2017). Researchers conducted experimental campaigns to characterize the mechanical properties of these steels under thermal conditions. They proposed reduction factors for key mechanical parameters, such as the elastic modulus, the yield strength, and the ultimate strength. Comparison with the proposals of different established design standards was also presented (Qiang *et al.* 2012, Li and Young 2017). Predictive equations and constitutive models were also developed (Shakil *et al.* 2020; Li and Young 2017), assessing material behaviour under different temperature ranges, and shedding light on the response of high strength steels at elevated temperatures. Additionally, Hassanein *et al.* (2022) suggested modifying the design codes to adequately predict the strength of S690 steels (Eurocode 3 Part 1.2 (CEN 2005) and AISC (AISC 2010)).

5.2 HSC reduction coefficients

The design provisions in EN1992-1-2 (CEN 2004) are applicable to normal weight concrete with characteristic compressive strength up to 90 MPa (cylinder strength), additional rules for concrete with strength above 50 MPa being given in its section 6. For compressive strengths ranging from C55/67 class to C90/105 class, Table 6.1N contains high strength concrete reduction coefficients. In turn, the Australian standard AS/NZ 2327 (2017) refers to EN1992-1-2 (CEN 2004) for the variation of the mechanical properties of concrete with temperature. In North America, the standard ACI 216.1-14 (ACI 2014) offers formulas to predict the behaviour of normal strength concrete at high temperatures. Despite the absence of direct specifications, this code is assumed not to encompass provisions applicable to high strength concrete. Facing the lack of specific guidelines, several researchers have proposed equations and temperature-dependent strength reduction coefficients for HSC (Phan and Carino 2003, Kodur *et al.* 2004, Matsudo *et al.* 2008). Other studies offered tabulated relationships between material properties and temperatures (Aslani and Bastami 2011). It is worth mentioning the extensive analysis performed by Elsanadedy (2019) where a profound analysis of design code provisions on this matter and literature proposals were made to be contrasted to experimental data.

5.3 Plastic resistance design equation for SR-CFST stub columns at elevated temperatures

The approach presented in this section for evaluating the plastic resistance of SR-CFST stub columns at elevated temperature is based on dividing the cross-section into five components, with different representative temperatures, see Fig. 17. The embedded steel profile is split into its flanges and web, while the concrete infill is divided into two parts: the concrete encased by the steel profile flanges and the concrete ring between the steel profile and outer tube. This approach aligns with the method proposed by Yang *et al.* (2020) and EN1994-1-2 Annex G (CEN 2005) provisions for partially encased composite columns.

In order to evaluate the mechanical contribution of each part of the section at a certain time period, a representative temperature needs to be obtained, which is subsequently used to reduce the material strength. To perform the assessment of the design equations in this section, these representative temperatures were derived from the experimental thermocouple measurements. The procedure for obtaining the five representative temperatures (θ_i) indicated in Fig. 17 was as follows. The temperature of the outer steel tube (θ_a) was derived by computing the mean value of thermocouples TC1 and TC6, resulting in a range between 650 to 770 ºC at failure time. For the steel profile flanges, the corresponding temperature (θ_f) was obtained

Table 3 Average error (ξ) obtained for the different HSS proposals assessed

Specimen	EN1993-1-2 (2005)	Qiang *et al.* (2012)	Li and Young (2017)	Li and Song (2020)	Shakil *et al.* (2020)	AS4100 (2020)
SR-CFST-C-TM2	0.94	1.07	1.15	1.11	1.12	1.13
SR-CFST-S-TM2	0.93	1.04	1.16	1.13	1.11	1.08
Mean	0.93	1.06	1.15	1.12	1.12	1.10
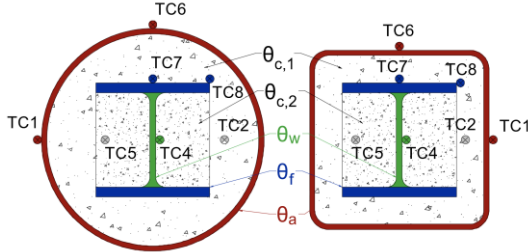
Fig. 17 Sub-division of the cross-section to calculate the plastic resistance at elevated temperatures

*As per Clause 2.2 of EN1993-1-12 (CEN 2015): "The standard is applicable to steels with grades greater than S460 up to S700 without further additional rules.

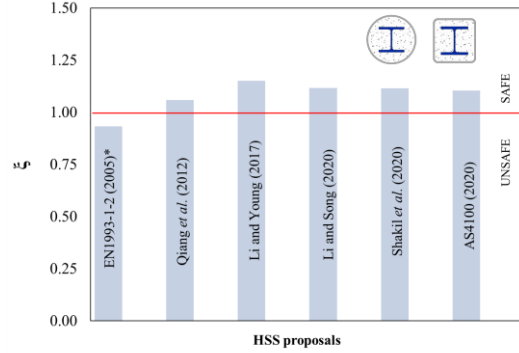Fig. 18 Predictions for columns SR-CFST-C-TM2 and SR-CFST-S-TM2 using different HSS proposals

using the average value from thermocouples TC7 and TC8. In turn, the temperature at the web of the embedded steel profile (θ_w) was determined solely by thermocouple TC4. The temperatures recorded at failure time for the inner profile ranged from 410 to 620 ºC. Regarding the concrete infill, the representative temperatures for the ring ($\theta_{c,1}$) and for the encased concrete ($\theta_{c,2}$) were given by thermocouples TC2 and TC5 respectively. The temperatures measured within the encased areas of the concrete infill spanned from 420 to 550 ºC at failure time, while the ring areas exhibited higher temperatures, ranging between 475 and 620 ºC.

Once this simplified temperature field is obtained, the plastic resistance to axial compression of a SR-CFST cross-section in case of fire ($N_{pl,Rd,fi}$) can be computed by adapting the equation given in Clause 4.3.5.1(4) of EN1994-1-2 (CEN 2005) for composite columns, as proposed in Eq. (3). To consider the inner steel profile, its contribution is added in the summation as proposed by Liew and Xiong (2015). Note that the area of the inner steel profile flanges (A_f) and web (A_w) has been split in this equation to consider their degradation with temperature separately, as well as the concrete infill, which has been divided into the two zones mentioned above: the concrete ring ($A_{c,1}$) and the encased concrete ($A_{c,2}$).

$$N_{pl,Rd,fi} = A_a \cdot f_y(\theta_a) + A_{c,1} \cdot f_c(\theta_{c,1}) + {} + A_{c,2} \cdot f_c(\theta_{c,2}) + A_w \cdot f_y(\theta_w) + 2 \cdot A_f \cdot f_y(\theta_f) \quad (3)$$

Eq. (3) was used to calculate the value of $N_{pl,Rd,fi}$ obtained when different sets of reductions coefficients for the high performance materials were applied (N_{pred} for each case). Various proposals were assessed comparing their prediction with the experimental results of the conducted tests.

The experimentally applied load (N_{exp}) was compared to the calculated cross-sectional resistance (N_{pred}) at the highest recorded temperatures by computing the error ξ, defined as given in Eq. (4):

$$\xi = \frac{N_{exp}}{N_{pred}} \quad (4)$$

High strength steel proposals

Using the values proposed for the reduction coefficients of high strength steels in the works commented above (Qiang *et al.* 2012, Li and Song 2020, Shakil *et al.* 2020, and Li and Young 2017), the predicted resistances are calculated and compared with the experimental loads.

The different high strength steel proposals were evaluated using specimens with HSS inner profiles and NSC (i.e., SR-CFST-S-TM2 and SR-CFST-C-TM2) to ensure a meaningful comparison. The results are summarised in the bar graph presented in Fig. 18 and in Table 3.

Note that a value of the average error ξ greater than one means that the proposal of reduction coefficients evaluated is safe in comparison with the experimental result - i.e., the value of the predicted cross-sectional resistance to compression of the SR-CFST column at elevated temperatures (N_{pred}) is less than the experimental load -.

From this comparison, it can be seen that the most accurate model from the literature is that proposed by Qiang *et al.* (2012), exhibiting deviations of about 6% from the experimental results. The models proposed by Li and Song (2020) and Shakil *et al.* (2020) lead to conservative predictions with a 12% deviation from the experimental values, while the proposal by Li and Young (2017) shows the lower agreement (15% deviation), although with conservative predictions.

The reduction coefficients in EN1993-1-2 (CEN 2005)

Table 4 Average error (ξ) obtained for the different HSC proposals assessed

Specimen	Phan and Carino (2003)	EN1992-1-2 Table 6.1N (2004)	Kodur *et al.* (2004)	Matsudo *et al.* (2008)	Aslani and Bastami (2011)
SR-CFST-C-TM3	1.16	1.00	0.99	1.21	1.02
SR-CFST-S-TM3	1.22	1.04	1.03	1.17	1.07
Mean	1.19	1.02	1.01	1.19	1.04

Fig. 19 Predictions for columns SR-CFST-C-TM3 and SR-CFST-S-TM3 using different HSC proposals
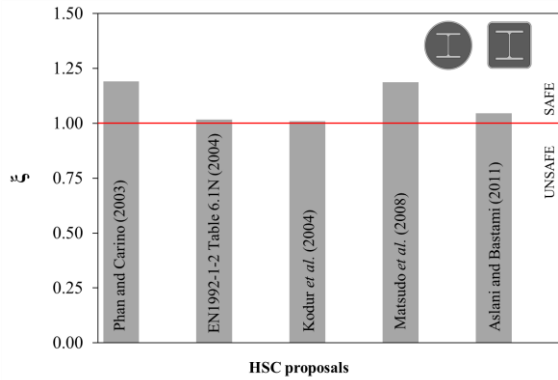

Fig. 20 Predictions for columns SR-CFST-C-TM4 and SR-CFST-S-TM4 combining HSS and HSC proposals

have also been included in this comparison, showing non-conservative predictions as compared to the experimental results, with a 7% overestimation. This may be due to a lack of calibration of the design code for this range of strengths, as the reduction coefficients are specifically derived for steel grades up to 460 MPa, although extended to 700 MPa as per Clause 2.2 of EN1993-1-12 (CEN 2015). Also the steel yield strength reduction proposal at elevated temperatures from AS4100 (2020) has been included in this comparison, showing conservative results, with an average error of 10%.

High strength concrete proposals

An identical procedure is applied in this section for the evaluation of the HSC proposals in the prediction of the cross-sectional resistance to compression of the SR-CFST columns at elevated temperatures. The different proposals were examined by using the appropriate test specimens for comparison (i.e., SR-CFST-S-TM3 and SR-CFST-C-TM3), see Fig. 19 and Table 4.

The HSC strength reduction coefficient proposals with temperature by Phan and Carino (2003), EN1992-1-2 (CEN 2004), Kodur *et al.* (2004), Matsudo *et al.* (2008), and Aslani and Bastami (2011) were studied.

As it can be seen in Fig. 19 and Table 4, the coefficients from Table 6.1N of EN1992-1-2 (CEN 2004), along with the models proposed by Kodur *et al.* (2004) and Aslani and Bastami (2011), demonstrate a significant accuracy in predicting the behaviour of the high strength concrete core with average errors of 1.02, 1.01 and 1.04 (lower than a 5% deviation), all of them lying on the safe side.

In turn, the reduction coefficients proposed by Phan and Carino (2003) and Matsudo *et al.* (2008) provide considerably conservative predictions, both with a deviation of a 19% from the actual column capacity at high
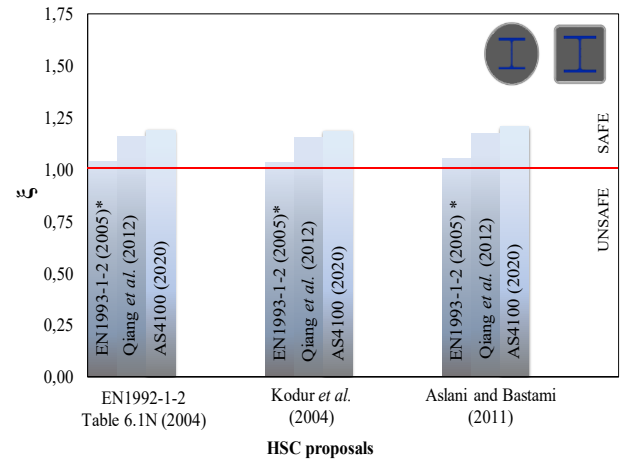
temperatures.

As can be observed, none of the proposals analysed provided unsafe predictions, which means that none of them overestimated the cross-sectional resistance to compression of the SR-CFST column at elevated temperatures.

Combination of proposals

Finally, a third comparison is conducted, using the insights gained from the HSS and HSC models studied in the previous sections. The best performing reduction coefficients for each material are selected (those not exceeding a 10% error in the previous evaluations) and compared against the experimental tests that make use of both HSS and HSC (test specimens SR-CFST-S-TM4 and SR-CFST-C-TM4). The results for this comparison can be observed in Fig. 20 and Table 5.

The aim of this analysis is to determine which combination is the most suitable to predict the cross-sectional resistance to compression of SR-CFST columns at high temperatures according to the experimental results presented above by the authors. For HSS, the proposals considered are the reduction coefficients from EN1993-1-2 (CEN 2005), as well as those by Qiang *et al.* (2012) and AS4100 (2020). In turn, for HSC, the selected proposals include the reduction coefficients from EN1992-1-2 (CEN 2004) and those by Kodur *et al.* (2004), and Aslani and Bastami (2011).

As can be seen in Fig. 20 and Table 5, irrespective of the HSC proposal employed, the three selected options for HSS result in conservative predictions, with average values above one. However, the best agreement between the predicted and the tested failure loads at elevated

Table 5 Average error (ξ) obtained for the combined HSS and HSC proposals assessed

Specimen	EN1992-1-2 (2004)			Kodur *et al.* (2004)			Aslani and Bastami (2011)		
	EN1993-1-2 (2005)	Qiang *et al.* (2012)	AS4100 (2020)	EN1993-1-2 (2005)	Qiang *et al.* (2012)	AS4100 (2020)	EN1993-1-2 (2005)	Qiang *et al.* (2012)	AS4100 (2020)
SR-CFST-C-TM4	1.06	1.18	1.22	1.05	1.17	1.21	1.17	1.19	1.23
SR-CFST-S-TM4	1.02	1.14	1.16	1.02	1.14	1.16	1.03	1.15	1.18
Mean	1.04	1.16	1.19	1.04	1.15	1.18	1.05	1.17	1.20

temperatures is obtained when combining the reduction coefficients for HSC from Table 6.1N of EN1992-1-2 (CEN 2004) and those for HSS in EN1993-1-2 (CEN 2005), with an average error of 1.04. Also the reduction coefficients proposed by Kodur *et al.* (2004) or Aslami and Bastami (2011), combined with EN1993-1-2 (CEN 2005), demonstrate a good agreement with the test results. The reduction coefficients for HSS proposed by Qiang *et al.* (2012) provide errors above a 15% when combined with the studied reduction coefficients for HSC, although they lay on the safe side. Finally, the provisions in AS4100 (2020) for the reduction of steel strength with temperature also result in safe predictions, although too safe-sided, with an error of about a 20%.

It should be noted that the present comparison is in its initial stages, relying on a limited number of experiments. Conclusions should be cautiously approached, as further research and validation are necessary to ensure sufficient accuracy. Additional experiments and extension to validated numerical models, accompanied by comprehensive parametric studies, are required for a reliable analysis before drawing firm conclusions that can lead to the development of design recommendations.

6. Conclusions

In this paper, the thermo-mechanical response of SR-CFST stub columns has been studied through the experimental investigation here described. The evolution of the cross-sectional temperatures with time and the axial displacement versus time histories were analysed. Ten SR-CFST specimens, four circular and six square, were tested together with two hollow steel tubes which served as reference. First, the columns were loaded at a certain load level and afterwards uniformly heated inside an electric furnace until failure. According to their external shape, eight of the columns were grouped into two series comprising circular and square geometries respectively (TM1-TM4) combining normal with high performance materials for the inner components (concrete infill and embedded steel profile). For the sake of comparison, the selected circular and square steel tubes had a comparable steel usage. Two of the square SR-CFST columns (TM5 and TM6) had high strength steel in the outer tube. From the results of the thermo-mechanical tests, some conclusions can be drawn:

• Temperatures were generally higher for the square SR-CFST columns than for the corresponding circular columns,

which may be due to the effect of the higher section factor of square columns as compared to their circular counterparts.

• The circular specimens reached higher failure times than the square columns. The failure time significantly increased with the use of high strength steel at the embedded steel profile, as well as with the use of high strength concrete as infill.

• From the fire design point of view, it is not worth to use neither a high amount of steel, nor a high steel grade at the outer tube.

The current design provisions for the evaluation of the cross-sectional plastic resistance of SR-CFST columns at elevated temperatures and the applicability of the currently available strength reduction coefficients for HSS and HSC from the design codes and the reviewed literature was assessed, by contrast with the experimental results. It was found that the strength reduction coefficients from the Eurocodes – EN1992-1-2 (CEN 2004) and EN1993-1-2 (CEN 2005) – provide the more accurate results in predicting the axial capacity at elevated temperatures of SR-CFST stub columns with high performance materials, followed by the proposal from Qiang *et al.* (2012) and the provisions in the Australian code AS4100 (2020), all of them leading to conservative results.

In the framework of the nationally funded project that overarches the present research (HIFICOMP) the authors will carry out further experimental tests and numerical studies to extend the conclusions drawn in this work and to be able to develop fire design recommendations for the use of high performance materials in SR-CFST columns.

Acknowledgments

References

ACI 216.1-14 (2014), *Code Requirements for Determining Fire Resistance of Concrete and Masonry Construction Assemblies*, American Concrete Institute; Farmington Hills, MI, USA.

ANSI/AISC 360-16 (2010), *Specification for Structural Steel Buildings,* American Institute of Steel Construction; Chicago, IL, USA.

AS 4100 (2020), *Steel structures*, Standards Australia Ltd.; Sydney, Australia.

AS/NZS 2327 (2017), *Composite structures - Composite steel-concrete construction in buildings*, Standards Australia/Standards New Zealand; Auckland, New Zealand.

Aslani, F. and Bastami, M. (2011), "Constitutive relationships for normal-and high-strength concrete at elevated temperatures" *ACI Mater. J.*, **108**(4), 355-364. https://doi.org/10.14359/51683106.

BS 5950-8 (2003), *Structural Use of Steelwork in Building Part 8: Code of Practice for Fire Resistant Design,* British Standards Institution; London, UK.

Dotreppe, J.C., Chu, T.B. and Franssen, J.M. (2010), "Steel hollow columns filled with self-compacting concrete under fire conditions." *Proceedings of the 3rd Congress of the International Federation for Structural Concrete (FIB) and PCI Conference*, Washington D.C., May.

Elsanadedy, HM. (2019), "Residual Compressive Strength of High-Strength Concrete Exposed to Elevated Temperatures", *Adv. Mater. Sci. Eng.*, **2019**, 6039571. https://doi.org/10.1155/2019/6039571

EN1363-1:2020 (2020), *Fire Resistance Tests - Part 1: General Requirements*, CEN European Committee for Standardization, Brussels, Belgium.

EN1992-1-2 (2004*), Eurocode 2: Design of Concrete Structures, Part 1.2: General rules – Structural Fire Design,* CEN European Committee for Standardization; Brussels, Belgium.

EN1993-1-2 (2005), *Design of Steel Structures, Part 1.2: General Rules – Structural Fire Design*, CEN European Committee for Standardization; Brussels, Belgium.

EN1994-1-1 (2004*), Eurocode 4: Design of Composite Steel and Concrete Structures. Part 1.1: General rules and rules for buildings*, European Committee for Standardization; Brussels, Belgium.

EN1994-1-2 (2005*), Eurocode 4: Design of Composite Steel and Concrete Structures. Part 1.2: General rules - Structural fire design*, European Committee for Standardization; Brussels, Belgium.

EN1993-1-12 (2015), *Design of Steel Structures, Part 1-12: Additional Rules for the Extension of EN 1993 up to Steel Grades S700*, CEN European Committee for Standardization; Brussels, Belgium

Espinos, A., Romero, M.L. and Lam, D. (2016), "Fire performance of innovative steel-concrete composite columns using high strength steels", *Thin-Wall. Struct.*, **106**, 113-128. https://doi.org/10.1016/j.tws.2016.04.014.

Hassanein, M.F., Zhang, Y.M., Shao, Y.B. and Zhou, M. (2022), "New AISC and EC3 design for S690 plate girders at elevated temperatures" *J. Constr. Steel Res.*, **194**, 107313. https://doi.org/10.1016/j.jcsr.2022.107313

ISO 12570:2000 (2000), *Hygrothermal performance of building materials and products — Determination of moisture content by drying at elevated temperature,* International Organization for Standardization, Geneva, Switzerland.

Kodur, V.K.R., Wang, T.C. and Cheng, F.P. (2004), "Predicting the fire resistance behaviour of high strength concrete columns", *Cem. Concr. Compos.*, **26**(2), 141-153. https://doi.org/10.1016/S0958-9465(03)00089-1.

Li, G.Q. and Song, L.X. (2020), "Mechanical properties of TMCP Q690 high strength structural steel at elevated temperatures", *Fire Saf. J.* **116**, 103190. https://doi.org/10.1016/j.firesaf.2020.103190

Li, H.T. and Young, B. (2017), "Material properties of cold-formed high strength steel at elevated temperatures", *Thin-Wall. Struct*, **115**, 289-299. https://doi.org/10.1016/j.tws.2017.02.019.

Liew, J.Y.R. and Xiong, M. (2015), *Design Guide for Concrete Filled Tubular Members with High Strength Materials to Eurocode 4*, Research Publishing, Singapore, Republic of Singapore.

Mao, W.J., Wang, W. and Zhou, K. (2022), "Fire performance on steel-reinforced concrete-filled steel tubular columns with fire protection", *J. Constr. Steel Res.*, **199**, 107580. https://doi.org/10.1016/j.jcsr.2022.107580

Mao, W.J., Wang, W., Zhou, K. and Du, E.F. (2021), "Experimental study on steel-reinforced concrete-filled steel tubular columns under the fire", *J. Constr. Steel Res.*, **185**, 106867.https://doi.org/10.1016/j.jcsr.2021.106867

Mao, W.J., Zhou, K. and Wang, W. (2023), "Investigation on fire resistance of steel-reinforced concrete-filled steel tubular columns subjected to non-uniform fire", *Eng. Struct.*, **280**, 115653. https://doi.org/10.1016/j.engstruct.2023.115653

Matsudo, M., Nishida, H., Ohtsuka, T., Hirashima, T. and Abe, T. (2008), "mechanical properties of high strength concrete at high temperatures", *J. Struct. Construct. Eng. Transact. AIJ*, **73**(624), 341-347. https://doi.org/10.3130/aijs.73.341.

Medall, M., Espinós, A., Albero, V. and Romero, M.L. (2022), "Simplified proposal for the temperature field of steel-reinforced CFST columns exposed to fire", *Eng. Struct.*, **273**, 115083. https://doi.org/10.1016/j.engstruct.2022.115083.

Meng, F.Q., Zhu, M.C., Clifton, G.C., Ukanwa, K.U. and Lim, J.B.P. (2020), "Performance of square steel-reinforced concrete-filled steel tubular columns subject to non-uniform fire", *J Constrct. Steel Res.*, **166**, 105909. https://doi.org/10.1016/j.jcsr.2019.105909.

Meng, F-Q., Zhu, M-C., Clifton, G.C., Ukanwa, K.U. and Lim, J.B.P. (2021), "Fire performance of edge and interior circular steel-reinforced concrete-filled steel tubular stub columns", *Steel Compos. Struct.*, **41**(1), 115-122. https://doi.org/10.12989/scs.2021.41.1.115

Phan, L.T. and Carino, N.J. (2006), "Code provisions for high strength concrete strength-temperature relationship at elevated temperatures", *Mater. Struct.*, **36**(256), 91-98. https://doi.org/10.1007/BF02479522.

Pons, D., Espinós, A., Albero, V. and Romero, M.L. (2018), "Numerical study on axially loaded ultra-high strength concrete-filled dual steel columns", *Steel Compos. Struct.*, **26**(6), 705-717. https://doi.org/10.12989/scs.2018.26.6.705.

Qiang, X., Bijlaard, F. and Kolstein, H. (2012), "Dependence of mechanical properties of high strength steel S690 on elevated temperatures", *Construct. Build. Mater.*, **30**, 73-79. https://doi.org/10.1016/j.conbuildmat.2011.12.018.

Romero, M.L., Espinos, A., Portolés, J.M., Hospitaler, A. and Ibañez, C. (2015), "Slender double-tube ultra-high strength concrete-filled tubular columns under ambient temperature and fire", *Eng. Struct.*, **99**, 536-545. http://dx.doi.org/10.1016/j.engstruct.2015.05.026.

Shakil, S., Lu, W. and Puttonen, J. (2020), "Experimental studies on mechanical properties of S700 MC steel at elevated temperatures", *Fire Saf. J.*, **116**, 103157. https://doi.org/10.1016/j.firesaf.2020.103157.

Yang, X., Tang, C., Chen, Y. and Qiao, T.Y. (2020), "Compressive behavior of steel-reinforced concrete-filled square steel tubular stub columns after exposure to elevated temperature", *Eng. Struct.*, **204**. https://doi.org/10.1016/j.engstruct.2019.110048.

DL

ANNEX I. COMPENDIUM OF PUBLICATIONS

ARTICLE 4

Fire design of steel-reinforced CFST stub columns with high-strength materials

David Medall [a], Manuel L. Romero [a], Huu-Tai Thai [b], Ana Espinós [a],*

[a] *ICITECH, Universitat Politècnica de València, Valencia, Spain*
[b] *Department of Infrastructure Engineering, The University of Melbourne, Australia*

ARTICLE INFO

ABSTRACT

Innovative composite sections are gaining popularity as they reduce the environmental impact of construction and take advantage of the collaboration of concrete and steel properties at room temperature and in fire. By introducing high-performance materials, these synergies are boosted. One typology is the steel-reinforced concrete-filled steel tubular (SR-CFST) section, in which a steel profile is embedded inside a CFST section. Despite their impressive load-bearing capacity and fire resistance, the available investigations on their thermo-mechanical capabilities are scarce. The present paper develops a numerical model to analyse the thermo-mechanical behaviour of SR-CFST stub columns subjected to fire. The model is validated against previous experiments conducted by the authors by comparing the temperature distribution and the mechanical behaviour with the experimental measurements. Afterwards, an extensive parametric study (1440 cases) is conducted to analyse the influence of several geometrical parameters – cross-sectional shape, outer tube dimensions and thickness, inner steel profile dimensions, section factor – and the use of high-strength materials for the concrete and the inner steel profile. Afterwards, a simplified temperature distribution proposal formerly designed by the authors for SR-CFST sections was tentatively tested. Based on this previous simplified temperature field and in line with the current provisions of EN1994-1-2, a new proposal is developed to evaluate the cross-sectional plastic resistance of SR-CFST stub columns under a fire scenario. This method unifies the initially developed thermal method and provides practical guidance for designers to evaluate the thermo-mechanical behaviour of SR-CFST columns, filling an existing gap in the European design code.

1. Introduction

The increase in popularity and use of steel-concrete composite structures has been pushing technological research in this field in recent years. Innovative sections and high-performance materials (i.e. high-strength concrete and high-strength steel) have allowed steel-concrete members – and more specifically, steel-concrete columns – increase their mechanical capacity and decrease their cross-sectional dimensions, thus reducing the environmental impact of construction. A new typology that has emerged recently, based on the widely extended concrete-filled steel tubular (CFST) sections, consists of embedding a steel profile inside a CFST: the so-called steel-reinforced concrete-filled steel tubular (SR-CFST) columns. The advantages of these sections at room temperature are well known. Additionally, this geometry also enhances the thermal behaviour of the section, granting intrinsic fire protection to the inner profile, which is thermally protected by the outer steel tube and the

surrounding concrete core, delaying the loss of its mechanical properties and postponing the failure of the member when exposed to elevated temperatures [1]. Therefore, using high-performance materials at the inner parts of these types of sections may further enhance their fire performance, increasing their load-bearing capacity both at room temperature and under fire conditions.

Due to their novelty, a reduced number of experimental investigations have been conducted so far on the fire behaviour of SR-CFST columns. The first work published on SR-CFST columns exposed to high temperature reported the tests conducted by Dotreppe et al. [2] at the University of Liege (Belgium). Ten slender composite columns with circular and square geometries were tested under constant load and fire conditions. Four of them were SR-CFST sections consisting of an outer circular tube of 219.1 mm filled with self-compacting concrete and an embedded HEB120 steel profile.

Meng et al. [3,4] carried out eight SR-CFST tests in Shanghai (China),

---

* Corresponding author.
E-mail address: aespinos@mes.upv.es (A. Espinós).

both uniformly and partially exposed to high temperatures. The columns were 1800 mm long and had a HW150x150 steel profile embedded inside. The authors noticed that including the steel profile considerably increased the load-bearing capacity of the columns under fire.

Other authors have tested a different type of SR-CFST column geometries featuring a cruciform steel section embedded inside [5–7]. These specimens were subjected to uniform and non-uniform fire conditions under the ISO-834 curve.

Lately, the authors of this manuscript have conducted a thermo-mechanical experimental campaign on SR-CFST stub columns with high-performance materials exposed to fire [8]. Ten columns (four circular and six square specimens) were tested in this study under constant load and high-temperature conditions. High-strength steel up to 777 MPa and high-strength concrete up to 86 MPa were used in the experiments for the inner steel profile and the concrete infill, respectively. The study concluded that using these materials greatly enhanced the fire resistance of SR-CFST stub columns.

Alternatively, researchers have studied the thermal and mechanical behaviour of these sections by employing numerical models. The numerical investigation of Espinós et al. [1] is worth mentioning, in which different innovative composite cross-sections were studied to evaluate possible alternatives to improve the fire resistance of traditional CFST columns. The FE models were developed using the finite element package ABAQUS. The study found that reducing the amount of steel in the outer tube and instead placing an equivalent amount of steel inside the embedded profile significantly increased the fire resistance of the sections as the inner steel resulted thermally protected by the surrounding concrete mass.

Other authors [9,10] studied the possibility of using stainless steel at the inner embedded profile of SR-CFST columns exposed to fire. It was found that including stainless steel at the inner profile enhanced the fire performance compared to regular carbon steel with the exact dimensions and load-bearing capacity.

Mao et al. [11] featured a numerical analysis of the fire behaviour of square-shaped SR-CFST sections. The influence of several parameters (i. e. the slenderness, concrete compressive strength, steel yield strength and steel ratio) over the thermo-mechanical performance of the columns was assessed. The relation between the steel used at the outer and inner parts of the section was found to be of major importance in the fire behaviour. The authors also noted the benefits of using high-strength steel at the embedded profile, which aligns with the previous conclusions of Espinós et al. [1].

Meng et al. [3,4] developed a numerical model for SR-CFST columns subjected to non-uniform fire exposure and validated it against several previous experiments by their research group [12]. The authors then conducted a series of parametric studies to study the possible application of fire assessment methods of CFST sections to SR-CFST columns. Given the lack of specific guidance in the European design codes for these sections, the method proposed by Albero et al. [13] for CFST columns (approved by CEN/TC250/SC4 to replace Annex H of EN1994-1-2 [14] and included in the new draft version of prEN1994-1-2:2021 [15]) was applied to SR-CFST sections. Conservative results were obtained, and the authors concluded that additional research should be developed to provide precise predictions for this innovative typology.

Most recently, the authors of this study have developed a thermal finite element model to analyse the temperature field of SR-CFST sections under fire conditions [16]. In this study, the authors developed a sectional 2D model with the nonlinear FE analysis software ABAQUS and validated it against several experimental campaigns of both SR-CFST columns and other composite section typologies. Parametric studies showed the influence of the cross-sectional slenderness, the steel area, the section factor, the inner steel profile dimensions and the concrete moisture content. Based on the parametric studies results, the authors developed a simplified proposal for evaluating the temperature distribution in SR-CFST by obtaining an equivalent temperature to represent each part of the section (i.e. steel tube, concrete infill and

embedded steel profile) that results in the same fire resistance as using the non-uniform temperature field.

Revising the available literature on SR-CFST columns showed that a reduced number of numerical and experimental investigations under fire conditions have been conducted to date. Furthermore, even fewer of these studies include the use of high-performance materials and their effect on the fire behaviour of the columns. Therefore, the present study aims to extend the research scope of SR-CFST sections to analyse the use of high-strength steel and high-strength concrete and their different combinations to understand their effect on the thermal and mechanical response of the columns under fire. Additionally, as previously mentioned, there is a lack of guidance in the international design codes and, more specifically, Eurocode 4 Part 1.2 [14] for this typology of sections. Thus, following from the previous investigation by the authors [16], this paper develops a unified proposal that adequately predicts the thermal and mechanical behaviour of SR-CFST stub columns exposed to high temperatures.

2. Development of the finite element model

A three-dimensional model was developed using the non-linear finite element software package ABAQUS [17].

2.1. Geometry and finite element mesh

The geometry of the finite element model is composed of an assembly of several parts. An outer steel tube, a concrete encasement, and an embedded steel profile form the column. Two plates are modelled at both ends of the column to provide a flat contact surface and apply the load evenly across the column section. Fig. 1 displays the different parts of the numerical model and Fig. 2 shows the assembly and finite element mesh of the model.

The concrete infill and inner steel profile are modelled for the thermal analysis using 4-node linear heat transfer tetrahedrons (DC3D4) with nodal temperature degrees of freedom. Meanwhile, the outer tube was meshed with 4-node heat transfer quadrilateral shell elements (DS4) with nodal temperature degrees of freedom. Regarding the mechanical analysis, the concrete infill and inner steel profile were modelled with 4-noded linear tetrahedron elements (C3D4) and the outer steel tube as 4-noded doubly curved thin shell elements (S4R) with reduced integration. The loading plates were meshed as discrete rigid elements with 4-noded 3-D bilinear rigid quadrilateral elements (R3D4). A maximum FE size of 20 mm was used at the inner steel profile and concrete infill, while a 15 mm size was employed at the outer steel tube based on previous sensitivity studies [16].

2.2. Thermo-mechanical analysis

A non-linear heat transfer analysis was conducted in ABAQUS [17] to compute the temperature field of the modelled steel-reinforced CFST columns. The loading plates were not included in the thermal analysis of the specimens. The heat balance equation based on Fourier's law, given in Eq. (1), was introduced in the model. The exposed surface of the outer steel tube was subjected to the thermal boundary conditions through the convection and radiation heat transfer mechanisms as stated in Eq. (2):

$$\nabla(k \cdot \nabla \theta) = \rho c_p \frac{\partial \theta}{\partial t} \tag{1}$$

$$-n \cdot k \cdot \nabla \theta = \alpha_c (\theta_m - \theta_g) + \Phi \cdot \varepsilon_m \cdot \varepsilon_f \cdot \sigma (\theta_r^4 - \theta_g^4) \tag{2}$$

where θ_m is the surface temperature of the exposed member, θ_g is the gas temperature near the exposed member and θ_r is the effective radiation temperature of the fire environment.

The EN1991-1-2 [18] recommended values for the heat transfer equation were adopted for the convection and radiation portions. The
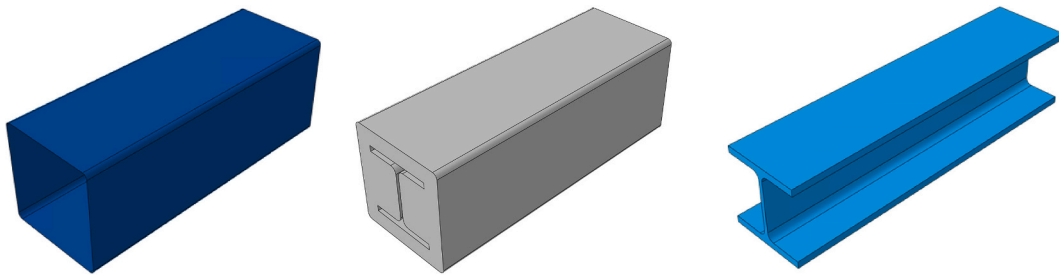
Fig. 1. Parts of the assembly of the finite element model: a) outer steel tube, b) concrete infill and c) inner steel profile.
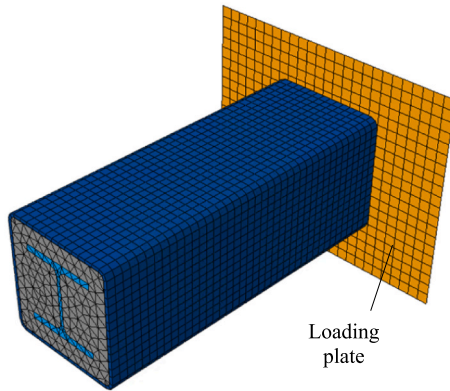

Fig. 2. Geometry and finite element mesh of the finite element model.

The heat transfer non-linear analysis results were the evolution of the nodal temperature (NT11) at all the FE of the model. Once the temperature evolution was obtained from the thermal model, the results of the nodal temperatures were imported into the mechanical model as a predefined temperature field and a sequentially coupled thermo-mechanical analysis was conducted.

2.3. Steel-concrete interaction

Several thermal interactions between the different parts of the model were defined. The inner steel profile was assumed to have a perfect thermal contact with the concrete core (i.e. no thermal resistance), as previous numerical investigations proved to provide accurate results [11,1]. As regards to the contact between the outer steel tube and the concrete infill, a gap conductance definition was introduced to emulate the effect of the expansion of the steel tube at elevated temperature, which separates transversally from the concrete core, creating an "air gap", thereby delaying the overall temperature rise across the section. As previous research from the authors in SR-CFST [16] and CFST [13] sections proved, a gap thermal conductance of 200 W/m²K provides accurate results to represent the temperature delay at this interface; therefore, this value was adopted in the numerical model.

Mechanically, a "steel-concrete" contact interaction property between the inner steel profile and the concrete part was defined, as well as between the outer steel tube and the inner concrete. The tangential behaviour of this interaction was defined by a friction coefficient of 0.3 as in previous studies of the authors [1], while the normal behaviour was modelled as a "hard contact", which prevented the penetration between the two parts. At the top end of the column, the contact between the steel plate and the concrete infill was defined with the same "steel-concrete" property. In turn, at the bottom end of the column, the steel tube and

convective coefficient at the outer steel tube surface was assumed to be $\alpha_c = 25\ W/m^2 K$. The surface emissivity of the member was set to $\varepsilon_m = 0.7$ at the steel surface, the emissivity of fire was assumed to be $\varepsilon_f = 1.0$ and the Stephan-Boltzmann constant was taken as $\sigma = 5.67 \cdot 10^{-8}\ W/m^2 K^4$. For the validation cases, the time-temperature evolution inside the furnace was measured and modelled accordingly in the numerical model. As the temperature distribution along the vertical dimension of the furnace varied significantly, three temperature exposure zones (upper, middle, and lower part of the column) were modelled in the validation to simulate the experimental conditions properly (see Fig. 3). In the parametric studies, the fire temperature evolution was assumed to follow the standard ISO-834 curve [19].
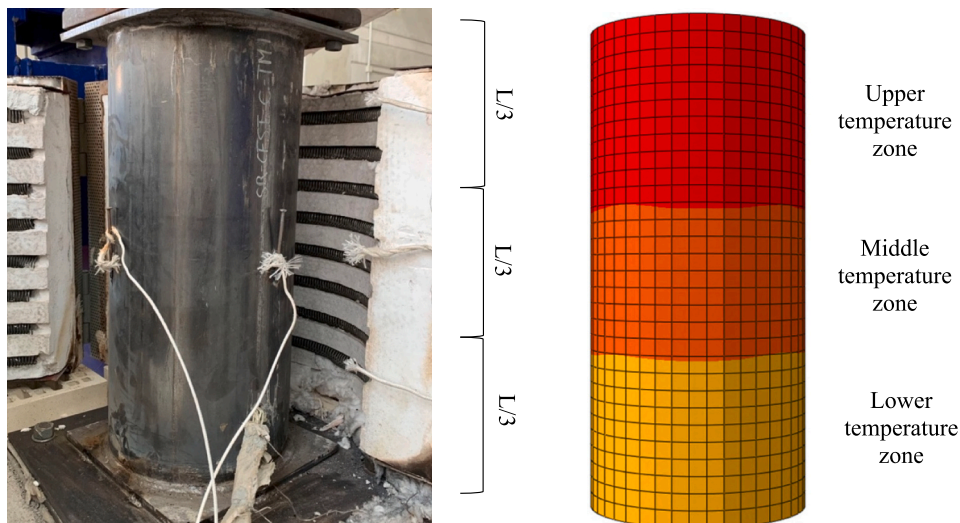

Fig. 3. Temperature exposure zones prescribed at the FE model as compared to the experimentally measured thermocouples in specimen SR-CFST-C-TM1.

inner profile were tied to the lower steel plate, since in the experiments these parts were welded together. The same tied interaction was prescribed between the outer steel tube and the top end plate.

2.4. Material properties at elevated temperatures

2.4.1. Thermal properties

The relevant thermal properties were the steel and concrete density, conductivity, and specific heat. A constant value of 7850 kg/m^3 was defined for the density of steel. In turn, the concrete density was considered temperature dependent according to 3.4(2) of EN1994-1-2 [14]. The conductivity of steel was defined as per Clause 3.3.1(7) of EN1994-1-2 [14]. The concrete conductivity was modelled using the new approach proposed in prEN1994-1-2 [15], which combines the upper and lower limit from the previous version of EN1994-1-2, being the formulation as follows:

$$\lambda_c = 2 - 0,2451(\theta_c/100) + 0,0107(\theta_c/100)^2 \text{ for } \theta_c \leq 140^\circ C \quad (3)$$

$$\lambda_c = -0,02604\,\theta_c + 5,324 \text{for } 140 < \theta_c < 160^\circ C \quad (4)$$

$$\lambda_c = 1,36 - 0,136(\theta_c/100) + 0,0057(\theta_c/100)^2 \text{ for } \theta_c \geq 160^\circ C \quad (5)$$

The specific heat of steel was introduced following Clause 3.3.1(4) of EN1994-1-2 [14], while in the case of concrete, the formulation given in Clause 3.3.2(4) was followed, introducing a peak value between 100 and 200 °C to account for the water evaporation, as stated in Clause 3.3.2(8) of the same code.

2.4.2. Mechanical properties

The constitutive models included in EN1994-1-2 [14] for the uni-axial behaviour at elevated temperatures were used for the steel and concrete, respectively. Thermal elongation was also included in the material definition in the mechanical model as defined in Clauses 3.3.1 (1) and 3.3.2(1) of EN1994-1-2 [14].

The mechanical behaviour of the materials was introduced in ABA-QUS [17] by means of different plasticity models. An isotropic elastic-plastic model with the von Mises yield criterion was used for steel, while for concrete, the Drucker Prager model was used. The input parameters for the Drucker Prager model were the friction angle, which was set to 25°, a flow-stress ratio of 0.8 and a dilation angle of 5°. For stablishing the suitable mechanical properties of high-strength steel and concrete, specific sensitivity studies were performed and are included in section 3.3 of this paper.

3. Validation of the model

This section describes the thermal and mechanical validation of the numerical model. The model is validated with available data from a previous thermo-mechanical experimental campaign on stub SR-CFST columns [8]. The main characteristics of the column specimens used for the validation are included in Table 1.

The experimental campaign consisted of twelve specimens: two reference empty tubes (circular and square, TM0), four circular SR-CFST columns (C-TM1 to C-TM4) and six square SR-CFST columns (S-TM1 to S-TM6). The dimensions of specimens TM1 to TM4 were designed to be equal in steel sectional area for comparison purposes, using the same inner profile dimensions. Specimens TM5 and TM6 possessed thicker outer tubes and were made from S700 high-strength steel.

All columns were tested thermo-mechanically under a constant load level (40% or 30%) applied by a 5000 kN hydraulic jack and an increasing temperature provided by a 10 kW electric furnace [8]. The applied load was calculated by computing the plastic resistance to axial compression of the columns as stated in Clause 6.7.3.2 of EN1994-1-1 [20] and multiplying the obtained values by the designated load level.

3.1. Validation of the thermal response

The thermal response of the columns was validated by comparing the data collected from the thermocouple locations in the experimental tests with the temperature evolution of the model in that location. The thermocouples were placed in the mid-section of the column, and the temperature of several parts of the SR-CFST column was recorded: steel profile flanges and web, concrete core at different depths, and outer steel tube. The concrete moisture content was measured at the time of the test for both mixtures. The considered moisture percentage for each specimen is included in Table 1. Fig. 4 shows an example of the numerically predicted temperature field across the section for specimen SR-CFST-S-TM1 [8] at two standard fire periods (60 and 120 min).

A comparison between the experimentally obtained temperatures and the numerical values from the FE model is included in Figs. 5-7 for specimens TM0 (empty tubes), TM1 to TM4 (SR-CFST with normal strength steel outer tube) and TM5 and TM6 (SR-CFST with high strength steel outer tube), respectively.

It is worth mentioning that the furnace temperature started in the range of 200 °C in the experiments, as an initial pre-heating was prescribed inside the furnace chamber in order to overcome the elevated thermal inertia of the electric furnace and allow for a faster heating of the columns.

As can be observed, the temperature recordings at the outer steel tube (TC1) differed in some cases from the numerically calculated ones (e.g. SHS-TM0, SR-CFST-C-TM3, SR-CFST-C-TM4). It should be taken into account that the external thermocouples were attached to the mid-section of the outer tube, which expanded significantly as the temperature raised, therefore creating a fluctuation on the measurements
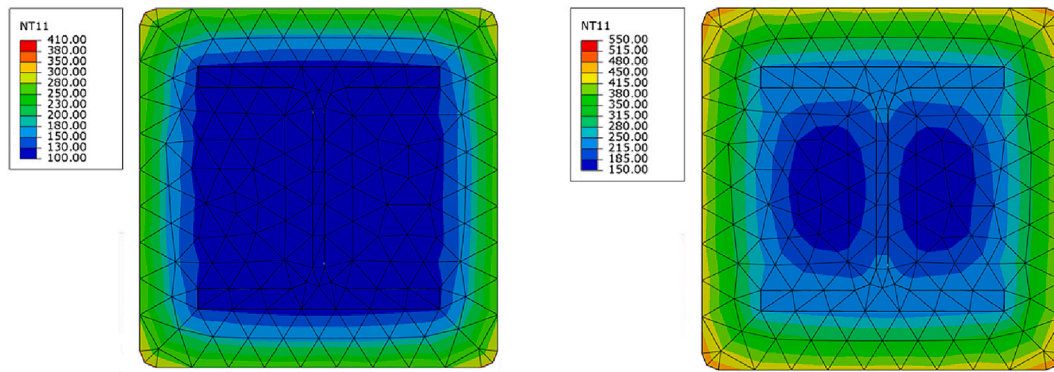
Table 1
Details of the tested specimens [8] used for the validation of the numerical model.*

Specimen	D o B (mm)	t (mm)	Inner profile	Moist. (%)	f_y (MPa)	f_c (MPa)	f_a (MPa)	μ (%)	t_{exp} (min)	t_{num} (min)	$\frac{t_{exp}}{t_{num}}$
CHS-TM0	273	6.3	–	–	413.33	–	–	40	63	–	1.14
SR-CFST-C-TM1	273	6.3	HEB140	6.28	413.33	29.73	315	40	267	240.53	1.07
SR-CFST-C-TM2	273	6.3	HEB140	6.28	413.33	29.73	777	40	405	358.02	1.06
SR-CFST-C-TM3	273	6.3	HEB140	2.11	413.33	86.16	315	40	317	303.02	0.98
SR-CFST-C-TM4	273	6.3	HEB140	2.11	413.33	86.16	777	40	383	389.02	1.16
SHS-TM0	220	6.3	–	–	495.84	–	–	40	43	–	1.03
SR-CFST-S-TM1	220	6.3	HEB140	6.28	495.84	29.73	315	40	239	201.01	1.09
SR-CFST-S-TM2	220	6.3	HEB140	6.28	495.84	29.73	777	40	308	299.71	1.04
SR-CFST-S-TM3	220	6.3	HEB140	2.11	495.84	86.16	315	40	285	260.57	1.03
SR-CFST-S-TM4	220	6.3	HEB140	2.11	495.84	86.16	777	40	294	283.81	0.96
SR-CFST-S-TM5	250	10	HEB140	6.28	824	29.73	315	30	274	267.19	1.14
SR-CFST-S-TM6	250	10	HEB140	2.11	824	86.16	777	30	395	414.02	1.07

* Note: D and B are the outer diameter or dimension for circular and square sections respectively; t is the outer steel tube thickness; f_y and f_a are the yield strength of steel for the inner embedded section and outer steel tube respectively; f_c is the concrete cylinder compressive strength; μ is the load level; t_{exp} is the experimental failure time; and t_{num} is the numerically calculated failure time.

Fig. 4. Numerically obtained temperature fields of the SR-CFST-S-TM2 stub column tested by the authors [8] at a) 60 min and b) 120 min.
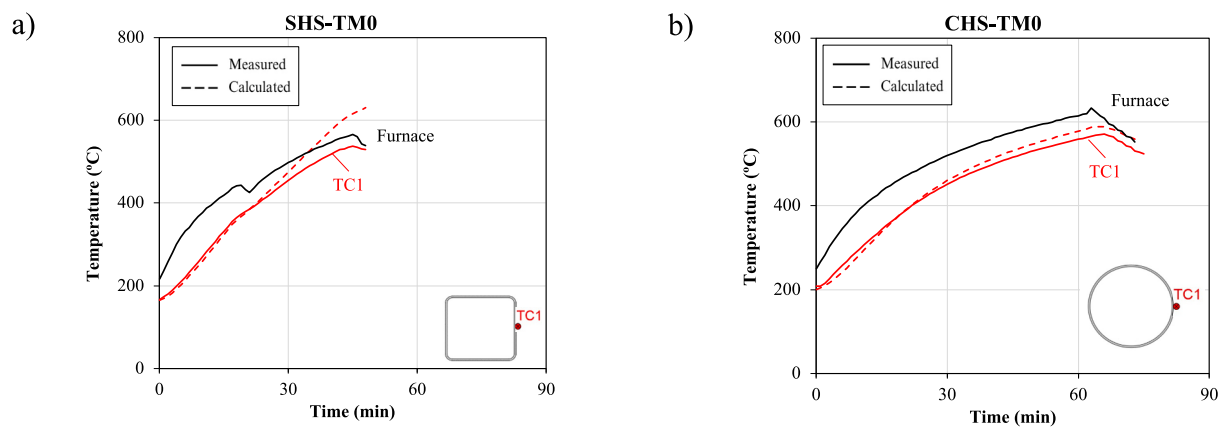

Fig. 5. Comparison between measured and computed temperature–time curves for the reference specimens (empty tubes) a) SHS-TM0 and b) CHS-TM0.

which may be responsible for the differences found between the computed and the experimental values.

3.2. Validation of the mechanical response

The mechanical response of the columns under fire was validated by simulating numerically the previously presented column specimens from the experimental campaign [8]. The boundary conditions for the validation were modelled as pinned-fixed (P—F) as they were considered the most accurate to the experimental conditions of the tests (hinge at the top, welded at the bottom).

The experimentally described time-displacement curves and the resulting failure times were compared with the ones obtained from the FE simulations. Table 1 shows the relative error of the numerical predictions, t_{exp}/t_{num}, in terms of failure time, where values greater than 1 mean safe predictions and lower than 1 mean unsafe predictions. An average value of 1.06 and a standard deviation of 6% were obtained, which denotes a good agreement and consistency between the numerically modelled cases and the experimental tests.

Fig. 8 compares the deformed shape for one of the experimentally tested columns and the one obtained with the FE model. As can be observed, there is good agreement between the failure mode of the column and the bulge location showed at the outer tube.

Additionally, Figs. 9-11 include a comparison between the experimental and numerical axial displacement versus time curves for the ten column specimens used for validation, showing good agreement between the numerical model and the experiments.

3.3. Sensitivity study of the mechanical properties of high-performance materials

Several models from the international design codes, together with those available in the revised literature were tested to select the most appropriate for the numerical model.

Regarding the material properties of steel, Qiang et al. [21] presented a series of experimentally obtained coefficients for high-strength steel grade S690 at temperatures between 20 and 700 °C. The research conducted by Li & Young [22] studied experimentally the material properties of high-strength steel that ranged from 690 to 960 MPa exposed to temperatures up to 1000 °C. Shakil et al. [23] presented several coefficients for the mechanical properties of S700 MC steel at temperatures up to 800 °C. Li & Song [24] investigated the mechanical properties of TMCP Q690 HSS at high temperatures ranging from 200 to 800 °C. Finally, as the range of application of EN1993-1-2 has been extended up to steel grades of S700 [25], it will also be considered in this sensibility study. The models from Qiang et al. [21], Li & Young [22], Shakil et al. [23], Li & Song [24] and EN1993-1-2 [26] are tested for specimens S-TM2 and C-TM2.

Concerning the mechanical properties of high-strength concrete, Phan and Carino (2003) [27] presented a strength-temperature relationship for high-strength concrete based on the results of several experiments. Kodur et al. [28], proposed a numerical model to predict the behaviour of high-performance concrete (HPC) columns exposed to fire. Matsudo et al. (2008) [29] also conducted experimental tests for HSC specimens at temperatures between 100 and 800 °C and proposed mathematical expressions to characterise the mechanical behaviour of the material. Other authors developed a constitutive relationship for both normal and high-strength concrete exposed to fire, where both the compressive and tensile properties of HSC were studied (2011) [30]. The
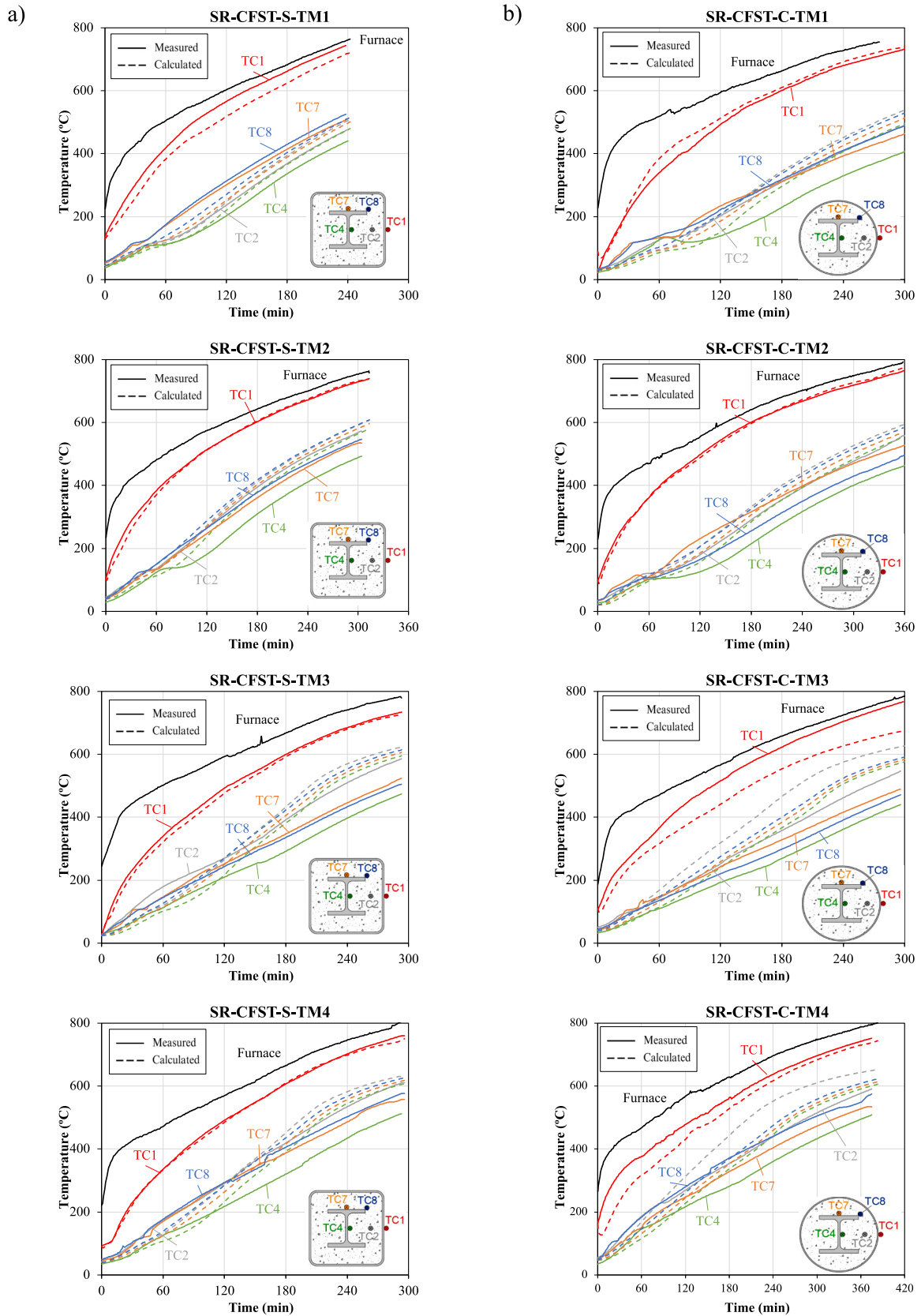
a)

b)

Fig. 6. Comparison between measured and computed temperature–time curves for a) square and b) circular SR-CFST specimens TM1 to TM4.

a)
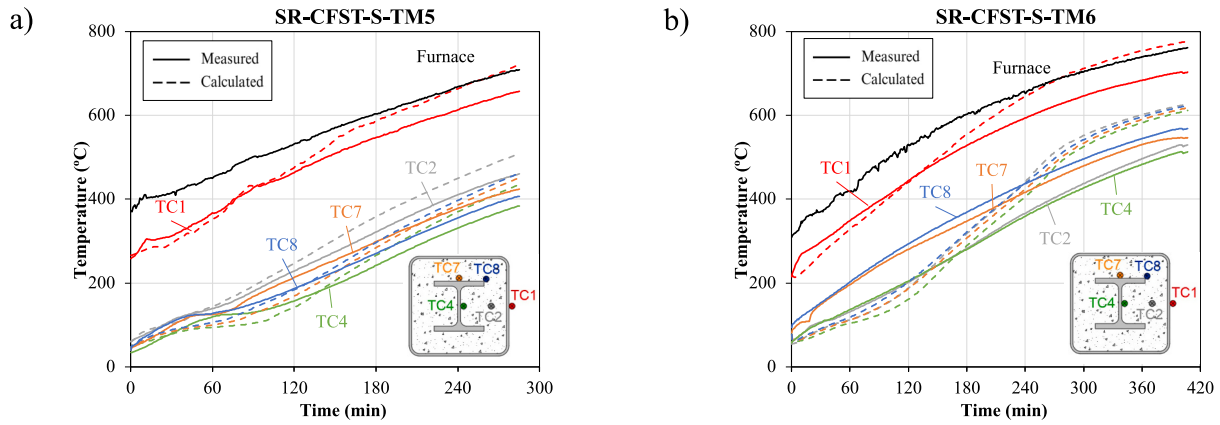
SR-CFST-S-TM5

b)

SR-CFST-S-TM6

Fig. 7. Comparison between measured and computed temperature–time curves for the SR-CFST specimens a) S-TM5 and b) S-TM6.

Fig. 8. Comparison between the experimental and numerical deformed shape for specimen SR-CFST-S-TM1.

models from Kodur et al. [28], Phan and Carino [27], Matsudo et al. [29], Aslani and Bastami [30] and the provisions included in the new draft of prEC1992-1-2:2021–09 [31] were tested for specimens S-TM3 and C-TM3.

Fig. 12 shows a comparison between the different steel models used in specimens SR-CFST-S-TM2 and SR-CFST-C-TM2, in which the inner steel profile was made of high-strength steel while the materials of the concrete infill and steel outer tube remained as normal-strength. This

way, the influence of the selected steel model can be isolated from the other material variables. Even though the coefficients indicated by Qiang et al. [21] have a good agreement in the S-TM2 specimen (see Fig. 12.a), they fail to predict the steel behaviour in the circular case adequately (see Fig. 12.b). As can be observed, while all the tested models provide good agreement with the experimental results, the model that gives the most precise simulations is the EN1993-1-2 [26] used following the indications of EN1993-1-12 [25] which extends the scope of the code to steels up to 700 MPa. As it can be seen, this material model provides the best agreement in terms of failure time.

A comparison between the previously mentioned high-strength concrete material models is included in Fig. 13. Experimental cases S-TM3 and C-TM3 are included as they are the only specimens with high-strength concrete in the infill with a normal-strength steel inner profile. The validation shows a good agreement of the numerical response when the Aslani and Bastami [30] material model is used. This model reduces the mechanical degradation of concrete, extending its failure time further than the rest of the compared models. As can be observed, the other models provide a rather conservative response, slightly more accurate in the case of prEN1992-1-2 [32] and Kodur et al. [28] formulation. Consequently, as the prEN1992-1-2 provides relatively precise and conservative results, it will be employed to conduct parametric studies on SR-CFST sections.

4. Parametric studies

Once the numerical model was thermo-mechanically validated, a parametric study was conducted. An extensive set of analysis cases was designed to analyse the influence of several parameters on the fire behaviour of SR-CFST sections.
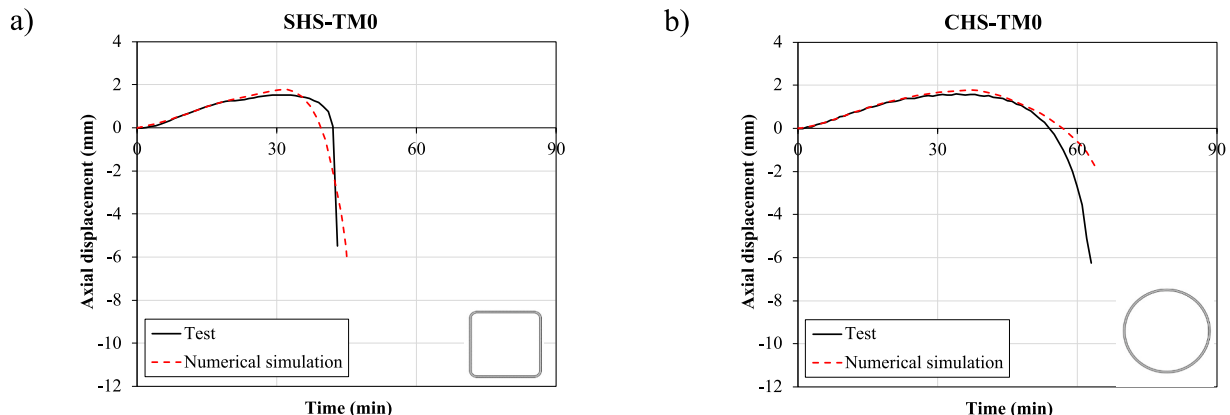
a)

SHS-TM0

b)

CHS-TM0

Fig. 9. Comparison between measured and computed axial displacement–time curves for specimens TM0, a) square, b) circular.
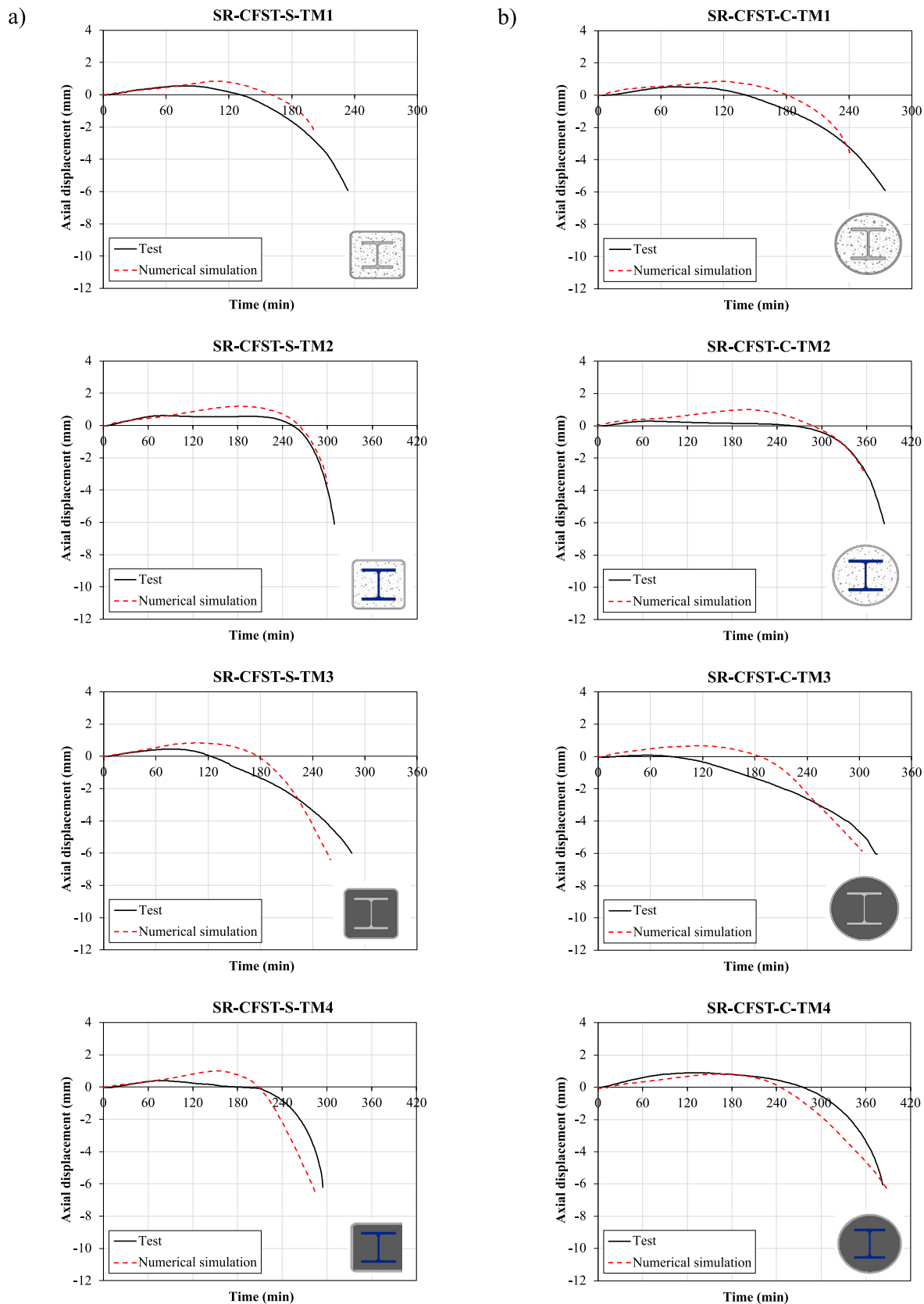
Fig. 10. Comparison between measured and computed axial displacement–time curves for specimens TM1 to TM4, a) square, b) circular.
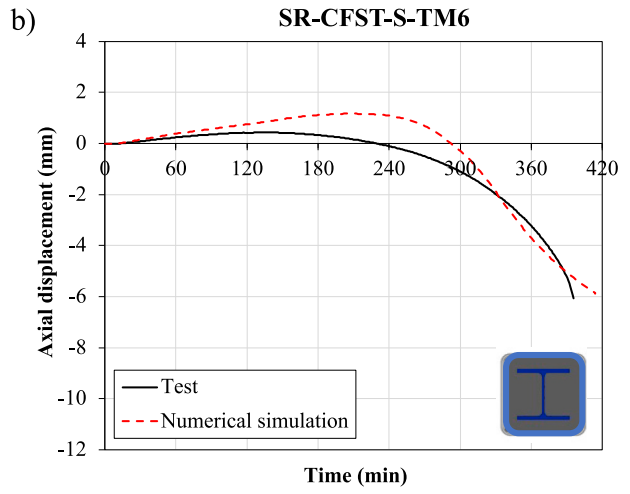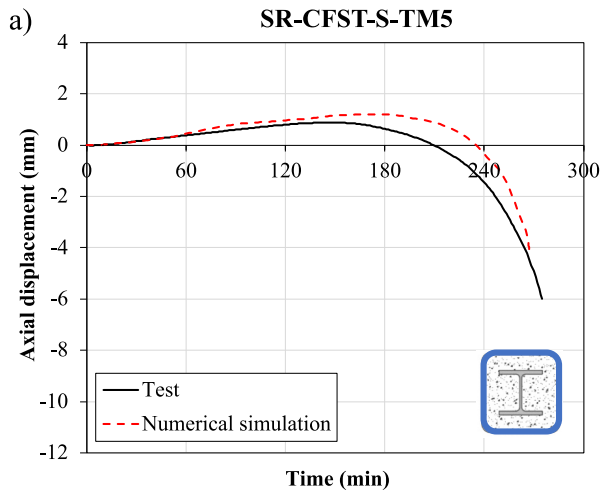
Fig. 11. Comparison between measured and computed axial displacement–time curves for specimens TM5 (a) and TM6 (b).
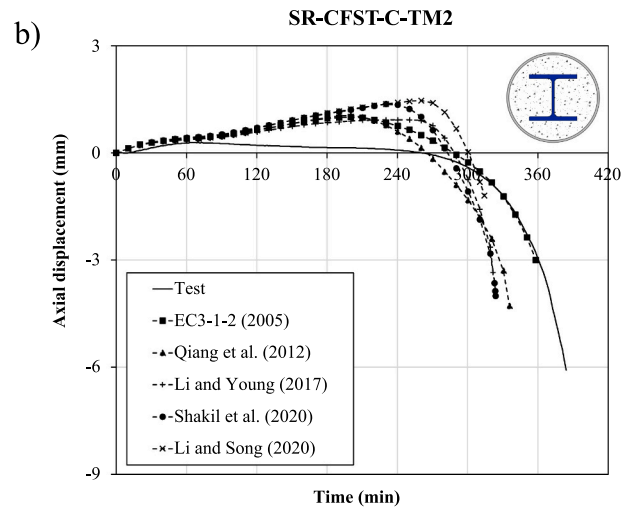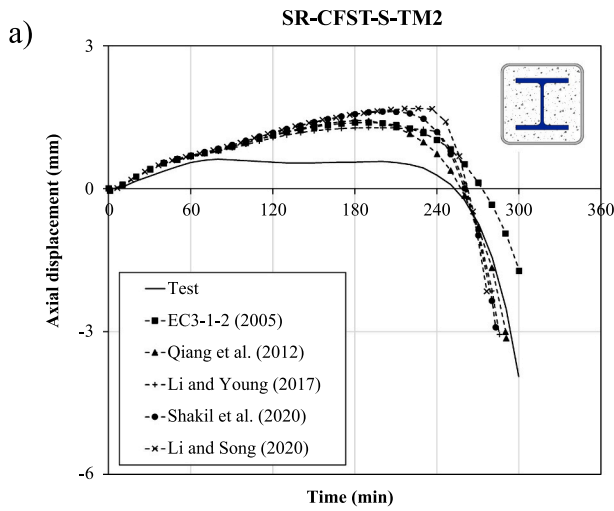

Fig. 12. Sensitivity analysis on the HSS material models for specimens a) SR-CFST-S-TM2 and b) SR-CFST-C-TM2.
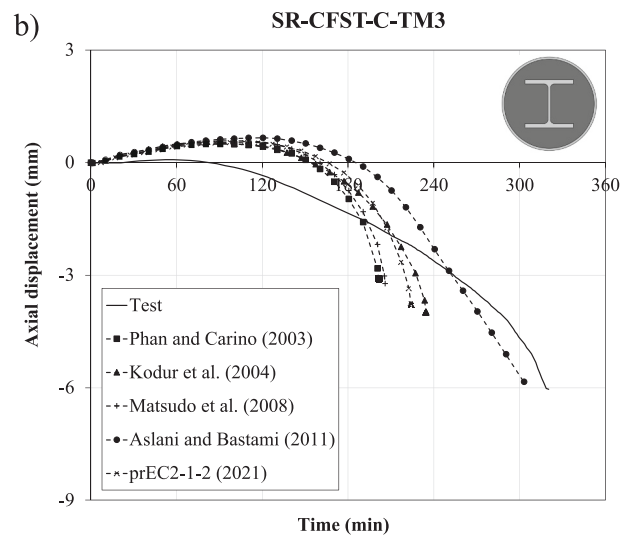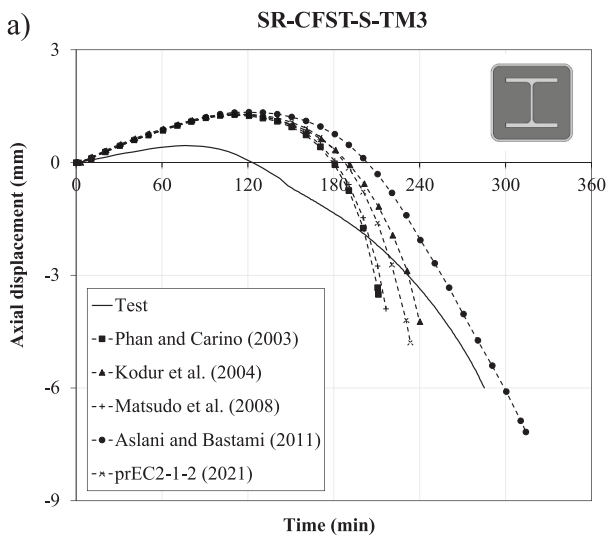

Fig. 13. Sensitivity analysis on the HSC material models for specimens a) SR-CFST-S-TM3 and b) SR-CFST-C-TM3.

4.1. Composite section used in the parametric study

The studied parameters were the outer dimensions of the SR-CFST section (*D* for the circular cases and *B* for the square ones), the thickness of the outer steel tube (*t*), the inner steel profile dimensions (expressed in terms of the cross-sectional inner steel area over the concrete infill area, A_{sp}/A_c), the load level (*μ*), the inner concrete compressive strength (*f_c*) and the inner steel profile yield strength (*f_y*). The designed dimensions for the parametric study combinations were selected based on the commercially available sections. Table 2 shows the combination of the parameters, resulting in a total of 1440 analysis cases, 720 circular and 720 square shaped, respectively.

For all the analysis cases, the relation between the area of the inner steel profile and the concrete core was within the range $0.04 \leq A_{sp}/A_c \leq 0.13$. The minimum concrete cover, defined as the distance from the centre of an embedded element (i.e., web or flanges of the steel profile) to the concrete outer surface, was set to $u_s \geq 35\ mm$. Both square and circular cases were designed to have a similar amount of total steel area (steel tube + inner profile), with a maximum difference of less than a 4%. Slender sections (i.e. Class 4) were also included among the hollow sections selected for the parametric studies. The boundary conditions of all the column specimens was set to "Pinned – Pinned" (P—P). The relation between the length of the columns and the outer dimension of the cross-section (L/D or L/B) was set to 1.5.

Three different concrete compressive strengths were used: 30, 60 and 90 MPa. The yield strength of the outer steel tube was maintained in all cases equal to 355 MPa, while the inner steel profile yield strength was varied between 275, 355, 460 and 690 MPa. The material combinations between the inner steel profile and the concrete infill were designed to meet the criteria established by Liew et al. [33], except for the cases with the highest steel strength (690 MPa), which are incompatible with any of the studied concrete mixes, according to these recommendations. It is worth mentioning that these suggestions are valid for CFST sections, and should be re-evaluated for steel-reinforced CFST columns.

For the thermal properties of steel, the coefficients included in Section 3.4 of EN1993-1-2 [26] were used. For the reduction factors of the mechanical properties of steel at elevated temperatures, Table 3.1 of the same code was used. As EN1993-1-12 [25] extends the field of application of EN1993-1-2 [26] to steels up to 700 MPa, the same coefficients were used for all the steels included in the parametric study.

Regarding the thermal properties of concrete, the coefficients included in Section 3.3 of EN1992-1-2 [32] were employed. The concrete moisture content was considered equal to 4% in all cases, as per Clause 3.3.2(7) of EN1994-1-2 [14]. For normal strength concrete, the mechanical reduction coefficients of Table 3.1 in EN1992-1-2 [32] were used, while the values given in Table 6-1N of the same code were utilized for the high-strength concrete elevated temperature reduction factors, which are more severe at as compared to the normal-strength concrete reduction coefficients.

4.2. Analysis of the results of the parametric study

Figs. 14-17 show the results of the parametric study regarding the effect of the studied parameters on the fire resistance of the SR-CFST columns. The vertical axis of the graphs represents the failure time (*FT*) of each column represented in minutes. The influence of the outer steel tube thickness (in terms of the cross-sectional slenderness, *D/t* or *B/t*), the section factor (A_m/V), the inner steel profile dimensions (through the A_{sp}/A_c ratio and the concrete cover, *c*) and the material properties of the concrete and steel is evaluated next. The influence of the different geometrical parameters was studied by subdividing all the analysis cases into smaller groups depending on their material properties. By doing so, the parameter influence could be isolated, and stronger conclusions could be drawn from the results.

4.2.1. Influence of the outer tube thickness

The cross-sectional slenderness (*D/t* or *B/t*) of the columns has a linearly positive influence on the failure time, as can be seen in Fig. 14. This effect is reduced when the load level is increased, its effect being notable in lower load levels (30%), less influential in medium levels (50%) and barely noticeable for high-load levels (70%). For a fixed outer dimension, when the *D/t* (or *B/t*) value is increased, the outer steel tube area decreases (thinner hollow section), increasing the quantity of embedded concrete as a result. As the outer steel section is directly exposed to fire, it degrades rapidly, losing most of its load-bearing capacity; by cutting the amount of material in this area the column capacity is enhanced. The effect decreases as the load level rises, as in higher load levels, the rapid loss of mechanical capacities in the outer tube transfers a considerable amount of load to the inner parts of the sections, which they cannot bear, not taking advantage of the added

Table 2
Combination of analysis cases for the parametric studies.

CIRCULAR CASES									
D (mm)	244.5		273		323.9		457		508	
t (mm) (D/t)	6.3 (39)	10 (24)	6.3 (43)	10 (27)	6.3 (51)	10 (32)	8 (57)	10 (46)	10 (51)	12.5 (41)
μ				0.3–0.5–0.7						
f_y (MPa)				275–355–460–690						
***f_c (MPa)**				C30/37 – C60/75– C90/105						
Profiles (A_{sp}/A_c)	HEB100 (0.07) HEB120 (0.09)	HEB100 (0.07) HEB120 (0.09)	HEB100 (0.05) HEB140 (0.09)	HEB100 (0.05) HEB140 (0.09)	HEB120 (0.05) HEB180 (0.09)	HEB120 (0.05) HEB180 (0.10)	HEB160 (0.04) HEB260 (0.08)	HEB160 (0.04) HEB260 (0.09)	HEB180 (0.04) HEB300 (0.09)	HEB180 (0.04) HEB300 (0.10)
SQUARE CASES										
B (mm)	200		220		260		350		400	
t (mm) (B/t)	6.3 (32)	10 (20)	6.3 (35)	10 (22)	6.3 (41)	10 (26)	8 (44)	10 (35)	10 (40)	12.5 (32)
Load (%)				30–50–70						
f_y (MPa)				275–355–460–690						
***f_c (MPa)**				C30/37 – C60/75– C90/105						
Profiles (A_{sp}/A_c)	HEB100 (0.08) HEB120 (0.11)	HEB100 (0.09) HEB120 (0.12)	HEB100 (0.06) HEB140 (0.11)	HEB100 (0.07) HEB140 (0.12)	HEB120 (0.06) HEB180 (0.12)	HEB120 (0.06) HEB180 (0.13)	HEB160 (0.05) HEB260 (0.12)	HEB160 (0.05) HEB260 (0.12)	HEB180 (0.05) HEB300 (0.13)	HEB180 (0.05) HEB300 (0.13)

* **Note:** The considered cylinder strength for the mixtures was 30 MPa, 60 MPa and 90 MPa, respectively.
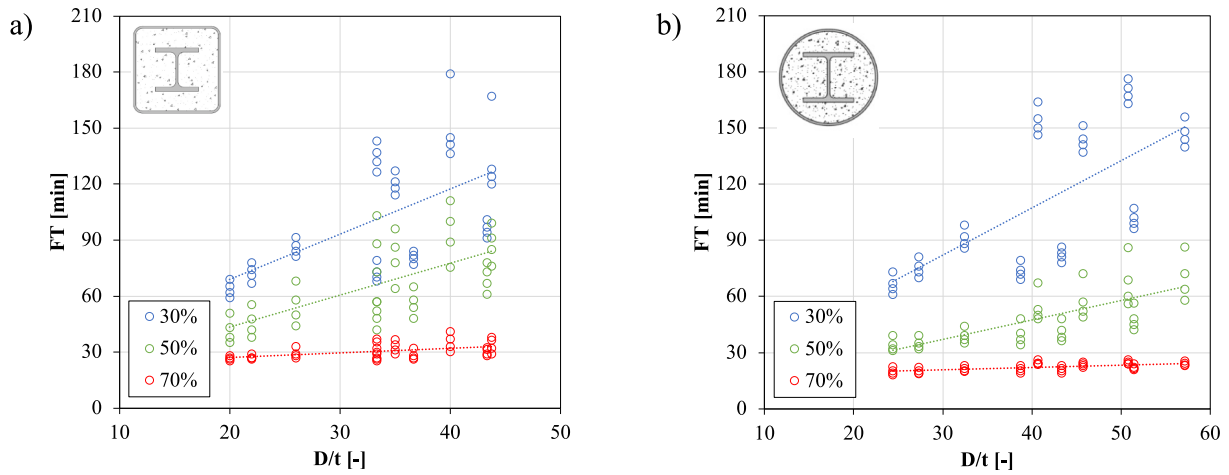
Fig. 14. Influence of the cross-sectional slenderness over the failure time of SR-CFST stub sections with both square (a) and circular (b) sections.
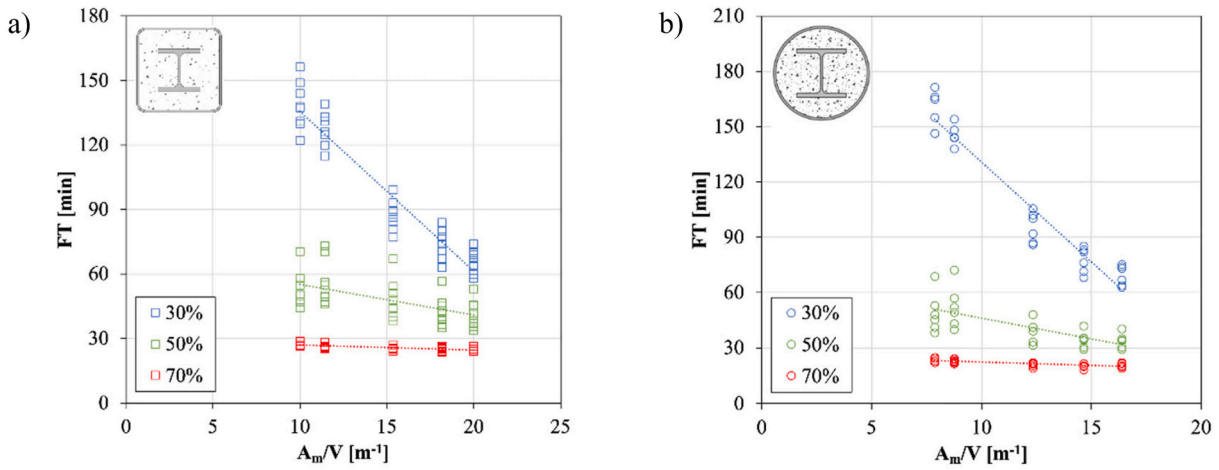

Fig. 15. Influence of the section factor (A_m/V) over the failure time of SR-CFST stub sections with both square (a) and circular (b) sections.
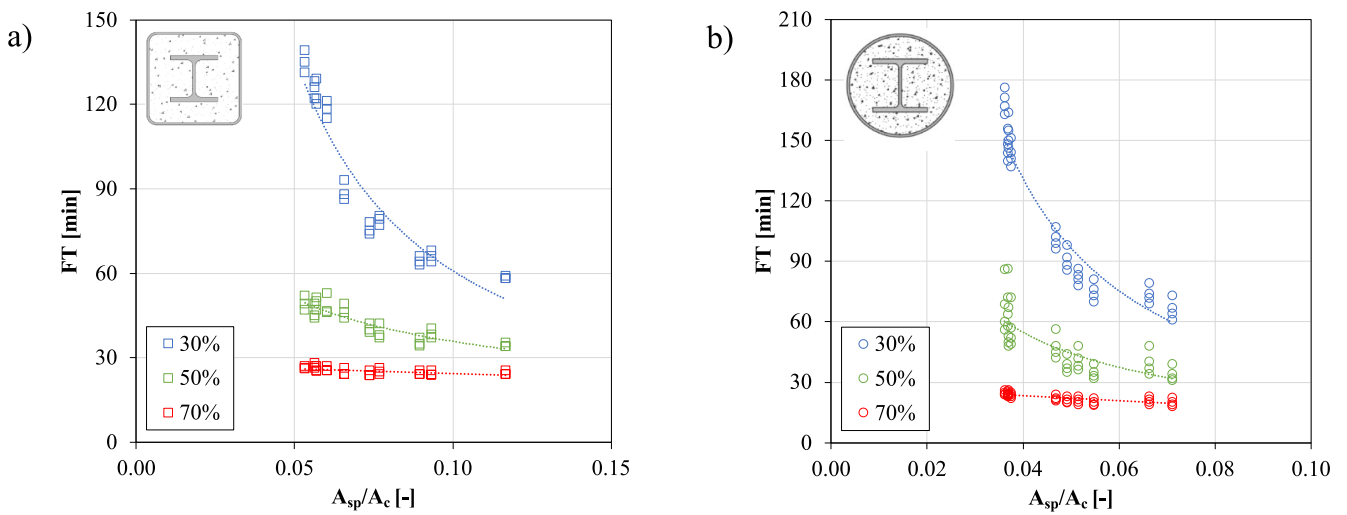

Fig. 16. Influence of the inner steel ratio (A_{sp}/A_c) over the failure time of SR-CFST stub sections with both square (a) and circular (b) sections.

thermal protection.

For the highly-loaded cases (70% load ratio) the cross-sectional slenderness appears to have almost no influence over the failure time of the columns. In these cases, the range of failure times obtained were

similar, as the column specimens fail right after the outer steel tube has lost its load-bearing capacity, since after that point, the concrete infill and inner steel profile are not able to sustain the applied load on their own.
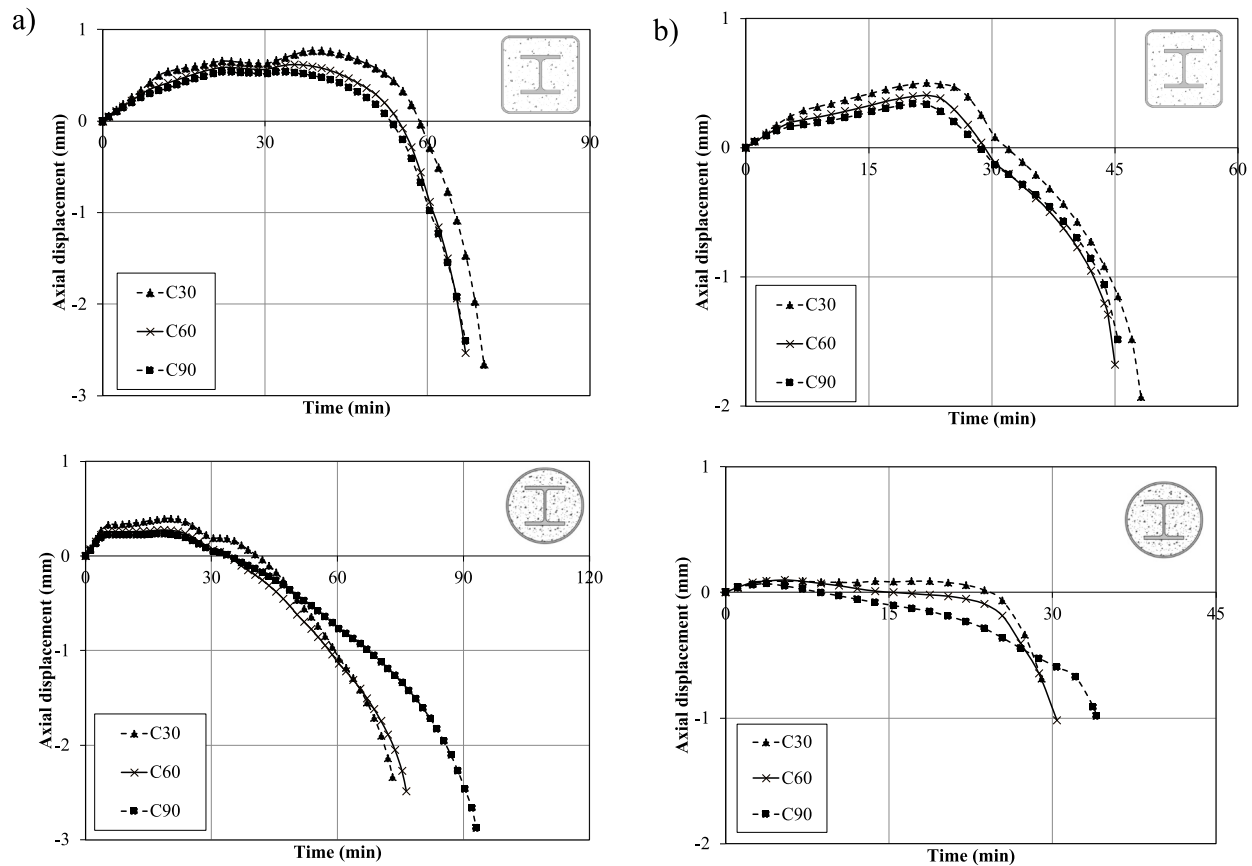
Fig. 17. Axial displacement-time curves comparing the three studied concrete grades of SR-CFST stub columns with both square (a) and circular (b) sections.

4.2.2. Influence of the section factor

Fig. 15 shows the influence of the section factor (A_m/V) parameter over the failure time of the SR-CFST columns. It is worth noting that the section factor (A_m/V) in a steel profile is defined as the fire-exposed perimeter of the section divided by the total steel area. In the case of SR-CST sections, despite this concept may have a different interpretation for composite sections, the section factor is defined by the authors similarly, by dividing the fire-exposed perimeter over the total area of the section (concrete plus steel), as it is also defined for partially encased sections in Annex G of EN1994-1-2 [14], as well as in the new method for CFST columns in Annex H of prEN1994-1-2:2021 [15]. [14] Consequently, in circular SR-CFST sections, the section factor is calculated as: $A_m/V = P_m/A = \pi D/(\pi D^2/4) = 4/D$, while in square SR-CFST sections as: $A_m/V = P_m/A = 4B/B^2 = 4/B$.

The section factor defines the quantity of exposed steel area to the fire source related to the volume of the member, which gives an insight into the influence of both the outer shape and the dimensions of a column. As can be observed, the relation is linearly negative, with more influence at lower load levels. As the section factor increases, a higher area is exposed to fire, resulting in faster column heating and, therefore, rapid degradation of the mechanical properties of steel and concrete. The included graphs are filtered by concrete mixture (C60) in the case of Fig. 15.a and by the steel yield strength in the case of Fig. 15.b The same relation is obtained in any other combination, but only these are included for clarity. Note that, for circular columns, the section factors tend to be lower than their square counterparts, thus resulting in better fire performance and slower degradation of the columns.

4.2.3. Influence of the dimensions of the inner profiles

The relation between the steel profile area and the concrete infill area (A_{sp}/A_c) studies the influence of the embedded steel profile

dimensions. To adequately study the influence of this parameter, the cases are compared by filtering them by concrete strength and steel profile grade. Therefore, Fig. 16 shows a comparison, one for square cases (Fig. 16.a) filtered by steel profile grade (S275) and one for circular cases (Fig. 16.b) filtered by concrete compressive strength (C90) in which the FT is plotted against the A_{sp}/A_c of the sections. The results show that a reduced A_{sp}/A_c provides better results as the inner steel is more protected and stays unaffected by thermal degradation. This effect is enhanced at low load levels and loses importance as the load increases.

4.2.4. Influence of the material properties

Concrete

The effect of the compressive strength of the concrete infill of the section is included in several examples of different sizes and geometries (see Fig. 17). The influence of this parameter must be analysed, considering the composition of the concrete mixes and their compressive strength. High-strength concrete has a different mechanical behaviour than normal-strength concrete, having a faster reduction in their mechanical capacity (almost double) at high temperatures (> 600 °C). Therefore, the added strength of the concrete is balanced by its worse thermal behaviour, reducing the influence of this parameter in the overall thermo-mechanical behaviour of the column. An example is the better mechanical behaviour of the lowest compressive strength (30 MPa) compared to the mixture with $f_c = 60$ MPa.

The results obtained are presented separately for the three studied concrete grades. While in the square cases, a significant percentage of the C30 cases have a higher failure time than the C90 cases, the opposite happens when analyzing the circular cases (see Table 3). Several factors may cause this phenomenon, a significant one being the slower temperature evolution in the circular cases due to a smaller section factor than square ones. A faster heating of the section causes the concrete to

Table 3
Influence of the concrete compressive strength over the failure time of the columns.

	$FT_{C30} > FT_{C90}$	$FT_{C90} > FT_{C30}$
Square	83.33%	16.67%
Circular	27.08%	72.92%

degrade, therefore losing most of its mechanical capacity. As the formulation indicates, the high-strength concrete mixtures lose capacity quicker than the normal-strength concrete at high temperatures, causing premature column failure in those cases for square columns. The processes are reversed in circular columns: the temperatures at the inside of the cross-section are lower, and the C90 concrete sustains its mechanical properties for longer, therefore bearing the load longer than the C30 mixture. The C60 mixture was the least favourable option of the three.

Steel

The influence of the steel profile yield strength (f_y) can be observed for several sections (different geometries and sizes) in Fig. 18. As can be observed, the influence of the steel grade is positive, effectively increasing the load-bearing capacity of the SR-CFST columns in all cases. Due to its location in the cross-section, the inner profile is inherently protected by the outer steel tube and the surrounding concrete. Henceforth, a stronger steel grade in this element provides a higher fire resistance as this profile remains below 400 °C long, thus retaining all of its mechanical capacities.

The effect is most prominent at lower load ratios but can be observed in higher loads, see Fig. 18. This may be explained by the application of a load level dependent on the room temperature capacity of the sections. As the steel grade directly influences that parameter, the load applied to steel sections with higher steel grades tends to be increased. When the load is transferred to the concrete and steel profile at high load levels, the column rapidly fails, not having time to benefit from this increase in the load-bearing capacity of the thermally protected section.

4.2.5. Summary of the analysis results

Through the results of the parametric study, it was found that the section factor has a negative direct effect on the temperature evolution of the sections. A higher section factor indicates a higher exposed area of steel as related to the member volume, therefore resulting in a faster heating of the column cross-section and a a worse thermo-mechanical behaviour. Regarding the SR-CFST columns, the influence of the outer steel tube dimensions has been found to be influential, as the increase in the cross-sectional slenderness (D/t or B/t), meaning a reduction in the thickness of the tube, has been found to enhance the fire behaviour of the columns. The inner steel profile dimensions also affect the fire

resistance of the columns, as including a smaller profile has proven to be a better option than a higher one in the fire scenario, as it remains unaffected for a more extended time and retains its mechanical properties intact for a longer period.

Regarding the influence of the materials, introducing a high-strength steel profile has proven to positively influence the fire behaviour of the SR-CFST column compared to normal-strength ones. On the other hand, the concrete compressive strength has a mixed influence. While stronger concrete can enhance the mechanical behaviour of the column, its faster degradation at high temperatures reduces its beneficial properties when in fire. All these insights will be used in the next section to develop a simplified model for predicting the plastic resistance of SR-CFST columns under fire conditions.

5. Development of a simplified calculation method for SR-CFST stub columns exposed to FIRE

When assessing the capacity of steel-concrete structures under the fire action, the reference code in Europe is EN1994-1-2 [14]. While this design code includes provisions for both totally and partially concrete encased columns as well as for concrete-filled tubular columns, there is no specific guidance for the novel typology studied in this investigation, which is a combination of both types. The authors previously addressed this issue in a numerical investigation that studied the thermal behaviour of these sections. While the code does not provide any simplified process to obtain the temperature field in an SR-CFST cross-section, the previous study [16] provided a simple method that predicted an equivalent temperature for each cross-section part: concrete core, web and flanges of the steel profile and outer steel tube, see Fig. 19.

In this investigation, the previously proposed equivalent temperature equations are used to predict -a simplified temperature field, and with those, the cross-sectional plastic resistance of the column after a certain fire exposure time is obtained. This way, the previous thermal method is extended to a full thermo-mechanical proposal, providing a new procedure to obtain the fire design plastic resistance of SR-CFST that fills an existing gap in the normative.

5.1. Application of the previous simplified method for the temperature field of SR-CFST sections

Initially, the simplified cross-sectional temperature field method proposed by the authors [16] is applied to the sections of the parametric study. The formulation used for obtaining the corresponding equivalent temperatures is included hereafter:
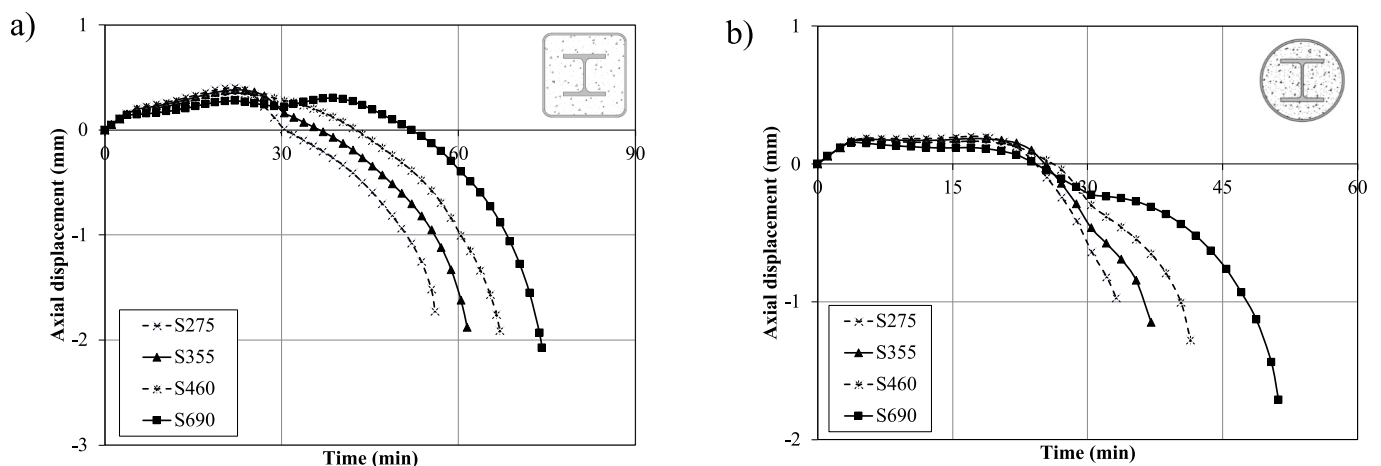
Fig. 18. Displacement-time curves comparing the three studied concrete grades of SR-CFST stub columns with both square (a) and circular (b) sections.
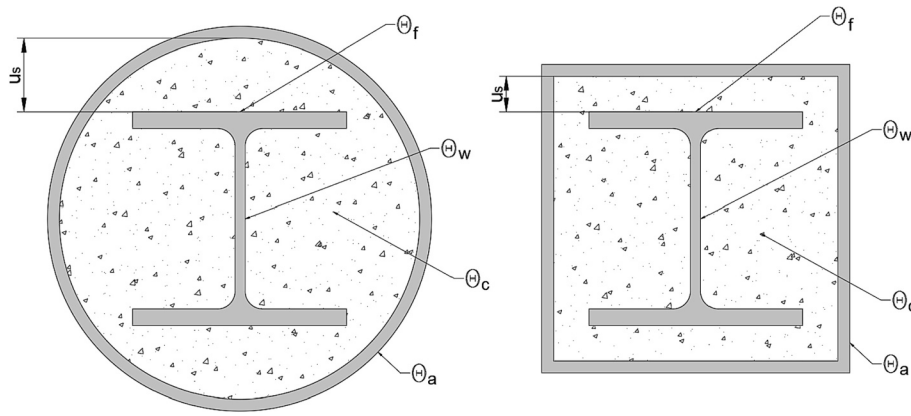
Fig. 19. Equivalent temperatures of the different parts of the composite section and definition of the parameter u_s in circular and square SR-CFST columns, extracted from [16].

$$\theta_{a,eq} = -824.667 + 5.579R + 0.007R^2 - 0.009R\left(A_m/V\right) + 645.076R^{0.269}(A_m/V)^{0.017} \tag{6}$$

$$\theta_{c,eq} = a_1 + b_1R + b_2R^2 + c_1(A_m/V) + c_2(A_m/V)^2 + d_1R(A_m/V) + e_1R^{f_1}(A_m/V)^{f_2} + g_1(A_{sp}/A_c) \leq 1200^oC \tag{7}$$

$$\theta_{f,eq} = a_1 + b_1R + b_2R^2 + c_1(A_m/V) + c_2(A_m/V)^2 + d_1R(A_m/V) + e_1R^{f_1}(A_m/V)^{f_2} + g_1u_s \tag{8}$$

$$\theta_{w,eq} = a_1 + b_1R + b_2R^2 + c_1(A_m/V) + c_2(A_m/V)^2 + d_1R(A_m/V) + e_1R^{f_1}(A_m/V)^{f_2} + g_1\left(A_{sp}/A_c\right) + g_2\left(A_{sp}/A_c\right)^2 \tag{9}$$

where the values of the coefficients a_1 to g_2 depend on the shape of the cross-section and are given in [16].

Therefore, the equivalent temperatures of the outer tube, concrete infill and the flanges and web of the inner steel profile are obtained for each section at the numerically obtained failure time. (see Fig. 19). Based on these, the steel and concrete temperature-dependent mechanical degradation coefficients are obtained. For steel, the coefficients are extracted from Table 3.2 of EN1994-1-2 [14] for both normal and high-strength steel. The coefficients for normal-strength concrete are extracted from Table 3.3 of EN1994-1-2 [14], while the values for high-strength concrete are obtained from Table 5.1 of prEN1992-1-2 [32].

The mechanical contribution of each of the parts of the section is then computed by multiplying its reduced material strength by its area to obtain the cross-sectional plastic resistance of the column at elevated temperature, which can be calculated with a simple addition of the components, adapting the expression given in Clause 4.3.5.1(4) of EN1994-1-2 [14] and extending it to include the inner steel profile:

$$N_{fi,pl,Rd} = A_a f_{y,\theta}\left(\theta_{a,eq}\right)/\gamma_{M,fi,a} + A_c f_{c,\theta}\left(\theta_{c,eq}\right)/\gamma_{M,fi,c} + A_f f_{y,\theta}\left(\theta_{f,eq}\right)/\gamma_{M,fi,sp} + A_w f_{y,\theta}\left(\theta_{w,eq}\right)/\gamma_{M,fi,sp} \tag{10}$$

where:

A_i is the area of part i of the cross-section ($i = a$ or c or f or w), where a stands for "outer steel tube", c for "concrete", f for "inner steel profile flanges" and w for "inner steel profile web";

$f_{i,\theta}\left(\theta_{i,eq}\right)$ is the design strength of part i at a temperature $\left(\theta_{i,eq}\right)$ which can be calculated through the reduction factors from Table 3.2 and Table 3.3 of EN1994-1-2 [14];

$\gamma_{M,fi,i}$ is the partial factor for the relevant material property of part i in the fire situation. As Clause 2.3(1) of EN1994-1-2 [14] indicates, these coefficients are assumed to be 1,0 in the fire situation.

5.2. Simplified plastic resistance proposal for SR-CFST sections under fire conditions

As a first approach, the previous expression (Eq. (10)) is directly used to evaluate the plastic resistance of the simulated column specimens in the parametric studies for both circular and square geometries. As shown in Fig. 20, the direct application of Eq. (10) adjusts well for high load levels (70%) but provides unsafe predictions for the reduced load levels (30%), while the intermediate load levels (50%) tend to deviate towards the unsafe side. Therefore, a correction is needed to obtain a robust equation that can be valid for different load levels.

A simple modification of the initial proposal in Eq. (10) is therefore suggested, which consists of adding two homogenization coefficients to the concrete infill and the flanges of the steel profile. It should be mentioned that, when exposed to fire, the flanges of the steel profile and the inner concrete suffer a significant temperature gradient, therefore two coefficients need to be introduced here to "homogenise" this steep gradient and allow for a representation of these parts with a single equivalent temperature each. For the outer steel tube and web of the inner profile, however, this correction is not needed, as their temperature distribution is mostly uniform, therefore they can be easily represented with a single equivalent temperature, regardless the fire exposure time.

Therefore, a modified equation is proposed for evaluating the cross-sectional plastic resistance of SR-CFST columns in fire, by including the homogenization coefficients for the concrete infill and steel profile flanges:

$$N_{fi,pl,Rd} = A_a f_{y,\theta}\left(\theta_{a,eq}\right)/\gamma_{M,fi,a} + k_{c,\theta}A_c f_{c,\theta}\left(\theta_{c,eq}\right)/\gamma_{M,fi,c} + k_{f,\theta}A_f f_{y,\theta}\left(\theta_{f,eq}\right)/\gamma_{M,fi,sp} + A_w f_{y,\theta}\left(\theta_{w,eq}\right)/\gamma_{M,fi,sp} \tag{11}$$

where:

$k_{f,\theta}$ and $k_{c,\theta}$ are the proposed homogenization factors for the steel profile flanges and concrete infill, respectively. The values of these coefficients, which depend on the standard fire exposure time (R), are included in Table 4.

The proposed method is designed to meet the CEN TC250 Horizontal Group Fire [34] accuracy criteria, which are as follows:

- The calculation result shall not be on the unsafe side by more than 15% of the reference result,
- A maximum of 20% of individual calculation results shall be on the unsafe side,
- The mean value of all percentage differences between calculation and reference results shall be safe.
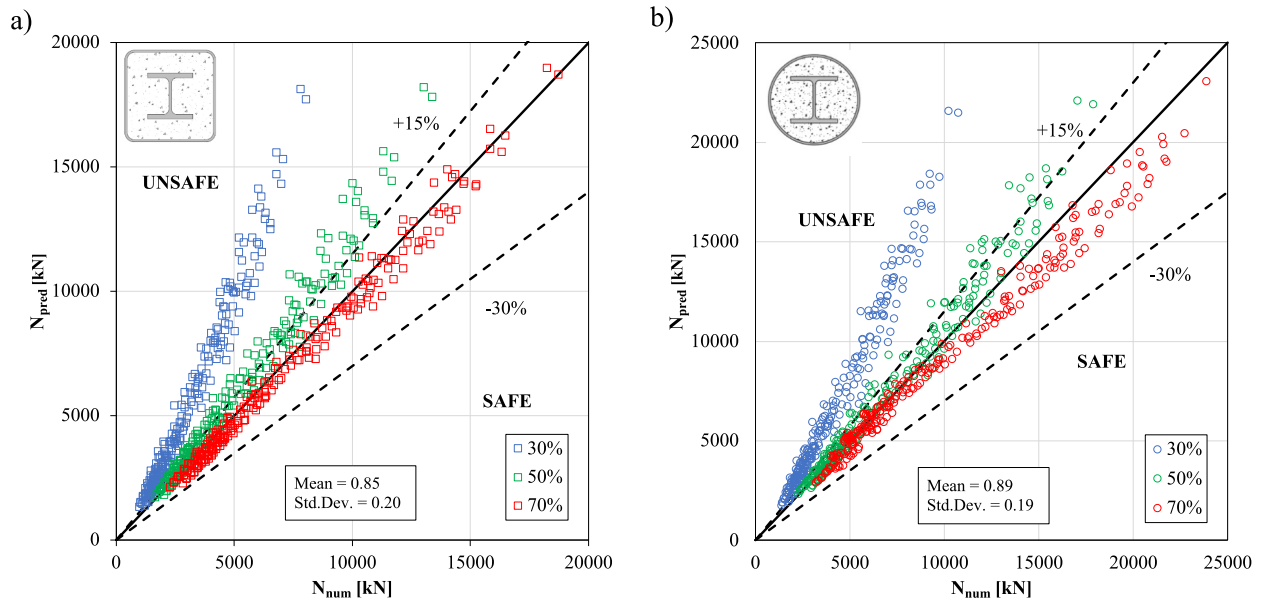
Fig. 20. Numerical vs. predicted fire plastic resistance obtained by directly applying Eq. (10) for a) square and b) circular SR-CFST stub columns.

Table 4
Proposed homogenization factors for the steel profile flanges and concrete infill.

R (min)	$k_{c,\theta}$	$k_{f,\theta}$
30	1.00	1.00
60	0.70	0.70
90	0.60	0.50
120	0.50	0.40
180		

Table 5
Summary of the verification of the CEN TC250 [34] accuracy criteria obtained with the proposed method.

	Maximum error	Unsafe results	Mean value
Square SR-CFST columns	14.90%	12.36%	1.10
Circular SR-CFST columns	12.06%	19.31%	1.09

Table 5 shows the results obtained for these parameters in the comparison with the parametric studies numerical database for both geometries (circular and square), proving that the designed method complies with the reference accuracy criteria.

Fig. 21 shows the predicted results by applying the proposal in Eq. (11) in comparison with the numerically predicted plastic resistance for all the analysis cases of the parametric studies.

As it can be seen, a good agreement is found for the two sets of data (circular and square columns) and the prediction results are quite homogeneous for the different load levels studied. Therefore, it is proved that the proposed design method improves the accuracy of the existing equation, with conservative and reliable results.

5.3. Applicability limits of the proposed method

The applicability limits of the previously presented simplified calculation method are as follows:

- For circular SR-CFST stub columns:

$$7.5 \leq A_m/V \leq 16.5$$
$$24.5 \leq D/t \leq 57$$
$$0.04 \leq A_{sp}/A_c \leq 0.10$$
$$u_s \geq 52\ mm$$

- For square SR-CFST stub columns:

$$10 \leq A_m/V \leq 20$$
$$20 \leq B/t \leq 44$$
$$0.05 \leq A_{sp}/A_c \leq 0.16$$
$$u_s \geq 30\ mm$$

- The method can be used for standard fire exposure times between 30 and 180 min.
- The method can be used for SR-CFST stub columns with concrete classes from C30 to C90 and steel grades from S275 to S690.

6. Summary and conclusions

A thermo-mechanical sequentially coupled FE model was developed using the nonlinear analysis package ABAQUS and was validated against the results obtained from the previous experimental campaign on stub SR-CFST columns carried out by the authors. The thermal results obtained in the FE model were compared to the time-temperature evolution registered by the thermocouple measurements at the mid-section of the columns. In turn, the mechanical part of the model was validated by comparing the displacement-time curves obtained from the experimental tests.

After the validation, an extensive parametric study comprising a total of 1440 cases (square and circular geometries) was developed. The influence of several geometrical parameters – section shape, outer tube dimensions and thickness, the relation between the inner steel profile are and the concrete infill area (A_{sp}/A_c) and, section factor – as well as the material properties of the concrete and steel – compressive concrete strength (f_c) and yield strength of steel (f_y) – was studied. It was found that the circular columns had better behaviour under the fire action than their square counterparts. Reducing the outer tube thickness, and therefore increasing the amount of concrete in the section, improved the fire resistance of the column, as the outer tube rapidly loses its mechanical properties when directly exposed to the heat source. The
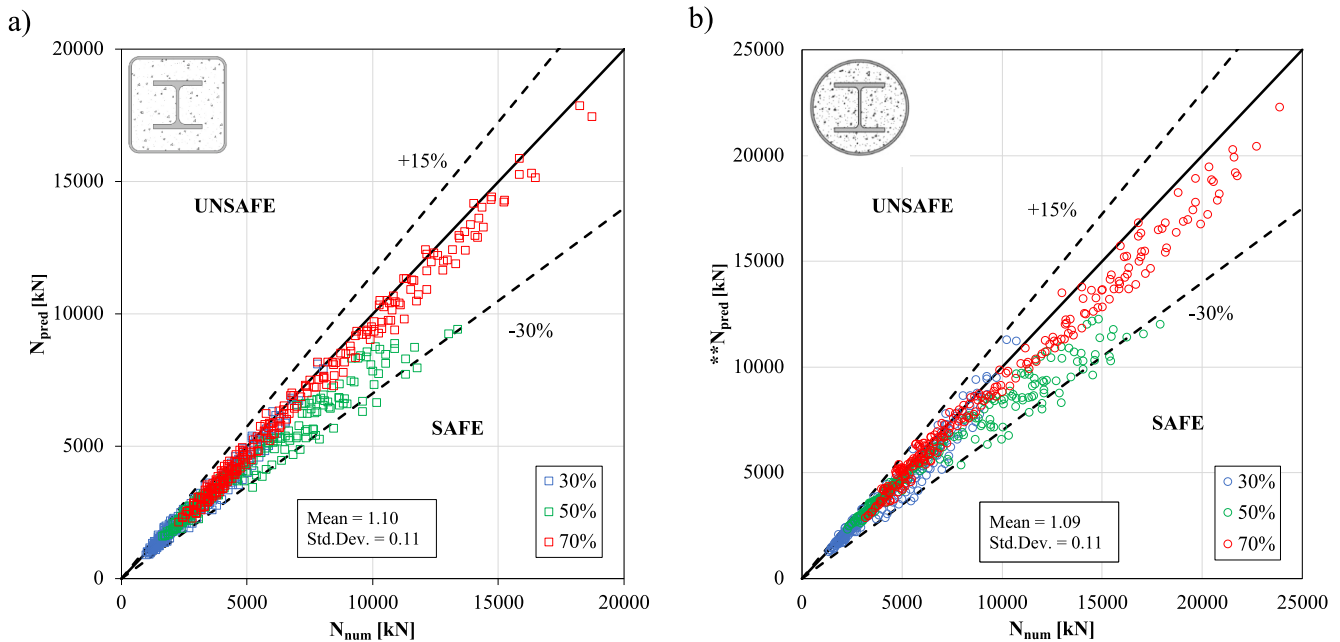
Fig. 21. Numerical vs. predicted fire plastic resistance obtained by applying the proposed simplified calculation method in eq. (13) for a) square and b) circular SR-CFST stub columns.

authors also pointed out that including a smaller inner profile of high-strength steel enhanced the fire performance of the sections, as while being protected by the surrounding concrete, its mechanical properties are retained for a longer period.

A new simplified calculation method was developed for evaluating the cross-sectional plastic resistance of SR-CFST stub columns subjected to fire. The equivalent temperature equations proposed by the authors for each part of the SR-CFST section – outer tube, concrete, web, and flanges of the steel profile – was combined with a new formulation proposed for evaluating the cross-sectional plastic resistance by addition of the mechanical contribution of the different parts of the section, in line with the current provisions in EN1994-1-2 [14]. This proposal extends the previous method proposed by the authors for CFST columns and provides a valuable tool for obtaining the cross-sectional plastic resistance of SR-CFST stub columns under high temperatures. The method has proven its accuracy by meeting the established CEN TC250 HGF criteria, providing safe and reliable predictions with a simplistic approach that will facilitate designers its practical application.

CRediT authorship contribution statement

David Medall: Writing – original draft, Validation, Methodology, Investigation, Formal analysis, Conceptualization. **Manuel L. Romero:** Writing – review & editing, Supervision, Project administration, Methodology, Funding acquisition, Conceptualization. **Huu-Tai Thai:** Writing – review & editing, Supervision, Resources, Conceptualization. **Ana Espinós:** Writing – review & editing, Validation, Supervision, Project administration, Methodology, Funding acquisition, Conceptualization.

Declaration of competing interest

The authors declare that they have no known competing financial interests or personal relationships that could have appeared to influence the work reported in this paper.

Data availability

Data will be made available on request.

References

[1] A. Espinós, M.L. Romero, D. Lam, Fire performance of innovative steel-concrete composite columns using high strength steels, Thin-Walled Struct. 106 (2016) 113–128, https://doi.org/10.1016/j.tws.2016.04.014.

[2] C. Dotreppe J, T. Binh Chu, R. Eng, J. Marc Franssen, Steel hollow columns filled with self-compacting concrete under fire conditions, 2010.

[3] F.-Q. Meng, M.-C. Zhu, G.C. Clifton, K.U. Ukanwa, J.B.P. Lim, Performance of square steel-reinforced concrete-filled steel tubular columns subject to non-uniform fire, J. Constr. Steel Res. (2020) 166, https://doi.org/10.1016/j.jcsr.2019.105909.

[4] Fan-Qin Meng, G. Mei-Chun Zhu, Charles Clifton, Kingsley U. Ukanwa, James B. P. Lim, Fire performance of edge and interior circular steel-reinforced concrete-filled steel tubular stub columns, Steel Compos. Struct. 41 (2021) 115–122.

[5] W.J. Mao, Wang W. Da, K. Zhou, E.F. Du, Experimental study on steel-reinforced concrete-filled steel tubular columns under the fire, J. Constr. Steel Res. 185 (2021) 106867, https://doi.org/10.1016/J.JCSR.2021.106867.

[6] W.J. Mao, Wang W. Da, K. Zhou, Fire performance on steel-reinforced concrete-filled steel tubular columns with fire protection, J. Constr. Steel Res. 199 (2022) 107580, https://doi.org/10.1016/J.JCSR.2022.107580.

[7] W.J. Mao, K. Zhou, Wang W. Da, Investigation on fire resistance of steel-reinforced concrete-filled steel tubular columns subjected to non-uniform fire, Eng. Struct. 280 (2023) 115653, https://doi.org/10.1016/J.ENGSTRUCT.2023.115653.

[8] D. Medall, C. Ibañez, A. Espinós, M.L. Romero, Thermo-mechanical compression tests on steel-reinforced concrete-filled steel tubular stub columns with high performance materials, Steel Compos. Struct. 49 (2023) 533–546.

[9] Q. Tan, L. Gardner, L. Han, Performance of steel-reinforced concrete-filled stainless steel tubular columns at elevated temperature, Int. J. Struct. Stab. Dyn. (2019) 19, https://doi.org/10.1142/S0219455419400029.

[10] Q.-H. Tan, L. Gardner, L.-H. Han, T.-Y. Song, Fire performance of steel reinforced concrete-filled stainless steel tubular (CFSST) columns with square cross-sections, Thin-Walled Struct. (2019) 143, https://doi.org/10.1016/j.tws.2019.106197.

[11] W.-J. Mao, W.-D. Wang, W. Xian, Numerical analysis on fire performance of steel-reinforced concrete-filled steel tubular columns with square cross-section, Structures 28 (2020) 1–16, https://doi.org/10.1016/j.istruc.2020.08.043.

[12] Zhu Meichun, Meng Fanqin, He Baojie, Experimental research on fire resistance of steel tubular columns filled with steel reinforced concrete, J. Build. Struct. 37 (2016) 36–43.

[13] V. Albero, A. Espinos, M.L. Romero, A. Hospitaler, G. Bihina, C. Renaud, Proposal of a new method in EN1994-1-2 for the fire design of concrete-filled steel tubular columns, Eng. Struct. (2016) 128, https://doi.org/10.1016/j.engstruct.2016.09.037.

[14] CEN. EN 1994-1-2, Eurocode 4: Design of composite steel and concrete structures. Part 1.2: General rules - Structural fire design, Comité Européen de Normalisation, Brussels, Belgium, 2005.

[15] CEN/TC250/SC4 N2192 - SC4.T7 Project Team final draft prEN 1994-1-2, Eurocode 4: Design of composite steel and concrete structures – Part 1–2: General – Structural fire design, 2021.

[16] D. Medall, A. Espinós, V. Albero, M.L. Romero, Simplified proposal for the temperature field of steel-reinforced CFST columns exposed to fire, Eng. Struct. 273 (2022) 115083, https://doi.org/10.1016/j.engstruct.2022.115083.

[17] Dassault Systèmes, Abaqus Unified FEA - SIMULIATM by Dassault Systèmes®, Dassault Systèmes Simulia, 2021.

[18] CEN. EN 1991-1-2, Eurocode 1: Actions on structures - Part 1–2: General actions - Actions on structures exposed to fire, Comité Européen de Normalisation, Brussels, Belgium, 2002.

[19] International Organization for Standardization, ISO 834-11 - Fire resistance tests — Elements of building construction, International Organization for Standardization, Geneva, Switzerland, 2014.

[20] CEN. EN 1994-1-1, Eurocode 4: Design of composite steel and concrete structures. Part 1.1: General rules and rules for buildings, Comité Européen de Normalisation, Brussels, Belgium, 2004.

[21] X. Qiang, F. Bijlaard, H. Kolstein, Dependence of mechanical properties of high strength steel S690 on elevated temperatures, Constr. Build. Mater. 30 (2012) 73–79, https://doi.org/10.1016/j.conbuildmat.2011.12.018.

[22] H.T. Li, B. Young, Material properties of cold-formed high strength steel at elevated temperatures, Thin-Walled Struct. (2017) 115, https://doi.org/10.1016/j.tws.2017.02.019.

[23] S. Shakil, W. Lu, J. Puttonen, Experimental studies on mechanical properties of S700 MC steel at elevated temperatures, Fire Saf. J. 116 (2020) 103157, https://doi.org/10.1016/J.FIRESAF.2020.103157.

[24] G.Q. Li, L.X. Song, Mechanical properties of TMCP Q690 high strength structural steel at elevated temperatures, Fire Saf. J. (2020) 116, https://doi.org/10.1016/j.firesaf.2020.103190.

[25] CEN., EN 1993-1-12: Eurocode 3 - Design of steel structures - Part 1–12: Additional rules for the extension of EN 1993 up to steel grades S 700. Design of Structural Elements, 2015.

[26] CEN. EN 1993-1-2, Eurocode 3: Design of steel structures, Part 1.2: General rules – Structural fire design, Comité Européen de Normalisation, Brussels, Belgium, 2005.

[27] L.T. Phan, N.J. Carino, Code provisions for high strength concrete strength-temperature relationship at elevated temperatures, Mater. Struct. (2003) 36, https://doi.org/10.1617/13811.

[28] V.K.R. Kodur, T.C. Wang, F.P. Cheng, Predicting the fire resistance behaviour of high strength concrete columns, Cem. Concr. Compos. (2004) 26, https://doi.org/10.1016/S0958-9465(03)00089-1.

[29] M. Matsudo, H. Nishida, T. Ohtsuka, T. Hirashima, T. Abe, Mechanical properties of high strength concrete at high temperatures, J. Struct. Construct. Eng. (Trans. AIJ) (2008) 73, https://doi.org/10.3130/aijs.73.341.

[30] F. Aslani, M. Bastami, Constitutive relationships for normal-and high-strength concrete at elevated temperatures, ACI Mater. J. (2011) 108, https://doi.org/10.14359/51683106.

[31] CEN/TC250/SC2 N1897 - Stable version prEN 1992-1-2:2021--09, Eurocode 2: Design of concrete structures - Part 1–2: General rules - Structural fire design, 2021.

[32] CEN. EN 1992-1-2, Eurocode 2: Design of concrete structures, Part 1.2: General rules – Structural fire design, Comité Européen de Normalisation, Brussels, Belgium, 2004.

[33] J.Y.R. Liew, M.X. Xiong, B.L. Lai, Design of Steel-Concrete Composite Structures Using High-Strength Materials, 2021, https://doi.org/10.1016/B978-0-12-823396-2.00041-1.

[34] J. Kruppa, CEN TC 250 Horizontal Group Fire. Document n° 99/130. Proposal for a Methodology to check the Accuracy of Assessment Methods, 1999.